

1963-64
Annual Summary Report

FACILITY FORM 802

N64-33207
(ACCESSION NUMBER)
373
(PAGES)
NASA CR 59002
(NASA CR OR TMX OR AD NUMBER)

(THRU)

(CODE)

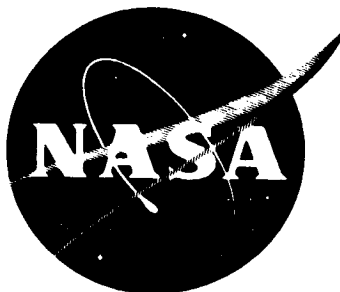
(CATEGORY)

POWER RELAY DESIGN

Extended Study of High Current Switching Devices

Contract No. NAS 8-2552

Prepared for:



George C. Marshall Space Flight Center
Huntsville, Alabama

OTS PRICE

XEROX

\$

2.00

MICROFILM

\$

2.00



SCHOOL OF ELECTRICAL ENGINEERING
OKLAHOMA STATE UNIVERSITY
Stillwater

1963 - 64

ANNUAL SUMMARY REPORT

Extended Study of High Current Switching Devices

Contract No. NAS 8-2552

Prepared for

N. A. S. A.

George C. Marshall Space Flight Center
Huntsville, Alabama

by

Dr. D. D. Lingelbach, Project Director
of
School of Electrical Engineering
Oklahoma State University
Stillwater

Report period 1 July 1963 - 30 June 1964

July 1, 1964

Reproduction of this document in any form by other than the National Aeronautics and Space Administration is not authorized except by written permission from the School of Electrical Engineering of the Oklahoma State University or from the George C. Marshall Space Flight Center.

OKLAHOMA STATE UNIVERSITY

Power Relay Design Personnel

Project Director

Dr. D. D. Lingelbach

Project Associates

W. A. Kyrk

R. M. Penn

L. C. Thomason

Project Assistants

A. F. Baker

A. L. Lindorfer

T. J. Pemberton

Project Technician

M. L. Colpitts

Project Secretary

(Mrs.) K. A. McBride

Office of Engineering Research

Director

Dr. Clark A. Dunn

Office Manager

(Mrs.) Glenna Banks

Editor

Bill Linville

NATIONAL AERONAUTICS AND SPACE ADMINISTRATION

George C. Marshall Space Flight Center

Technical Supervisors

Wayne J. Shockley

Richard Boehme

FOREWORD

This annual report is the third of a series of similar summary reports and is a compilation of the information in the five bimonthly interim reports submitted during the period July 1, 1963 to June 30, 1964. The first summary report, submitted July 1, 1962, contained the results of six months of investigation and the second summary report, submitted July 1, 1963, contained the results of the next 12 months of investigation.

abstract 33207
This report is organized into six parts. The first part is a summary containing the table of contents, the scope of work as defined in the contract, a brief summary of the technical material in the report, and a summary of the work time of each one of the project personnel. The remaining five parts contain the technical information and data and is divided into the major technical subject areas of investigation. The major areas of study are convenient in that it helps in defining the areas of investigation for the research personnel. The major subject areas are: analysis and performance, contacts, design, vibration and design theory. Each subject has a brief summary presented at the beginning of that part along with a table of contents.

Author
The information contained in each of the technical parts is compiled from the various interim report sections and consequently contains the section numbering used in that particular interim report. In order to maintain continuity of presentation the interim report sections used to make up each part of this report may not be in chronological order. In case the chronological order is desired the tabs identifying the sections in a given interim report are assigned a particular color. The numbering of the interim was started with the first one covering the period of

January and February 1962. The interim report numbers for the period of this summary report are the 9th, 10th, 11th, 12th and 13th. The tab color code associated with the interim reports is as follows. 9th - orange, 10th - rose, 11th - green, 12th - blue, and 13th - yellow.

This report presents findings of investigations involving only high current switching devices as required by the basic contract and subsequent modifications. As instructed, the proposal submitted for Modification No. 2 covered study of high voltage switching devices, but this aspect of the work was not included in the modification when formally included in the contract. Further expansion of the scope of work is recommended so that characteristics of higher voltage switching devices can be studied, covering both contactors and motor-driven switches to distribute 56 volts dc power in space vehicle circuitry.

The various sections of the interim reports are written by different project personnel. Effort has been made to make the different sections conform to a consistent pattern of presentation and format but inevitably some differences exist.

The project technical personnel consist of graduate research assistants who are actively pursuing M.S. or Ph.D. degrees and faculty in the College of Engineering. It is through their effort and the technical supervisors at the George C. Marshall Space Flight Center that this report is possible.

TABLE OF CONTENTS

Part A SUMMARY

Title Page	i
Personnel List	ii
Foreword	iii
Table of Contents	v
Report Summary	vii
Scope of Work	x
Summary of Man Hours	xiii

TECHNICAL INFORMATION AND DATA

Part B	<u>ANALYSIS AND PERFORMANCE</u>	<u>Section</u>	<u>Interim Report</u>
	Contactors Evaluation by Means of the Coil Current Derivative- - - - -	III	10th
	Influence of Temperature on the Dynamic Operation of a Hermetically Sealed Contactor- - -	II	11th
	Transient Analysis of the Economized Parallel Coil Contactor- - - - -	IV	12th
	The Energy Cycle Curve- - - - -	V	10th
	Leakage Flux Within a Relay- - - - -	I	11th
	Approximating Armature Movement and Leakage Flux of Sealed Relays- - - - -	III	12th
	Armature Movement Detection and Approximation- - - - -	VI	13th
	Proposed Figure of Merit for Power Relays- - - - -	III	13th
Part C	<u>CONTACTS</u>		
	The Contact Subsystem - Objectives of Research- - - - -	I	10th
	Contact Simulation on the Digital Computer- - - - -	III	11th

	<u>Section</u>	<u>Interim Report</u>
Some Energy, Temperature and Material Transfer Relations for Relay Contacts- - - - -	V	13th
Part D <u>DESIGN</u>		
Force-Physical Shape Relations for the Bipolar Type Coil Arrangement- - - - -	II	9th
A Study of Pole Face Configurations- - - - -	II	10th
Further Discussion of Pole Face Configurations- - - - -	IV	13th
Relay Drop-Out Time- - - - -	I	12th
Design Modification of the Parallel Coil 300 Ampere Contactor- - - - -	I	13th
Part E <u>VIBRATION</u>		
Applications of Vibration Theory in Relay Design- - - - -	IV	9th
Vibration Testing of a 75 Ampere Rotary Type Relay (part 1)- - - - -	II	12th
Vibration Testing of a 75 Ampere Rotary Type Relay (part 2)- - - - -	II	13th
Part F <u>DESIGN THEORY</u>		
Use of Abstract Models in Relay Design- - - - -	I	9th
An Investigation of an Alternate Design Map- - - - -	III	9th
Methods for Obtaining Allowed Specification Sets- - - - -	IV	10th

Tab Color Code

Orange	9th Interim	1 July - 30 Sept., 1963
Rose	10th Interim	1 Oct. - 30 Nov., 1963
Green	11th Interim	1 Dec., 1963 - 31 Jan., 1964
Blue	12th Interim	1 Feb. - 31 March, 1964
Yellow	13th Interim	1 April - 31 May, 1964

REPORT SUMMARY

The general objective pursued in this study was the development of mathematical models which represent the various energy conversion systems making up a power relay. The models were and are to be used to predict the performance, to optimize various characteristics and to study ways to obtain the greatest information from the use of such models. Also, part of this objective involved investigating better ways to measure the response of the hermetically sealed unit.

The scope of work, as defined in this contract modification, has been divided into five areas of investigation. The subject areas of investigation are: analysis and performance, contacts, design, vibration and design theory.

Presented in the part on analysis and performance is the use of the transient coil current derivative along with the transient coil current as a means of studying the influence of temperature on the dynamic operation of the power relay. Also presented is the development of a means to calculate the approximate armature motion of a hermetically sealed device by taking measurements from the x - y presentation of the transient coil current and the average transient coil flux. Included in this part is the development of a proposed relationship which allows the quantitative comparison of power relays by including the effects of various characteristics of the unit.

In the contact area work was initiated into the determination of the relationship between the contact material transferred and the arc energy and also the relationship among the parameters and the arc

energy. A numerical solution for the arc energy as a function of the arc characteristics is presented. Only a limited amount of experimental data has been obtained to date on arc energy and material transferred. Some theory on the "short arc" is also presented.

In design the objective was the determination of parameters that can be optimized and relationships to represent the device. A study of circular and square cross section cores reveals that the circular cross section core is 1.27 times more efficient in terms of the pull per watt. Also, presented is a study of the influence of the apex angle of shaped pole pieces on maximum pull. The angle for maximum pull is a function of the ratio of the working circuit reluctance to the non-working circuit reluctance. Also included is the result of a design modification of the 300 ampere contactor. The modification was to determine if it is possible to eliminate the coil switching arrangement by maximizing the pull per watt. The theoretical development indicates that a one coil unit, with no switching of the coil and using essentially the same holding power as the original design, is possible. An experimental verification of this modification is desirable because of the assumptions that had to be made to use the existing mathematical model.

The vibration part of this report presents the results of a thorough study of the resonant conditions existing in the 75 ampere rotary type relay. Different mounting arrangements have been evaluated and at present it has been possible to shift the resonant frequency from about 600 cps to about 1500 cps. To obtain a satisfactory unit the resonant frequency will have to be shifted out beyond 2000 cps.

The design theory part presents two techniques for checking the consistency of a set of selected parameters of a mathematical model. Also, a procedure for determining whether or not a group of relationships is independent is presented.

SCOPE OF WORK January 1, 1962

The work will consist of the following:

- (a) Review several contactor designs presently employed for space vehicle applications and select the most promising design for further analysis.
- (b) Analyze in detail the design to determine the parameters which are not consistent with the requirements.
- (c) Propose a modified design which would more nearly satisfy the required performance.
- (d) The design performance of the contactor is as follows:
 - (1) Withstand 20G or more vibration with a frequency range of 10 to 2000 cps.
 - (2) That the contactor have a minimum life of 10,000 operations at rated load.
 - (3) Temperature limits - 65° to + 125° F.
 - (4) Contactor shall be contained in hermetically sealed package.
- (e) Evaluate modified design unit

MODIFICATION I July 1, 1962

1. Progress thus far has provided data from transient coil current build-up traces to determine the particular form of certain design relationships. Because of apparent armature delay during operation, the total function time of the armature will be divided into initial and final periods. Each interval will have a pick-up transit time. It appears that agreement exists between theoretically developed relationships and the form of the measured traces. Transient coil current decay will be used with current coil build-up data to verify the form of the

design relationships.

2. It is the intended purpose to develop equations and from these equations develop a mapping technique to analyze, not only the electrical relationships, but also, the mechanical and contact relationships in order to arrive at a means for determining the parameters which may be consistent with the specification requirements. With this approach, it is the goal from these studies to determine if a design will meet specification requirements by analysis rather than trial and error production, and continued testing and modification. Particular attention will be spent, in the first few weeks of this additional effort, in testing existing contactor designs and writing suitable performance equations which relate mass, spring tension, and other variables. These equations will then be used, with the design procedure which has already been developed, to design a contactor which will withstand 20G vibration with a frequency range of 10 to 2000 cps.

3. Contactors which were tested at rated contact current and high inductance were found to overheat. Test runs of load on the contacts of a given contactor under various loading of current and inductance with several ambient temperature conditions need to be performed. Information is required to determine the characteristic temperature equations to use in the design procedure.

4. It is the intent of this contract to be able at its completion to specify the parameters that prevent a contactor from meeting a given specification and also to be able to give the parameters to design a new unit.

MODIFICATION II July 1, 1963

a. Study of design of the thermal characteristics from extreme low temperatures to 125^o C for a relay.

b. Study of materials which influence design and those materials which influence relay performance at extreme low temperature to 125^o C (springs, coils, insulation).

c. Attempt to design the coil of a relay for use at a temperature range of - 85^o C to + 125^o C. If this is not feasible, recommend designs which should be recommended for use at low temperatures.

d. Continue study of the design of the mechanical system of a relay in an attempt to design the mechanical system to reduce its susceptibility to vibration.

e. Continue study of a relay (or contactor) design to determine maximum pull per watt and if possible maximum pull per watt per unit of weight over a range of stability factors for various parameters to obtain design for optimum conditions.

f. Make a study of relay contacts in an attempt to design and specify contacts.

g. Make a study of relay design parameters to find optimum design relationships and criteria.

h. Translate word specifications to significant design parameters.

i. Assist relay manufacturer with design or modification of design for specific performance as required for space application.

SUMMARY OF MAN HOURS

Annual Summary Report: 1 July, 1963 to 30 June, 1964

Interim Report Periods:

9th	1 July to 30 Sept., 1963*
10th	1 Oct. to 30 Nov., 1963
11th	1 Dec., 1963 to 31 Jan., 1964
12th	1 Feb. to 31 March, 1964
13th	1 April to 31 May, 1964

		Periods					
		9th	10th	11th	12th	13th	June
(a) Engineering							
D. D. Lingelbach	50%						
Project Director	100%						
A. F. Baker	50%						
	100%		100% August				
W. A. Kyrk	50%						
		Started September 1					
A. L. Lindorfer	25%						
	50%		50% July				
T. J. Pemberton	25%						
	100%						
R. M. Penn	50%						
L. C. Thomason	50%						
		Started September 1					
H. W. Shira	50%						
P. K. Shih	25%						
M. E. Council	25%						
G. C. Stone	50%		50% July				
	100%		100% August				
(b) Secretarial							
K. A. McBride	100%						
(c) Technician							
M. L. Colpitts	100%						

The academic staff of the Oklahoma State University is appointed for nine months plus a vacation of one month for a given salary. When a person works two months during the summer, this pay is at the rate of ten per cent of his pay for the academic year per month. Working hours are 40 hours per week except where vacation periods are established by the University. Research personnel are assigned a given percentage of their total time to a project, and relieved of other duties for the corresponding time assigned to the project.

TABLE OF CONTENTS

Part B

ANALYSIS AND PERFORMANCE

<u>SUMMARY</u>	<u>Section</u>	<u>Interim Report</u>
Contactator Evaluation by Means of the Coil Current Derivative- - - - -	III	10th
Influence of Temperature on the Dynamic Operation of a Hermetically Sealed Contactator- - - - -	II	11th
Transient Analysis of the Ecomonized Parallel Coil Contactator- - - - -	IV	12th
The Energy Cycle Curve- - - - -	V	10th
Leakage Flux Within a Relay- - - - -	I	11th
Approximating Armature Movement and Leakage Flux of Sealed Relays- - - - -	III	12th
Armature Movement Detection and Approximation- - - - -	VI	13th
Proposed Figure of Merit for Power Relays- - - - -	III	13th

Tab Color Code

Orange	9th Interim	1 July - 30 Sept., 1963
Rose	10th Interim	1 Oct. - 30 Nov., 1963
Green	11th Interim	1 Dec., 1963 - 31 Jan., 1964
Blue	12th Interim	1 Feb. - 31 March, 1964
Yellow	13th Interim	1 April - 31 May, 1964

SUMMARY

Part B

Analysis and Performance

The information presented in this part is the result of pursuing the objective of trying to find better ways to obtain more and better data about the response of a hermetically sealed power relay.

The testing techniques are essentially limited to making electrical tests at the terminals of the device. From these tests it is desired to obtain the mechanical, magnetic as well as the electrical response of the device. The simultaneous presentation of the response of more than one variable gives more accurate information so the use of the dual beam oscilloscope is almost mandantory. The combination of data obtained by steady state and transient tests results in much more useful information than the data of either by itself. More complete information is obtained from the transient data than the steady state data since the transient information is available for all periods of the operation while the steady state is limited to certain periods.

The first section of this part shows that the transient coil current time derivative presented along with the transient coil current gives additional and more conclusive information about the response of the device than the transient coil current alone. Data of the transient response obtained from sample open type units can be used with the transient data from sealed units to determine mechanical and magnetic behavior of the unit by comparing the various transient coil currents and their time derivatives. In the second section of this part the coil current derivative technique was used to show the possibility of obtaining information about the influence of temperature on the spring constants and

overtravel distances of a hermetically sealed power relay.

The third section of this part is another example of the greater effectiveness of using transient information to examine the response of a sealed unit. The unit tested was a two coil operate-one coil hold arrangement and by using transient data it was possible to show that the control switch used to switch the coil malfunctioned on certain occasions. Some of this information would have been impossible to obtain by a steady state test. In fact an error in the schematic diagram was determined by using the transient test.

The next four sections of this part presents the development of a technique referred to as the Energy Cycle Curve. This energy cycle curve is a presentation of the transient coil current and the transient average coil flux as an x - y plot. The relationship between the coil current and coil flux is the magnetic reluctance. Utilizing the transient value of reluctance it is possible to obtain an approximation to the armature motion as a function of time from the energy cycle curve. This can be done on a hermetically sealed device.

The last section of this part deals with a proposed way to quantitatively compare the required and desirable characteristics of several possible contactors. The main problem is the determination of weighting factors to associate with the parameters being considered.

SECTION III

CONTACTOR EVALUATION BY MEANS OF THE COIL CURRENT DERIVATIVE

The transient response of the coil current and contact voltage of a contactor to a given input voltage has resulted in an effective way to analyze its performance. To date, the analysis has been limited essentially to examining the current or voltage trace presented on the oscilloscope as recorded on film. Additional ways are being investigated to obtain more or other types of information from the transients associated with the contactor.

In the analysis of the performance of the contactor, ultimately the tests must be those that can be used on a hermetically sealed device. To obtain information about the mechanical dynamics of the contactor in terms of electrical quantities is the main objective of examining these transients. The technique explained in this section is the possibility of electronically differentiating the coil current transient and using this information to help understand the performance of the contactor, especially the mechanical dynamics.

The coil current signal is fed to an operational amplifier connected such that the output signal is the time derivative of the input signal. The coil current signal and its derivative signal is then applied to a dual beam oscilloscope which results in the simultaneous display of both signals. More useful information is obtained by the simultaneous display than by each one separately. This dictates the use of a dual beam scope for best results.

One result more readily available from the coil current derivative than from the coil current itself is the change in armature velocity caused by it picking up the contacts on make. This action is shown by the two traces in the oscillogram shown in Figure 1. To emphasize this change in armature velocity when making with the contacts, one of two things may be changed. Decreasing the coil

voltage or increasing the resistance in series with the coil will cause these changes in armature velocity to be exaggerated. This is demonstrated by making a comparison of the traces shown respectively in Figures 1, 2, 3 and 4 or by studying the three sets of traces in Figure 5. Figure 5 shows the results of putting three sets of information on the same oscillogram which may be, at first, a little difficult to interpret. It has the definite advantage of being able to make a more direct comparison of the results.

For the contactor under examination, decreasing the voltage not only increases the pick-up and closing times but results in the armature changing its velocity considerable when making with the contacts and associated overtravel springs. This is shown in the coil current traces by the presence of the double cusp, and in the differential of the coil current trace, by the presence of the two negative spikes.

The existence of some armature rebound is noticable in the derivative of the coil current by the occurrence of the "high" frequency oscillations in these traces. One note of caution might be appropriate here and that is the derivative of a signal is susceptible to including noise which can be the cause of some of the "high" frequency oscillations in the trace. The reason noise was ruled out in this case is that the observed oscillations appear to occur only after the armature is supposed to strike something and does not show up before these times.

The series of oscillograms shown by Figures 1, 2, 3 and 4 show the influence of increasing the coil voltage from a value near pick-up to the rated value. At the lower voltages the influence of the contacts making, which results in the slowing down of the armature, is readily obvious. The resulting change in the coil current because of this phenomena is a function of the "closeness" of the magnetic coupling of the coil and the sensitivity of the magnetic flux to changes in armature air gap. The derivative of the coil current contains two negative

spikes in Figure 1. The second spike is of greater amplitude than the first. This may be caused by two possible reasons. One reason the second spike is longer than the first is that the air gap is small at this point, since the armature is seating on the pole piece. Consequently, a given change in air gap, at this position, results in a greater percentage change than when the air gap is in the open position. Another reason why the second spike might be larger than the first is that the impact of the armature with the pole face is more violent than the impact with the contacts, because of the overtravel springs when making with the contacts.

Increasing the coil voltage tends to "smooth" out the second cusp in the coil current trace as shown by comparison of Figures 1 and 2. In Figure 2, the change caused by the making of the contacts is not as noticeable because of the increased magnetic pull at this increased voltage.

Figure 3 shows the result of increasing the coil voltage from 13.6 v for Figure 2 to 16 v for Figure 3. The coil current cusp is now essentially smooth and shows little evidence, if any, of the contacts making. However, the coil current derivative trace still shows a marked change in its position at the point where the armature reacts to the making of the contacts. This is one of the main advantages of recording or analyzing the coil current derivative is that it is more sensitive to changes in the armature motion. In analyzing the performance of hermetically sealed contactors electrical measurements are the only source of information about both the magnetic and mechanical behavior of the contactor.

Figure 4 is the result of applying rated voltage to the coil. A scale change was necessary in this oscillogram to keep the traces on the coordinates but the results still show that the coil current cusp is very smooth now and the coil

current derivative is also essentially smooth. However, close examination of the coil current derivative will show a slight change about one half the way down the negative spike which unfortunately fell exactly on the center coordinate in this oscillogram. Figure 12 shows the same result but was obtained by changing the resistance in series with the coil and in this figure the change in the coil current derivative is more noticable since it is not on the coordinate.

Figure 5 shows the coil current and coil current derivative for three values of coil voltage. It allows a more direct comparison of the effects of the increase in voltage on the armature change in velocity caused by the making of the contacts.

Changing the coil voltage is not the only way the influence of the making of the contacts on the armature motion phenomena can be studied. The series of Figures 6, 7, 8, 9, 10, 11 and 12 show the influence of this armature motion change on the coil current and coil current derivative. One basic difference of the series resistance approach over the variable coil voltage approach, is that the value of the coil current derivative at $t = 0$ (the time the coil voltage is applied) is the same for all values of series resistance. In the variable voltage case the value of the coil current derivative at $t = 0$ should vary directly with the coil voltage applied. Even though the traces in the series of Figures 1, 2, 3 and 4 look similar to those in the series of Figure 6 to 12 there are a number of differences. Cases which are taken at the same steady state coil current are different since in the series resistance case the time constant of the circuit is changed, while in the variable voltage case the time constant of the circuit is not changed, but the initial rate of change of the current is changed. Even the shape of the coil current cusp is different, being flatter for the series resistance case.

This discussion and samples of oscillograms showing transient coil currents and coil current derivatives has been presented to show that additional information can be obtained about the dynamic behavior of the contactor by studying the coil current derivatives in conjunction with the transient coil current. The main problem involved with the derivative of the coil current is that of noise since the noise is differentiated along with the coil current signal.

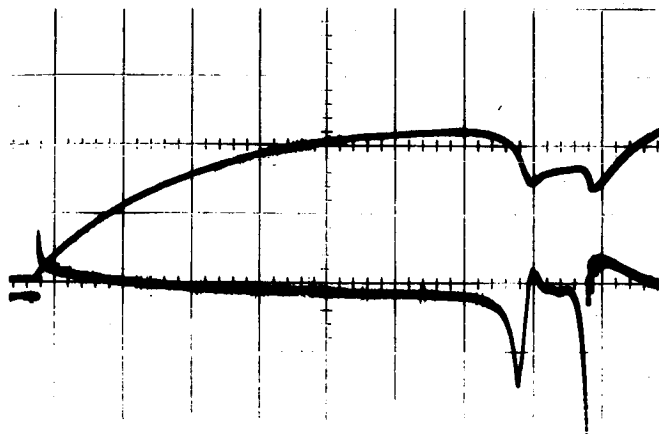


Figure 1

Vertical axis: Upper trace - coil current
 Lower trace - coil current derivative
 Horizontal axis: Time

Time scale: 10 milliseconds/cm
 Current scale: 100 milliamperes/cm

*Coil voltage: 13.25 volts dc
 *Coil current: 238 milliamperes

Test Circuit values:
 Shunt 1 ohm, sensitivity 100 mv/cm

Differentiator constants:
 $Z_i = 0.1\mu f$, $Z_f = 0.1$ meg
 Sensitivity 0.2v/cm uncalibrated

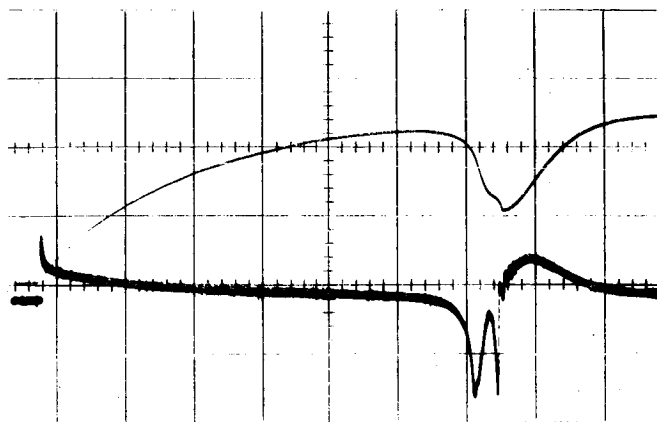


Figure 2

Vertical axis: Upper trace - coil current
 Lower trace - coil current derivative
 Horizontal axis: Time

Time scale: 10 milliseconds/cm
 Current scale: 100 milliamperes/cm

*Coil voltage: 13.6 volts dc
 *Coil current: 245 milliamperes

Test circuit values:
 Shunt 1 ohm, sensitivity 100 mv/cm

Differentiator constants:
 $Z_i = 0.1 \mu f$, $Z_f = 0.1 \text{ meg}$
 Sensitivity 0.2v/cm uncalibrated

*Changed from previous figure

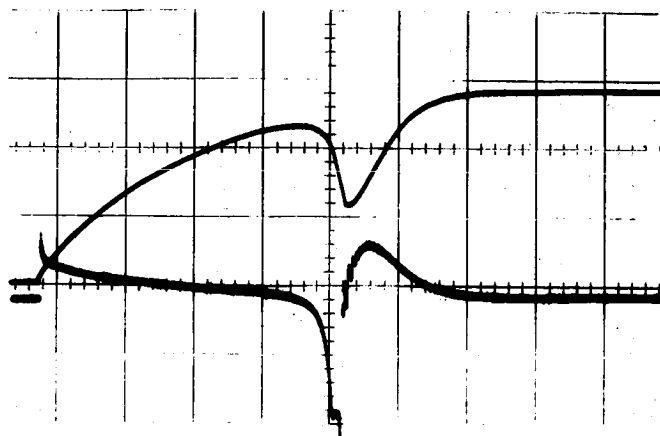


Figure 3

Vertical axis: Upper trace - coil current
 Lower trace - coil current derivative
 Horizontal axis: Time

Time scale: 10 milliseconds/cm
 Current scale: 100 milliamperes/cm

*Coil voltage: 16 volts dc
 *Coil current: 289 milliamperes

Test circuit values:
 Shunt 1 ohm, sensitivity 100 mv/cm

Differentiator constants:
 $Z_i = 0.1 \mu f$, $Z_f = 0.1 \text{ meg}$
 Sensitivity 0.2v/cm uncalibrated

*Changed from previous figure

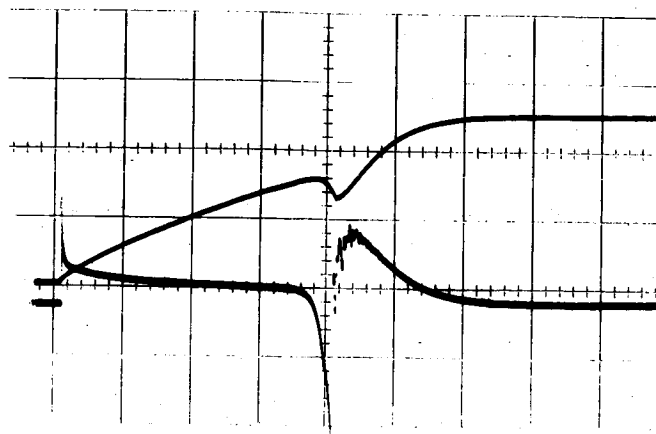


Figure 4

Vertical axis: Upper trace - coil current
 Lower trace - coil current derivative
 Horizontal axis: Time

*Time scale: 5 milliseconds/cm
 *Current scale: 200 milliamperes/cm

*Coil voltage: 28 volts dc
 *Coil current: 496 milliamperes

Test circuit values:
 Shunt 1 ohm, sensitivity 200 mv/cm*

Differentiator constants:
 $Z_i = 0.1 \mu f$, $Z_f = 0.1 \text{ meg}$
 Sensitivity 0.5v/cm calibrated*

*Changed from previous figure

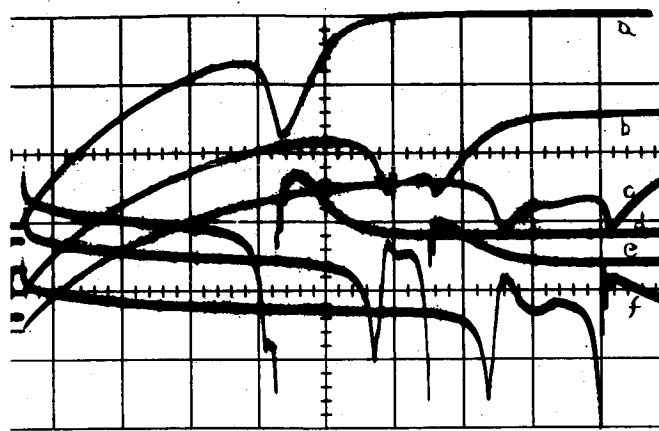


Figure 5

Vertical axis: Traces a, b, c coil current
Traces d, e, f coil current derivative
Horizontal axis: Time

*Time scale: 10 milliseconds/cm

*Current scale: 100 milliamperes/cm

*Coil voltage: Traces a & d = 17.7v; traces b & e = 14.5v;
traces c & f = 13.3v

*Coil current: Traces a & d = 320ma; traces b & e = 260ma;
traces c & f = 240ma

Test circuit values:

Shunt 1 ohm, sensitivity 100 mv/cm*

Differentiator constants:

$Z_i = 0.1\mu f$, $Z_f = 0.1$ meg

Sensitivity 0.2v/cm uncalibrated*

*Changed from previous figures

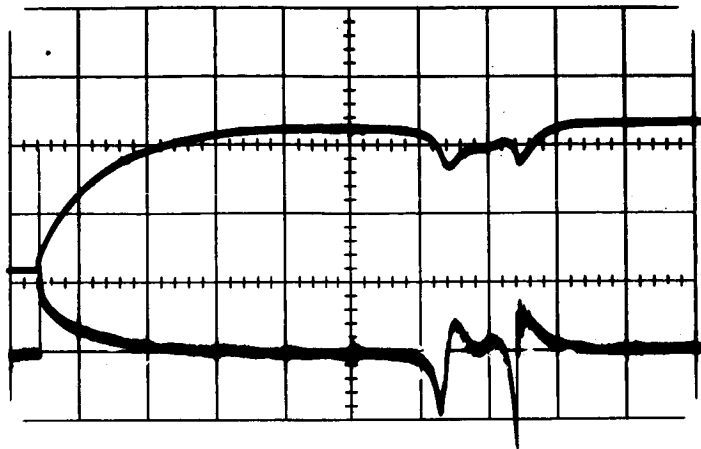


Figure 6

Vertical axis: Upper trace - coil current
 Lower trace - coil current derivative
 Horizontal axis Time

Time scale: 10 milliseconds/cm
 Current scale: 100 milliamperes/cm

*Coil voltage: 28 volts dc
 *Coil current: 219 milliamperes

Test circuit values:
 Shunt 1 ohm, sensitivity 100 mv/cm

Differentiator constants:
 $Z_i = 0.1 \mu f$, $Z_f = 0.1 \text{ meg}$
 Sensitivity 0.2v/cm uncalibrated

*Changed from previous figure

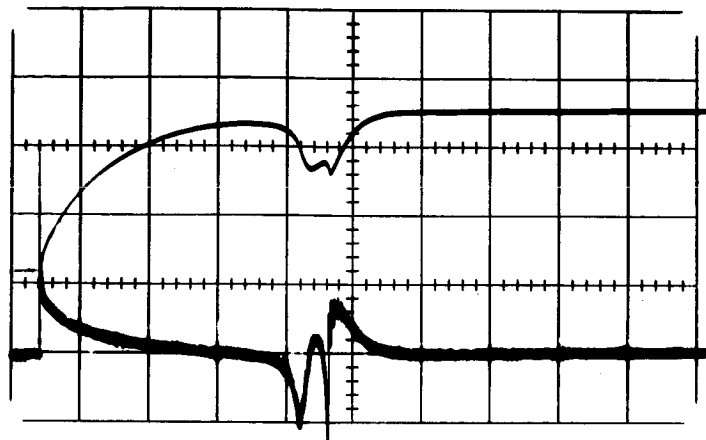


Figure 7

Vertical axis: Upper trace - coil current
 Lower trace - coil current derivative
 Horizontal axis: Time

Time scale: 10 milliseconds/cm
 Current scale: 100 milliamperes/cm

Coil voltage: 28 volts dc
 *Coil current: 230 milliamperes

Test circuit values:
 Shunt 1 ohm, sensitivity 100 mv/cm

Differentiator constants:
 $Z_i = 0.1 \mu f$, $Z_f = 0.1 \text{ meg}$
 Sensitivity 0.2v/cm uncalibrated

*Changed from previous figure

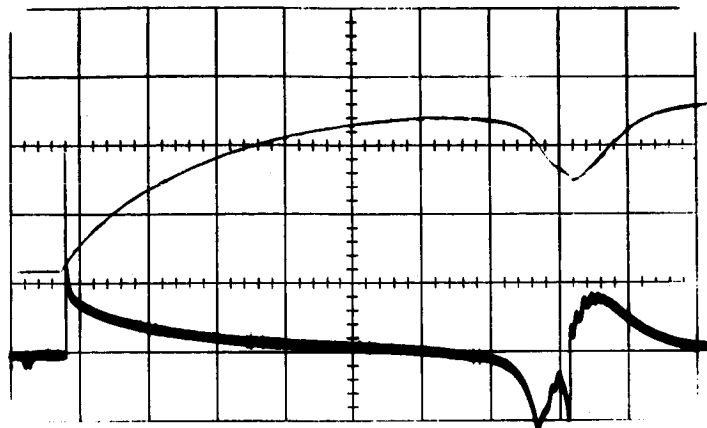


Figure 8

Vertical axis: Upper trace - coil current
 Lower trace - coil current derivative
 Horizontal axis: Time

Time scale: 10 milliseconds/cm
 Current scale: 100 milliamperes/cm

Coil voltage: 28 volts dc
 *Coil current: 249 milliamperes

Test Circuit values:
 Shunt 1 ohm, sensitivity 100mv/cm

Differentiator constants:
 $Z_i = 0.1\mu f$, $Z_f = 0.1$ meg
 Sensitivity 0.2v/cm uncalibrated

*Changed from previous figure

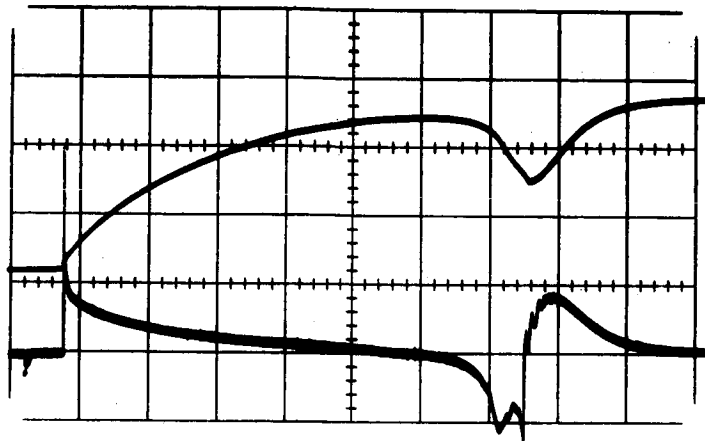


Figure 9

Vertical axis: Upper trace - coil current
 Lower trace - coil current derivative
 Horizontal axis: Time

Time scale: 10 milliseconds/cm
 Current scale: 100 milliamperes/cm

Coil voltage: 28 volts dc
 *Coil current: 260 milliamperes

Test circuit values:
 Shunt 1 ohm, sensitivity 100 mv/cm

Differentiator constants:
 $Z_i = 0.1 \mu f$, $Z_f = 0.1 \text{ meg}$
 Sensitivity 0.2v/cm uncalibrated

*Changed from previous figure

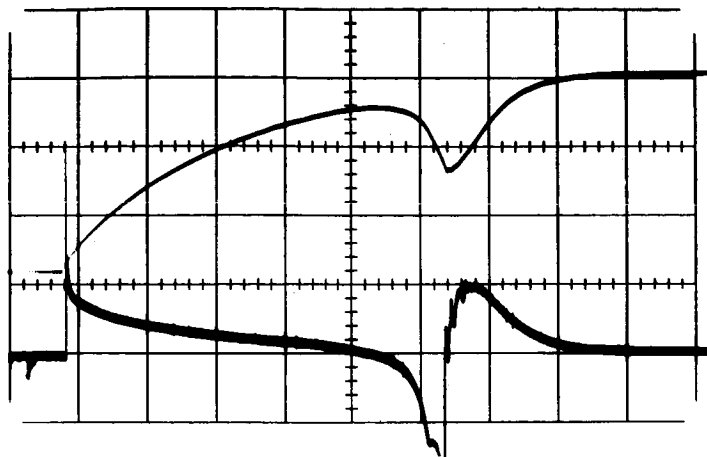


Figure 10

Vertical axis: Upper trace - coil current
 Lower trace - coil current derivative
 Horizontal axis: Time

Time scale: 10 milliseconds/cm
 Current Scale: 100 milliamperes/cm

Coil voltage: 28 volts dc
 *Coil current: 296 milliamperes

Test circuit values:
 Shunt 1 ohm, sensitivity 100 mv/cm

Differentiator constants:
 $Z_i = 0.1\mu f$, $Z_f = 0.1$ meg
 Sensivity 0.2v/cm uncalibrated

*Changed from previous figure

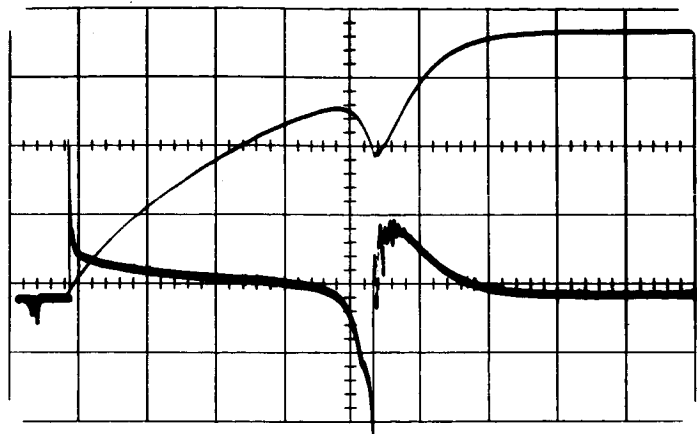


Figure 11

Vertical axis: Upper trace - coil current
 Lower trace - coil current derivative
 Horizontal axis: Time

Time scale: 10 milliseconds/cm
 Current scale: 100 milliamperes

Coil voltage: 28 volts dc
 *Coil current: 400 milliamperes

Test circuit values:
 Shunt 1 ohm, sensitivity 100 mv/cm

Differentiator constants:
 $Z_i = 0.1 \mu f$, $Z_f = 0.1 \text{ meg}$
 Sensitivity 0.2v/cm uncalibrated*

*Changed from previous figure

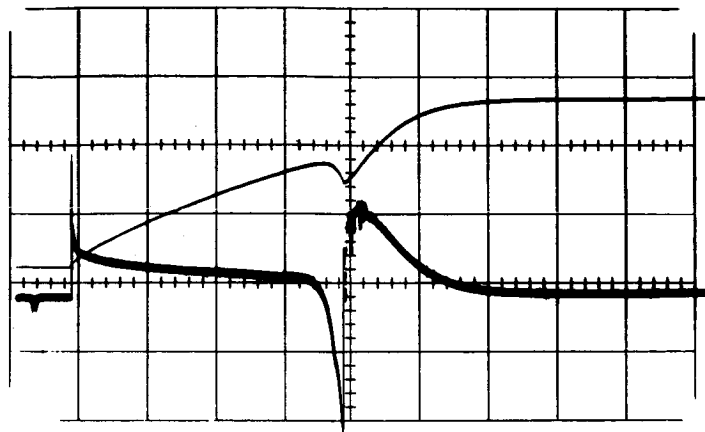


Figure 12

Vertical axis: Upper trace - coil current
 Lower trace - coil current derivative
 Horizontal axis: Time

Time scale: 10 milliseconds/cm
 *Current scale: 200 milliamperes/cm

Coil voltage: 28 volts dc
 *Coil current: 493 milliamperes

Test circuit values:
 Shunt 1 ohm, sensitivity 200. mv/cm

Differentiator constants:
 $Z_i = 0.1 \mu f$, $Z_f = 0.1 \text{ meg}$
 Sensivity 0.2v/cm uncalibrated

*Changed from previous figure

SECTION II
INFLUENCE OF TEMPERATURE ON THE DYNAMIC OPERATION
OF A HERMETICALLY SEALED CONTACTOR

Analysis of a hermetically sealed device is primarily limited to that information that can be obtained by electrical measurements at the terminals of the device. By using the transient coil current and its time derivative and the contact voltage a certain amount of useful information about the dynamic performance of the device can be obtained. The amount of useful information is related to having previously correlated the variations of the instantaneous coil current with other measurable quantities on an open device embodying similar principles. Familiarity of the mechanics of the operation then allows one to obtain useful information from the transient coil current.

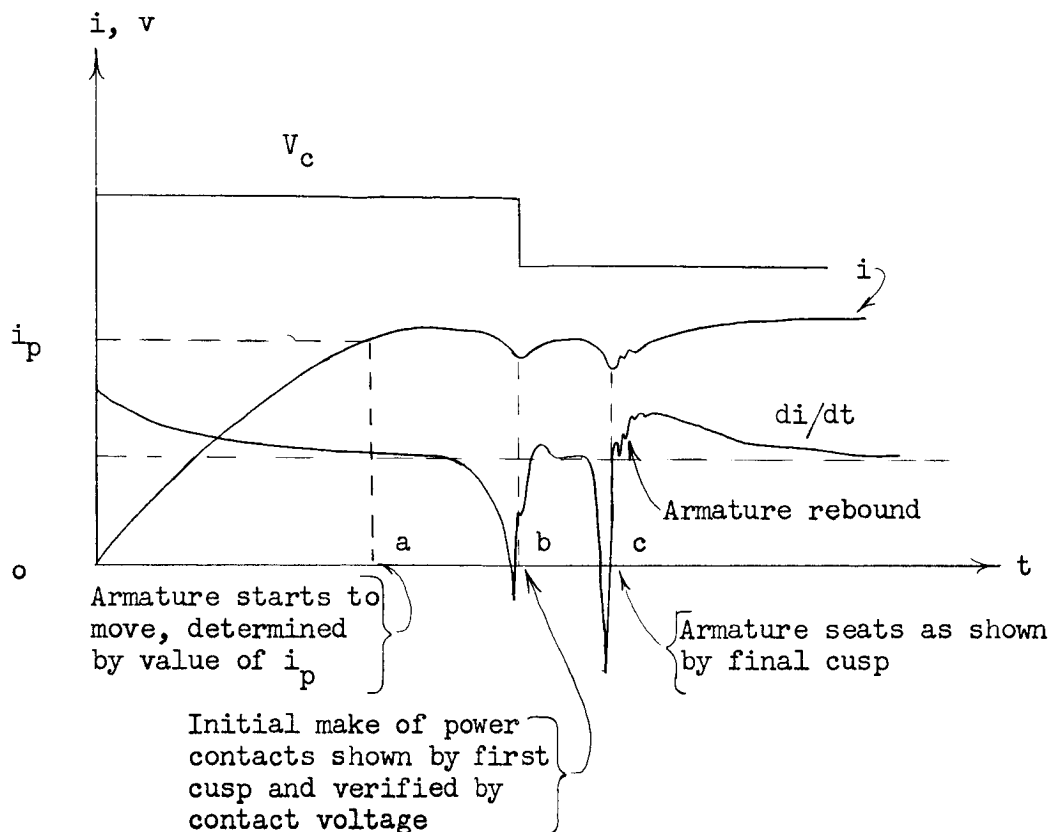
In this investigation it was desired to determine the changes in the mechanical system caused by the changes in temperature. In order to do this meant that the change in the coil current, caused by the change in resistance resulting from a change in temperature, must be compensated for so that constant steady state current was maintained. Constant steady state current was maintained by applying constant voltage and adding a suitable series resistance in the coil circuit. By maintaining constant voltage and constant total resistance, then that part of the transient coil current, from the instant the coil was energized until the armature started to move, was unchanged. Therefore, changes in the instantaneous coil current at different temperatures should be caused by changes in the mechanical operation.

One effective way of determining changes in the instantaneous coil current is to examine the time derivative of the coil current. The

instantaneous coil current and its derivative are shown in Figures 1 through 5. Both of these are shown simultaneously, to develop a familiarity of the shape of the coil current derivative, which will be used in other figures along with the contact voltage. The only significant change in these traces as the temperature decreased is the slight increase in negative slope of the coil current derivative commencing when the armature begins to move. On the oscillograms in Figures 1 through 5, this point of movement occurs about 2 centimeters (10 milliseconds) after the coil was energized. (A centimeter is a major full line division on the oscillogram). This increase in the negative slope of the derivative indicates a change in the operation of the mechanical system as the temperature decreases.

These oscillograms in Figures 1 - 5 were all taken with rated voltage applied to the coil. It has been found that if the analysis is performed on the contactor at reduced voltage then changes in the mechanical operation are more effective in causing changes in the coil current. Therefore, the set of oscillograms in Figure 6 through 15 were obtained in order to show what part of the mechanical system is more susceptible to changes in temperature. This set of oscillograms show the contact voltage across one pair of contacts and the coil current derivative simultaneously. Again, the steady state value of the coil current was maintained constant as the temperature decreased by adding a suitable series resistance to the coil circuit. However, the voltage applied, in this case, was near the room temperature pick-up value. For these oscillograms the voltage applied was 13.5 volts dc. To help understand the various points on the trace, the general shape of the traces are shown and explained in the sketch below. For purposes of discussion the time represented by Oa is called pick-up time, the time represented by

ab contact transit time and the time represented by bc as the contact overtravel time. The time represented by Ob is commonly referred to as the operate time.



One problem which arises, when data are collected for the steady state coil current near the pick-up valve, is that the behavior of the contactor is more random in nature than at rated value. This makes it a little more difficult to establish trends in the changes which occur. Therefore, a record of the randomness that occurs is presented in the first oscillogram and this is shown in Figure 6. This shows four consecutive operations of the contactor with all known parameters constant. This happens to be taken at a temperature of -80°F but the same kind of variation is present at other temperatures. There was no noticeable change

in the variations at different temperatures but this point will be considered at another time. The variations in operate time was about 7.0 milliseconds out of a total operate time of about 60 milliseconds or about a 10 percent change. The variation in the contact overtravel time is about 8 milliseconds out of 24 milliseconds.

Figures 7 through 15 shows the influence of the mechanical operation on the coil current derivative. The major trends are an increase in the operate time (represented by Ob in sketch) and an increase in the contact overtravel time (represented by bc in the sketch). The shape of the coil current derivative during the operate time shows no significant change except in total time. The coil current derivative during the contact overtravel time show some changes in shape but those seem to be the result of the increase in time.

Inspection of the kinematics of the mechanical system of this contactor is planned in order to establish what mechanical changes are taking place caused by temperature changes that could result in the changes recorded in the oscillogram.

It should be mentioned that the actual performance of the contactor at low temperatures would exhibit a shorter operate time because of the decrease in the coil resistance resulting in a greater steady state value of the coil current at constant supply voltage. In this test the coil circuit resistance was adjusted to keep the steady state value of the coil current constant in order to study the changes in the mechanical system as the temperature was decreased.

One interesting phenomena occurred in the recording of this data and this is the proximity effect. The contactor under test was sealed in a non-magnetic container and the first measurement was taken at room temperature on a wooden bench and its operation is shown in Figure 1.

When the unit was placed in the temperature chamber it was placed on a metal support to allow better air circulation around it and the oscillogram shown in Figure 16 is its operation under these conditions and a temperature of 40°F. A noticeable change in the coil current derivative is evident on the oscillogram about 3 1/2 centimeters after the point of coil energization. The change recorded at this point shows that the slope of the coil current increased in a region where no or little motion of the armature should occur. Also, the nature of the change is not like the change caused by armature motion. From previous tests this increase in the value of the coil current derivative is known to be caused by magnetic saturation. When the oscillogram in Figure 16 was first recorded, it was thought this change was caused by the temperature. However, after recording the oscillogram shown in Figure 17 which was at a temperature of 20°F it was evident that temperature was not the cause. Recalling the conditions at the room temperature made it evident that the metal support in the temperature chamber was the cause of the magnetic saturation. This implies that the leakage flux associated with this device in the armature open position is fairly large. Close packaging of units of this kind with the more sensitive relays might result in problems.

The results of these tests indicate that the mechanical system does change in such a manner that the operate time and the contact overtravel time increase with a decrease in temperature. A study is planned of the kinematics of the mechanical system to ascertain the mechanism by which this change occurs.

The results also show that the proximity effect can cause a significant change in the transient coil current and the performance of the device.

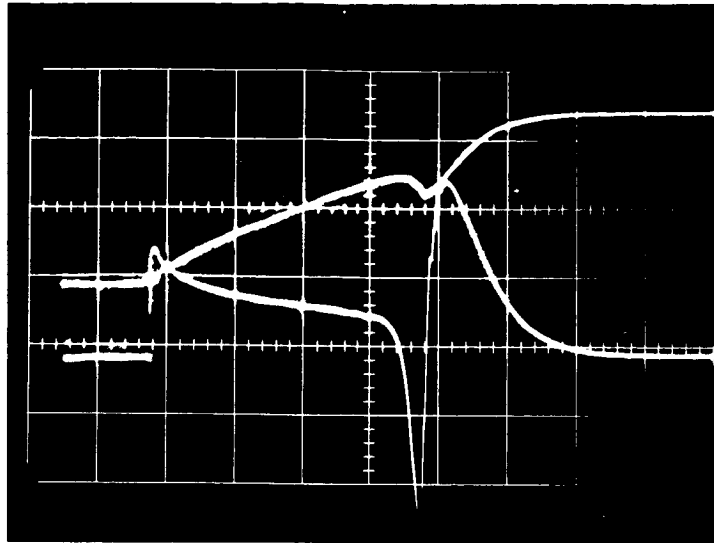


Figure 1

Vertical axis: Upper trace - coil current

Lower trace - coil current derivative

Horizontal axis: Time

Time scale: 5 milliseconds per centimeter

Current scale: 200 milliamperes per centimeter

Coil voltage: 28 volts dc

Coil current: 526 milliamperes

Test circuit values: 0.5 ohm shunt
0.1 volt/cm sensitivity
73°F

Differentiator constants: $Z_i = 1\mu f$, $Z_f = 0.1$ meg ohm
1 volt/cm sensitivity

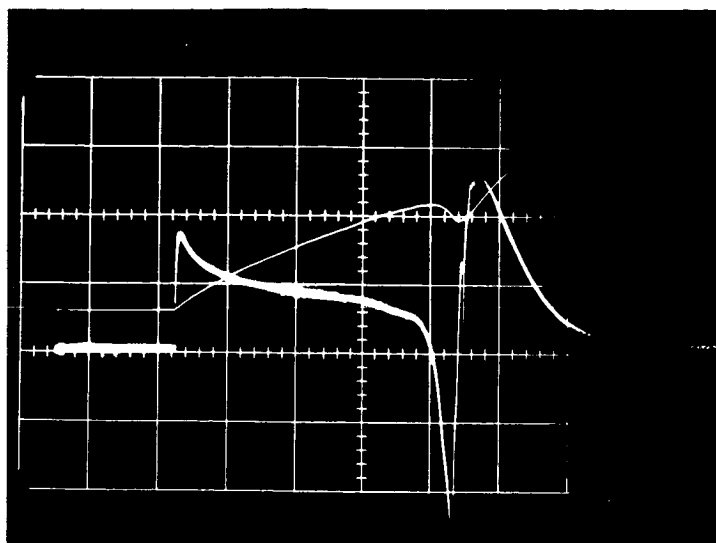


Figure 2

Vertical axis: Upper trace - coil current

Lower trace - coil current derivative

Horizontal axis: Time

Time scale: 5 milliseconds per centimeter

Current scale: 200 milliamperes per centimeter

Coil voltage: 28 volts dc

Coil current: 526 milliamperes

Test Circuit values: 0.5 ohm shunt
0.1 volt/cm sensitivity
0°F*

Differentiator constants: $Z_i = 1\mu f$, $Z_f = 0.1 \text{ meg ohm}$
1 volt/cm sensitivity

*Changed from previous figure

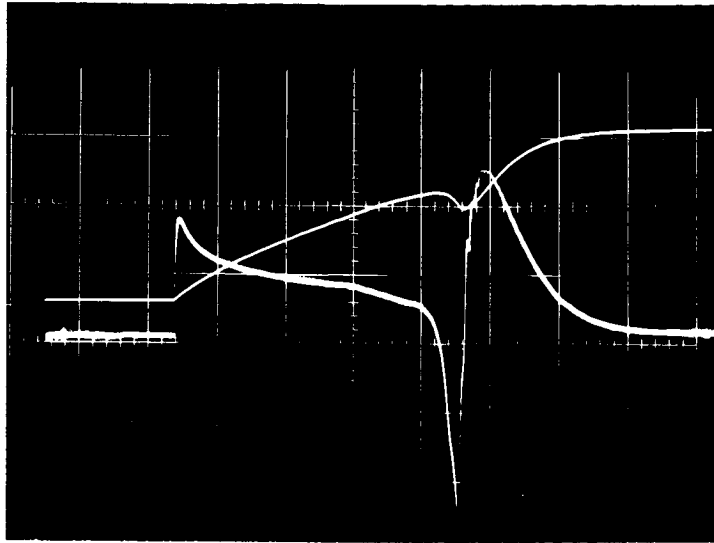


Figure 3

Vertical axis: Upper trace - coil current

Lower trace - coil current derivative

Horizontal axis: Time

Time scale: 5 milliseconds per centimeter

Current scale: 200 milliamperes per centimeter

Coil voltage: 28 volts dc

Coil current: 526 milliamperes

Test circuit values: 0.5 ohm shunt
0.1 volt/cm sensitivity
-60°F**

Differentiator constants: $Z_i = 4\mu f$, $Z_f = 0.1 \text{ meg ohm}$
1 volt/cm sensitivity

*Changed from previous figure

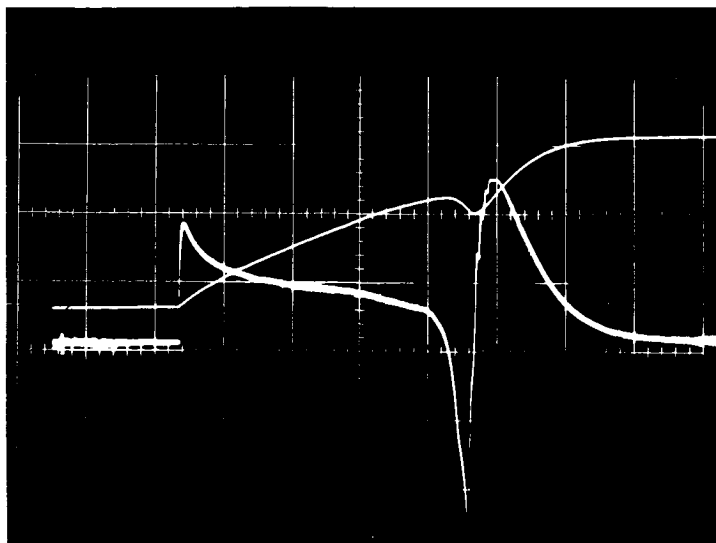


Figure 4

Vertical axis: Upper trace - coil current

Lower trace - coil current derivative

Horizontal axis: Time

Time scale: 5 milliseconds per centimeter

Current scale: 200 milliamperes per centimeter

Coil voltage: 28 volts dc

Coil current: 526 milliamperes

Test circuit values: 0.5 ohm shunt
0.1 volt/cm sensitivity
-100°F*

Differentiator constants: $Z_i = 1\mu f$, $Z_f = 0.1$ meg ohm
1 volt/cm sensitivity

*Changed from previous figure

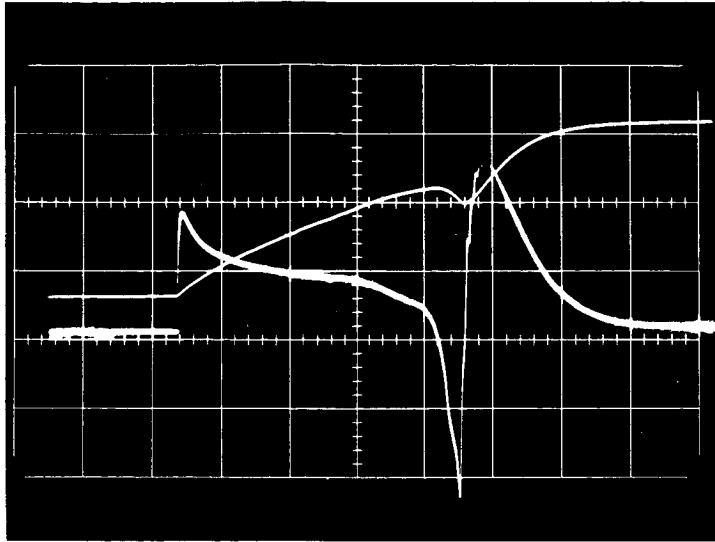


Figure 5

Vertical axis: Upper trace - coil current

Lower trace - coil current derivative

Horizontal axis: Time

Time scale: 5 milliseconds per centimeter

Current scale: 200 milliamperes per centimeter

Coil voltage: 23 volts dc

Coil current: 526 milliamperes

Test circuit values: 0.5 ohm shunt
0.1 volt/cm sensitivity
-120°F*

Differentiator constants: $Z_i = 1\mu f$, $Z_f = 0.1 \text{ meg ohm}$
1 volt/cm sensitivity

*Changed from previous figure



Figure 6

Vertical axis: Upper trace* - contact voltage

Lower trace - coil current derivative

Horizontal axis: Time

*Time scale: 10 milliseconds per centimeter

*Voltage scale: 5 volts per centimeter

*Coil voltage: 13.5 volts dc

*Coil current: 245 milliamperes

*Test circuit values: -80°F

Differentiator constants: $Z_1 = 1\mu\text{f}$, $Z_f = 0.1 \text{ meg ohm}$
1 volt/cm sensitivity

*Changed from previous figure

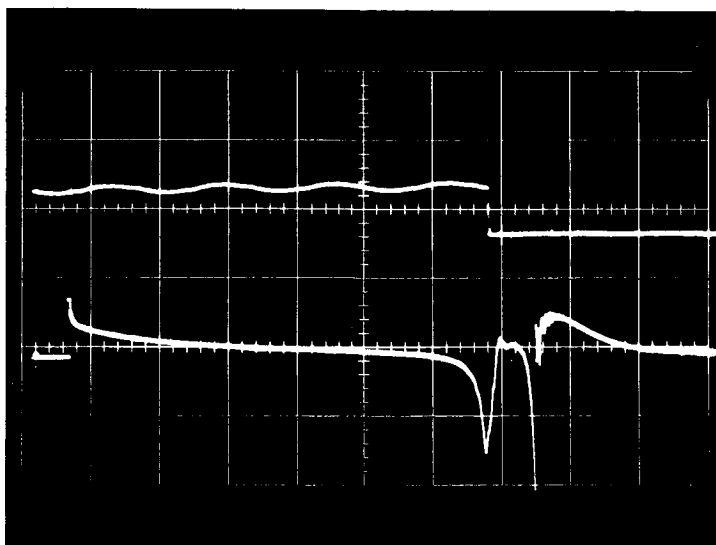


Figure 7

Vertical axis: Upper trace - contact voltage

Lower trace - coil current derivative

Horizontal axis: Time

Time scale: 10 milliseconds per centimeter

Voltage scale: 5 volts per centimeter

Coil voltage: 13.5 volts dc

Coil current: 245 milliamperes

*Test circuit values: 73°F

Differentiator constants: $Z_1 = 1\mu\text{f}$, $Z_f = 0.1 \text{ meg ohm}$
1 volt/cm sensitivity

*Changed from previous figure

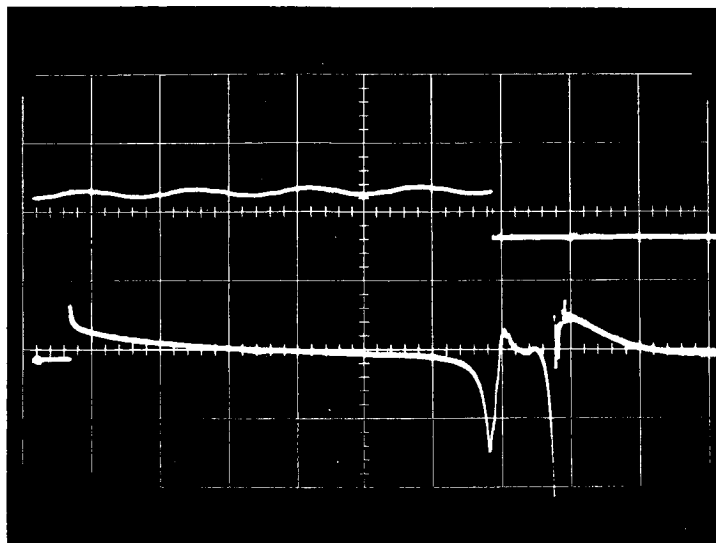


Figure 8

Vertical axis: Upper trace - contact voltage

Lower trace - coil current derivative

Horizontal axis: Time

Time scale: 10 milliseconds per centimeter

Voltage scale: 5 volts per centimeter

Coil voltage: 13.5 volts dc

Coil current: 245 milliamperes

*Test circuit values: 40°F

Differentiator constants: $Z_i = 1\mu f$, $Z_f = 0.1 \text{ meg ohm}$
1 volt/cm sensitivity

*Changed from previous figure

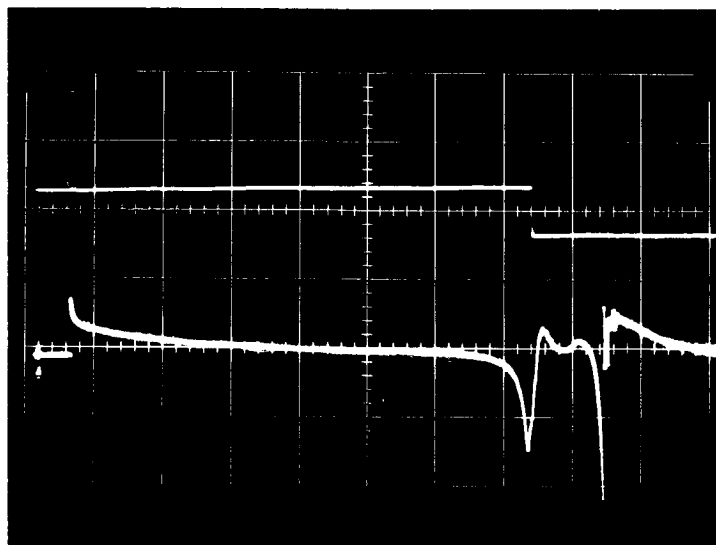


Figure 9

Vertical axis: Upper trace - contact voltage

Lower trace - coil current derivative

Horizontal axis: Time

Time scale: 10 milliseconds per centimeter

Voltage scale: 5 volts per centimeter

Coil voltage: 13.5 volts dc

Coil current: 245 milliamperes

*Test circuit values: 0°F

Differentiator constants: $Z_1 = 1\mu f$, $Z_f = 0.1$ meg ohm
1 volt/cm sensitivity

*Changed from previous figure

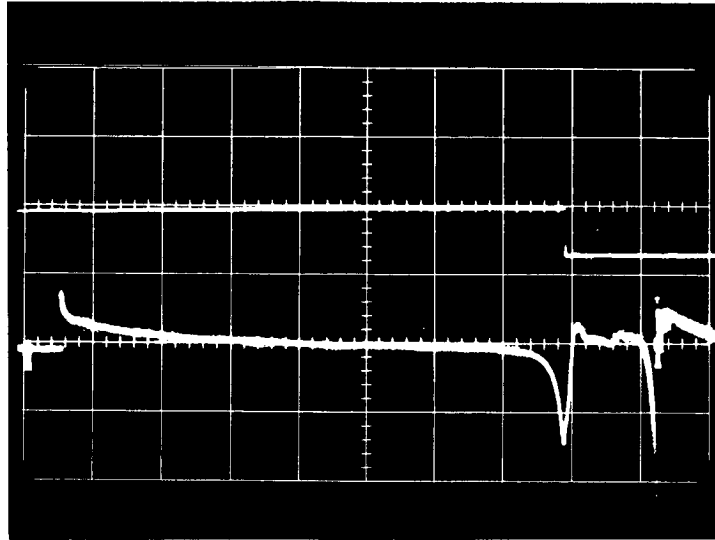


Figure 10

Vertical axis: Upper trace - contact voltage

Lower trace - coil current derivative

Horizontal axis: Time

Time scale: 10 milliseconds per centimeter

Voltage scale: 5 volts per centimeter

Coil voltage: 13.5 volts dc

Coil current: 245 milliamperes

*Test circuit values: -40°F

Differentiator constants: $Z_i = 1\mu\text{f}$, $Z_f = 0.1\text{ meg ohm}$
1 volt/cm sensitivity

*Changed from previous figure

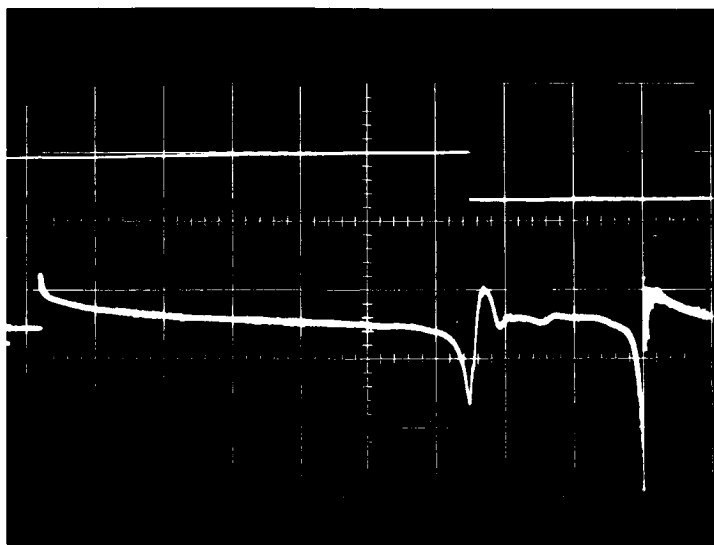


Figure 11

Vertical axis: Upper trace - contact voltage

Lower trace - coil current derivative

Horizontal axis: Time

Time scale: 10 milliseconds per centimeter

Voltage scale: 5 volts per centimeter

Coil voltage: 13.5 volts dc

Coil current: 245 milliamperes

*Test circuit values: -60°F

Differentiator constants: $Z_i = 1\mu f$, $Z_f = 0.1$ meg ohm

1 volt/cm sensitivity

*Changed from previous figure

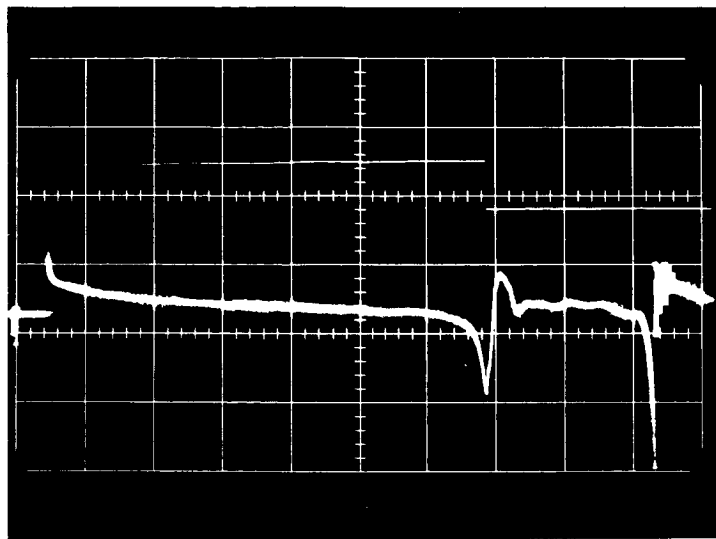


Figure 12

Vertical axis: Upper trace - contact voltage

Lower trace - coil current derivative

Horizontal axis: Time

Time scale: 10 milliseconds per centimeter

Voltage scale: 5 volts per centimeter

Coil voltage: 13.5 volts dc

Coil current: 245 milliamperes

*Test circuit values: -80°F

Differentiator constants: $Z_i = 1\mu\text{f}$, $Z_f = 0.1 \text{ meg ohm}$

1 volt/cm sensitivity

*Changed from previous figure

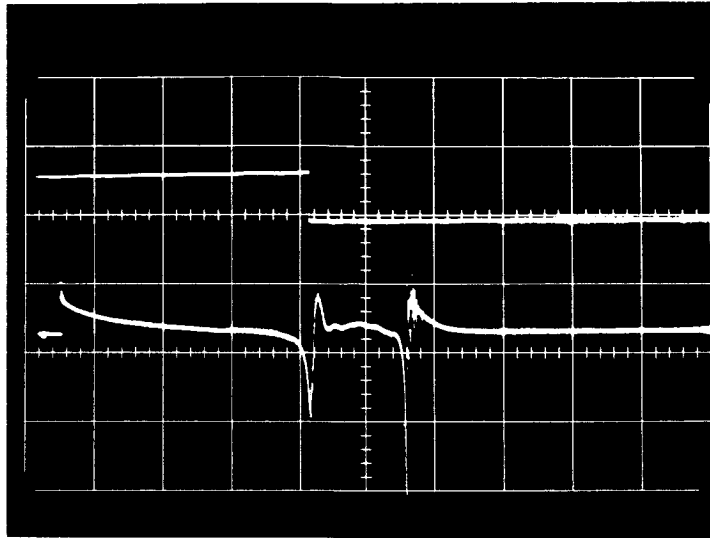


Figure 13

Vertical axis: Upper trace - contact voltage
Lower trace - coil current derivative

Horizontal axis: Time

*Time scale: 20 milliseconds per centimeter

Voltage scale: 5 volts per centimeter

Coil voltage: 13.5 volts dc

Coil current: 245 milliamperes

Test circuit values: -80°F

Differentiator constants: $Z_1 = 1\mu f$, $Z_f = 0.1 \text{ meg ohm}$

1 volt/cm sensitivity

*Changed from previous figure

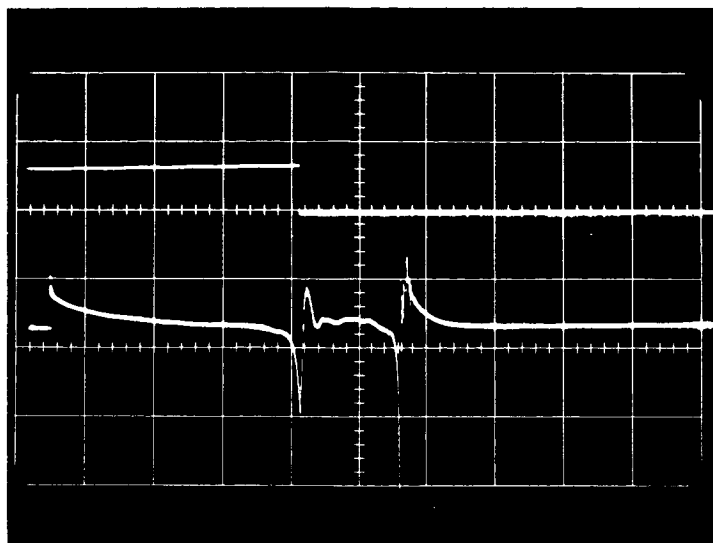


Figure 14

Vertical axis: Upper trace - contact voltage

Lower trace - coil current derivative

Horizontal axis: Time

Time scale: 20 milliseconds per centimeter

Voltage scale: 5 volts per centimeter

Coil voltage: 13.5 volts dc

Coil current: 245 milliamperes

*Test circuit values: -100°F

Differentiator constants: $Z_i = 1\text{ }\mu\text{f}$, $Z_f = 0.1\text{ meg ohm}$

1 volt/cm sensitivity

*Changed from previous figure

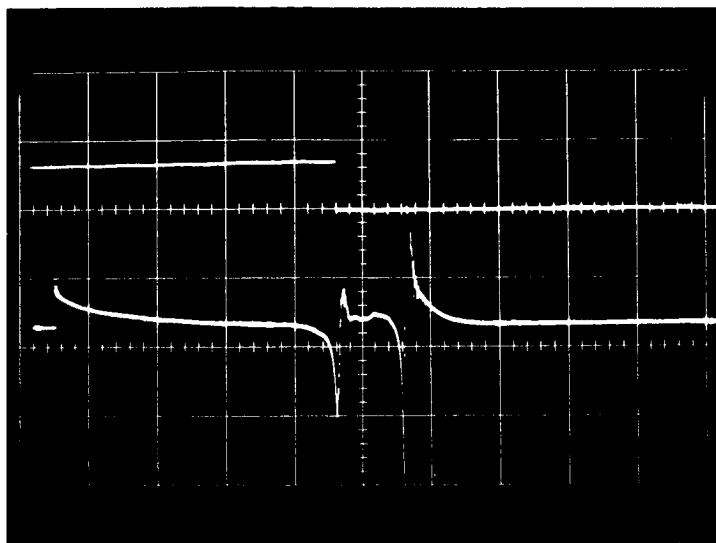


Figure 15

Vertical axis: Upper trace - contact voltage

Lower trace - coil current derivative

Horizontal axis: Time

Time scale: 20 milliseconds per centimeter

Voltage scale: 5 volts per centimeter

Coil voltage: 13.5 volts dc

Coil current: 245 milliamperes

*Test circuit values: -120°F

Differentiator constants: $Z_i = 1\mu\text{f}$, $Z_f = 0.1\text{ meg ohm}$
1 volt/cm sensitivity

*Changed from previous figure

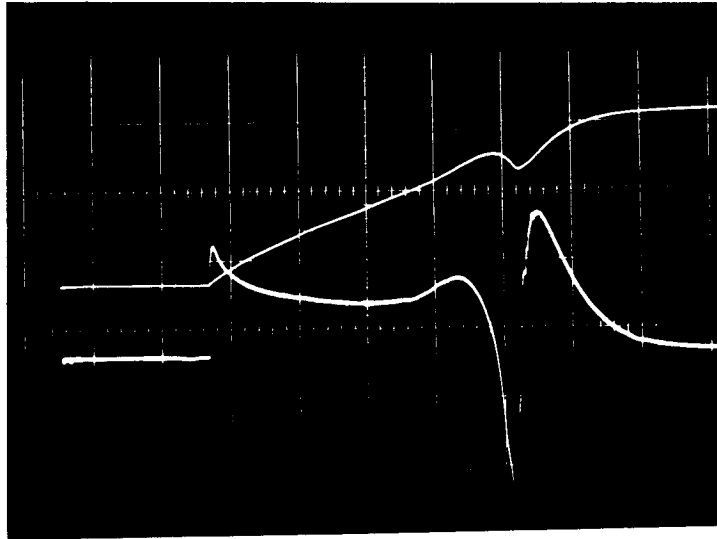


Figure 16

*Vertical axis: Upper trace - coil current
Lower trace - coil current derivative

Horizontal axis: Time

*Time scale: 5 milliseconds per centimeter

*Current scale: 200 milliamperes per centimeter

*Coil voltage: 28 volts dc

*Coil current: 526 milliamperes

*Test circuit values: 0.5 ohm shunt
0.1 volt/cm sensitivity
40°F
Metal structure

Differentiator constants: $Z_1 = 1\mu\text{f}$, $Z_f = 0.1 \text{ meg ohm}$
1 volt/cm sensitivity

*Changed from previous figure

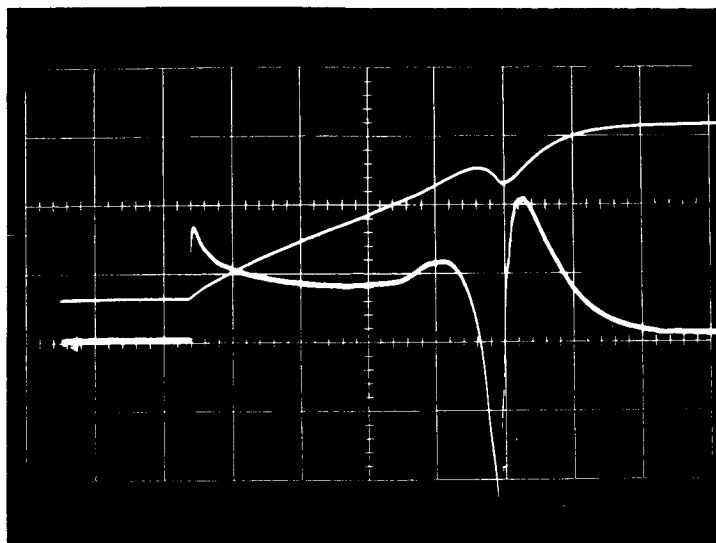


Figure 17

Vertical axis: Upper trace - coil current

Lower trace - coil current derivative

Horizontal axis: Time

Time scale: 5 milliseconds per centimeter

Current scale: 200 milliamperes per centimeter

Coil voltage: 28 volts dc

Coil current: 526 milliamperes

Test circuit values: 0.5 ohm shunt
0.1 volt/cm sensitivity
20°F*
Metal structure

Differentiator constants: $Z_1 = 1\mu f$, $Z_f = 0.1$ meg ohm
1 volt/cm sensitivity

*Changed from previous figure

SECTION IV
TRANSIENT ANALYSIS OF THE ECONOMIZED
PARALLEL COIL CONTACTOR

The "economized" coil arrangement is one attempt to approach a low holding power contactor with a "minimum" volume. The economized coil arrangement consists of two coils connected in such a way that one coil connection is used for the operate cycle and another coil connection is used for the hold cycle. The switching of the coil connection is accomplished internally by the use of an auxiliary switch actuated by the plunger in the contactor.

The first economized coil contactor analyzed and reported in the section A-b and A-c of the Summary Report of 1 July, 1962 to 30 June, 1963 was a series arrangement where one coil was used to operate and both coils used to hold. This particular connection required that one coil be short circuited during the operate cycle. Since the two coils were magnetically coupled together the transient current supplied by the source was greater during most of the operate cycle than it would have been with only one operate coil on the core. To reduce the transient coil current for the series arrangement would require a make before break contact arrangement. The coil current is then reduced by keeping the second coil open circuited during the operate part of the cycle. A disadvantage of series coil arrangement is that only part of available coil volume is being used for the operate part of the cycle while all of the coil is used for the hold cycle. It would be desirable to interchange this arrangement because of the inverse relationship between coil power and coil volume. The parallel coil arrangement utilizes all the available

coil volume during the operate part of the cycle and only part of the coil volume for the hold condition. This is a better arrangement because the magnetic pull for a given power is greater in the closed plunger position than it is in the open position.

The one possible disadvantage of the economized coil arrangement is the necessity of the auxiliary control switch and its possible failure to function properly. The reason for this point is given by some of the data presented by the oscillograms in the Figures 1 through 5.

Figures 1, 2 and 3 presents data which demonstrates the malfunctioning of the control switch used to switch from the operate to hold coil connection. The tests were performed at room temperature on a hermetically sealed model of the contactor. The tests had to be made at reduced coil voltage to show this malfunctioning. Figure 1 shows that the switch eventually functioned but was late in its operation. The operating point of the switch is indicated by the pulse on the trace occurring about 20 ms after the plunger seated. The coil current after the switching operation is continually decreasing.

Figure 2 shows essentially the same malfunctioning of the control switch but with a different horizontal scale. For Figure 2 the time scale is 10 milliseconds per centimeter while for Figure 1 it is 20 milliseconds per centimeter. The transient coil current, after the switching operation rises initially and then decreases indicating a different switching operation than that shown in Figure 1.

Figure 3 shows the condition where the control switch never functioned. Two operations are shown which indicates that this malfunctioning was not a one time occurrence.

It was not possible to get the contactor to malfunction at rated voltage during the time these data were being recorded. The operation at rated voltage is shown in Figure 4 which shows both operate and release.

Figure 5 shows three consecutive operations of the contactor at rated voltage. Some differences are noticeable in the control switch operation but comparison with Figure 4 is necessary to show the kind of variation that can exist between operations.

A temperature run was made on the contactor to determine if the malfunctioning of the control switch was a function of the temperature. In order to study only the mechanical changes in the performance at various temperatures the coil circuit resistance was held constant at its value at the highest temperature by inserting the suitable series resistance values. Data were recorded for two values of coil voltage. One was rated voltage and the other was as near the must operate value as possible. The results of the influence of high temperature on the transient performance of the contactor are presented in Figures 6 through 11. The control switch functioned throughout the temperature run and no trends as a function of temperature were noted in the functioning of the contactor. It appears that the malfunctioning of the control switch had corrected itself and was not aggravated by the heat run.

A cold run was made down to -120°F to determine if the low temperatures had any influence on the malfunctioning of the control switch. The results are presented in Figures 12 through 17. As in the heat run the coil circuit resistance was kept constant at its highest temperature value by inserting suitable resistance values in the coil

circuit. Inspection of the traces shows no malfunctioning and no trends as a function of temperature as the temperature was decreased.

As the test data were being recorded it became evident that the malfunctioning of the control switch was decreasing with the number of operations. Since this is a hermetically sealed unit it was not possible to examine the control for possible causes of malfunctioning. The test data presented in the first five figures indicates that possible malfunctioning of the control switch might be a problem.

It is planned to make calculations to determine if it is possible by optimizing the pull per watt to eliminate the control switch but still not change the coil volume or holding coil power. This will be reported in the next interim report.

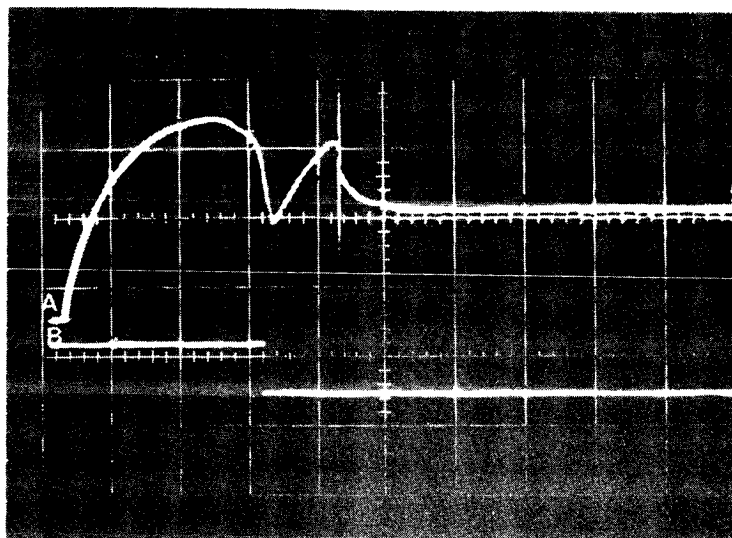


Figure 1

Trace: a - Coil current build-up

b - Contact voltage, operate

Time scale: 20 ms/cm

Current scale: 200 ma/cm

Coil voltage: 16v dc

Temperature: 70°F

Discharge resistance: Not measured

Coil circuit resistance: Not measured

Steady state coil current: 328 ma

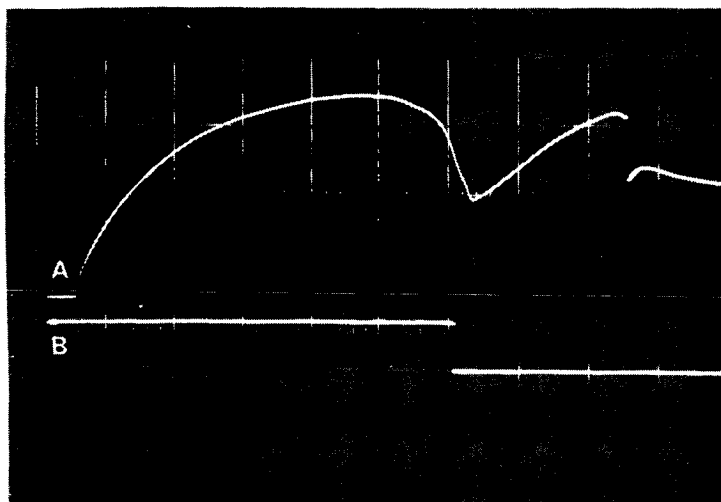


Figure 2

Trace: a - Coil current build-up

b - Contact voltage, operate

Time scale: 10 ms/cm*

Current scale: 200 ma/cm

Coil voltage: 16v dc

Temperature: 70°F

Discharge resistance: Not measured

Coil circuit resistance: Not measured

Steady state coil current: 328 ma

*Changed from previous figure

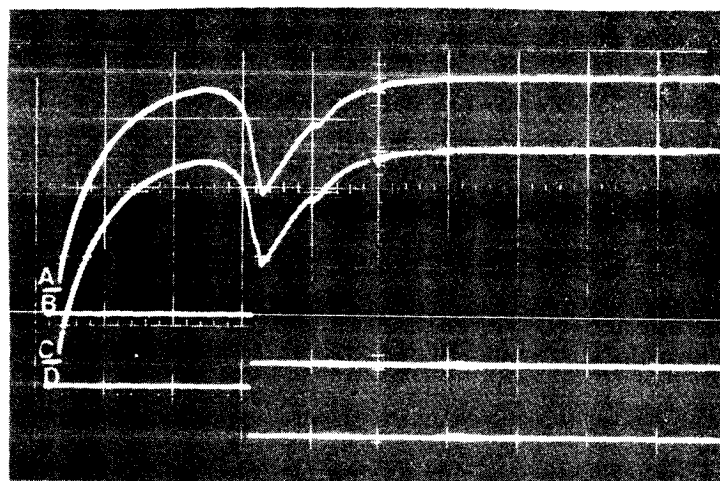


Figure 3

Trace: a - Coil current build-up
 b - Contact voltage, operate
 c - Coil current build-up
 d - Contact voltage, operate

Time scale: 20 μ s/cm*

Current scale: 200 μ A/cm

Coil voltage: 16v dc

Temperature: 70°F

Discharge resistance: Not measured

Coil circuit resistance: Not measured

Steady state coil current: Not measured

*Changed from previous figure

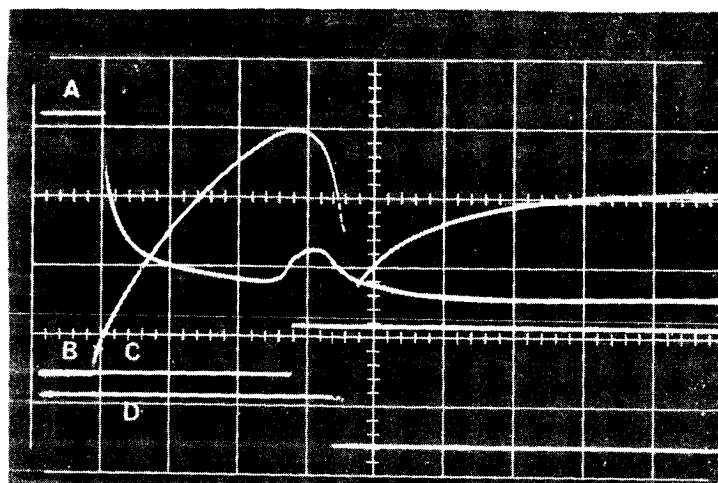


Figure 4

Trace: a - Coil current decay
 b - Coil current build-up
 c - Coil voltage, release
 d - Coil voltage, operate

Time scale: 5 ms/cm*

Current scale: 200 ma/cm

Coil voltage: 28v dc*

Temperature: 70°F

Discharge resistance: diode

Coil circuit resistance: Not measured

Steady state coil circuit: Not measured

*Changed from previous figure

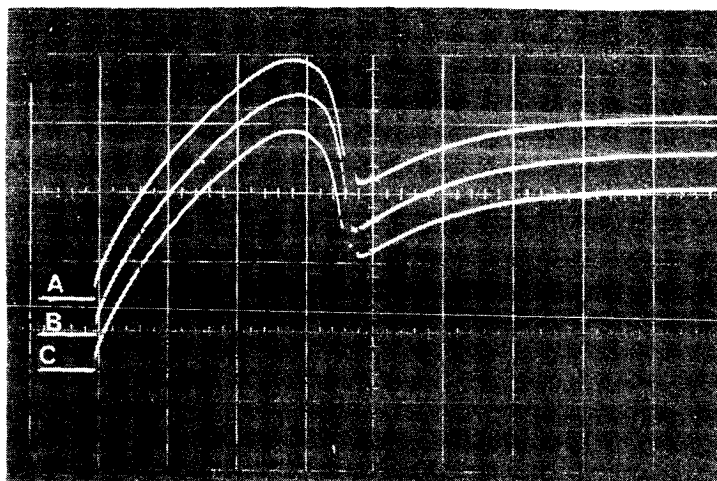


Figure 5

Trace: a - Coil current build-up
b - Coil current build-up
c - Coil current build-up

Time scale: 5 ms/cm

Current scale: 200 ma/cm

Coil voltage: 28v dc

Temperature: 70°F

Discharge resistance: Not measured*

Coil circuit resistance: Not measured

Steady state coil current: Not measured

*Changed from previous figure

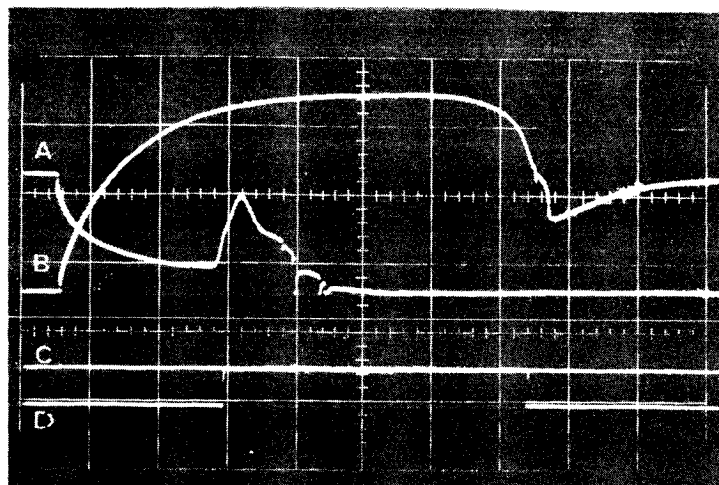


Figure 6

Trace: a - Coil current decay
 b - Coil current build-up
 c - Coil voltage, operate
 d - Coil voltage, release

Time scale: 10 ms/cm*

Current scale: 200 ma/cm

Coil voltage: 21.25v dc*

Temperature: 90°F*

Discharge resistance: diode*

Coil circuit resistance: 34Ω*

Steady state coil current: 354 ma*

*Changed from previous figure

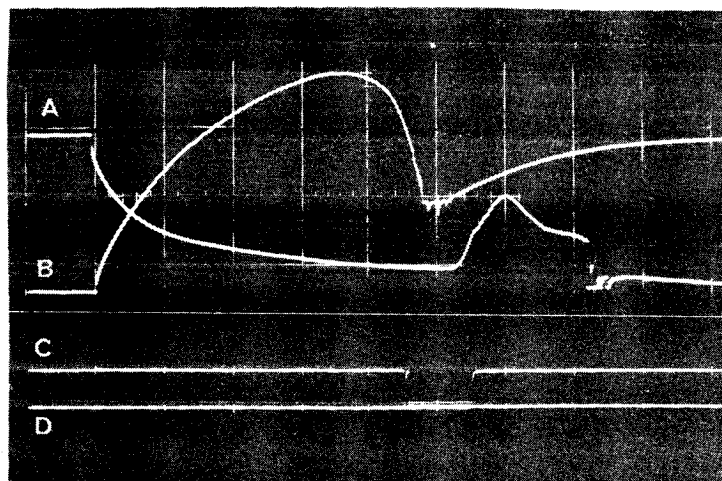


Figure 7

Trace: a - Coil current decay
 b - Coil current build-up
 c - Coil voltage, operate
 d - Coil voltage, release

Time scale: 5 ms/cm*

Current scale: 200 ma/cm

Coil voltage: 28v dc*

Temperature: 90°F

Discharge resistance: diode

Coil circuit resistance: 34Ω

Steady state coil current: 480 ma*

*Changed from previous figure

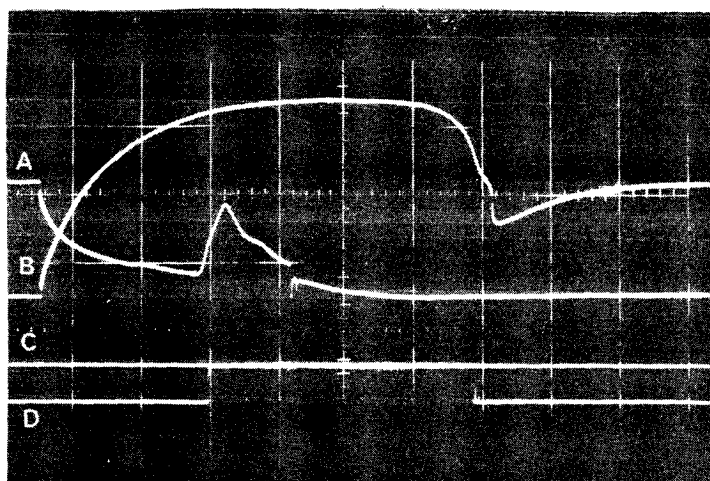


Figure 8

Trace: a - Coil current decay
 b - Coil current build-up
 c - Coil voltage, operate
 d - Coil voltage, release

Time scale: 10 ms/cm*

Current scale: 200 ma/cm

Coil voltage: 21.25v dc*

Temperature: 130°F*

Discharge resistance: diode

Coil circuit resistance: 34Ω

Steady state coil current: 342 ma*

*Changed from previous figure

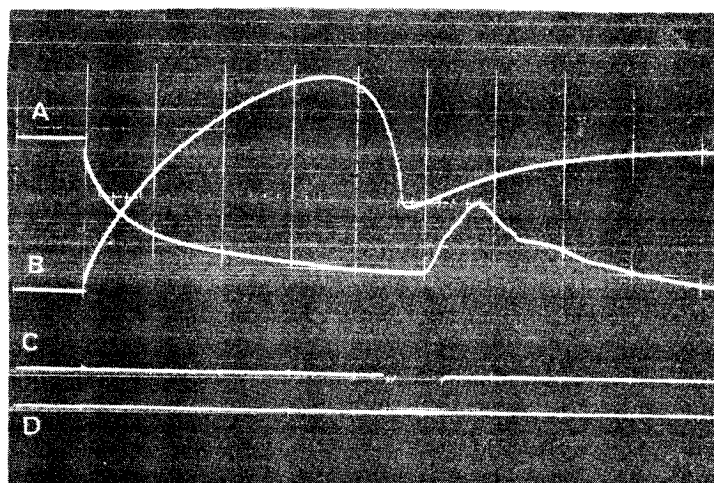


Figure 9

Trace: a - Coil current decay
 b - Coil current build-up
 c - Coil voltage, operate
 d - Coil voltage, release

Time scale: 5 ms/cm*

Current scale: 200 ma/cm

Coil voltage: 28v dc*

Temperature: 130°F

Discharge resistance: diode

Coil circuit resistance: 34Ω

Steady state coil current: 450 ma*

*Changed from previous figure

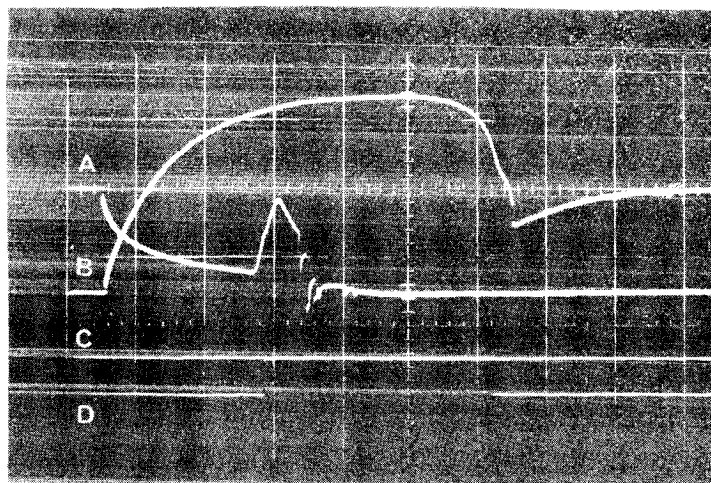


Figure 10

Trace: a - Coil current decay

b - Coil current build-up

c - Coil voltage, operate

d - Coil voltage, release

Time scale: 10 ms/cm*

Current scale: 200 ma/cm

Coil voltage: 21.25v. dc*

Temperature: 248°F*

Discharge resistance: diode

Coil circuit resistance: 34Ω

Steady state coil current: 310 ma*

*Changed from previous figure

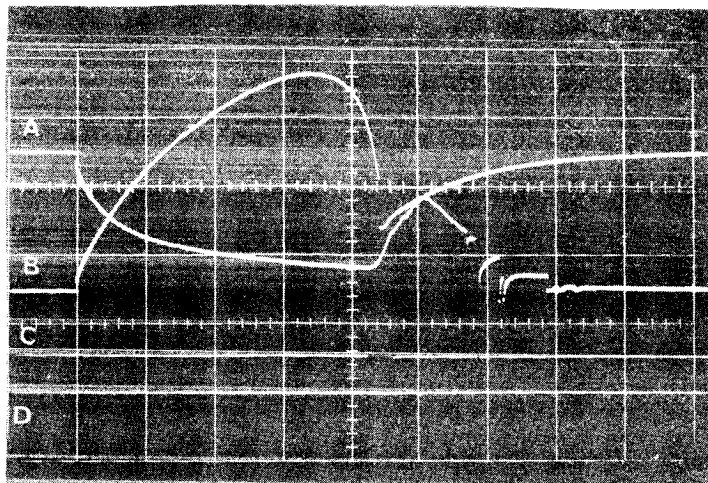


Figure 11

Trace: a - Coil current decay

b - Coil current build-up

c - Coil voltage, operate

d - Coil voltage, release

Time scale: 5 ms/cm*

Current scale: 200 ma/cm

Coil voltage: 28v dc*

Temperature: 248°F

Discharge resistance: diode

Coil circuit resistance: 34Ω

Steady state coil current: 415 ma*

*Changed from previous figure

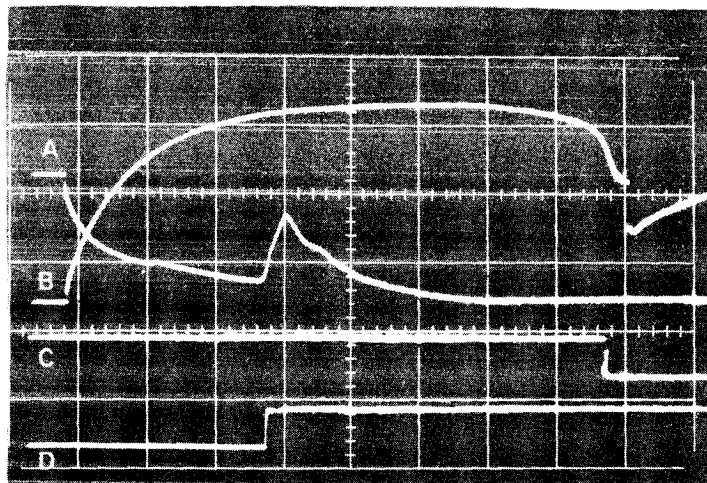


Figure 12

Trace: a - Coil current decay
 b - Coil current build-up
 c - Coil voltage, operate
 d - Coil voltage, release

Time scale: 10 ms/cm*

Current scale: 200 ma/cm

Coil voltage: 21.25v dc*

Temperature: 10°F*

Discharge resistance: diode

Coil circuit resistance: 34Ω

Steady state coil current: 380 ma*

*Changed from previous figure

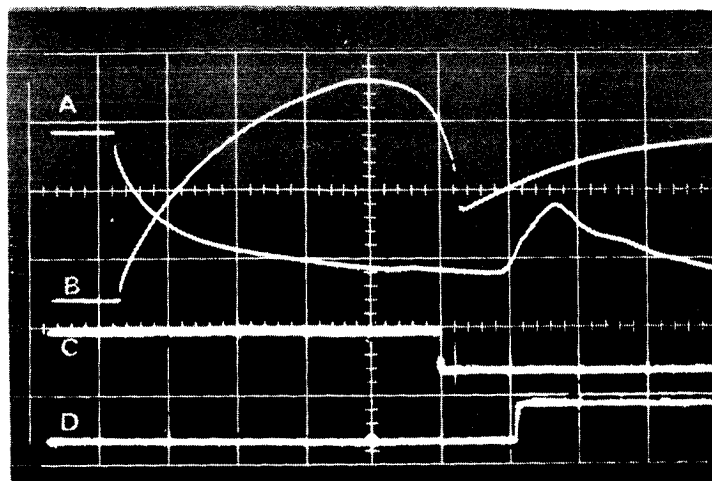


Figure 13

Trace: a - Coil current decay
 b - Coil current build-up
 c - Coil voltage, operate
 d - Coil voltage, release

Time scale: 5 ms/cm*

Current scale: 200 ma/cm

Coil voltage: 28v dc*

Temperature: 10°F

Discharge resistance: diode

Coil circuit resistance: 34Ω

Steady state coil current: 490 ma*

*Changed from previous figure

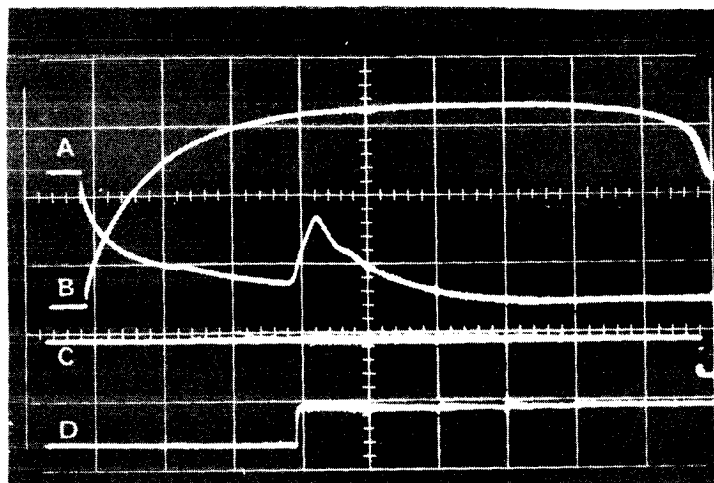


Figure 14

Trace: a - Coil current decay
 b - Coil current build-up
 c - Coil voltage, operate
 d - Coil voltage, release

Time scale: 10 ms/cm*

Current scale: 200 ma/cm

Coil voltage: 21.25v dc*

Temperature: -50°F*

Discharge resistance: diode

Coil circuit resistance: 34Ω

Steady state coil current: 400 ma*

*Changed from previous figure

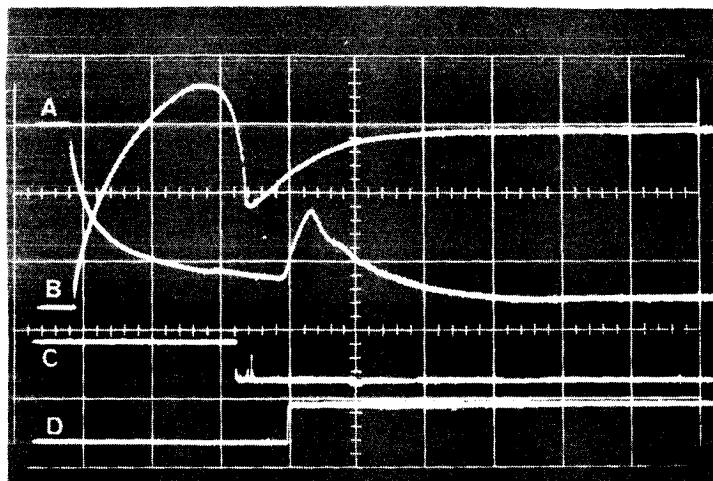


Figure 15

Trace: a - Coil current decay
 b - Coil current build-up
 c - Coil voltage, operate
 d - Coil voltage, release

Time scale: 5 ms/cm*

Current scale: 200 ma/cm

Coil voltage: 28v dc*

Temperature: -50°F

Discharge resistance: diode

Coil circuit resistance: 34Ω

Steady state coil current: 540 ma*

*Changed from previous figure

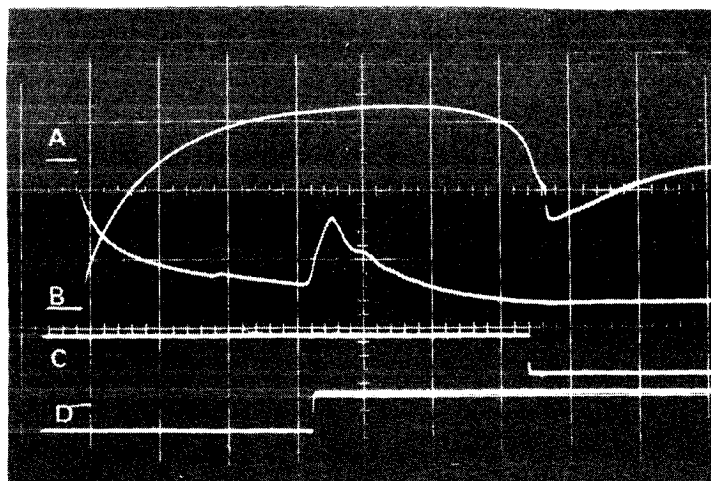


Figure 16

Trace: a - Coil current decay
 b - Coil current build-up
 c - Coil voltage, operate
 d - Coil voltage, release

Time scale: 10 ms/cm*

Current scale: 200 ma/cm

Coil voltage: 21.25v dc*

Temperature: -120°F*

Discharge resistance: diode

Coil circuit resistance: 34Ω

Steady state coil current: 440 ma*

*Changed from previous figure

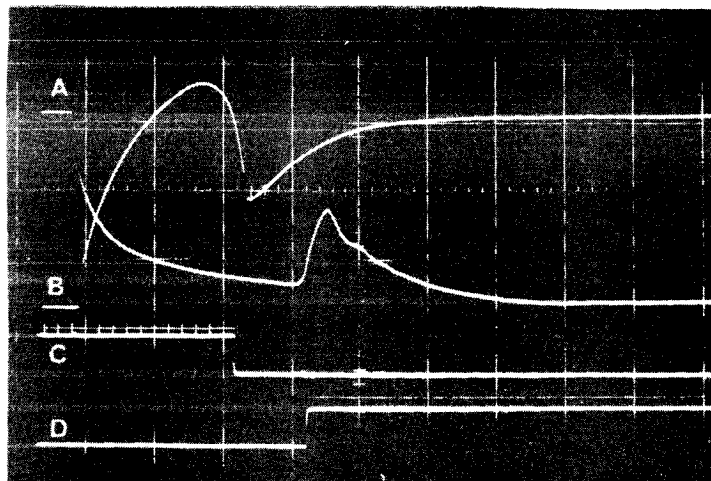


Figure 17

Trace: a - Coil current decay

b - Coil current build-up

c - Coil voltage, operate

d - Coil voltage, release

Time scale: 5 ms/cm*

Current scale: 200 ma/cm

Coil voltage: 28v dc*

Temperature: -120°F

Discharge resistance: diode

Coil circuit resistance: 34Ω

Steady state coil current: 580 ma*

*Changed from previous figure

SECTION V

THE ENERGY CYCLE CURVE

This investigation was started to determine a method of describing and predicting the operation of relays. The required testing of a sealed relay in various environments requires a method of remote evaluation. It is hoped that a definite division of operations states can be made on the energy cycle curve which will identify the energy transformed into the field before operation, the energy transformed into mechanical friction and acceleration, and the energy transformed into the fields after the operation.

This report will describe the method of obtaining the energy cycle curve.

The basic energy balance can be written as follows.

Energy input from electrical source minus resistances losses	=	Increase in energy stored in coupling field plus associated losses	+	Mechanical energy output plus friction and associated losses
---	---	---	---	--

$$dW_{\text{elect}} = (v_t - i_r) i dt = e i dt = dW_{\text{fields}} + dW_{\text{mechanical}}$$

A block diagram illustrates the system in Figure 1.

The electrical energy input is equal to: $dW_{\text{elect}} = e i dt$. Where the back emf e is equal to the change in flux linkage with respects to the change in time.

$$e = \frac{d\lambda}{dt} \quad \text{or} \quad e dt = d\lambda. \quad \text{Substituting this in equation (1) gives:}$$

$$dW_{\text{elect}} = i d\lambda = Ni d\phi = Fd\phi, \text{ or}$$

$$W_{\text{elect}} = \int_{\lambda_0}^{\lambda_1} i d\lambda. \quad (\lambda \text{ is flux linkages})$$

Therefore, a change of electrical energy in the system is proportional to a change of flux linkage, and the flux linkage is equal to the integral of the back emf with respect to time.

The back emf e was obtained electrically from the bridge circuit illustrated in Figure 2. With the switch (S_1) closed, the bridge was balanced to zero voltage at points "a" and "b". Thus, any sudden change of voltage would unbalance the bridge due to the inductance of the relay coil or back emf.

On one oscilloscope the integral of the voltage or flux linkage versus current was plotted. This plot represents the energy transformed in the relay. See Figure 7.

The back emf can be measured easily by the bridge method and is illustrated by the lower beam in Figure 3. The three traces are identified as, the armature blocked open, the armature free to operate and the armature blocked closed.

Figure 5 is "part I" of the integrator calibration. The back emf versus time was plotted on the scope for calibration purposes. The upper beam is the signal from a calibrating oscillator which was used to calibrate all amplifiers. The lower beam is a step voltage of two tenth volts (.2V) amplitude used to calibrate the integrator.

The integrator output is illustrated in Figure 6. Each centimeter of height on the curve is equal to the area under the curve "b", Figure 5, for the same time interval. By this method the integrator is calibrated directly in volt-seconds or weber-turns.

The source for the current display was obtained in the usual method by sensing the voltage across the shunt resistor, Figure 2. The three current traces for the test relay are illustrated in Figure 3, upper curve.

Figure 7 illustrates the first energy cycle curve for a relay with its armature free to operate. The area enclosed represents the energy transformed during one cycle of operation.

$$W_{\text{elect}} = \int_{\lambda_0}^{\lambda_1} i_a dt - \int_{\lambda_1}^{\lambda_0} i_b d\lambda$$

The operate and release portion of the curve is represented by the closed curve (0, a, b, c). Point "0" represents zero flux linkage and zero current. Point "a" corresponds to the stop of armature movement. Between points "a" and "1" additional energy storage occurs for the closed armature position. On the release cycle, the armature movement can be detected between points "c" and "0".

Figure 8 illustrates the energy cycle for the armature blocked open curves (a & b) and the armature blocked closed curves (c & d). It would be expected to have more field losses with armature operated due to the lowering of reluctance in the core.

Three energy cycle curves are superimposed in Figure 9. The influence of the mechanical motion of the armature can clearly be seen. The slope of the line (0, e) in the region of armature movement is equal to the change of flux-linkage with respect to the change of current. This relation provides an indication of the change in permeance during the armature travel time.

$$\text{Slope} = \frac{\lambda}{i}, \quad \lambda = N\Phi, \quad \Phi = \frac{\lambda}{N},$$

$$i = \frac{F}{N}, \quad F = Ni$$

$$\text{therefore } P \text{ (permeance)} = \frac{\Phi}{F} \approx \frac{\lambda}{i}$$

The self-inductance is defined as the flux-linkage in weber-turns per ampere.

$$L = \frac{\lambda}{i} = \text{Slope}$$

A family of Energy Cycle Curves has been plotted in Figure 10. This set of curves was obtained by varying the supply voltage in increments of one volts from one volt to ten volts.

The Energy Cycle Curve seems to express an over all evaluation of a relay. Investigation of the Energy Cycle Curve in relation to various specific properties will be the subject of the next report.

Block Diagram of Energy Distribution

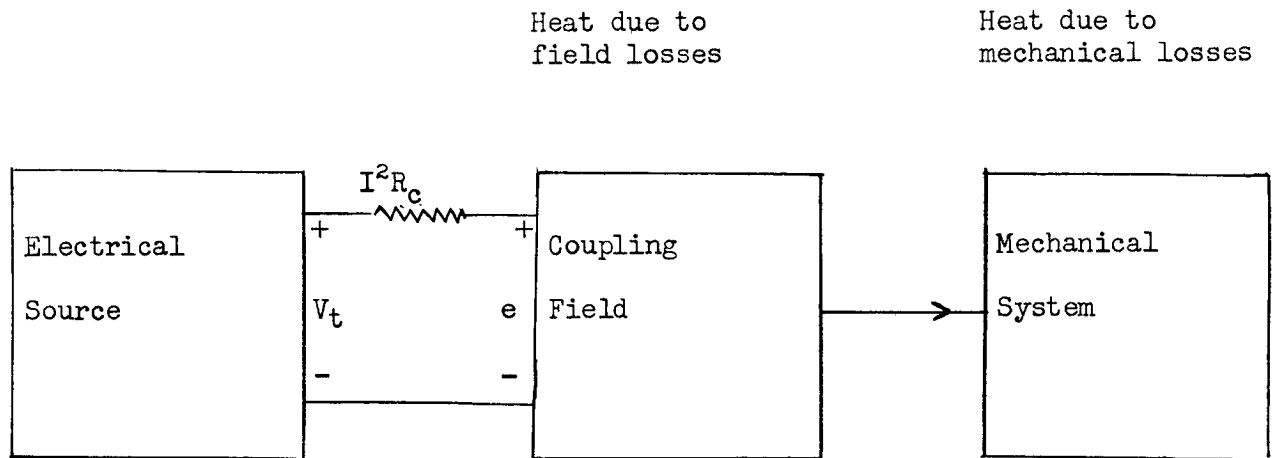


Figure 1

Energy input from
electrical source
minus resistances
losses

=

Increase in energy
stored in coupling
field plus associated
losses

+

Mechanical energy
output plus
friction and
associated losses

$$dW_{\text{elect}} = (v_t - i_r) i dt = e i dt = dW_{\text{field}} + dW_{\text{mechanical}}$$

Block Diagram of Laboratory Setup

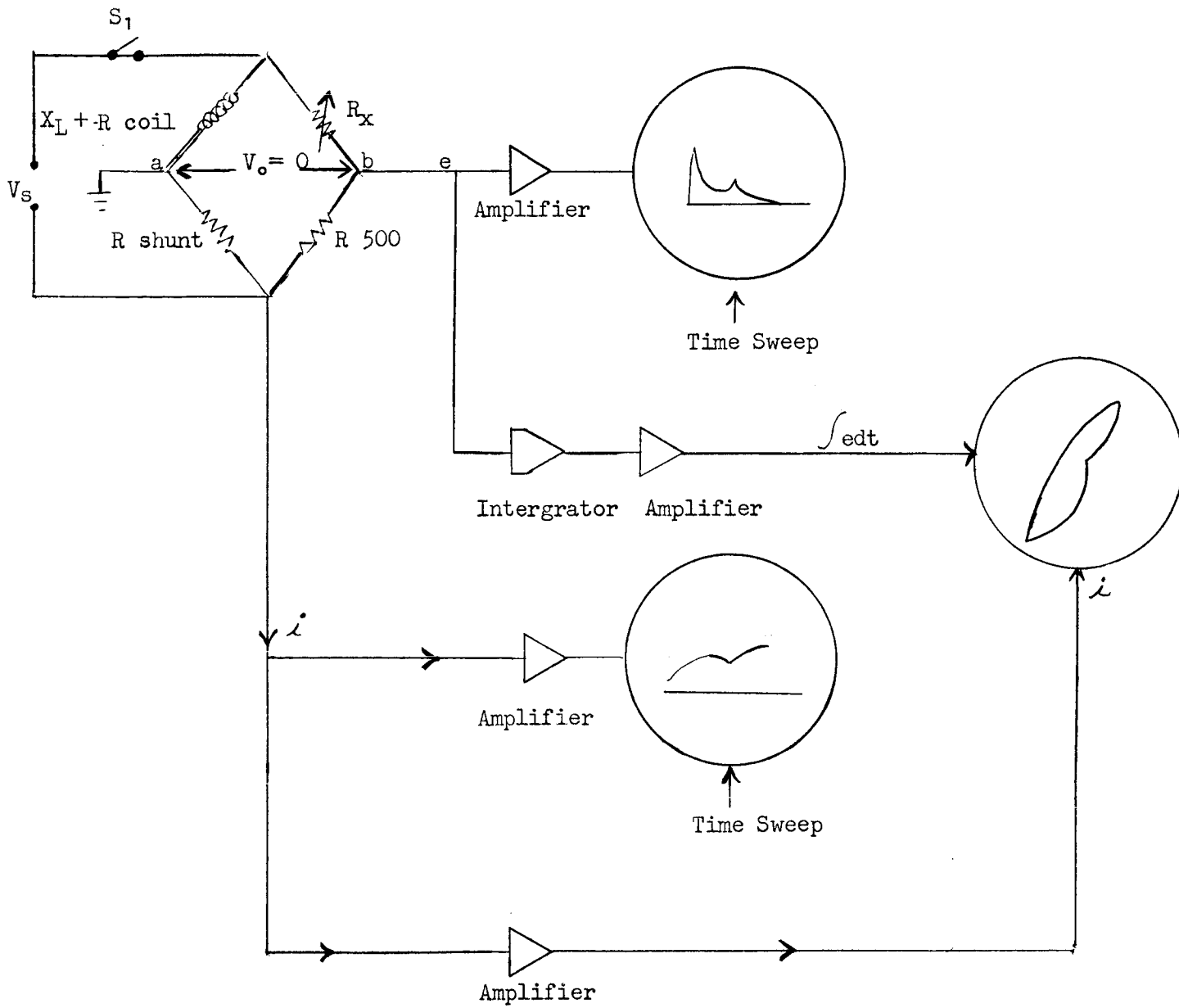


Figure 2

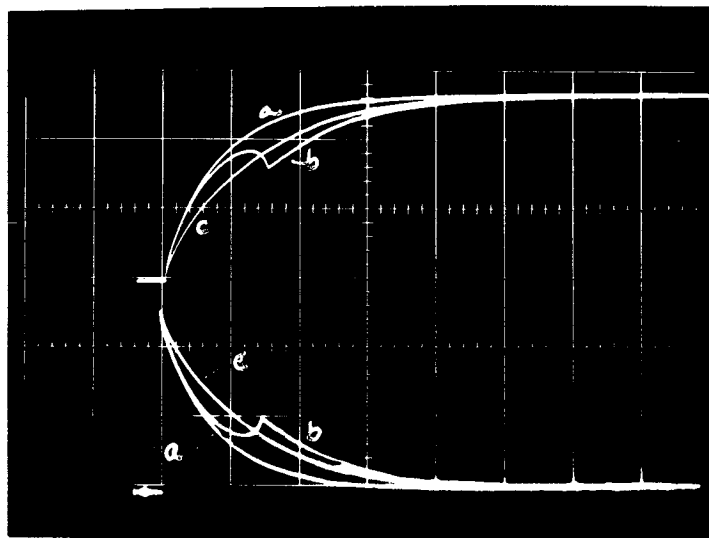


Figure 3

Transient Operate Current and Voltage Vs Time

Traces:

Upper - (a) current with relay blocked open

(b) current with relay free to operate

(c) current with relay blocked closed

Lower - (a) back generated voltage with relay blocked open

(b) " " " " " free to operate

(c) " " " " " blocked closed

Oscillogram:

Time scale = 10 milliseconds per centimeter

Current scale = .136 amperes per centimeter

Voltage scale = .1 volt per centimeter

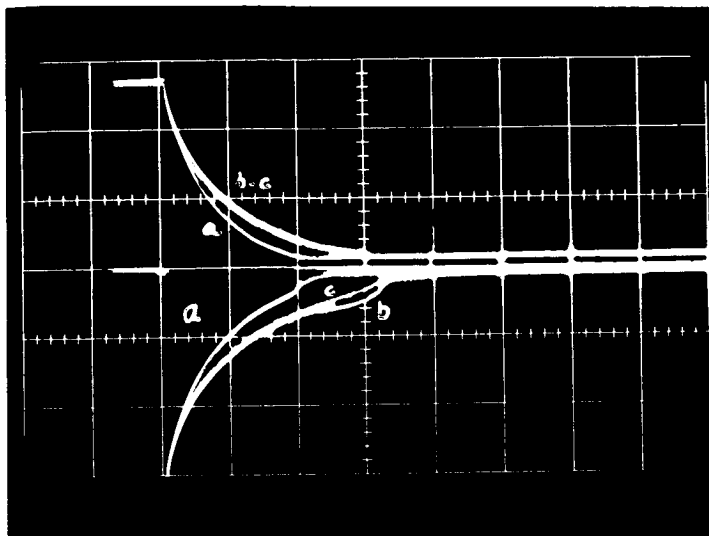


Figure 4

Transient Release Current and Voltage Vs Time

Traces:

Upper - (a) current with relay blocked open

(b) current with relay free to operate

(c) current with relay blocked closed

Lower - (a) back generated voltage with relay blocked open

(b) " " " " " free to operate

(c) " " " " " blocked closed

Oscillogram:

Time scale = 10 milliseconds per centimeter

Current scale = .136 amperes per centimeter

Voltage scale = .1 volt per centimeter

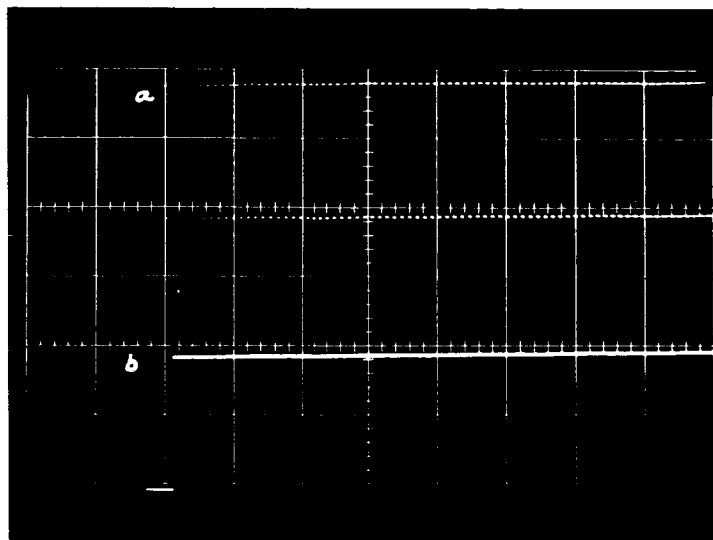


Figure 5

Calibration of Integrator, Part I

Traces:

- a. Internal square wave calibration signal from the oscilloscope (.2V amplitude)
- b. Step voltage input to calibrate integrator

Oscillogram Data:

Time scale: 10 milliseconds per centimeter

Voltage scale upper curve: .1 volt per centimeter

Voltage scale lower curve: .1 volt per centimeter

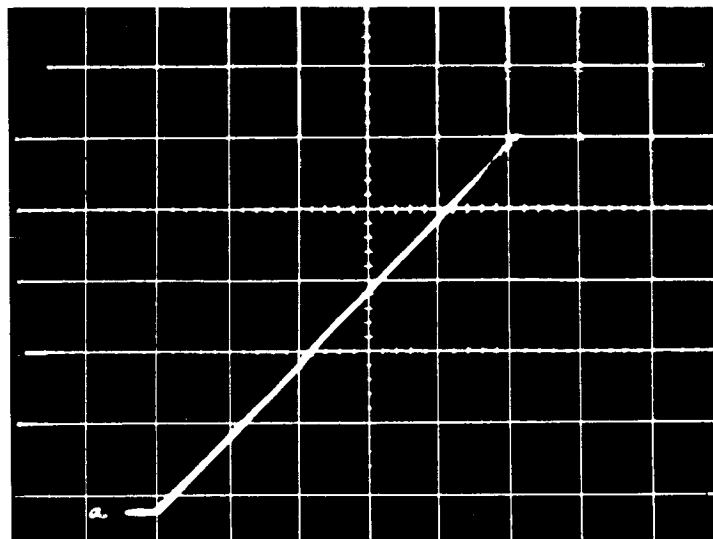


Figure 6

Calibration of Integrator, Part II

Trace:

(a) Integration of step function, Figure 5 b

Oscilloscope Data:

Time scale: 10 milliseconds per centimeter

Flux-Linkage scale: Volt-seconds or Weber-turns

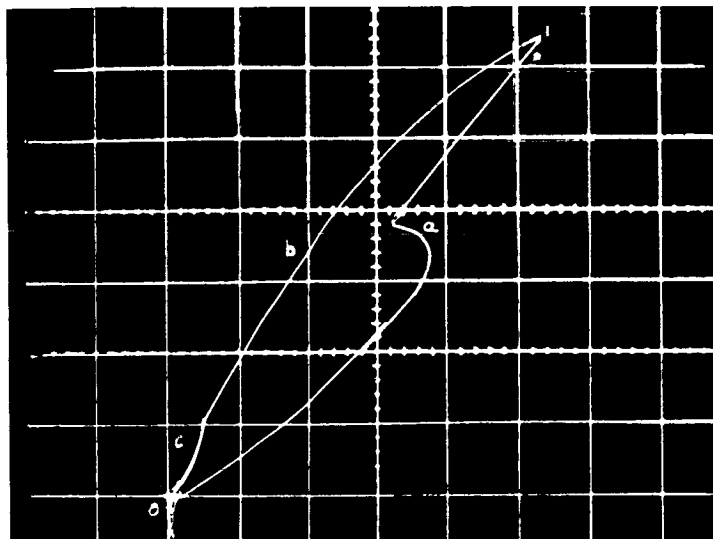


Figure 7

Energy Cycle Curve Relay Free To Operate

Traces:

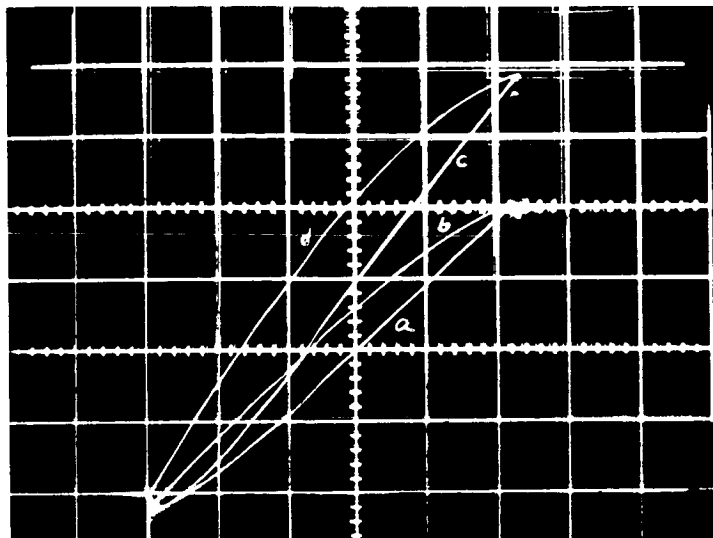
- (a) Flux-linkage vs current during the operate cycle.
- (b) Flux-linkage vs current during the release cycle

Oscillogram Data:

Current scale = .068 amperes per centimeter

Flux-linkage scale = 2 Weber-turns per centimeter

Flux-linkage



current amperes

Figure 8

Energy Cycle Curves

Relay Blocked Open & Relay Blocked Closed

Traces:

- a. Relay blocked open, coil energized
- b. Relay blocked open, coil deenergized
- c. Relay blocked closed, coil energized
- d. Relay blocked closed, coil deenergized

Oscillogram Data:

Flux-Linkage scale: 2 weber-turns/per centimeter

Current scale: .063 ampere per centimeter

Supply voltage: 6 volts d.c.

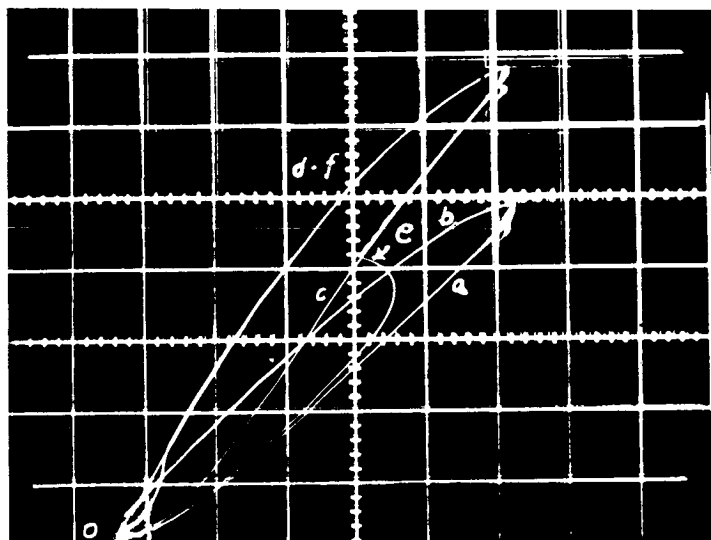


Figure 9

Energy Cycle Curve For Relay Free To Operate,
Relay Blocked Open & Relay Blocked Closed

Traces:

- a. Relay blocked open, coil energized
- b. Relay blocked open, coil deenergized
- c. Relay blocked closed, coil energized
- d. Relay blocked closed, coil deenergized
- e. Relay free to operate coil energized
- f. Relay free to operate coil deenergized

Oscillogram Data:

Flux-Linkage scale: 2 weber-turns/per centimeter

Current scale: .068 ampere per centimeter

Supply voltage: 6 Volts d.c.

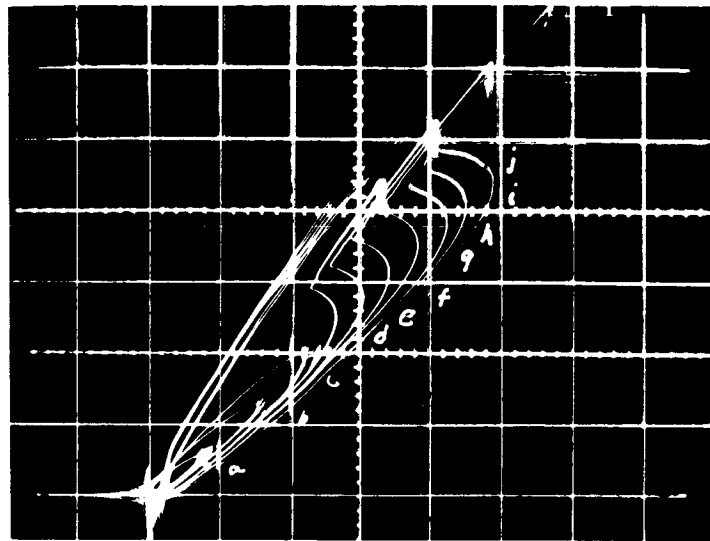


Figure 10

A Set of Energy Cycle Curves For A Relay

Traces:

- | | | |
|-----|---|------------------|
| (a) | Energy cycle with 1 volt supply voltage | |
| (b) | " " " 2 " " " | |
| (c) | " " " 3 " " " | |
| (d) | " " " 4 " " " | (Relay operated) |
| (e) | " " " 5 " " " | |
| (f) | " " " 6 " " " | |
| (g) | " " " 7 " " " | |
| (h) | " " " 8 " " " | |
| (i) | " " " 9 " " " | |
| (j) | " " " 10 " " " | |

Oscillogram Data:

Flux-Linkage: 2 weber-turns/per centimeter

Current scale: .068 amperes/per centimeter

SECTION I

LEAKAGE FLUX WITHIN A RELAY

An effort is being made to verify the energy curve as a method of analyzing various characteristics of relays from the terminals.

The bridge method of measuring the back electromotive force provides a means of determining the total flux linkage developed. The integral of back electromotive force is flux linkage. If the number of turns in the coil is known, then the total flux generated can be determined.

The mechanical operation of a relay effects only the flux across the air gap. In order to relate the mechanical characteristics of a relay in terms of flux changes, some methods must be obtained which will describe the flux across the air gap. Considering the flux leakage as the difference between the total flux produced and flux across the air gap, it is necessary to eliminate flux leakage components from the measured values.

$$\phi_{\text{leakage}} = \phi_{\text{total}} - \phi_{\text{air gap}} \quad (1)$$

The leakage flux should consist of two components.

(1) The partial flux leakage produced by the magnetic field within the winding space.

(2) The flux which is present in the coil core which does not appear across the air gap. The partial flux produced in the winding space should be small and would not appear in the core of the coil. The value should depend on coil configuration and be constant for any particular type of relay. An experiment was conducted to verify this reasoning.

The second component of the leakage flux presents a greater problem. This flux must leave the core at some point between the coil and the armature end of the core. The path must include a large air gap, many times longer than the armature air gap in conventional designs. The flux across an air gap is proportional to the magnetomotive force producing it. The reluctance of air is very much greater than the reluctance of iron. Hence, there will be much more magnetic energy present in passing the leakage flux across the linear air gap than in passing the leakage flux through the non linear core. Based on the above reasoning the leakage flux through the core component of flux leakage will be linear with respect to the magnetomotive force. The flux energy across the air gap equals the total flux energy minus the linear leakage flux energy. Therefore, the energy curve is a linear representation of the energy across the air gap. A second experiment was conducted to verify the above analogy.

EXPERIMENT I

This experiment was made to insure the value of back electromotive force across points (a) and (b) of the bridge was correct. Figure 1 was representative of the flux existing in the core.

The method of obtaining this information was by monitoring the flux actually developed in the core and comparing this value with the indicated flux by the bridge method. A special one layer monitor winding of 100 turns was placed next to the core of the relay. The monitor winding was connected directly to the input of a high impedance oscilloscope amplifier. A primary winding of 4800 turns was wound on top of the monitor winding. The primary winding was connected across the bridge as described in the interim report of October 1 to November 30, 1963, Section V. By evaluating the flux indicated in each winding, one can determine what portion of

the overall flux is produced in the core, as indicated by the bridge measurement.

In calculating the flux the following assumptions were made.

1. The core loss is negligibly small.
2. No current in the secondary.

Figure 1 illustrates the laboratory arrangement and Figure 3 illustrates the back electromotive force measured by the bridge, and the induced electromotive force measured by the special secondary coil. The upper trace represents the back electromotive force measured from the bridge. The lower trace was taken directly from the special secondary coil. Figure 3 also indicates that both voltage curves have the same wave forms. The relationship of the voltage to the flux is given by: $e = N d\phi/dt$. The actual back electromotive force of the primary coil may be calculated as follows:

$$\text{VOLTAGE}_{\text{primary}} = (\text{Centimeters indicated in Figure 2}) \times (\text{Ratio of resistance of bridge}) \times (\text{Gain of amplifier})$$

$$\text{Cm Figure 2} = 2.2$$

$$\text{Gain} = .05 \text{ Volts/Cm.}$$

$$\text{Resistance Ratio} = \frac{R_x}{R_{100}} = \frac{10000}{100} = 100$$

$$V_p = 2.2 \quad \times \quad .05 \quad \times \quad 100 \quad = \quad 11 \text{ Volts}$$

The voltage for the special secondary is:

$$\text{VOLTAGE}_{\text{secondary}} = (\text{Centimeter indicated in Figure 2}) \times (\text{Gain of amplifier})$$

$$V_s = \text{Cm. Figure 2} \times \text{Gain} = 2.2 (1) = .22 \text{ Volts}$$

The change of flux with respect to time is equal to the induced voltage divided by the number of turns of the winding.

$$\frac{d\phi_p}{dt} = \frac{E_p}{N_p} = \frac{11\text{Volts}}{4800\text{turns}} = .002292 \frac{\text{weber}}{\text{sec.}} = 229200 \frac{\text{Gilberts}}{\text{sec.}}$$

$$\frac{d\phi_s}{dt} = \frac{E_s}{N_s} = \frac{22\text{Volts}}{100\text{turns}} = .0022 \frac{\text{weber}}{\text{sec.}} = 220000 \frac{\text{Gilberts}}{\text{sec.}}$$

N_p = turns on primary winding = 4800

N_s = turns on secondary winding = 100

The bridge method is indicating approximately 4% higher flux change than exists in the core for the relay tested. This value would represent the maximum error which would exist. The error is due to the flux produced by the magnetic field component within the winding space and never reaches the core.

From the information given one can conclude that the back electromotive force, as indicated by the bridge method, will give a slightly higher value of flux than exists in the core due to the flux produced in the winding space. But the value indicated would not vary from any one type relay tested.

EXPERIMENT II

This experiment was conducted to verify the existence of a linear leakage flux component in conventionally designed relays. The results of this experiment was verified by direct measurement.

The relay used in this experiment is illustrated in Figure 2. A special winding was placed at the end of the core next to the armature. The winding of 48 turns was used to detect the flux in the armature air

gap. The primary winding of 4800 turns was connected to the bridge for the usual back electromotive force measurement.

From the voltage measurements of the two coils, the flux was calculated and plotted graphically. The value of air gap flux obtained by the special winding was checked by direct measurement with a gauss meter. The results checked very close.

Figures 4 and 5 are calibration diagrams made to set the scale of the integrator. This procedure is described in the Tenth Interim Report, Section V.

Figure 6 illustrates the voltages versus time for both windings on the relay.

The values measured by the bridge must be corrected for resistance ratios in the bridge. The integral of this voltage is flux linkage in volt-sec. or weber turns. Division of the flux linkage by the turns of a winding gives the flux passing through the winding. By this method, Figure 9 was plotted from Figure 8.

The following is a sample calculation of the information taken from Figures 6 and 8.

From Figure 6

Voltage primary = (Centimeters, Figure 6) x (Scale of amplifier) x
(Resistance ratio of bridge)

$$E_p = (.8) (.05) \frac{(10000)}{52} = 8 \text{ volts}$$

Voltage secondary = (Centimeters, Figure 6) x (Scale of amplifier)

$$E_s = (1.2) (.05) = .06 \text{ volts}$$

From Figure 8

$$e = N \frac{d\phi}{dt}$$

$$\phi = \frac{1}{N} \int_0^t e \, dt$$

Data for the sample calculations was taken from Figure 8 on the release cycle at a current of .042 amperes.

$$\begin{aligned} \lambda_{\text{primary coil}} &= \int_0^t e_p dt = (2.1 \text{ centimeters}) \times (.18 \text{ volt-second/cm}) \\ &= .378 \text{ volt-second.} \end{aligned}$$

$$\begin{aligned} \lambda_{\text{secondary coil}} &= \int_0^t e_s dt = (3.3 \text{ centimeters}) \times (.0009 \text{ volt-second/cm}) \\ &= .00297 \end{aligned}$$

$$\begin{aligned} \phi_{\text{primary}} &= \frac{1}{N_p} \int_0^t e_p dt = \frac{1}{4800} (.378) = .0000786 \text{ webers} \\ &= .0000786 \times 10^{-8} \text{ maxwells} \end{aligned}$$

$$\begin{aligned} \phi_{\text{secondary}} &= \frac{1}{N_s} \int_0^t e_s dt = \frac{1}{48} (.00297) = .000063 \text{ webers} \\ &= .00063 \times 10^{-8} \text{ maxwells} \end{aligned}$$

λ = flux linkage

ϕ = flux

The calculated flux of both windings was plotted against the mmf in the primary winding. Since no current was flowing the secondary winding, no energy was dissipated. The magnetic energy in the air gap would be represented by the flux existing across the gap times the mmf in the winding producing the flux.

Magnetomotive force = MMF = ampere turns = 1.257 NI Gilberts

The following is a table of calculated data used to plot Figure 9. The source for this information was taken from Figure 8.

Figure 8		Primary Turns	Primary Flux	Figure 8	Secondary Turns	Secondary Flux	Operate Cycle	Release Cycle	MMF
I	$\int e_p dt$	$1/N_p$	ϕ_p	$\int e_s dt$	$1/N_s$	ϕ_s	ϕ_s/ϕ_p	ϕ_s/ϕ_p	MMF
Amp.	Volt-sec	$1/4800$	Maxwells	Volts-sec	$1/48$	Maxwell			Gilberts
OPERATE									
.01	.036	2.08×10^{-4}	749	1.8×10^{-4}	2.08×10^{-2}	375	.50		60.3
.02	.072	"	1500	4.5×10^{-4}	"	939	.625		120.7
.026	.108	"	3250	6.93×10^{-4}	"	1440	.64		181.
.03	.117	"	2433	$.9 \times 10^{-4}$	"	1895	.78		241.
.04	.198	"	4118	14.4×10^{-4}	"	3000 x	.726		
.041	.234	"	4867	14.4×10^{-4}	"	3000	.62		
.05	.306	"	6400	25.2×10^{-4}	"	5240	.82		301.
.06	.415	"	8700	333×10^{-4}	"	6900	.79		362.
.064	.45	"	9400	35.1×10^{-4}	2.08×10^{-2}	7340	.78		
RELEASE									
.05	.415	"	8650	31.5×10^{-4}	"	6580		.76	
.04	.36	"	9500	27.9×10^{-4}	"	5810		.77	
.03	.305	"	6390	23.4×10^{-4}	"	4900		.78	
.02	.216	"	4500	17.1×10^{-4}	2.08×10^{-2}	3560		.79	
.014	.126	"	2630	11.7×10^{-4}	"	2440		.93	
.01	.108	"	2750	6.3×10^{-4}	"	1320		.58	

The ratio of secondary flux to the primary flux could be used as an indication of leakage flux.

For any particular operational state the ratio is fairly constant. Before the relay operates the value is close to 63%. After operation the value jumps to 79%. On the release cycle with the relay operated the ratio still remains constant at 79%. The values near zero are too small to be measured with any accuracy.

The information of the previous page indicates that the leakage flux is reasonably constant for any state of the relay. Also, only 60% of the flux generated is passing the armature air gap for the relay tested.

One point on Figure 9 was checked by direct measurement. A gauss meter probe was inserted in the air gap and the flux density was measured.

The area of the air gap was calculated from direct measurement. Fringing was compensated for in the measurement.

The following results were obtained.

$$A = .84 \text{ cm}^2$$

$$\phi_d = B (A) = (\text{gauss})(\text{cm}^2) = (1041)(.84) = 871 \text{ maxwells}$$

$$I = .02 \text{ amperes}$$

$$B = 1040 \text{ Gauss}$$

$$A = .84 \text{ centimeter squared}$$

$$\phi_d = 871 \text{ maxwells}$$

The flux obtained by direct measurement and the flux obtained by experimentally data compared within 94% of each other. It is believed the value of the experiments are acceptable.

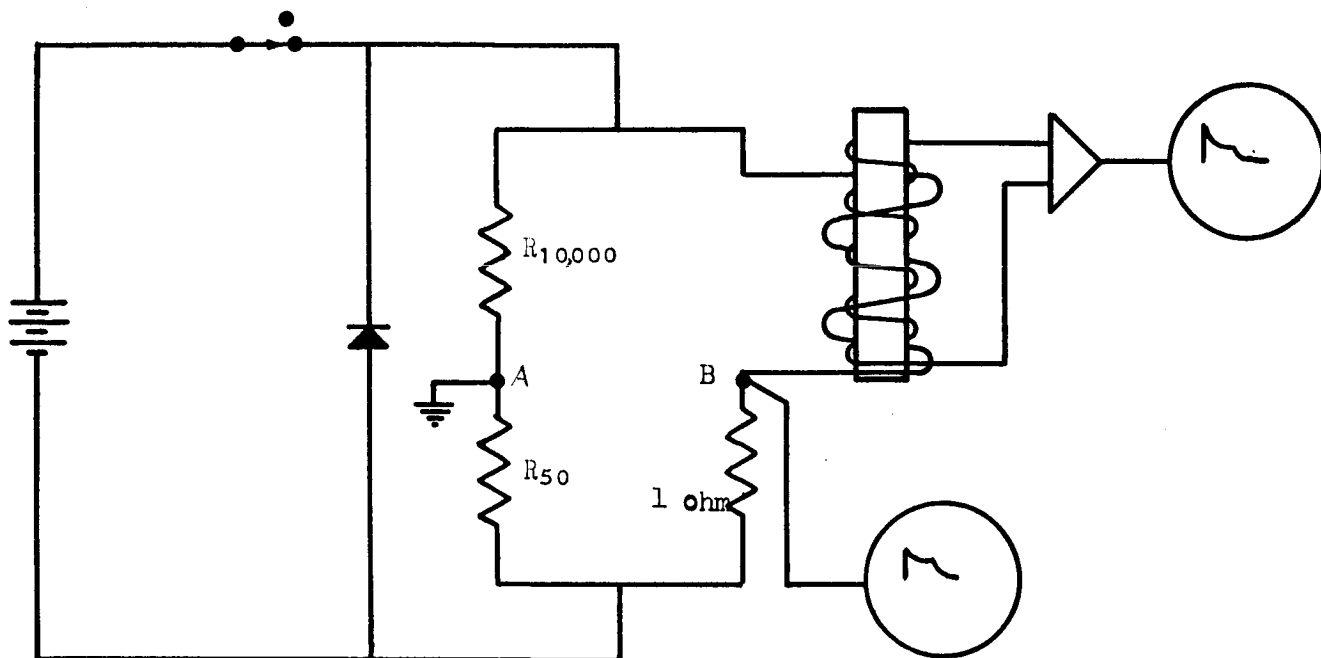


Figure 1

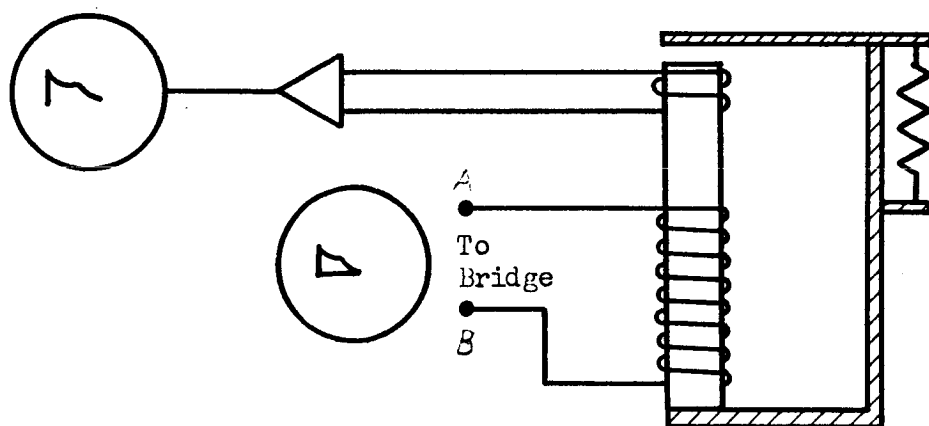


Figure 2

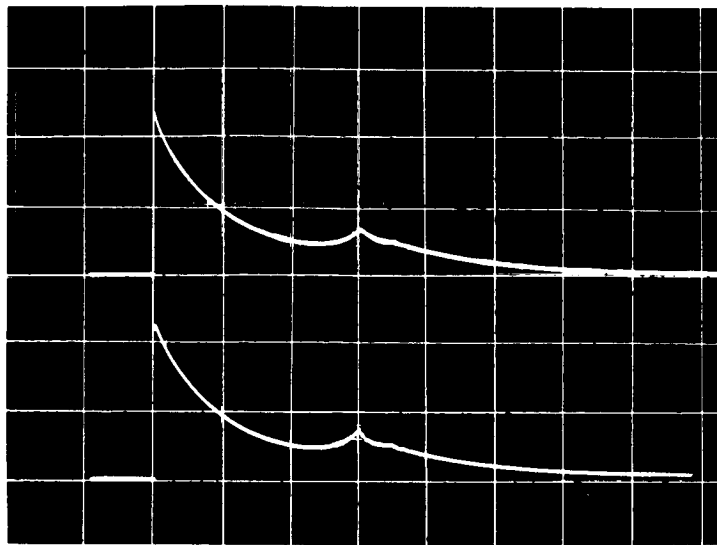


Figure 3

Back Electromotive Force Vs. Time &
Induced Operate Voltage Vs. Time

Traces: Upper - Back emf measured by the bridge method.

Lower - Induced voltage on special coil wound
next to core.

Oscillogram: Time scale - 10 milliseconds/cm.

Voltage scale on upper curve - 5 volts/cm.

Voltage scale on lower curve - .1 volts/cm.

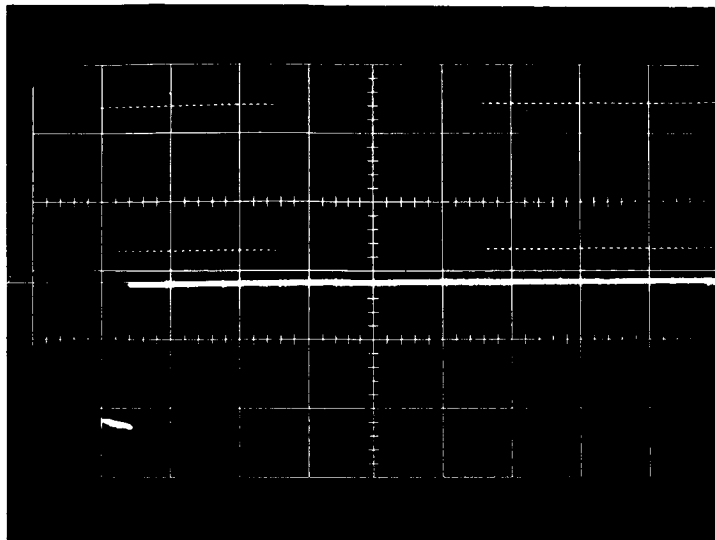


Figure 4

Integrator Calibration (Part One)

D.C. Signal Calibration

Traces: Upper - .1 volts total or .5 volts per centimeter
from the calibrator of the oscilloscope.

Lower - .1 volts total or 0.5 volts per centimeter
from direct current power supply.

Oscillogram: Time scale - 10 milliseconds per centimeter.

Voltage scale on upper trace 0.5 volts per centimeter.

Voltage scale on lower trace 0.5 volts per centimeter.

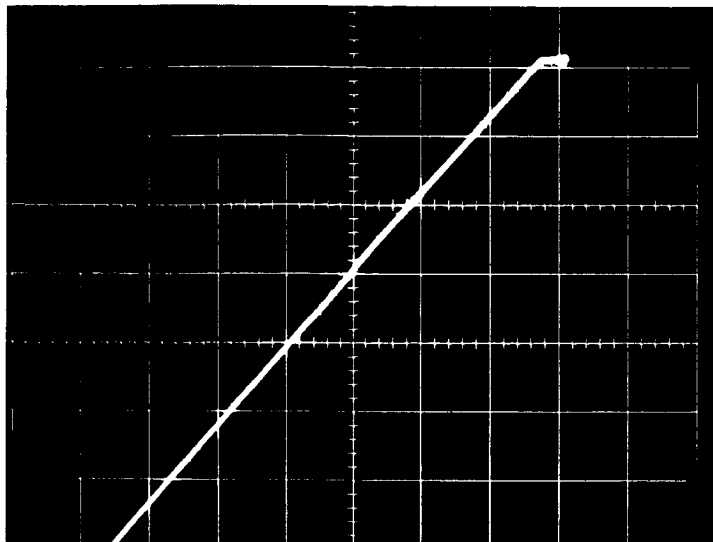


Figure 5
Integrator Calibration (Part Two)

Traces: Integration of direct current voltage of part one.
Oscillogram: Time scale - 10 milliseconds per centimeter.
Integrator scale - .0009 volt-seconds per centimeter.

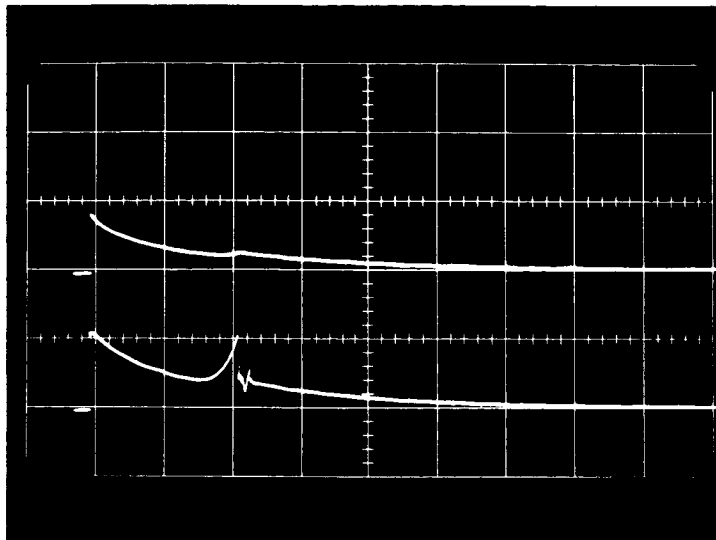


Figure 6

Back Electromotive Force Measurement by Bridge Method &
Induced Voltage Measurement Vs Time

Traces: Upper - Back electromotive force measured by
bridge method.

Lower - Induced voltage measurement on secondary winding.

Oscillogram: Time scale - 10 milliseconds per centimeter.

Upper trace - .05 volts per centimeter.

Lower trace - .05 volts per centimeter.

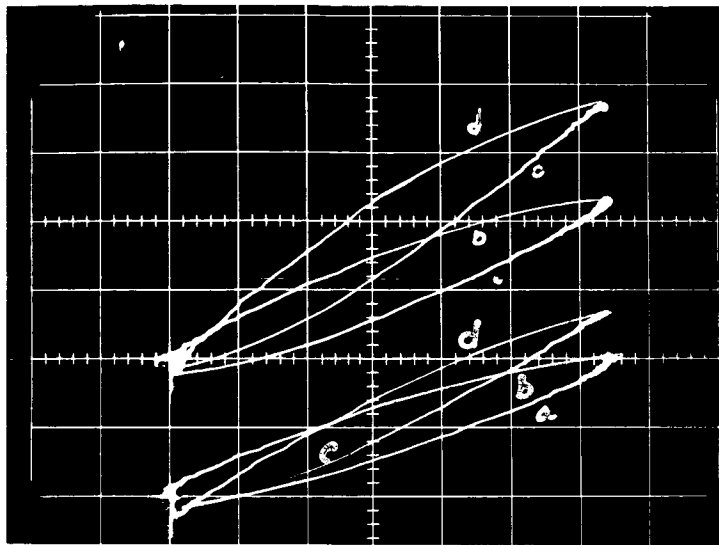


Figure 7

Energy Cycle Curve With Relay Blocked Open and Closed

Traces: Upper - Energy cycle curve made with secondary winding placed at the armature end of the core.

- (a) energization transition relay blocked open
- (b) deenergization transition relay blocked open
- (c) energization transition relay blocked closed
- (d) deenergization transition relay blocked closed

Lower - Energy cycle curve made with bridge at the relay terminals.

- (a) energization transition relay blocked open
- (b) deenergization transition relay blocked open
- (c) energization transition relay blocked closed
- (d) deenergization transition relay blocked closed

Oscillogram: Current scale - .01 ampere per centimeter

Upper curve - volt-second scale - .0009 volt-second per centimeter.

Lower curve - volt-second scale - .18 volt-second/cm

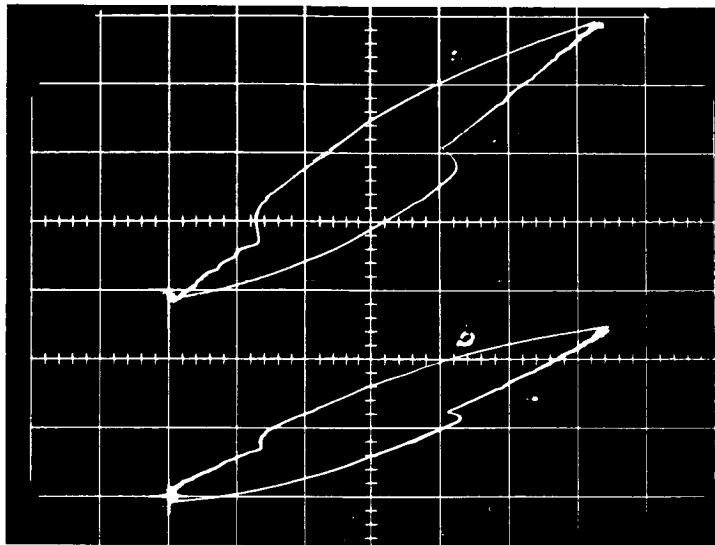


Figure 8

Energy Cycle Curve With Relay Free To Operate

Traces: Upper - Energy cycle curve made with secondary winding placed at the armature end of core.

- (a) energization transition relay free to operate
- (b) deenergization transition relay free to operate

Lower - Energy cycle curve made with bridge at the relay terminals

- (a) energization transition relay free to operate
- (b) deenergization transition relay free to operate

Oscillogram: Current scale - .01 ampere per centimeter

Upper curve - volt-second scale - .0009 volt-second/cm

Lower curve - volt-second scale - .13 volt-second/cm

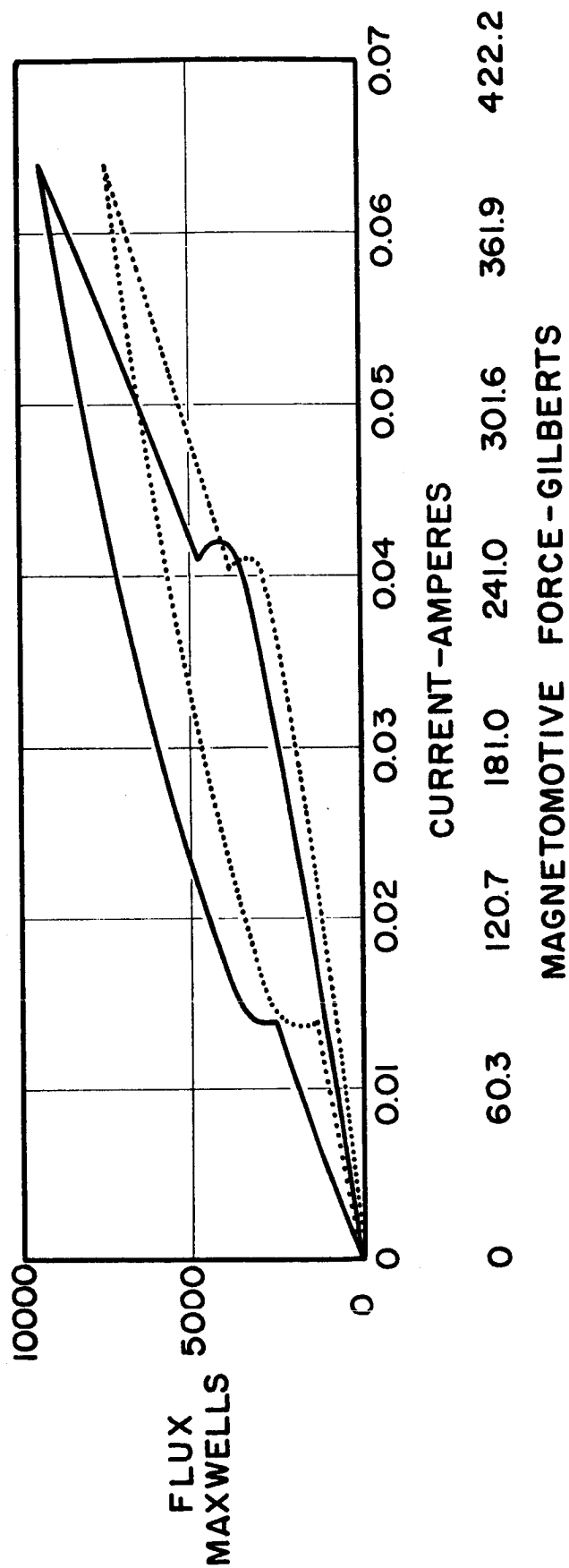


Figure 9

SECTION III
APPROXIMATING ARMATURE MOVEMENT AND LEAKAGE FLUX
OF SEALED RELAYS

The purpose of this report is to determine the armature displacement versus time of a sealed relay and check the results with direct measurements. If this information could be obtained accurately, various other mechanical properties could be deduced from terminal information of a relay.

A relation relating the magnetic properties with the electrical properties of a relay is illustrated. The graphical results obtained are empirical due to undefined variations of leakage flux and core saturation. The method used compensates for leakage flux and core saturation if present.

The method is based on the Energy Cycle Curve which was described in Section V on interim report October - November, 1963. This Energy Cycle Curve represents a graphical correlation of the total flux linkage versus current of a relay. Knowing the number of turns on the coil, the units of the plot can be converted to flux (Maxwells) and magnetomotive force (Gilbert). The magnitude represents the input to the system and includes all losses. This is logical since the measurements are made externally. Figure I illustrates a basic curve. It is desired to modify or reproduce the same curve to represent the variables which exist across the air gap during the mechanical transition of the armature.

By modulating the beam of a cathode ray oscilloscope with a differential square wave, additional information could be represented on the plot. The square wave generator was calibrated to indicate spots

at one-millisecond intervals. A beam modulated curve is illustrated in Figure II.

The slope of any point on the curve represents the permeance of the magnetic system.

$$P = \frac{\phi}{MMF}$$

The reluctance is represented by the reciprocal.

$$R_T = R_i + R_a + KR_L = \frac{MMF}{\phi} = \mu_i \frac{l_i}{A_i} + \mu_a \frac{l_a}{A_a} + \left[\frac{MMF}{\phi_L} \right] K$$

$$R_a = R_T - (R_i + KR_L) = [R_a + R_i + KR_L] - [R_i + KR_L]$$

If the plot of the relay Energy Cycle Curve could be obtained with the armature of the relay blocked closed, and another plot with the armature free to operate, the difference of reluctance could be observed for any value of flux. Any difference could be due to the varying length of the armature air gap. The relay is assumed to have the following constants.

0. Reluctance of air gap = (R_a)
1. Reluctance of leakage flux = (R_L)
2. Total reluctance = (R_T)
3. Area of iron core = (A_i)
4. Length of iron = (l_i)
5. Area of armature air gap = (A_a)
6. Permeability of iron and air = (μ_i) and (μ_a)
7. Magnetomotive force = (MMF)
8. Armature pick-up flux = (ϕ_p)
9. Subscripts "B", "C", and "D" also refers to points on figures.

The reluctance of the leakage flux path is in parallel with the reluctance of the air gap. The constant "K" would include a coefficient which is the equivalent to the series reluctance. The only unknown variable which exists in the above equation is the length of the air gap (ℓ_a).

The above statements are expressed mathematically as follows:

$$R_T = R_D, R_B = R_i + KR_L$$

$$R_a = R_D - R_B = \frac{MMF_D}{\phi_p} - \frac{MMF_B}{\phi_p} = \frac{1}{\phi_p} (MMF_D - MMF_B)$$

$$MMF_a = MMF_D - MMF_B = \phi_p (R_D - R_B) = \phi_p \left[\left(\mu_a \frac{\ell_{aD}}{A_a} + \mu_i \frac{\ell_i}{A_i} + KR_L \right) - \left(\mu_i \frac{\ell_{iB}}{A_i} + KR_L \right) \right]$$

$$MMF_D - MMF_B = \phi_p [K\ell_{aD}] = K_i \ell_{aD}$$

Assuming various values of flux (ϕ_n) the difference between the magnetomotive forces of the relay can be obtained from the plot during the armature transition. The difference of magnetomotive force with armature block closed and magnetomotive force with armature free to operate is proportional to the air gap length. Such a curve can be marked in one millisecond increments and the results plotted as armature air gap versus time.

Figure III illustrates two characteristic curves, one with the armature free to operate, the other is with the armature blocked closed. The curves superimpose each other except during the armature transition and before the armature pick-up point.

The curve in Figure III must be modified to represent the condition existing across the air gap of the relay. It is known that the magnetomotive force across the air gap is continually decreasing when the armature is moving toward the pole piece. The armature in the operated condition establishes a magnetic circuit in the relay of very low reluctance. Therefore, most all the flux exists in the low reluctance path. Any distortion due to saturation existing in the curve for the armature blocked closed, will exist in the core during the armature transition state for the same flux value.

The two conditions which must be satisfied in correcting a curve for leakage flux are:

- (1) The difference between the magnetomotive forces for any value of flux must be continually decreasing as the armature moves from the open to the closed position.
- (2) The tangent to the corrected curve and the original curve (armature free to operate) through the points intersected by the pick-up flux line must be parallel. .

If the above two conditions are met, the difference of magnetomotive force for any value of flux between the pick-up flux and the operated flux value should be proportional to the reluctance of the air gap.

The armature of a sealed relay cannot be blocked closed. However, various segments of the trace can be obtained, making a close approximation possible. The upper portion of the curve will define the trend. By reducing the voltage and making additional characteristic curves as illustrated in Figure IV, the trend can be extended. The curve must start from the zero vertex.

Figure V illustrates three Energy Cycle Curves of a relay. The armature blocked open, blocked closed and free to operate. The beam of the oscilloscope was modulated and each dot represents one millisecond. The curve was redrawn to scale and enlarged in Figure VI. The pick-up point of the armature is represented by " D_p " on the curve. There are 18 dots between " D_p " and "A" which represent 18 milliseconds for the mechanical transition of the armature. Line " B_p ", "A" is a curve segment for the relay blocked closed. This segment is rotated clockwise about "A" correcting for the leakage reluctance. The line at point " C_p " is tangent with the line at point " D_p ". The distance " D_p ", " C_p " represents the magnetomotive force existing across the air gap at a flux value of " ϕ_p ". The length of " D_p ", " C_p " is proportional to the length of air gap. Therefore, this distance must continually decrease as the armature air gap becomes smaller.

Figure VII represents two additional plots of the same rotary relay as Figure V. The lower trace represents armature travel versus time and was made by direct measurement. Figure VIII illustrates the plots of armature displacement versus time. One plot was obtained from the Energy Cycle Curve. The other plot was the result of direct measurement.

Figure II illustrates a typical curve which could be obtained from a sealed relay. This curve is redrawn and enlarged in Figure IX. The line "A", " B_p " has been projected through the original. The projection represents the completion of the Energy Cycle Curve with the relay blocked closed. The projected line "A", " B_p " was rotated clockwise about point "A" until the line at " C_p " is tangent with the line at " D_p " and the distance between " C_p " and " D_p " is decreasing as the flux " ϕ " is increasing. " C_n " represents any point on the line between " C_p " and "A". " D_n " represents any point on the line between " D_p " and "A" which has

the same value of flux " ϕ " as " C_n ".

The distance between " D_n " and " C_n " for each millisecond is plotted on Figure X.

Figure XI represents the armature travel versus time for a clapper type relay. The measured curve on Figure X was obtained from Figure XI. The measured and calculated plots correlates very close for the clapper type relay.

The accuracy of the Armature Air Gap curves was not good. A method of enlarging the small oscillograms would improve the accuracy of the plots. The process of obtaining the Energy Cycle Curve must also be done with care, since unbalance in the bridge will cause an error in the integration.

Considering Figure IX, the line " B_p ", "A" represents the reluctance locus of the system with no air gap as the flux increases. The line " B_p ", "A" could also represent the reluctance locus of the iron and leakage flux path as the flux increases. The line " C_p ", "A" represents the reluctance locus of the iron in the system.

If the leakage flux path is all the flux of a system which does not cross the armature air gap, then the reluctance of the leakage path would act in parallel with the reluctance of the iron. The total reluctance could be described as follows:

$$R_T = \frac{R_L R_i}{R_L + R_i}$$

Solving for the leakage reluctance (R_L)

$$R_L = \frac{R_i R_T}{R_i - R_T}$$

The value for the total reluctance with armature closed and leakage reluctance can be obtained from Figure IX as follows:

$$\begin{aligned} R_T &= \frac{\text{magnetomotive force at point "B"}}{\text{flux at point "B"}} = \frac{95}{1600} \\ &= 5.9 \times 10^{-2} \frac{\text{gilberts}}{\text{maxwell}} \end{aligned}$$

The reluctance of the iron from the corrected curve is:

$$\begin{aligned} R_i &= \frac{\text{magnetomotive force at point (A - C)}}{\text{flux at point (A - C)}} = \frac{245 - 10}{4560 - 1600} = \frac{235}{2960} \\ &= .232 \frac{\text{gilberts}}{\text{maxwell}} \end{aligned}$$

A classification factor of any magnetic circuit design could be obtained by using a ratio of reluctance of the iron divided by the total reluctance. The classification factor of the clapper type relay discussed could be:

$$\text{classification factor} = \frac{R_i}{R_i + R_L} = \frac{7.9 \times 10^{-2}}{7.9 \times 10^{-2} + .232} = .254$$

The reluctance of the leakage flux path is dependent on the physical configuration of the relay and could be used in a general system of relay classification.

TABLE OF SYMBOLS

A_a	=	Area of air gap
A_i	=	Area of iron core
A_e	=	Effective area
l_a	=	Length of air gap
l_i	=	Length of iron core
l_e	=	Effective length
ϕ_p	=	Pick-up flux
MMF	=	Magnetomotive force
ϕ_L	=	Leakage flux
ϕ_T	=	Total flux
P	=	Permeance
μ_i	=	Permeability of iron
μ_T	=	Total permeability
μ_a	=	Permeability of air
R_L	=	Reluctance of leakage flux path
R_T	=	Reluctance of magnetic system
R_i	=	Reluctance of iron core
MMF_a	=	Magnetomotive force across air gap

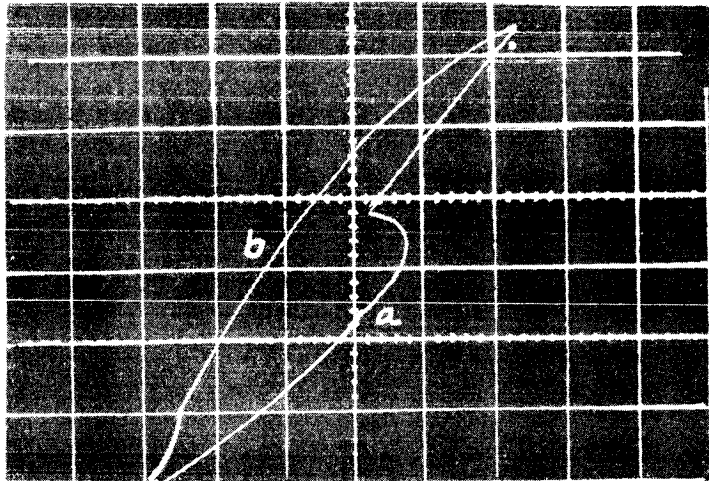


Figure I

Energy Cycle Curve For Armature Free To Operate

Traces: (a) Flux-linkages versus current during operate cycle
(b) Flux-linkages versus current during release cycle

Oscillogram Data:

Current scale = .068 amperes per centimeter

Flux-linkage scale = 2 weber-turns per centimeter

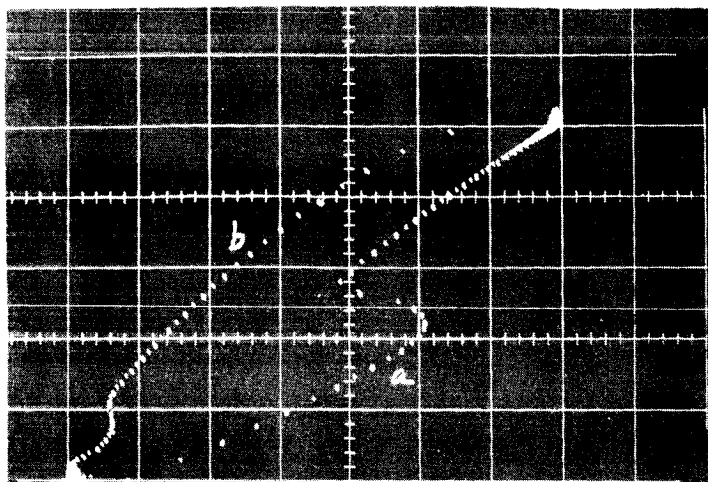


Figure II

Energy Cycle Curve With Cathode Ray Oscilloscope Beam
Modulated At One Millisecond Intervals

Traces: (a) Flux-linkage versus current or

Flux versus magnetomotive force for the coil energizing
cycle with armature free to operate

(b) Flux-linkage versus current or

Flux versus magnetomotive force for the coil deenergizing
cycle with armature free to operate

Oscillogram Data:

Flux-linkage scale = .014 weber-turns

Flux scale = 1600 maxwell per centimeter

Current scale = 50 milliamperes per centimeter

Magnetomotive force scale = 63 gilberts

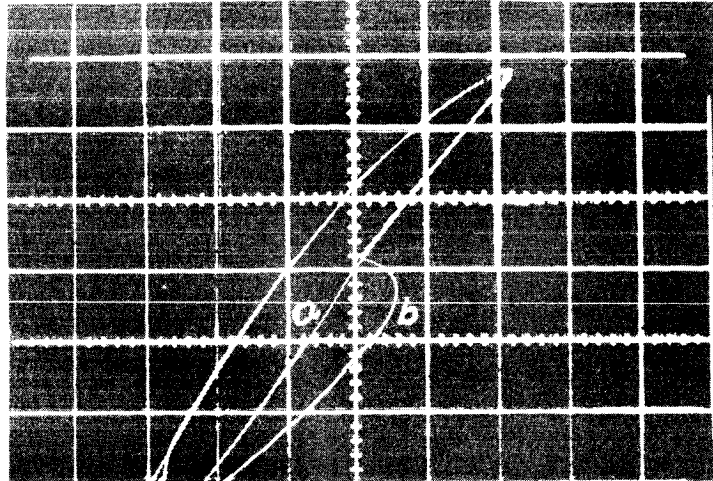


Figure III

Superimposed Energy Cycle Curves With Armature Free To Operate And
Armature Blocked Closed

Traces: (a) Flux-linkages versus current with armature blocked closed
(b) Flux-linkages versus current with armature free to operate

Oscillogram Data:

Flux-linkage scale = 2 webers-turns per centimeter

Current scale = .068 amperes per centimeter

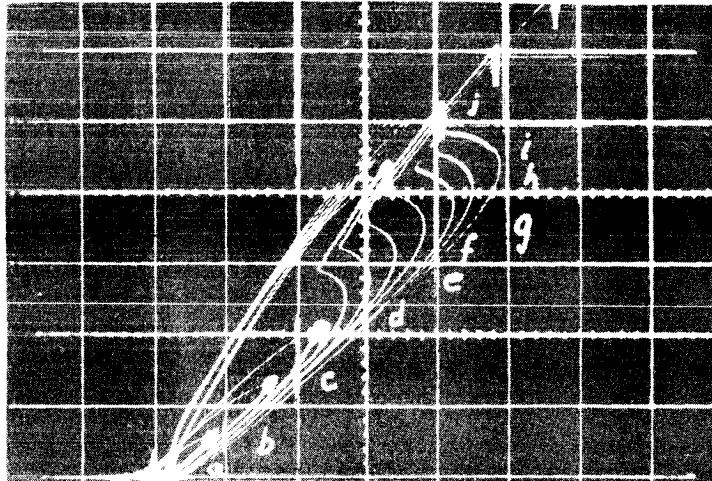


Figure IV
A Set Of Energy Cycle Curves For
Various Supply Voltages

Traces:	(a)	Flux	versus	current	with	1	volt	supply
	(b)	"	"	"	"	2	"	"
	(c)	"	"	"	"	3	"	"
	(d)	"	"	"	"	4	"	"
	(e)	"	"	"	"	5	"	"
	(f)	"	"	"	"	6	"	"
	(g)	"	"	"	"	7	"	"
	(h)	"	"	"	"	8	"	"
	(i)	"	"	"	"	9	"	"
	(j)	"	"	"	"	10	"	"

Oscillogram Data:

Flux-linkage = 2 webers-turns per centimeter

Current scale = .068 amperes per centimeter

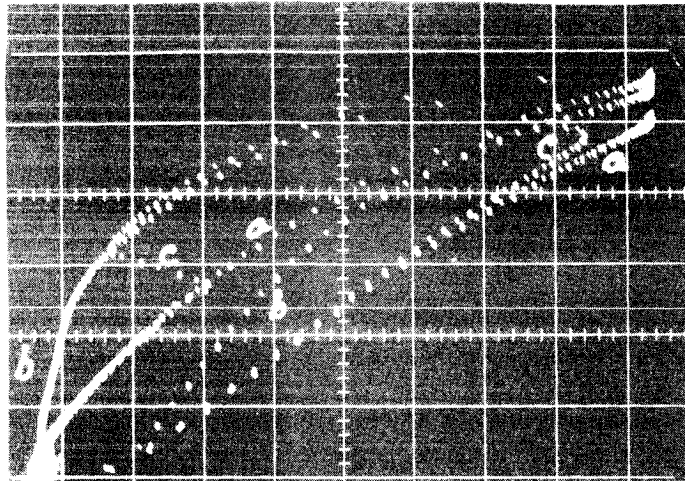


Figure V
Energy Cycle Curve With Time Modulation Of A
Rotary Type Relay

Traces: (a) Flux versus magnetomotive force with armature blocked open
(b) " " " " " " " closed
(c) " " " " " " " free to operate

Oscillogram Data:

Flux scale = 1 unit per centimeter

Magnetomotive force scale = 1 unit per centimeter

Time scale = 1 millisecond per dot

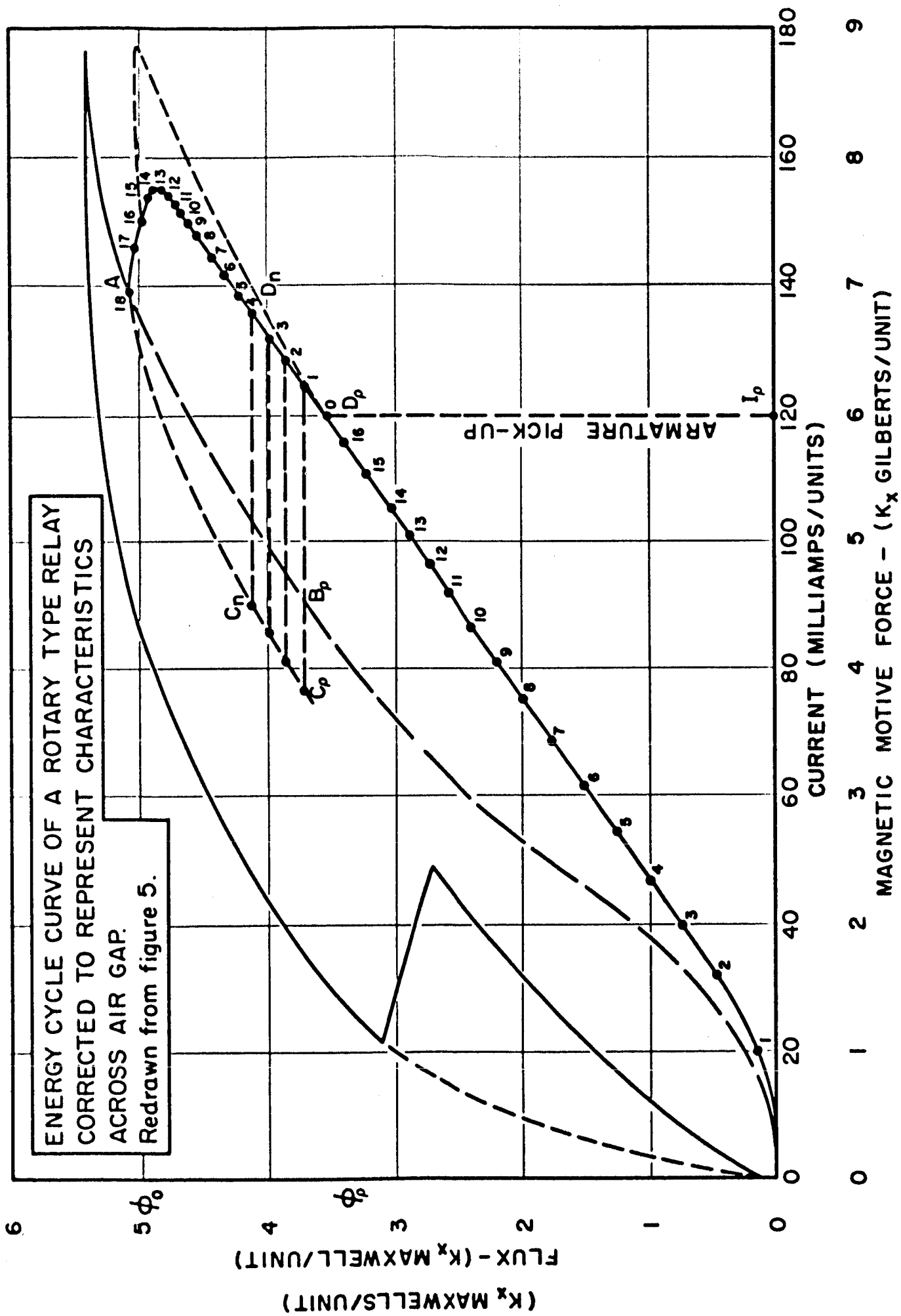


FIGURE VI

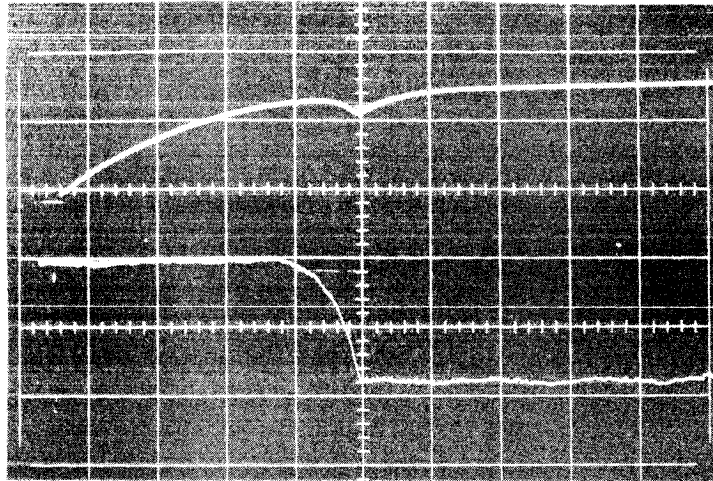


Figure VII

Characteristic Curves Of A Rotary Type Relay

Traces: Upper - Coil current versus time

Lower - Armature air gap versus time

Oscillogram Data:

Current Scale = 100 milliamperes per centimeter

Armature air gap length = 55% total air gap per centimeter

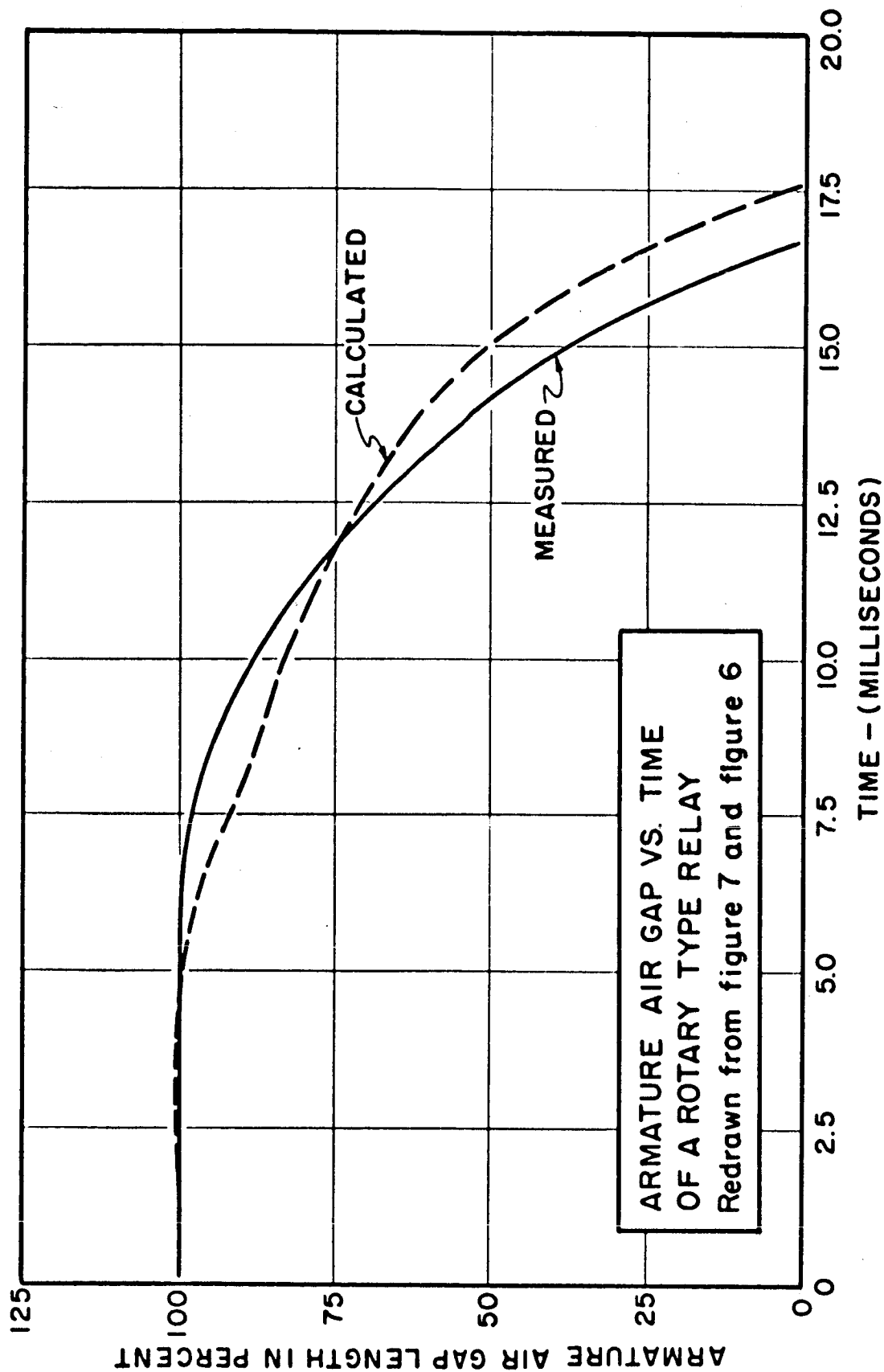


FIGURE VIII

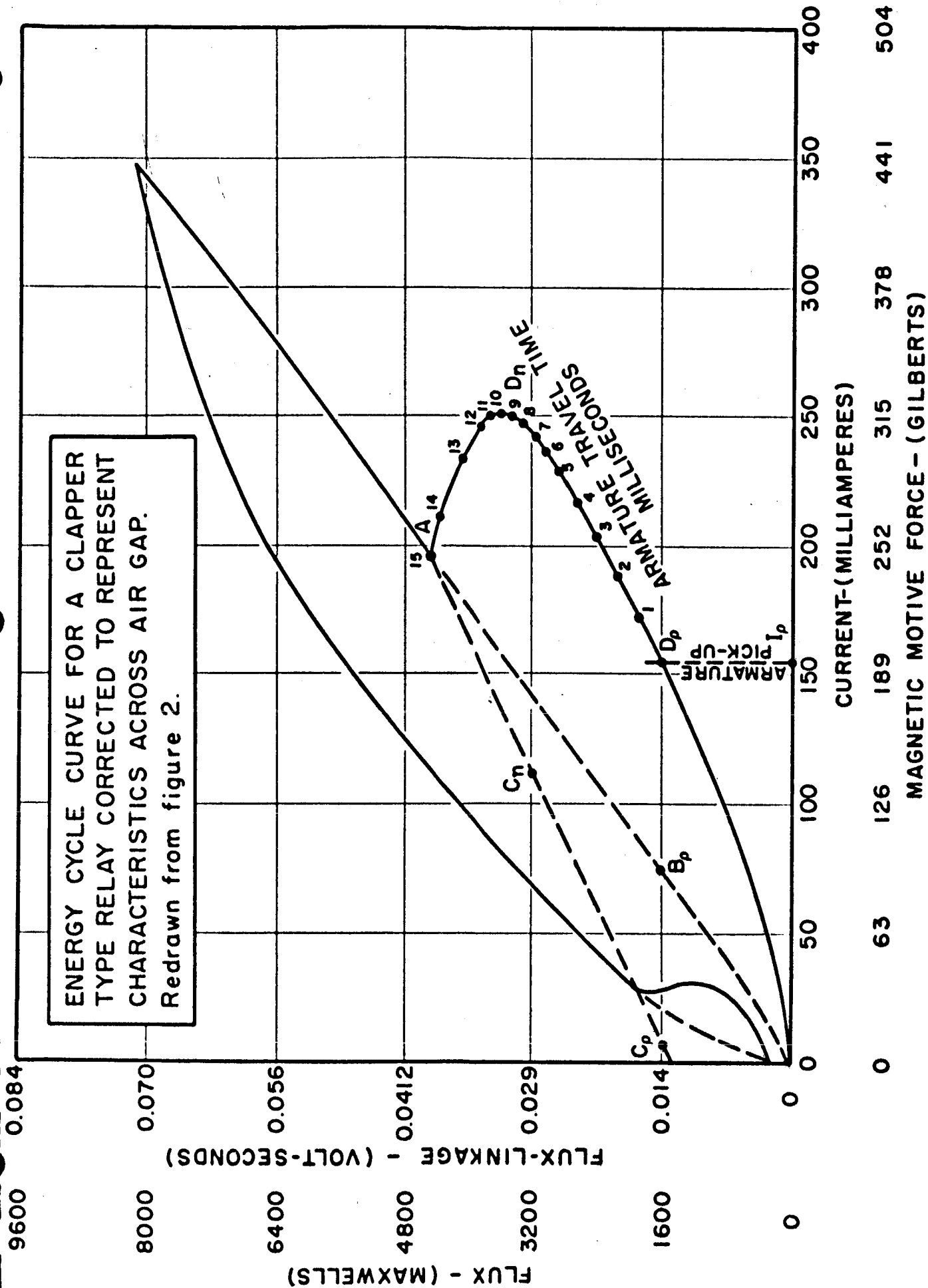


FIGURE IX

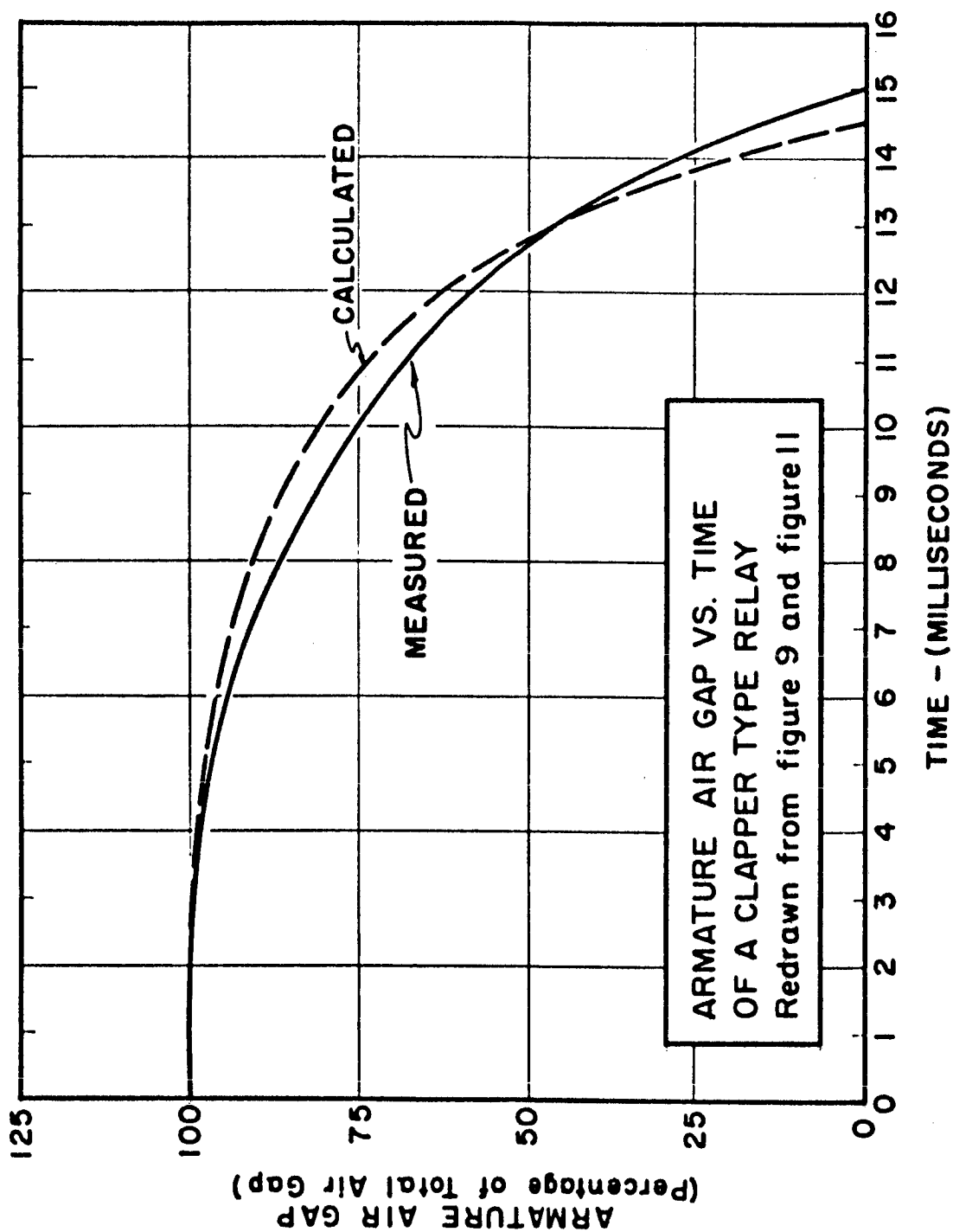


FIGURE X

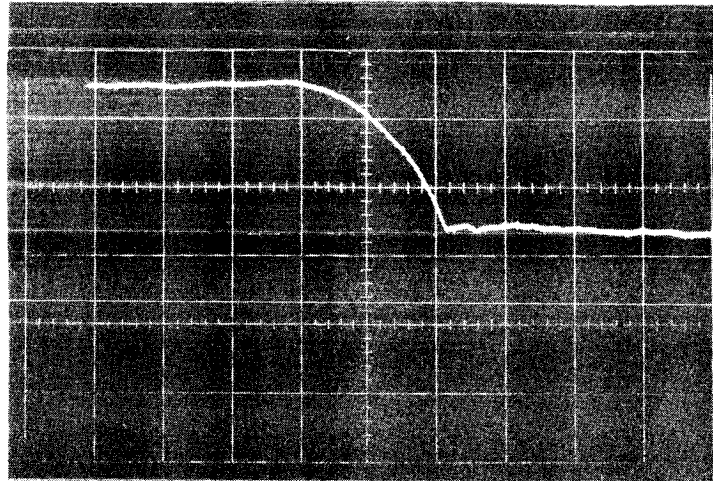


Figure XI

Armature Air Gap Versus Time Of A

Clapper Type Relay

Traces: Armature air gap versus time

Oscillogram Data:

Armature air gap scale = 45% total air gap per centimeter

time scale = 5 milliseconds per centimeter

SECTION VI

ARMATURE MOVEMENT DETECTION AND APPROXIMATION

A part of the work of the Twelfth interim period was devoted to the collection of more sample information. The approximation of armature travel versus time of a sealed relay was verified by a few examples and the results were fair. This work was continued in an effort to improve the accuracy of the approximation by enlarging the oscillograms and carefully plotting the results.

For each set of information, simultaneous oscillograms were taken of the relay. One oscillogram represented the flux versus magnetomotive force, and the other represented the armature movement versus time.

The detection of armature movement was made directly from the relay. Difficulty was experienced in obtaining this information. Two different methods were used. One method used a photo-electric tube measuring the quantity of light variation. The light method printed a line proportional to the armature movement. Noise and stability was a problem with this method. The other method used a differential transformer with a high frequency directly superimposed. As the coupling was unbalanced the amplitude of the carrier frequency increased. The system displayed an envelope on the oscilloscope. The amplitude was proportional to the armature movement. The linkage of the system presented a problem as is illustrated in Figure 7 by the indicated extra curve at "a" which is not due to armature movement. A new transformer is being prepared to overcome this difficulty.

Figure 1 illustrates a typical energy cycle curve for a relay with normal operating voltages. Figure 2 illustrates the current and armature displacement versus time for the same relay. Figure 1a is an enlargement of the oscillogram in Figure 1. Figure 2a shows the results obtained by

calculation and by measurements. The results give a good approximation but is not as accurate as desired. The photo-electric method was used for measuring the armature displacement curve. Figure 3 illustrates a calibration oscillogram for this system with four equal settings of the armature. The measuring system was not entirely linear.

Figure 4 illustrates another energy cycle curve for a relay with typical operating voltage. Figure 5 is the corresponding current and armature displacement curve for the same relay. After the armature was seated additional movement was indicated by the detector. Figures 4a and 5 were used to obtain the comparison of results. Again, the results were reasonable.

By detecting a change in velocity of the armature, one should be able to determine the closure or breakage position of the contacts with respect to the armature travel. The armature of a relay operating on very low voltage will decrease in velocity if additional spring tension is present from the contact springs. In some cases the armature seems to be stationary during a certain portion of the curve. Figure 6a is an enlargement of the oscillogram in Figure 6. Figure 7 illustrates the direct measurement of the armature movement and verifies that the armature is stationary during a certain portion of its travel as indicated at point "b".

Figure 7a illustrates a comparison of the measured and calculated armature travel versus time. It is seen the direct measurement indicated the armature is stationary at a different position than is indicated by the calculated curve.

Another relay was investigated using a low voltage supply. Figures 8, 8a, 9 and 9a illustrate the results obtained. The results were similar to the previous case. The armature was indicated as stationary at two different locations.

The results of the armature displacement versus time curves indicates the reluctance obtained for the air gap is not exact. Referring to curves 2a, 7a and 9a, all curves should stop at the same point on the time axis. The difference observed is due to the interpretation of the oscillograms. All the curves have the same slope during the last few millisecons of operation. During the first few milliseconds of armature movement, the calculated portion of the curve indicates more displacement than was measured by the armature motion detector. The differences between the two curves is believed to be due to the measured values of the back electromotive force. Any high frequency component of a wave would be shunted in the relay. Referring to the 11th Interim Report, Section I, Figure 6; the back electromotive force measured by the bridge is compared with the induced voltage of a search coil positioned near the air gap of a relay. The wave form of the back electromotive force measured by the bridge has less characteristics than the search coil movement. The energy cycle curve which is dependent on the bridge measurement also lacks definition. In a hermetically sealed device an exact representation of the air gap flux can not be obtained for any operating condition. However, a good approximation can be obtained if the armature motion is smooth and continuous. The armature displacement versus time curve is completely dependent on an accurate measurement of the relay air gap flux.

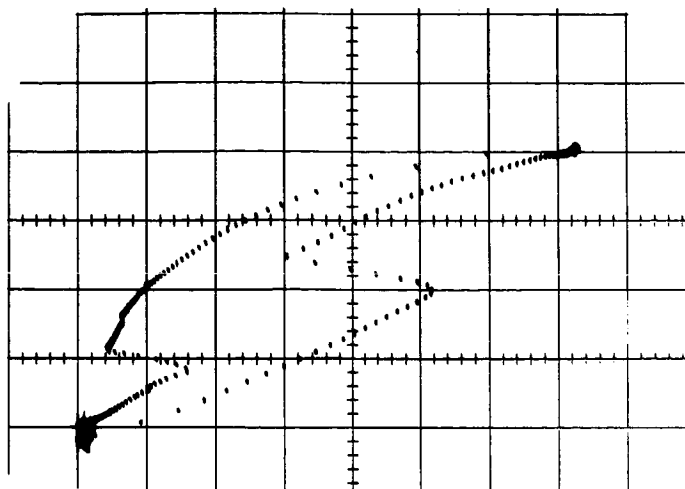


Figure 1
Oscillogram of a Plunger Type Relay

Traces:

- (a) Vertical axis: Flux linkage
- (b) Horizontal axis: Current
- (c) Trace modulated with equal increments of time

Oscillogram data:

Current scale: 50 milliamp per centimeter

Flux linkage scale: .0064 volt seconds per centimeter

Time scale: each dot as one millisecond

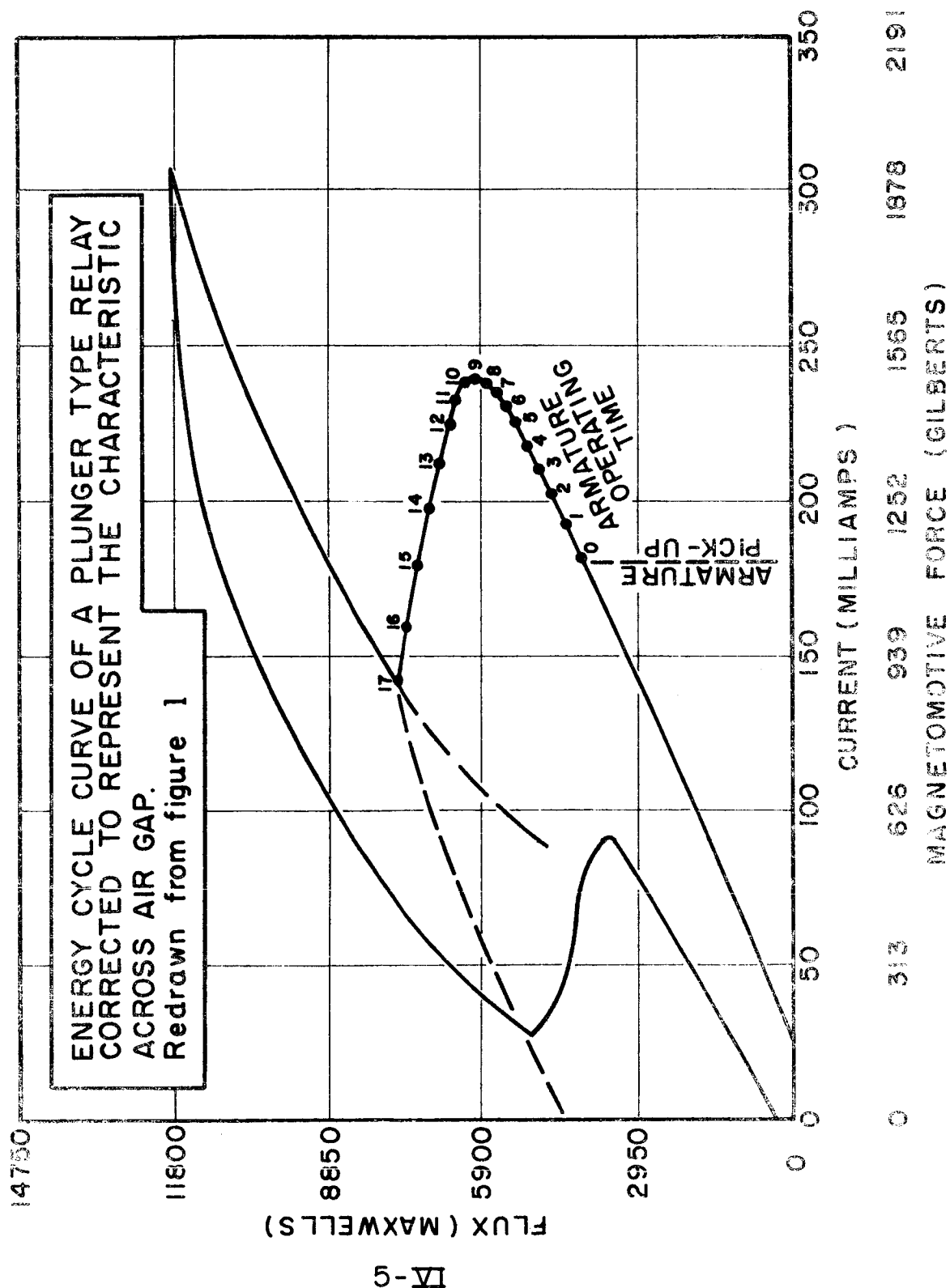


Figure 1a

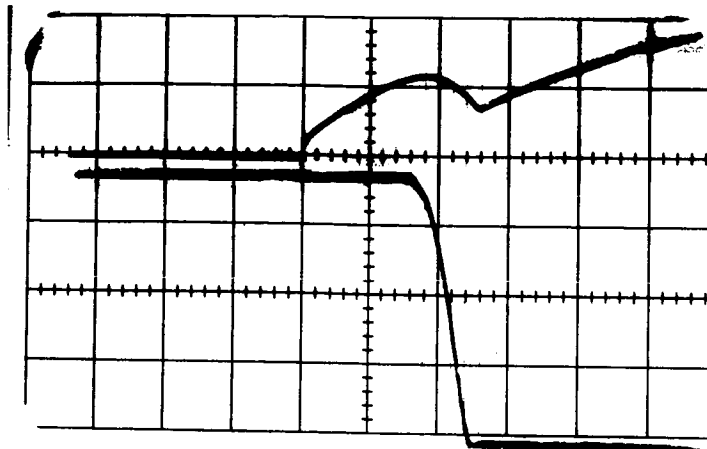


Figure 2

Oscillogram of Current and Armature Displacement
of a Plunger Type Relay

Traces:

Upper curve: Vertical axis is current

Lower curve: Vertical axis is armature displacement

Horizontal axis is time

Oscillogram data:

Current scale: 200 milliamp per centimeter

Armature displacement scale: 25% total armature travel
per centimeter

Time scale: 10 millisecond per centimeter

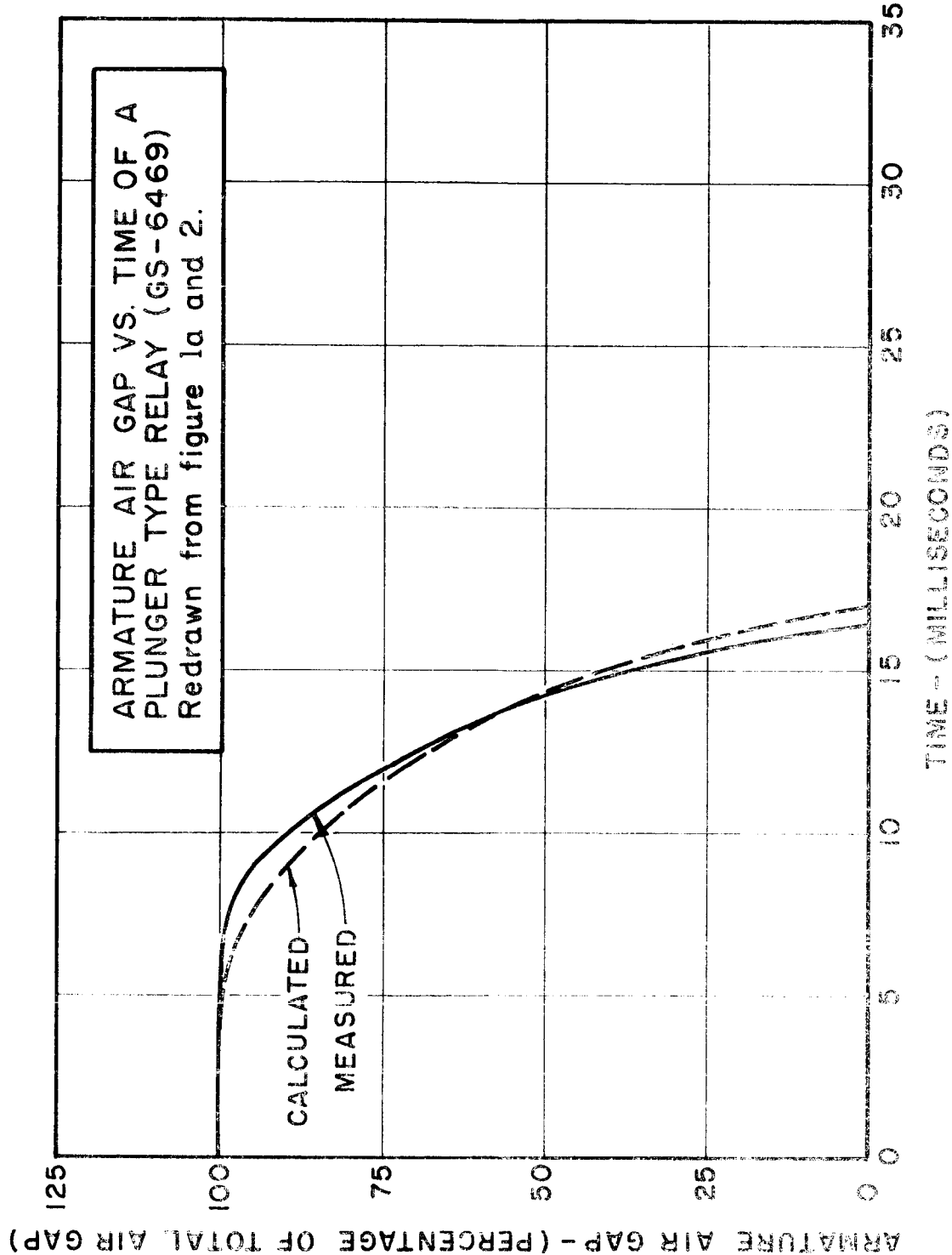


Figure 2a

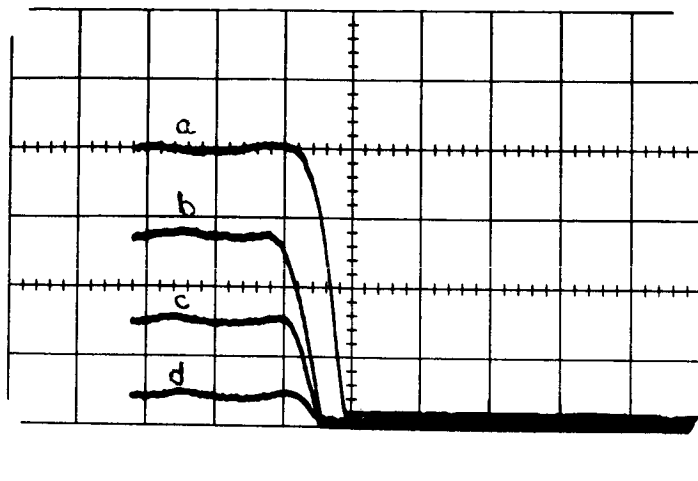


Figure 3

Calibration Curve of Armature
Displacement Detector

Traces:

- (a) Armature transition from open to close position
- (b) Armature displaced .015" from open position
- (c) Armature displaced .03" from open position
- (d) Armature displaced .045" from open position

Oscillogram data:

Vertical axis: percent of armature displacement

Horizontal axis time: 10 milliseconds per centimeter

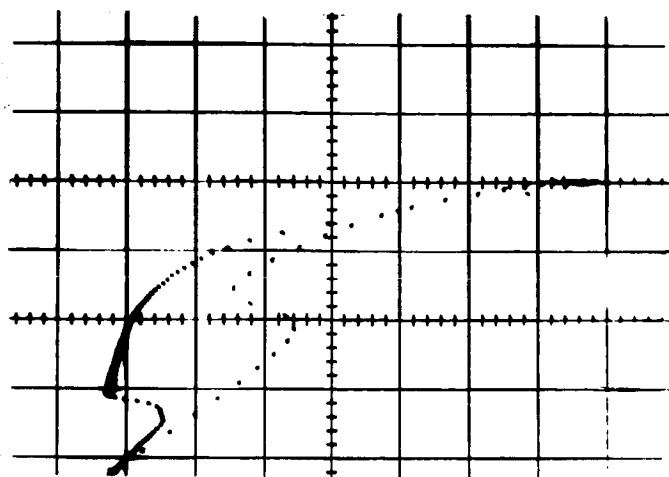


Figure 4

Oscillogram of a Clapper Type Relay "B"

Traces:

Vertical axis: flux

Horizontal axis: magnetomotive force

Oscillogram data:

Flux scale: K_y maxwells per unit

Magnetomotive force: K_x gilberts per unit

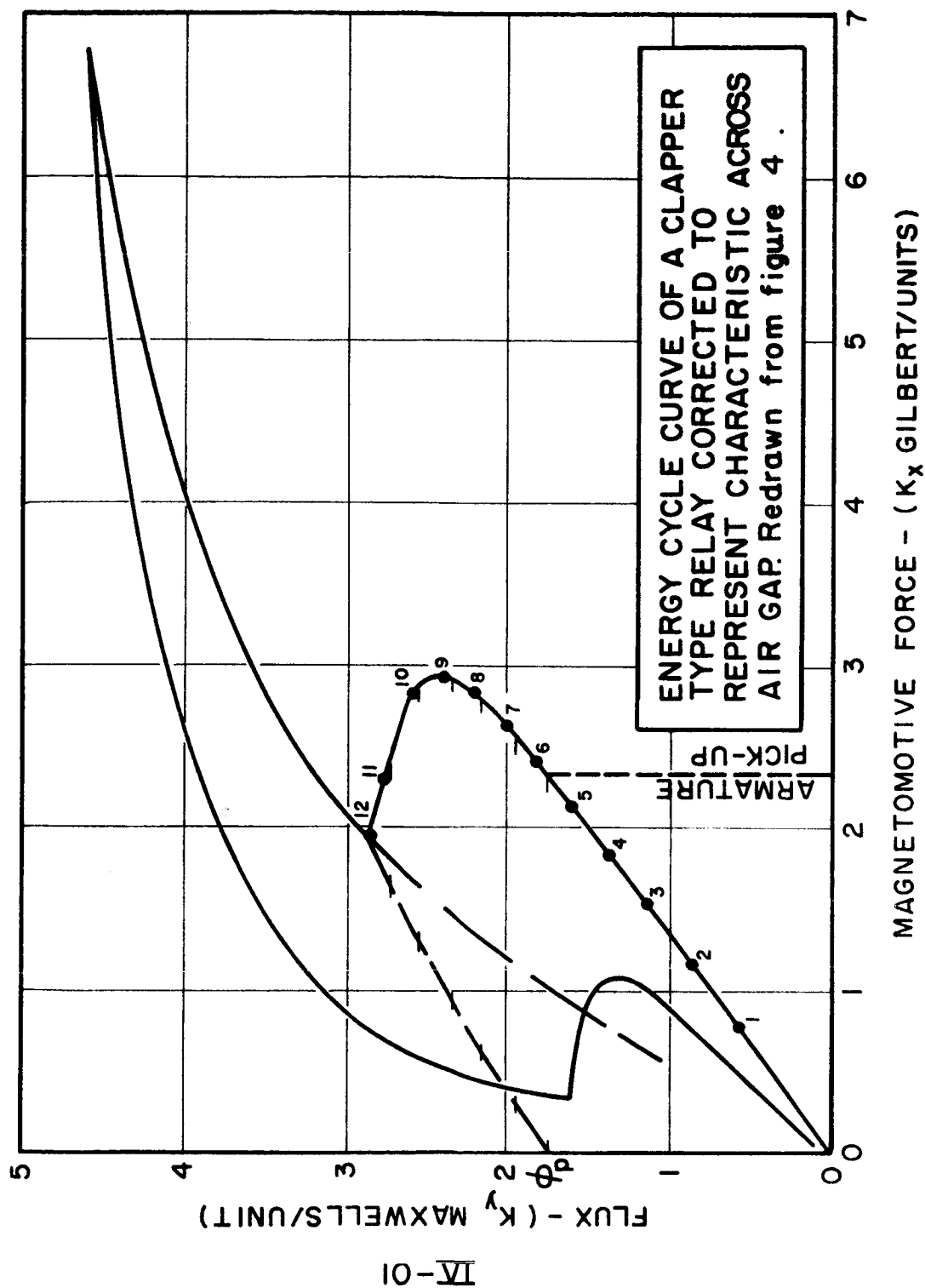


Figure 4a

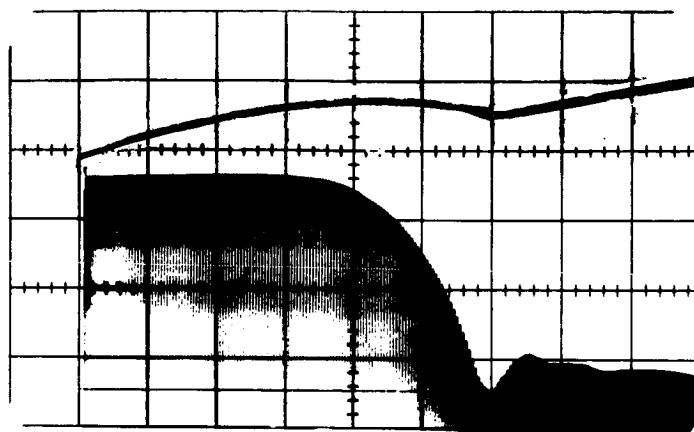


Figure 5

Oscillogram of Current and Armature Displacement
of a Clapper "B" Type Relay

Traces:

Upper curve: vertical axis current

Lower curve: Vertical axis armature displacement

Horizontal axis: Time

Oscillogram data:

Current scale: 50 milliamps per centimeter

Armature displacement scale: 33% total armature travel
per centimeter

Time scale: 2 milliseconds per centimeter

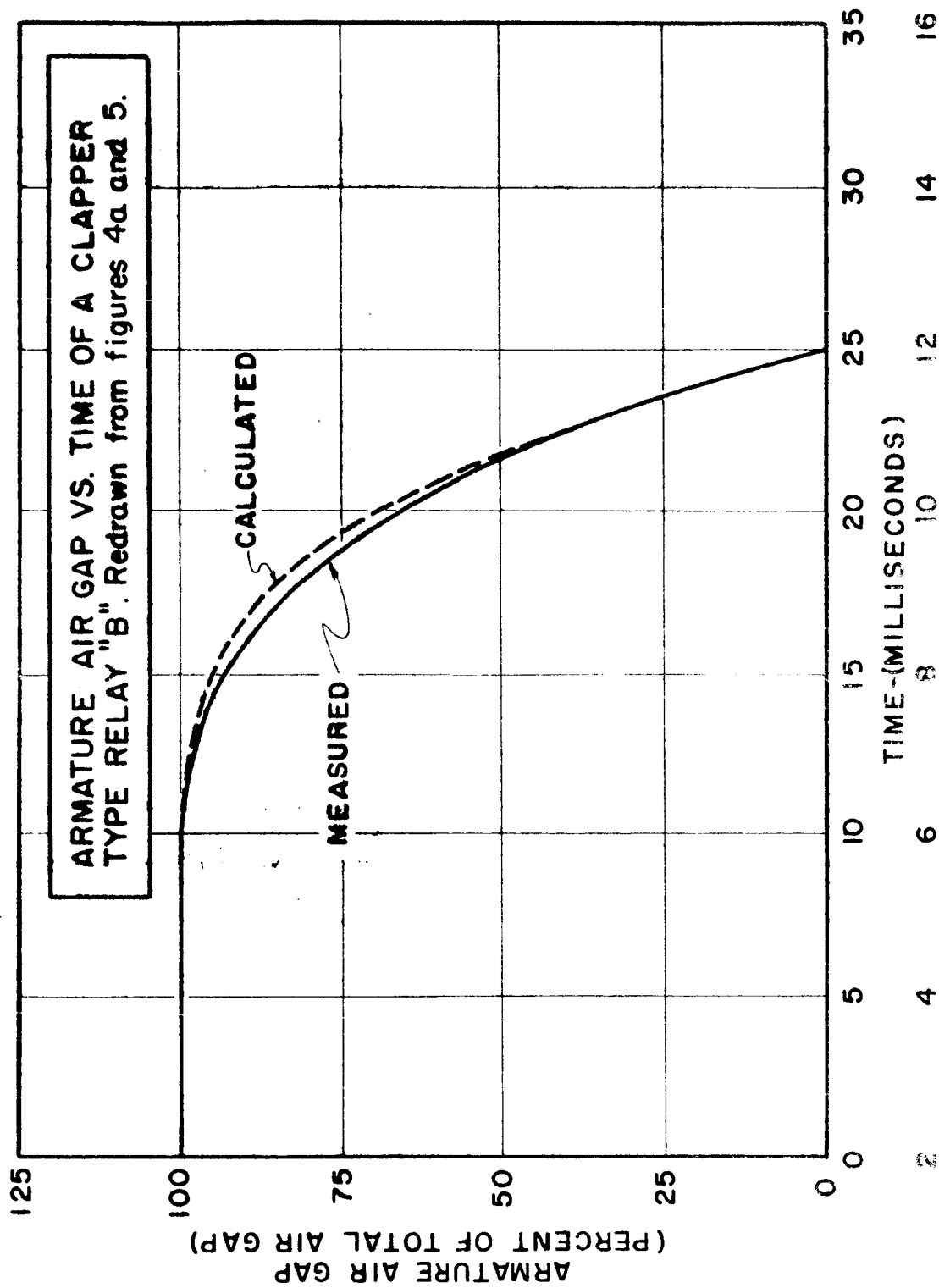


Figure 5a

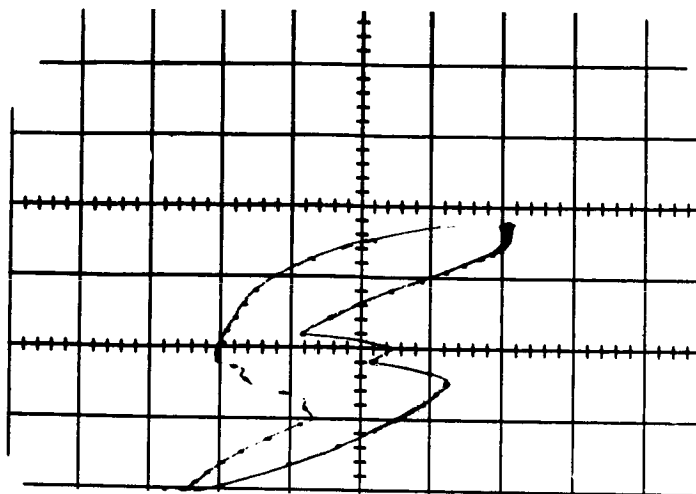


Figure 6

Oscillogram of Clapper Type Relay "A"
Operated on Low Voltage

Trace:

Vertical axis: Flux

Horizontal axis: Magnetomotive force

Trace: Modulated in equal increments of time

Oscillogram data:

Flux scale: K_y maxwells per centimeter

Magnetomotive force: K_x gilberts per centimeter

Time scale: 5 milliseconds per dot on trace

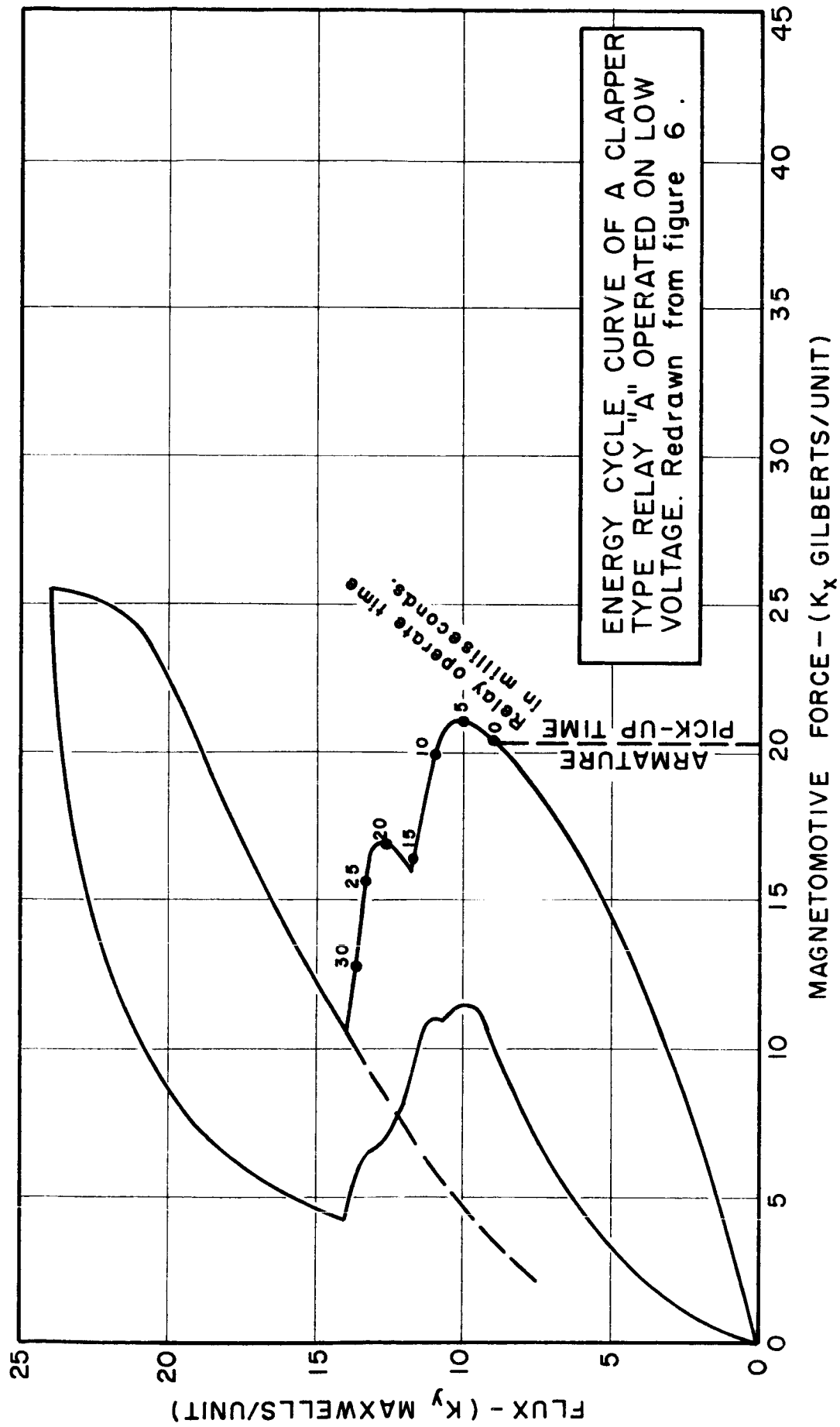


Figure 6a

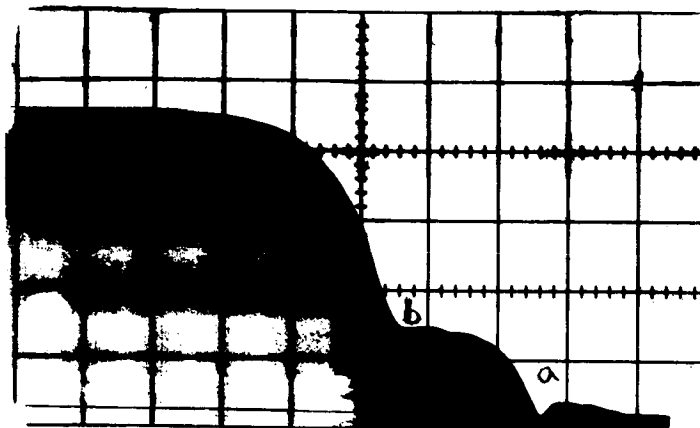


Figure 7

Oscillogram of Clapper Type Relay "A"
Operated on Low Voltage

Traces:

Vertical axis: Armature displacement

Horizontal axis: Time

Oscillogram data:

Armature Displacement Scale: 20% total armature travel
per centimeter

Time scale: 5 milliseconds per division

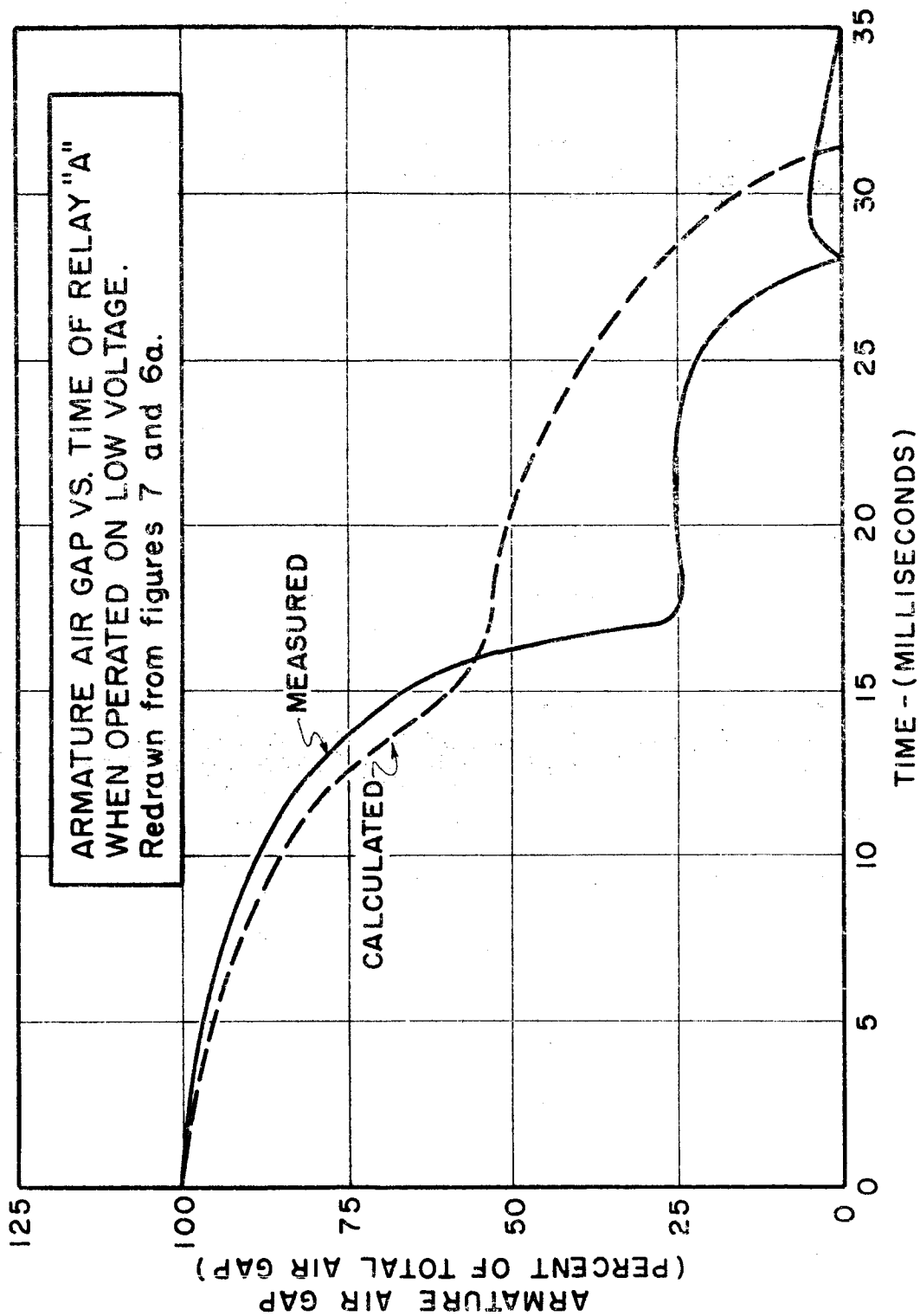


Figure 7a

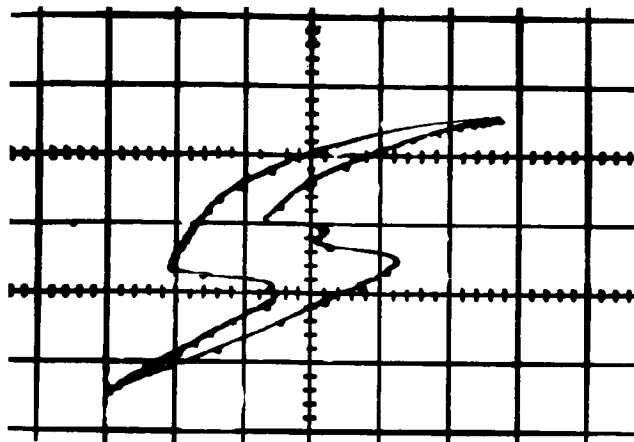


Figure 8

Oscillogram of Clapper Type Relay "A₁"
Operated on Low Voltage

Traces:

Vertical axis: Flux

Horizontal axis: Magnetomotive force

Trace: Modulated in equal time increments

Oscillogram data:

Flux scale: K_y maxwells per centimeter

Magnetomotive force scale: K_x gilberts per centimeter

Time scale: 5 milliseconds per dot on trace

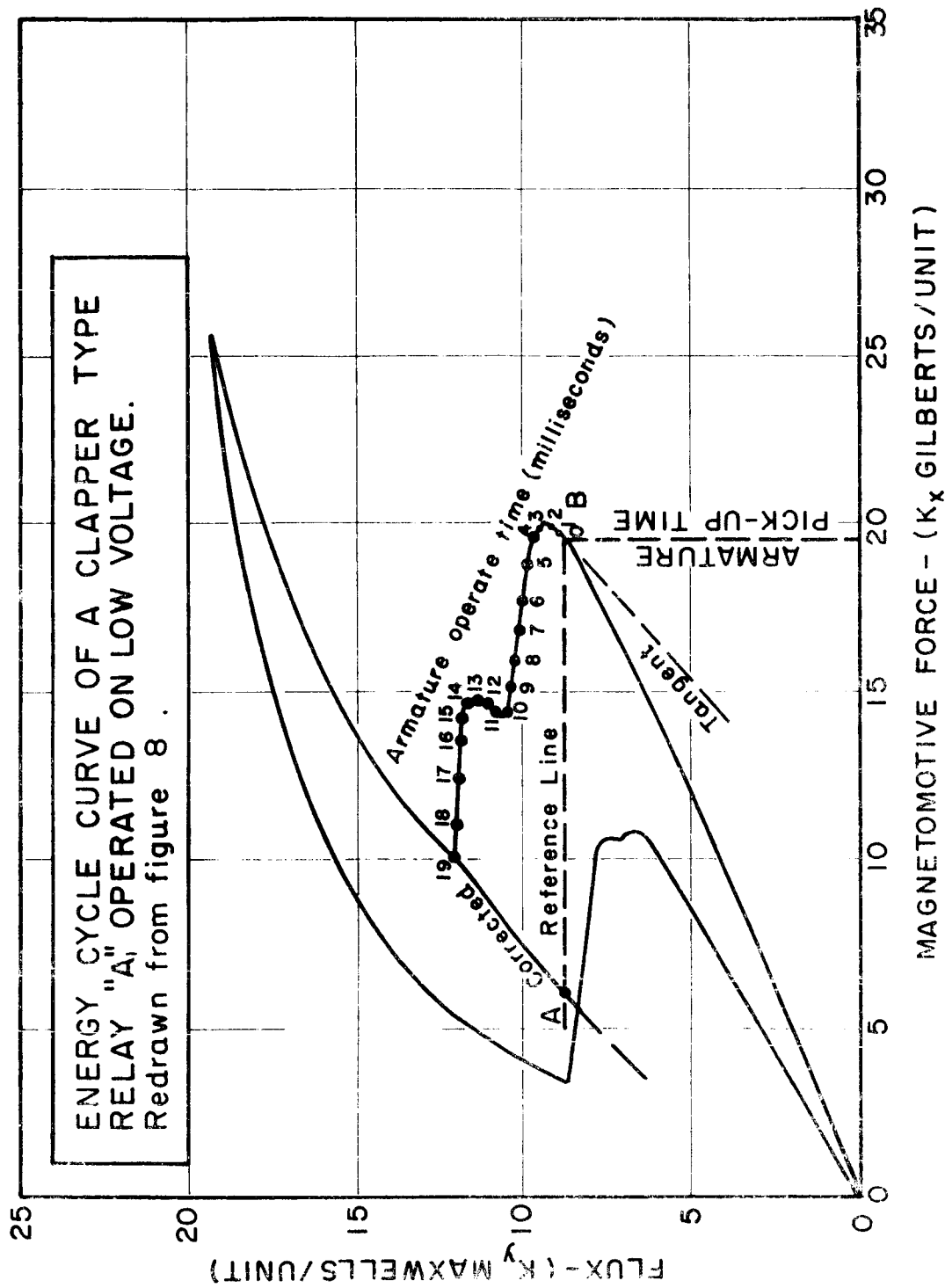


Figure 8a

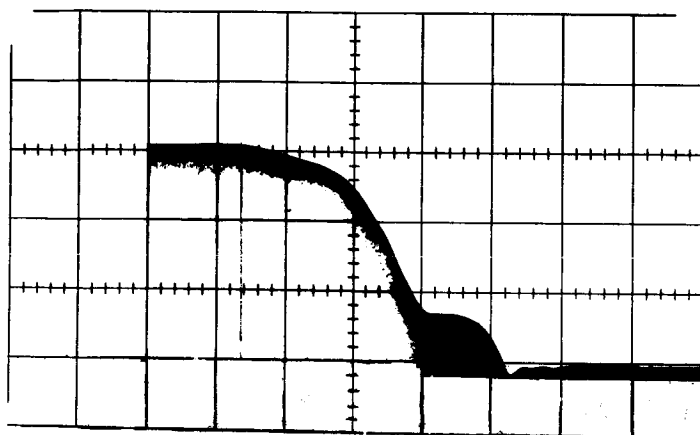


Figure 9

Oscillogram of Clapper Type "A₁" Relay

Trace:

Vertical axis: Armature displacement

Horizontal axis: Time

Oscillogram data:

Armature displacement scale: 33% of armature travel
per centimeter

Time scale: 5 milliseconds per centimeter

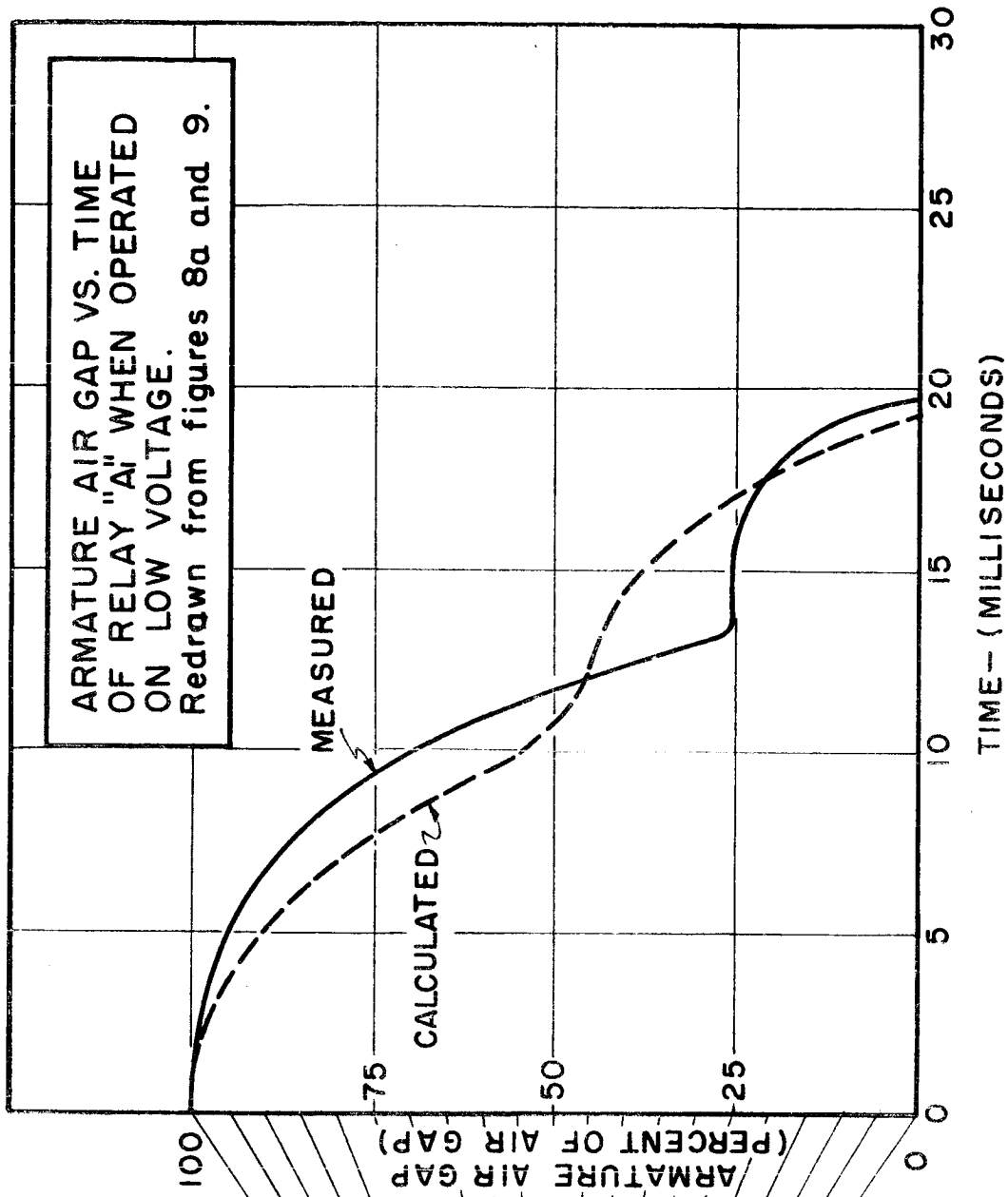
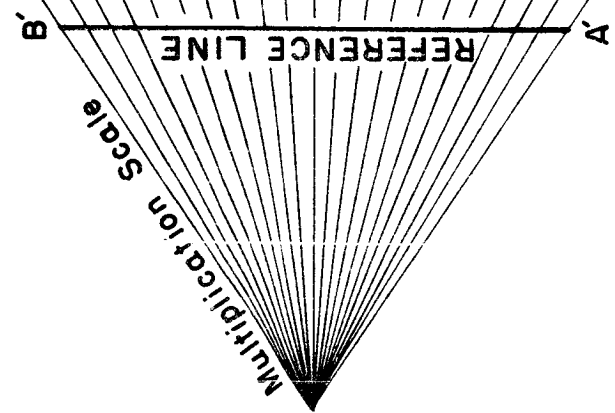


Figure 9a



SECTION III

PROPOSED FIGURE OF MERIT FOR POWER RELAYS

It is desirable to have some qualitative measure to aid in the evaluation of one power relay type for its suitability for missile application relative to another power relay type. One possible solution is to develop a relationship which contains those requirements which must be satisfied and those other parameters which represent desirable, but not critical requirements.

In general, the final design of a device is a compromise and it is necessary to be able to determine if the compromise is essentially an optimum one. By this is meant that it might be possible to adjust one parameter a small amount and thereby gain a greater amount on another parameter of equal importance. For example, because of the interrelationship between the coil power and the coil volume for a given amount of mechanical work, one type of design might decrease the coil volume and thereby increase the required coil power to do a given job while another might use a larger coil volume and thereby use less power. It would be desirable, therefore, to have some means to account for this "trade off". A problem associated with this determination of a figure of merit for a power relay is the fact that every parameter does not have the same weighting factor associated with it. For example, if the relationship between power and weight associated with the power supply is 40 watt-hours per pound of weight then a different weighting factor would probably apply than if the relationship was 80 watt-hours per pound. These weighting factors would, in general, be the same for any particular evaluation and so every device under consideration would have the same factors applied to it. Since this figure of merit is proposed as a relative evaluation and not as an absolute evaluation, then the value of the weighting factors is not as critical because the same value is

used in all cases. In this discussion all factors will be considered to have equal weight.

Determination of the parameters which make up the figure of merit involves including those which are important and those which should have some kind of bound on them. In missile applications, the G level the device will stand is of absolute importance. Other parameters such as coil power, relay weight and/or volume are also important. Factors such as contact voltage and current ratings are important since they indicate the amount of mechanical work the actuator must perform. Another parameter which should be considered is the operate time since this is influenced by coil power and coil volume and since too large a value for this might be unsatisfactory. The number of the predicted operations of the contacts might also be a factor.

To develop this figure of merit, these factors should be arranged so that the most desirable values of these factors will either maximize or minimize the figure of merit. Assume that it is desirable to arrange to have the figure of merit be large for the "best" values of the parameters. With this assumption, let the figure of merit be by the following form.

$$\text{merit} = \frac{G \Sigma V_c I_c}{(t_s)(P_c)(\text{wt.})(\eta)} \quad (1)$$

where G = acceleration in G's
 V_c = contact voltage rating
 I_c = contact current rating
 t_s = plunger or armature seating time
 P_c = coil power at rated voltage
 wt = weight
 Σ = sum of ' - - -

η = stability factor (ratio of pick-up to
steady state current)

These factors are so placed that a larger value of the figure of merit indicates a more acceptable device. In order to get some idea of the values involved, the following several cases are given.

For the parallel two coil 300 amp power relay the values of the parameters in equation 1 are

V_c = 28 volts

I_c = 300 amps

one set of power contacts

t_s = 18.2 ms

P_c = $(28)^2/24 = 32.7$ watts (operate coils)

wt = 26 oz.

η = 0.55

G = 20 (as given by manufacturer, failed
20G in one plane at 330 cps)

The merit figure for this relay not including the power rating of the auxiliary contacts is

$$\text{merit} = \frac{20 (28)(300)}{(18.2)(32.7)(26)(.55)}.$$

merit = 19.75 (operate position)

Since this is a two coil operate, one coil hold arrangement, a more indicative value would be determined by using the hold coil power required and not the operate coil power required. The hold coil power is 16.35 watts so the merit figure is

merit = 39.5 (hold position)

The next case is the series two coil 300 amp power relay. The values of the parameters involved are:

$V_c = 28$ volts
 $I_c = 300$ amps
one set of power contacts
 $t_s = 22.5$ ms
 $P_c = 27.6$ watts (operate power)
 $P_c = 7.55$ watts (hold power)
 $wt = 30$ oz.
 $\eta = 0.52$
 $G = 20$

The merit figure is

$$\text{merit} = \frac{20 (28)(300)}{(22.5)(27.6)(30)(.52)}$$

merit = 17.3 (operate position)

merit = 63.2 (hold position)

The 75 amp rotary modified unit will be considered next. The values of the parameters involved are:

$V_{c1} = 28$ volts
 $I_{c1} = 75$ amps
two sets of power contacts and two sets of auxiliary contacts
 $V_{c2} = 28$ volts
 $I_{c2} = 25$ amps
 $t_s = 17.8$ ms
 $P_c = 19.5$ watts

$$\begin{aligned} \text{wt} &= 38.4 \text{ oz.} \\ \eta &= .436 \\ G &= 5G \text{ (measured)} \end{aligned}$$

The merit figure is

$$\begin{aligned} \text{merit} &= \frac{5[2(28)(75) + 2(28)(25)]}{17.8 (19.5)(38.4)(.436)} \\ \text{merit} &= 4.8 \end{aligned}$$

For additional comparison, consider the 3 pole 25 ampere flat clapper type. The value of the parameters involved are:

$$\begin{aligned} V_c &= 28 \text{ volts} \\ I_c &= 25 \text{ amps} \\ 3 \text{ pole} \\ t_s &= 20 \text{ ms} \\ P_c &= 14.8 \text{ watts} \\ \text{wt} &= 19.2 \text{ oz.} \\ \eta &= .41 \\ G &= 10 \end{aligned}$$

The merit figure for this type is

$$\begin{aligned} \text{merit} &= \frac{10[3(25)(28)]}{20(14.8)(19.2)(.41)} \\ \text{merit} &= 9.0 \end{aligned}$$

On the basis of holding power the figure of merit values for the four cases are:

Parallel two coil - - 39.5
Series two coil - - - 63.2
Modified rotary - - - 4.8
3 pole clapper - - - 9.0

Two of the types at present do not meet the minimum G requirement so probably should not be compared on the same basis as the two types which meet the minimum G requirements. On the modified rotary it now appears possible to redesign the unit so that it will meet the minimum G level of 20 g's. This will probably require some additional weight but the increase in G level will be much greater than the corresponding increase in weight.

In comparison of the figures of merit, the two types involving the operate-hold arrangement have much larger values of merit figures. One reason this is so is that only the hold coil power is used in the comparison listed above. Comparing them on the basis of the steady state power associated with the operate position the following list results:

Parallel two coil - - 19.75

Series two coil - - - 17.3

Modified rotary - - - 4.8

3 pole clapper - - - 9.0

One obvious problem associated with the operate-hold two coil arrangement is the switch used to control the coil arrangement. Possible malfunctioning of it could result in the relay not operating. Another point in regard to the series two coil arrangement is that the instantaneous current into the coil terminals is larger than the steady state current. This is caused by the fact the operate coil is magnetically coupled to the short circuited hold coil.

The figure of merit approach does help point out in a quantitative manner the influence of the values of the parameters. For example, the series two coil type shows up as having the largest value of merit figure mainly because of its low holding power. While the modified rotary has such a low value because of its low G level. The figure of merit approach apparently

brings out these advantages or deficiencies which ever is the case.

The next work to be undertaken in this approach is to determine what values other parameters should have to maximize the figure of merit. Until a more quantative relationship is developed for the voltage-current rating of the contacts, work on maximizing this merit figure will not be too productive.

TABLE OF CONTENTS

Part C

CONTACTS

<u>SUMMARY</u>	<u>Section</u>	<u>Interim Report</u>
The Contact Subsystem - Objectives of Research- - - - -	I	10th
Contact Simulation on the Digital Computer- - - - -	III	11th
Some Energy, Temperature and Material Transfer Relations for Relay Contacts- - - - -	V	13th

Tab Color Code

Orange	9th Interim	1 July - 30 Sept., 1963
Rose	10th Interim	1 Oct. - 30 Nov., 1963
Green	11th Interim	1 Dec., 1963 - 31 Jan., 1964
Blue	12th Interim	1 Feb. - 31 March, 1964
Yellow	13th Interim	1 April - 31 May, 1964

SUMMARY

Part C

Contacts

The primary objective being pursued in this area is the determination of the relationship between the contact material transferred and the probability of failure and the determination of the companion relationship between material transferred and the contact system parameters. The contact system parameters involve those which are mechanical such as, contact forces, impact and opening velocities and accelerations, bounce, thermal conductivity and temperature, those which are environmental such as, atmosphere temperature, gas mixture, pressure, humidity and rate of gas flow.

In section two of this part a calculation of the energy transformed in the arc during contact opening is determined by numerically solving the differential equations which represents the arc characteristics, the power source and load characteristics. Only limited experimental data has been obtained so that correlation of calculated and experimental data is also limited. Equipment has been developed and is being assembled to measure the arc energy per operation and also to measure the contact material transferred. This data is to be correlated to determine the relationship existing between contact material transferred and arc energy.

The last section presents some of theory associated with the mechanism by which the material from the contact is transferred. This discussion and energy balance development is limited to the "short arc" condition.

SECTION I
THE CONTACT SUBSYSTEM:
OBJECTIVES FOR RESEARCH

I Introduction

The objective of relay contact study is, in general terms, to develop principles and relations which will allow the design engineer to select materials and construct a contact system to meet a specified set of requirements. In more specific terms (see reference 1) the design process may be defined in the following way:

Given a set of criteria (requirements to be met by the system) the design process consists of establishing a set of specifications (materials, size, etc.) that satisfy the given criteria.

The set of all criteria and specifications constitute the parameters of the contact system. The objective of relay contact research, then, is to obtain relations between the parameters of the contact system. The ultimate goal, of course, is to relate the criteria to the specifications.

II Definition of the Contact System

The switching contact is known to be an extremely complex device. One class of phenomena associated with contact operation can be described empirically but are not understood theoretically. Another group of characteristics of contacts has never been studied with the objective of relating the criteria of operation to the specifications. Because of this lack of carefully organized information, it is necessary to define carefully the device under study. A tentative definition of the contact subsystem is as follows.

Contact Subsystem

The contact subsystem is defined to be the contact material and the atmosphere surrounding the contacting surfaces.

This definition provides careful delineation of several phenomena associated with contact operation. The circuit subsystem, as well as the mechanical subsystem, must be coupled to the contact subsystem as shown below in Figure 1.

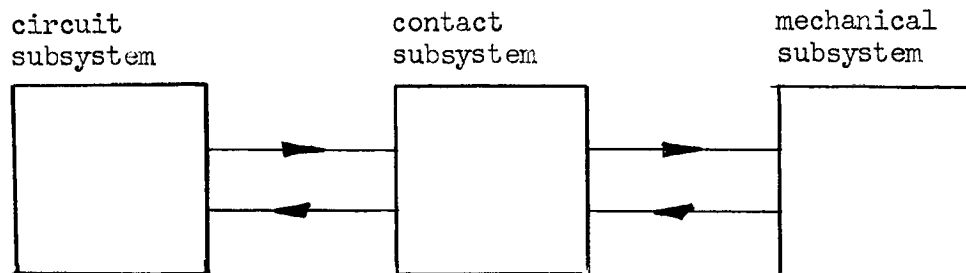


Figure 1

This system diagram helps to place in perspective the inter-relation among the three major classes of parameters of interest. Here, the contact circuit subsystems will (most often) unilaterally influence the design of the contact subsystem. On the other hand, design parameters relating the contact subsystem to the mechanical subsystem will generally be adjusted bilaterally. As the interest here is in high current contactors, this discussion will be limited to contact subsystems in this class.

III Design Criteria

The criteria to be applied to the design process will depend upon the particular application at hand. However, if the contact research engineer is to work efficiently toward his objective, he must have at hand at least a set of fundamental criteria. Each specific criteria represents a goal of one phase of the research project. A few of the criteria fundamental to contact design are:

- (a) number of operations to failure of relay
- (b) contact resistance
- (c) contact linearity
- (d) time to circuit open after operation initiated
- (e) time to circuit close after operation initiated
- (f) duty cycle
- (g) cost
- (h) size and weight

IV Design Parameters

The parameters which influence the design of the contact subsystem may be divided into two classes. A group of these parameters will be specified by the application at hand; these we shall call the specified parameters. Another group will be determined by the specified parameters and the criteria. The specified parameters are of particular interest to the research engineer since they should form conceptually a set of independent variables of the system. A number of specified parameters associated with the contact subsystem are listed below. Not all of these will be specified in every application however.

I Specified parameters of the contact circuit subsystem

- (a) current (steady state and transient)
- (c) open circuit voltage (a.c. or d.c.)
- (d) impedance of the circuit (including any nonlinearities)

II Specified parameters of the mechanical subsystem

- (a) force on closing contacts
- (b) speed of opening and closing contacts
- (c) acceleration of opening and closing contacts

- (d) bounce (frequency and magnitude)
- (e) thermal conductivity
- (f) temperature

III Specified parameter of the contactor subsystem

- (a) temperature of the atmosphere
- (b) gas content of the atmosphere
- (c) humidity of the atmosphere
- (d) velocity of the atmosphere

V Relations for the Design Process

The complex nature of the contact system provides a number of challenging problems for the research engineer. Some of these are difficult because of the nature of the system involved; others have not previously been studied. The very fact that materials play a primary role in the design process is important. The thermal, electrical, and mechanical properties of materials commonly used for contacts do not follow the linear relationships to which the design engineer is accustomed. This is especially true of the electro-mechanical phenomena associated with contact operation.

One of the most important design criteria of the contact subsystems is the number of operations to failure. There are several types of failure of particular interest. These are:

- (a) contact circuit will not open
- (b) contact circuit will not close
- (c) contact circuit closes when contacts are in open position
- (d) contact circuit opens when contacts are in closed position

Failures of type (a) and (b) are of special interest to the high current relay designer. Here, material removed from the contacts upon opening may

establish a steady arc in the space between the contacts, preventing the circuit from opening. On the other hand, if the circuit does open, the material removed from the contacts during the trial of the arc may prevent reclosing the circuit.

Relations have not been established to relate the material transfer during the switching operation of the contacts to the probability of failure. Material transfer is defined as follows:

Material transfer is the removal of material from the contact regardless of where it is deposited.

Thus, the relations between probability of failure and material transfer may be classified in two ways.

- (a) The probability of failure due to material transfer in which the material is not deposited on the contactor subsystem.
- (b) The probability of failure due to material transfer in which the material is deposited on the contactor subsystem.

Material transfer in high current contactors is known to be due primarily to three phenomena (reference 2).

- (a) Bridge transfer (sometimes called fine transfer.) A molten bridge of the contact material is formed at small spacings, especially upon opening the contacts.
- (b) Short arc transfer. Material is transferred here by the ion current of the arc. This arc is distinguished from the plasma arc (c) by the fact that its diameter is several times greater than the length.
- (c) Plasma arc transfer. Material is transferred by the ion current and diffusion.

While there has been an appreciable amount of work on the relations between material transfer and the parameters of the circuit subsystem, no generally acceptable result has been established for the high current contactor.

The other criteria listed in section III are, for the most part, directly related to the phenomena described above. Thus, once the material transfer process is understood, the research engineer will be prepared to study the other criteria, searching for the relations of interest to the design engineer.

VII Specific Research Objectives

As indicated above the research objective at this time quite naturally involves a study of the relations between (1) material transfer and the probability of failure, and (2) material transfer and the circuit parameters. Because of the complexity of the problem and the radically different phenomena involved, it is necessary to limit the field of study. The hope is, of course, to be able to enlarge the area being studied at a later time. Initially, failures of type (a) and (b) will be studied. Failures of type (c) occur primarily in high voltage circuits and those of type (d) are not common to high current contactors. Short arc and plasma material transfers are of primary interest in the high current contactor and the investigation will deal first with these.

References:

1. Analyze, Study, and Establish An Optimum Power Relay Design; January 1 to June 30, 1962; NAS 8-2552.
2. Electric Contacts Handbook; R. Holm, 3rd Edition; Berlin, 1958.

SECTION III
CONTACT SIMULATION ON
THE DIGITAL COMPUTER

In Section I of the Tenth Interim Report (1) it was stated that one of the immediate objectives of contact research was to study the relations between contact material transfer and the parameters of the circuit connected to the contacts. One of the present areas of investigation (1) is the relation between the energy dissipated by the arc of the opening contacts and the material transferred. Historically the current through a pair of opening contacts has been thought to strongly influence the amount of material transferred. Thus, with the overall objective in mind, a method of calculating the current, voltage, instantaneous power and total energy dissipated by a set of opening contacts has been developed and checked experimentally.

During the course of the investigation it became apparent that the original objective was not complete, and should be restated. In the Tenth Interim Report, referred to above, the relay contact system was divided into three parts for ease of analysis. These were: (1) circuit subsystem, (2) contact subsystem, and (3) mechanical subsystem. The objective should be restated to include each of the three subsystems. Thus, the goal is to determine a relation between material transfer and the parameters of the three subsystems. These will be described in detail below.

The digital computer was programmed to solve the nonlinear differential equation relating the three subsystems described above. A great deal of insight can be obtained from these calculations. For example, it is quite easy to vary a parameter of one of the subsystems without affecting any of the other mechanisms involved. Thus, the effect of certain contact

design changes over a wide range of values can be observed rapidly. These calculations will form the background for experimental work to follow.

Method of Calculation

The contact subsystem was represented by the circuit diagram shown in Figure 1. An important feature of this calculation is the ability to solve the circuit containing inductance.

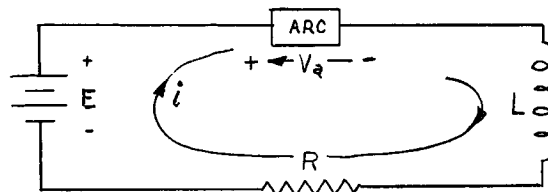


Figure 1

Representing the voltage across the arc by V_a , a function of the dependent current i and the independent variable time, t , we can write the first order differential equation of the circuit,

$$L \frac{di}{dt} + Ri + V_a(i, t) = E$$

The motion of the contact is started at $t = 0$. Thus, the initial current is

$$i(0) = \frac{E}{R}$$

The ability to solve this system hinges upon the information available for the arc voltage, V_a . A large volume of data collected by Ragana Holm (2) and others has shown that the steady state volt ampere characteristic of an arc can be represented by a set of "normalized" characteristic curves and three parameters which are chosen to characterize the material under study. The normalized curves are shown for different contact spacings in Figure 2. If I is the abscissa and V the ordinate of this normalized curve,

one may approximate.

$$V_a = \zeta(V + V_m)$$

$$I_a = I + I_m$$

Here V_m is the so called minimum voltage of the arc corresponding to the cathode material; I_m is the minimum current of the arc approaching the value of the anode material, and ζ is a correction factor to correct for plasmas in which the voltage gradient is unusually high. These parameters are influenced by the type of atmosphere, humidity, cleanness of contact, and shape of the electrode.

It is reasonable to question the application of these static curves to the dynamic problem under study. In this regard it is interesting to consider the analogous relation between the arc v-i curves and similar static curves for vacuum tubes and transistors. Static curves for these devices are useful for dynamic conditions below the frequencies at which the capacity of the nonlinear device becomes significant. Perhaps it is possible to apply the static curves of the arc over a similar range of dynamic conditions. Experimental evidence presented later seems to verify this conclusion. While the capacity of the arc does play an active part in the circuit, it does not seem to influence appreciably the average current, voltage, and power of the arc. The other dynamic parameters such as temperature, ion recombination, mass transfer and electromagnetic radiation will, it seems reasonable to expect, more significantly influence the arc characteristic as the arc energy becomes large and the contact opening speed becomes greater.

Each arc length curve of the v-i characteristic is treated as the grid line of a vacuum tube characteristic. The mechanical subsystem is coupled to the contact subsystem through these curves. The spacing is,

of course, a function of time determined by the opening characteristic of the mechanical subsystem. It may be possible to simulate contact bounce through this mechanism. Thus, with a v-i characteristic to represent the arc characteristic as a function of current and time, a numerical solution can proceed. The numerical methods and program details are not of particular interest here. These are presented in the Appendix.

Calculated and Experimental

Data

Calculated and experimental data for a 2 amp relay are presented in Figures 3 through 7. The contact was used to open a circuit with the following parameters,

$$E = 25.2 \text{ volts}$$

$$R = 12.6 \text{ ohms}$$

$$L = .110 \text{ henry (air core).}$$

The maximum contact spacing was set at 1 mm and the mechanical opening time measured at 11.4 m. sec. Thus, the velocity was 87.7 mm/sec. Values of $V_m = 12.0$, $I_m = 0.0$, and $\zeta = 1.0$ were selected from data tabulated by R. Holm (2) for silver plated contacts operating in air at an elevated temperature.

The agreement between the experimental and calculated data in Figure 3 is striking. It is especially important to note that the area under the V-I plot is the total energy dissipated by the contact subsystem. Clearly the calculated value of 16.8 watt-sec. is in good agreement with the experimental data. Figures 4 and 5 do not indicate the same degree of agreement. It is quite possible that the armature did not move with the constant velocity assumed for the calculation. If, for example, the elastic

force of the molten bridge slowed the initial velocity, the computed voltage would be higher than the experimental value.

Figures 8 and 9 illustrate the effect of the mechanical subsystem on the energy of the arc. Here the circuit parameters and material constants were held constant as the speed of contact opening was increased. The maximum opening distance was held constant at 1 mm. Note the large increase in arc energy for slow opening speeds.

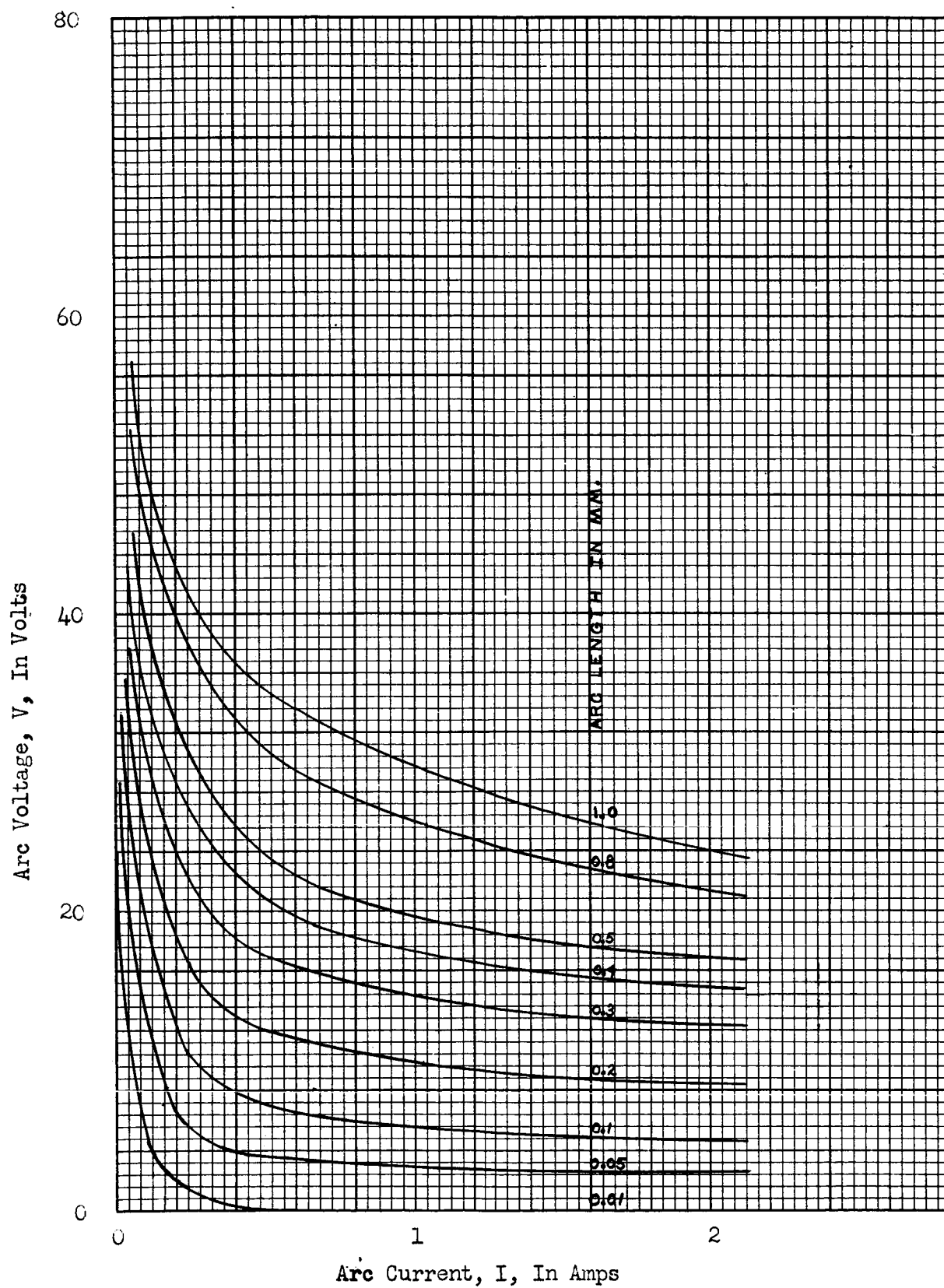


Figure 2

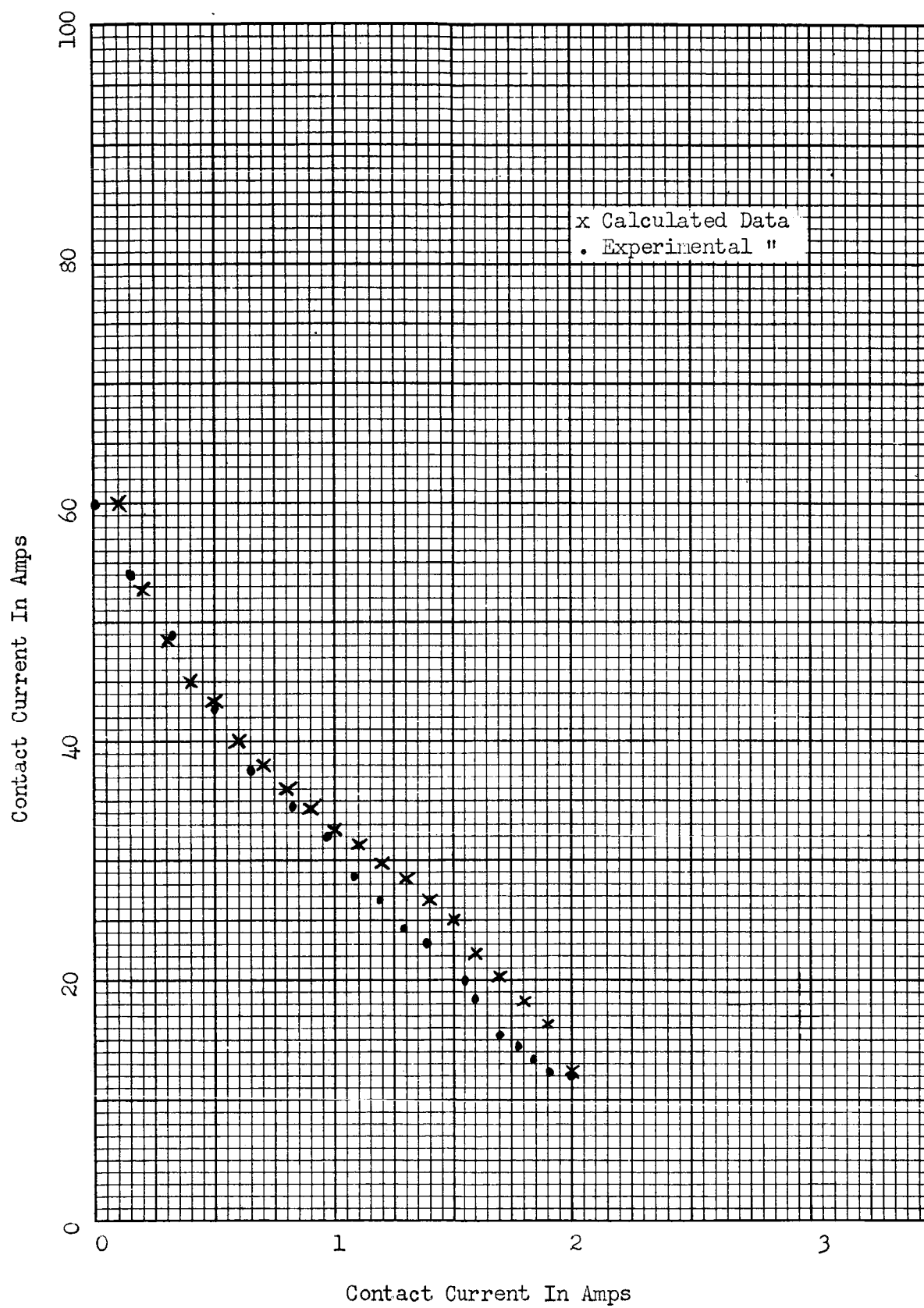


Figure 3

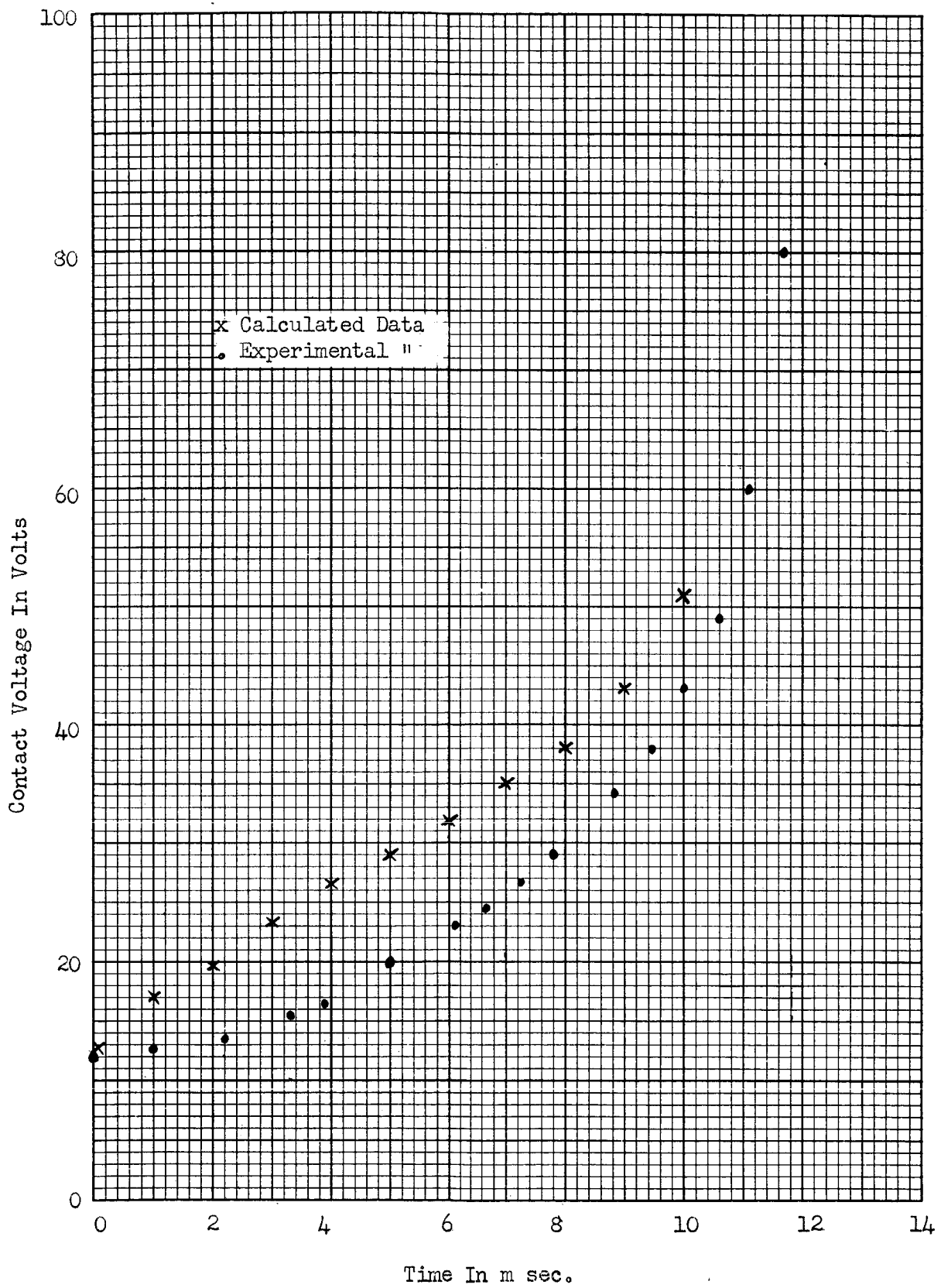
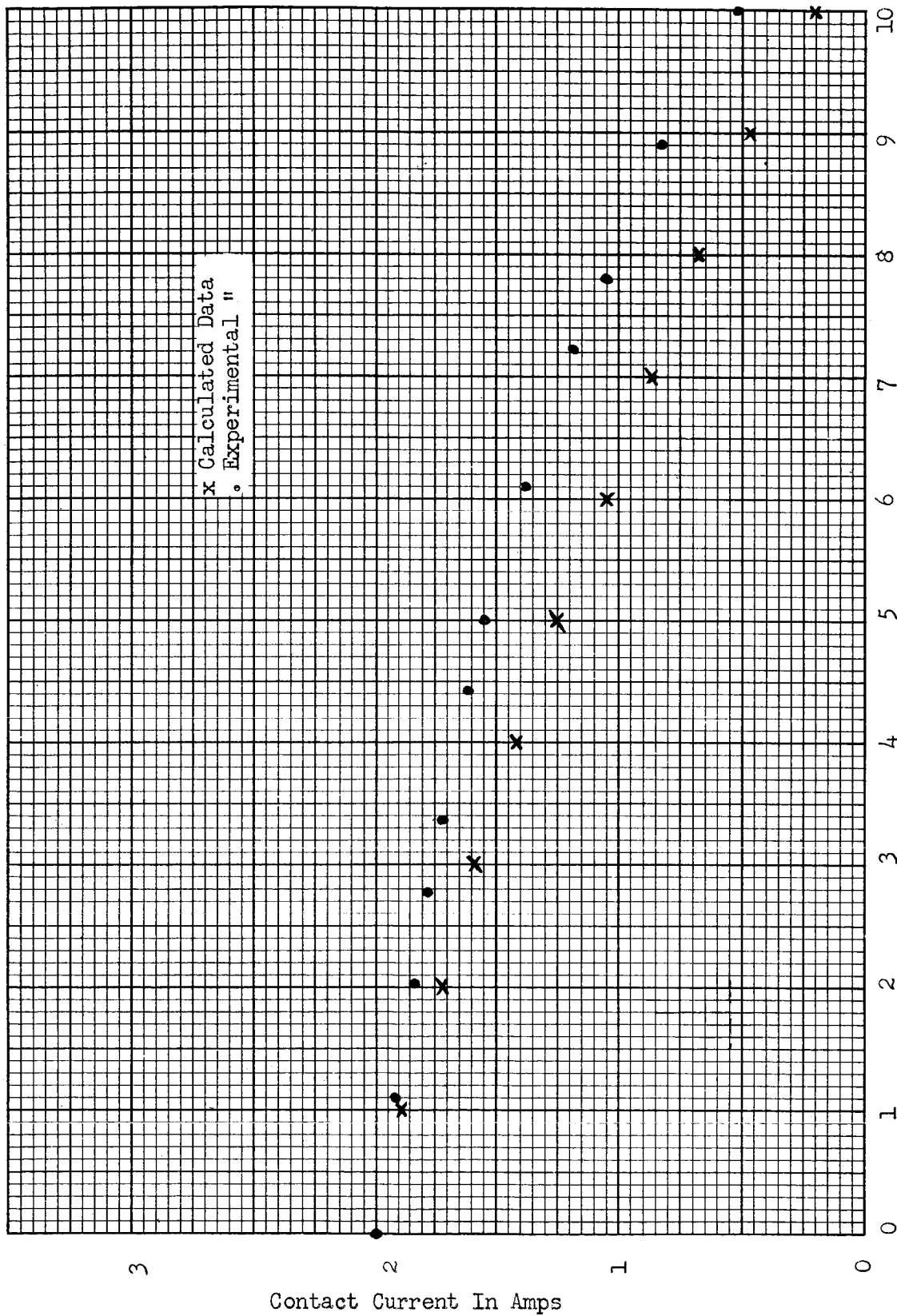


Figure 4



Time In m sec.

Figure 5

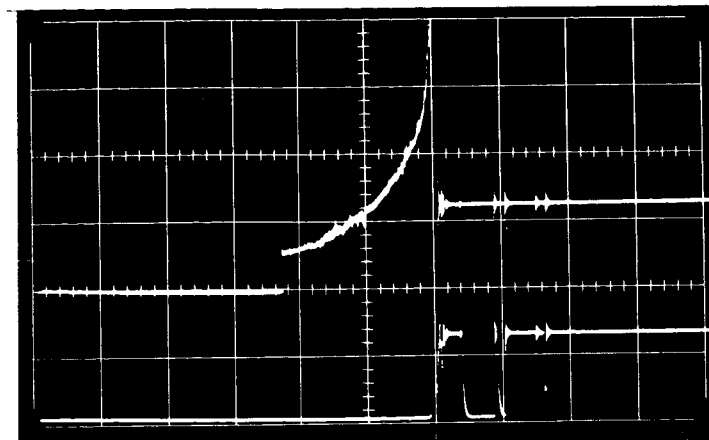


Figure 6

Contact Voltage

Vertical Scale: 20 volts/cm
 Horizontal Scale: 5 milliseconds/cm
 $E = 25.2$, $R = 12.6$, $L = 0.110$

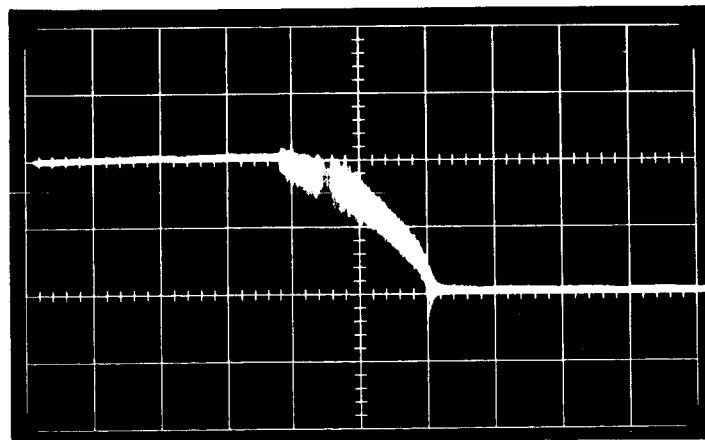


Figure 7

Contact Current

Vertical Scale: 1 amp/cm
 Horizontal Scale: 5 milliseconds/cm
 $E = 25.2$, $R = 12.6$, $L = 0.110$

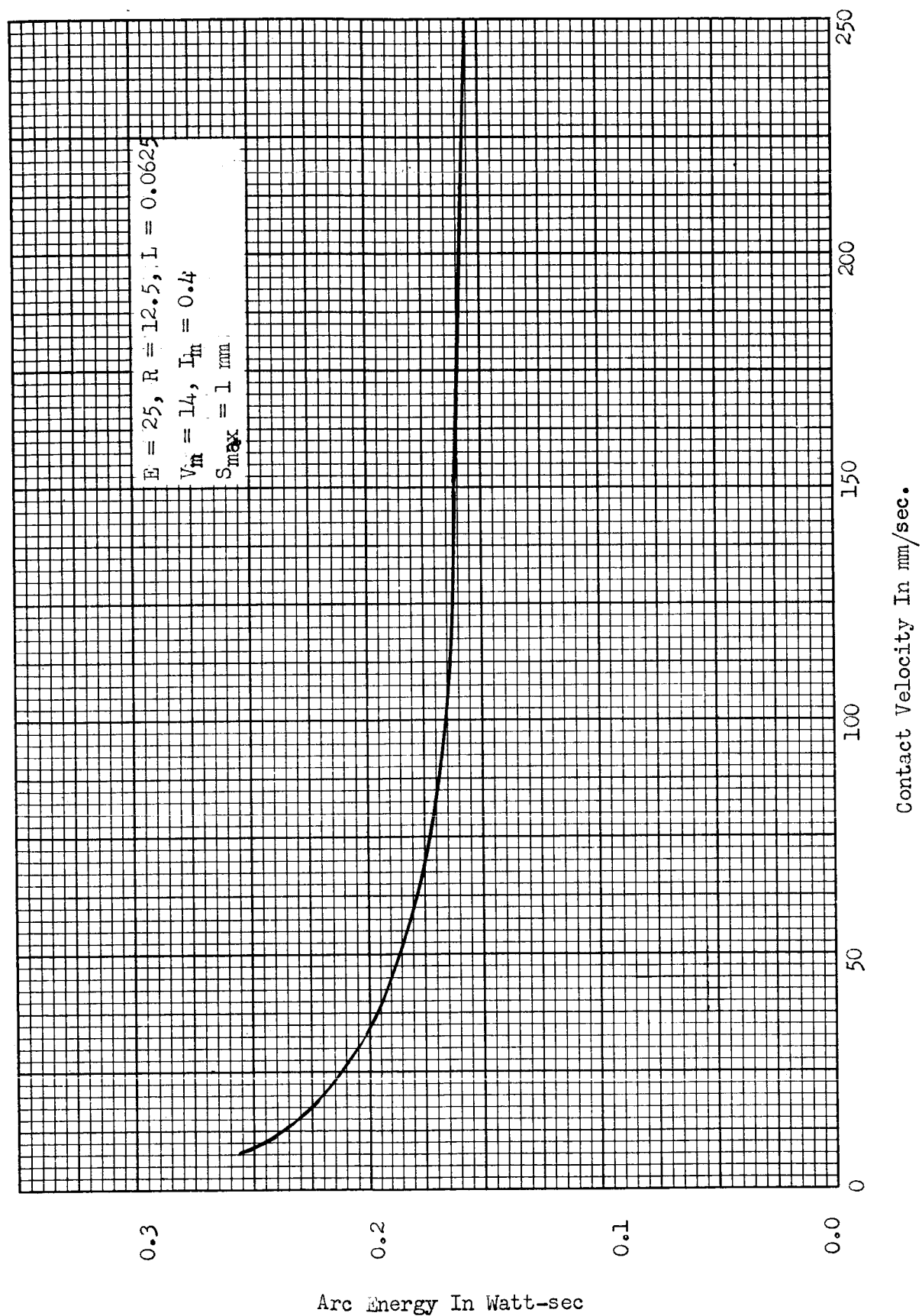


Figure 8

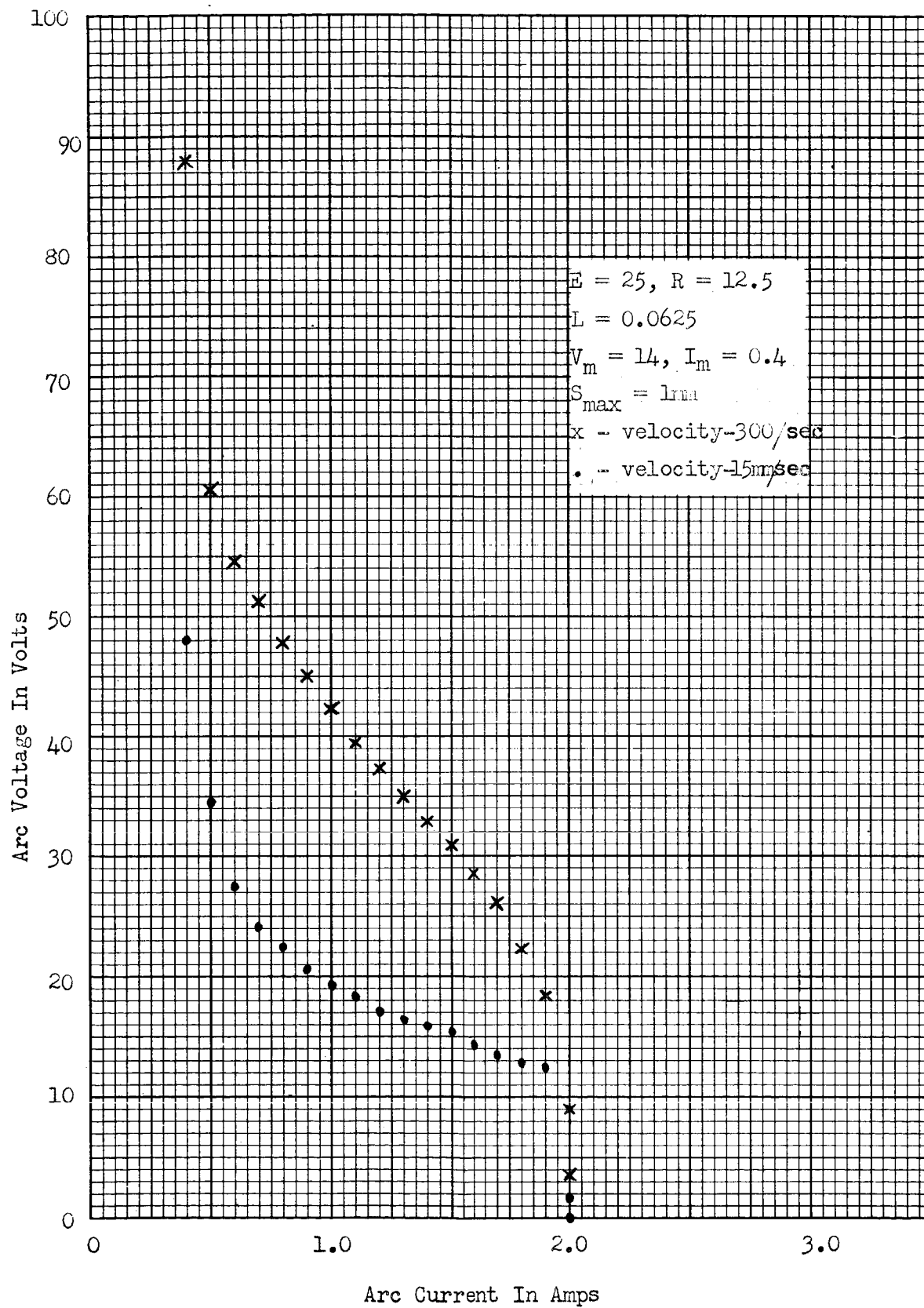


Figure 9

Appendix

A block diagram of the computer program is shown in Figure B and a listing of the program follows this section. Two aspects of the computational scheme are of particular interest. The integration procedure deserves some special comments and a method for calculating V_a will be discussed.

A predictor corrector method of integration is used to solve the differential equation. This method utilizes the slope of the curve at the present point of the solution and the value of the solution at one back point to predict the next solution point. Thus

$$y_p = y_{n-1} + 2hy'_n,$$

where y_p is the predicted solution at the point $n+1$, y'_n is the slope at the middle point n , and y_{n-1} is the solution at one back point. Having estimated the next solution point, the true value is corrected by the equation

$$y_c = y_n + h \frac{y'_{n+1} + y'_n}{2}.$$

Here the average of the slopes y'_{n+1} and y'_n is used to get the corrected solution point y_c . Expanding by a Taylor series (3) the error term can be shown to be

$$-\frac{h^3}{12} y'''(t)$$

The program is arranged to calculate this error and check to see if it is less than the value specified by the user. If the required tolerance has

been reached the value of the curve at the new point is printed. On the other hand, the program reduces the size of the interval h and repeats the above process.

Since the current curve is rather slowly changing for time near zero the integration will be quite slow. To speed the process the program estimates an increment h based upon the largest current step the user will allow. Thus, the program automatically selects the optimum interval.

The arc voltage, V_a , is interpolated from a table of numerical values taken from Figure I. Given the current I_o and a contact spacing S_o , four values of arc voltage are read from the table. These correspond to values of current and spacing on either side of the desired I_o , S_o , as indicated in Figure A.

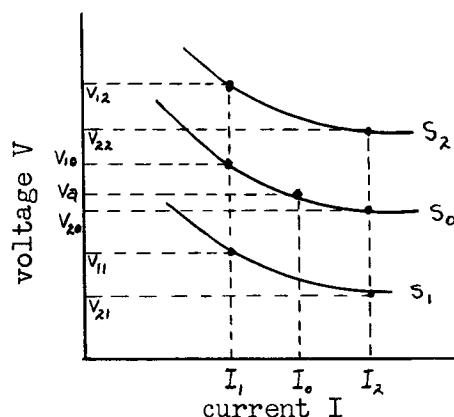


Figure A

The two values, V_{10} and V_{20} , are calculated by the linear interpolation equations

$$V_{10} = V_{11} + (V_{12} - V_{11}) \left(\frac{S_o - S_1}{S_2 - S_1} \right)$$

$$V_{20} = V_{21} + (V_{22} - V_{21}) \left(\frac{S_o - S_1}{S_2 - S_1} \right).$$

A curve of the form

$$V_a(I) = (A + BI)^{-1}$$

is used to calculate the arc voltage V_a at the point

$$I = I_o .$$

The constants A and B are calculated to pass the curve through the points V_{10} and V_{20} . The equations for A and B are

$$B = \frac{V_{10} - V_{20}}{V_{10} V_{20}(I_2 - I_1)} ,$$

and

$$A = \frac{1}{V_{10}} - BI_1 .$$

Thus, V_a can be calculated as

$$V_a (I_o, S_o) = (A + BI_o)^{-1} .$$

The process described above is quite fast considering the length of the table look up and interpolation scheme. A complete calculation with an accuracy of one tenth of one percent or greater can be performed in about ten minutes.

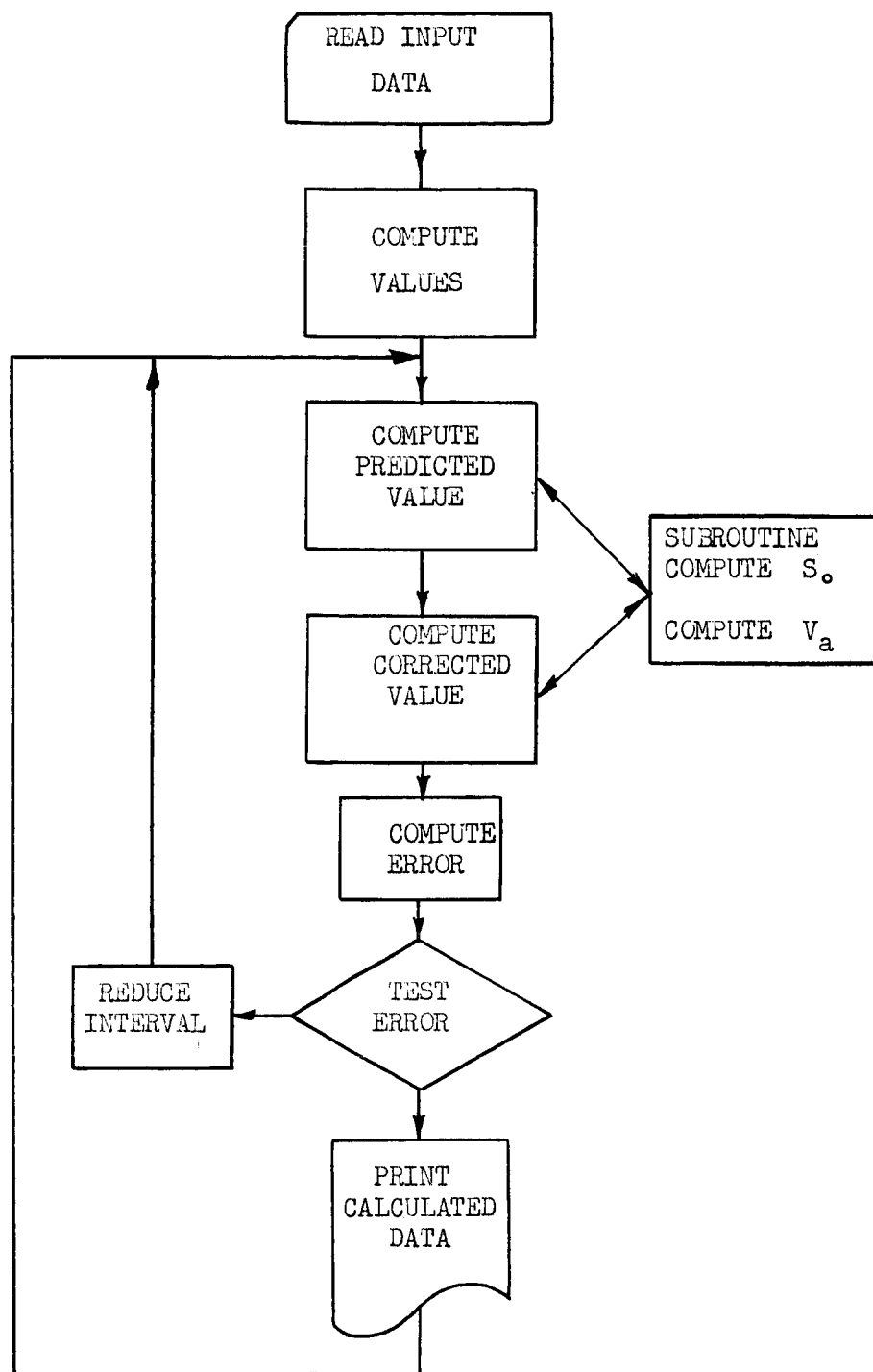


Figure B

1. The Contact Subsystem: Objectives for Research; October 1 to November 30, 1963; NAS 8-2552.
2. Electric Contacts Handbook; R. Holm, 3rd Edition; Berlin, 1958.
3. Numerical Methods for Scientists and Engineers; R. W. Hamming, New York, 1962.


```

C CONTACT SUBSYSTEM SIMULAT ON
C READ 9130,NCTL
C SUBROUTINE TO READ IN V-I DATA
C DIMENSION CS(41),VS(10,41),C(41),V(10,41),S(10)
0001 READ 9000,NS,NC
C ROUTINE TO READ V(I,J) USES C(I) FOR AUX STORAGE
D0 0010 I=1,NC
READ 9010,C(1),C(2),C(3),C(4),C(5),C(6),C(7),C(8),C(9),C(10)
D0 0010 I=1,NS
VS(I,J)=C(I)
C ROUTINE TO READ AND CALCULATE C(I)
0010 READ 9010,CS(1),CINC
C D0 0020 I=2,NC
CS(I)=CS(I-1)+CINC
C ROUTINE TO READ IN S(I) VALUES
0020 READ 9010,S(1),S(2),S(3),S(4),S(5),S(6),S(7),S(8),S(9),S(10)
C END SUBROUTINE
C ROUTINE TO ADJUST V-I DATA
0025 READ 9010,VM,CM
D0 0030 I=2,NS
D0 0030 I=1,NC
V(I,J)=VS(I,J)+VM
D0 0040 I=1,NC
C(I)=CS(I)+CM
0040 END ROUTINE
C *****
C ROUTINE TO READ IN CONSTANTS OF THE PROBLEM
C READ 9010,E
C READ 9010,R
C READ 9030,DUC
C READ 9010,AA
C READ 9010,W
C READ 9010,XMAX
C READ 9010,DELI
C READ 9010,TOL
C READ 9030,HMAX
C PRINT 9040
C PRINT 9050,VM,CM
C PRINT 9060,E,R,DUC
C PRINT 9070,AA,W,XMAX
C PRINT 9080,DELI,TOL

PRINT 9090
PRINT 9100
END ROUTINE
C *****
C COMPUTE INITIAL VALUES
ENER=0 0
X=0 0
VA=0 0
YO=E/R
Y1=Y0
T0=0.0
T1=1.0E-12
ESTIMATE H
C0=Y1
T=T1
KX=1
GO TO 3000
S0=X
KVA=1
GO TO 1000
YD1=(E-VA-R*Y1)/DUC
H=DELI/ABSF(YD1)
IF (H-HMAX)0125,0125,0126
H=HMAX
C *****
C COMPUTE PREDICTOR
T2=T1+H
YP=Y0+(T2-T0)*YD1
C COMPUTE CORRECTOR
C0=YP
T=T2
KX=2
GO TO 3000
S0=X
KVA=2
GO TO 1000
YD2=(E-VA-R*YP)/DUC
YC=Y1+(T2-T1)*(YD2+YD1)/2.0
C COMPUTE ERROR
ERROR=ABSF((YC-YP)/(YC+YP))*100.0

```

```

0150 IF (ERROR-TOL)0160,0160,0150
      H=H/2.0
      GO TO 0125
C     ESTABLISH DATA POINT
0160 Y2=YC+(YP-YC)/5.0
      PA=VA*Y2
      VD=DUC*YD2+R*Y2+VA-E
      PRINT 9110,T2,Y2,VA,PA,VD,ERROR
      ENER=ENER+PA*(T2-T1)
      Y0=Y1
      T0=T1
      Y1=Y2
      T1=T2
      IF (Y1-C(1))0170,0170,0105
0170 PRINT 9120,ENER
      PRINT 9130,NCTL
      GO TO 0025
C     *****
C     SUBROUTINE TO CALCULATE VA
1000 IF (S0)1020,1010,1030
1010 VA=0.0
      GO TO 1130
1020 K=1
      GO TO 2000
1030 IF (S0-S(NS))1040,1040,1020
1040 DO 1050 I=1,NS
      IF (S0-S(I))1060,1060,1050
1050 CONTINUE
1060 IS=1
      S2=S(I)
      S1=S(I-1)
      AUX1=(S0-S1)/(S2-S1)
      IF (C0)1080,1070,1090
1070 VA=V(IS-1,I)+(V(IS,1)-V(IS-1,1))*AUX1
      GO TO 1130
1080 K=2
      GO TO 2000
1090 IF (C0-C(NC))1100,1100,1080
1100 DO 1110 I=1,NC
      IF (C0-C(I))1120,1120,1110
1110 CONTINUE
1120 IC=1
      C2=C(I)
      C1=C(I-1)

```

```

V22=V(IS,IC)
V21=V(IS-1,IC)
V12=V(IS,IC-1)
V11=V(IS-1,IC-1)
V20=V21+(V22-V21)*AUX1
V10=V11+(V12-V11)*AUX1
B=(V10-V20)/(V10*V20*(C2-C1))
A=1.0/V10-B*C1
VA=1.0/(A+B*C0)
CONTINUE
1130 GO TO (0120,0140),KVA
C     END OF SUBROUTINE
C     *****
C     ERROR SUBROUTINE
2000 PRINT 9020,K
      PAUSE
      GO TO 0105
C     END OF SUBROUTINE
C     *****
C     SUBROUTINE TO COMPUTE CONTACT OPENING
3000 IF (W*T-1.5708)3010,3020,3020
3010 X=AA*SINF(W*T)
      IF (X-XMAX)3030,3030,3020
3020 X=XMAX
      GO TO (0110,0130),KX
3030 GO TO 0130
C     END OF SUBROUTINE
C     *****
9000 FORMAT (F7.2,F7.2,F7.2,F7.2,F7.2,F7.2,F7.2,F7.2,F7.2)
9010 FORMAT (1X,13HPROGRAM ERROR,13)
9020 FORMAT (E10.4,2X,E10.4,2X,E10.4,2X,E10.4,2X,E10.4,2X,E10.4)
9030 FORMAT (1X,30HCONTACTS IMULATION, INPUT DATA)
9040 FORMAT (1X,5HVM = ,F6.2,5X,5HIM = ,F6.2)
9050 FORMAT (/1X,5HSHW = ,F6.2,5X,5HSHL = ,E10.4)
9060 FORMAT (/1X,5HE = ,F6.2,5X,5HHR = ,F6.2,5X,5HHL = ,E10.4)
9070 FORMAT (/1X,5HAA = ,E10.4,5X,5HWA = ,E10.4,5X,5HWA = ,E10.4)
9080 FORMAT (/1X,7HDELI = ,E10.4,5X,6HTOL = ,E10.4)
9090 FORMAT (/1X,11HOUTPUT DATA)
9100 FORMAT (/6X,4HTIME,12X,4HAMP,12X,2HVA,14X,2HVD,14X,5HERR
      10R)
9110 FORMAT (1X,6E16.6)
9120 FORMAT (/1X,13HARC ENERGY = ,E14.8)
9130 FORMAT (11)
      END

```

SECTION V

SOME ENERGY, TEMPERATURE AND MATERIAL TRANSFER RELATIONS FOR RELAY CONTACTS

I. Introduction

One specific objective of contact research is to identify and describe by a mathematical model the parameters of the relay contact subsystem which control the probability of failure of the contacts. An important aspect of this study is the determination of the material transferred in the region of the contact electrodes. The material transferred during contact operation is influenced by many factors. For example, the phenomena at contact opening is quite different from that at contact closing. The circuit parameters and mechanical subsystem can change the character of the opening and closing operation radically.

Here we will consider some of the aspects of contact opening. In particular, the circuit parameters and mechanical subsystem are assumed to produce an arc upon contact opening which is a "short arc". The bridge transfer which precedes the short arc formation is neglected. This assumption appears reasonable for medium (25 to 100 amp) current contactors operating in inductive circuits with short time constants. By short arc we mean an arc whose length s is shorter than the radius of the arc a .

$$\frac{a}{s} \geq 10 \quad (\text{See Ref. 1 and 2})$$

II. Short Arc Phenomena

We will represent the contact electrodes and the arc by the model shown in Figure 1.

Model of Short Arc

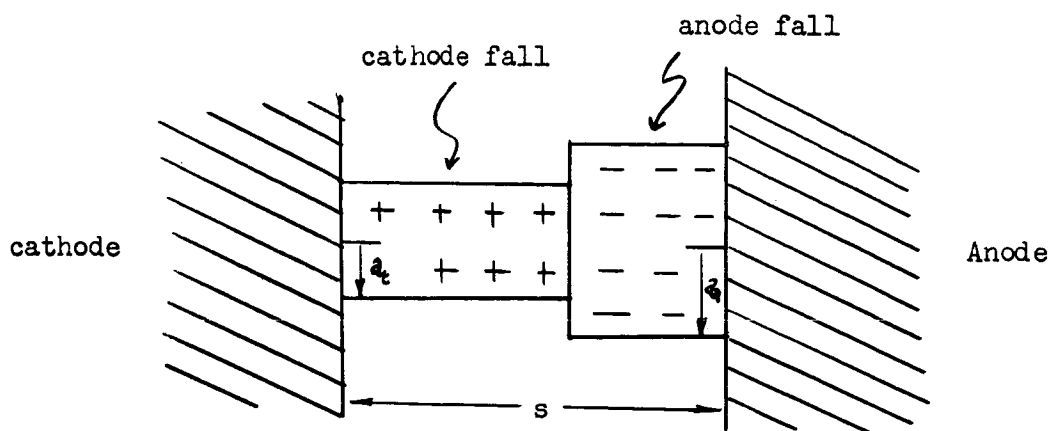


Figure 1

The cathode fall region contains a high concentration of ions. If the contacts are operating in a gaseous atmosphere, the cathode fall region will contain a mixture of gas and metallic ions. A significant flow occurs in this region. The glow is due to the photon energy released by an electron as it neutralizes an ion. Experimental evidence indicates that most of the deionization occurs on the cathode surface. The anode fall region is a dense electron cloud region.

The total voltage across the electrodes will be denoted by V , while the anode and cathode fall will be V_a and V_c , respectively. The potential distribution in the arc region is well known³.

Using Poisson's one dimensional equation

$$\frac{d^2V}{dx^2} = - \frac{\sigma}{\epsilon} \quad (1)$$

and the charge density given by

$$\sigma = - \frac{J}{v} \quad (2)$$

the potential distribution is

$$V = \frac{2}{3} \left(\frac{2J}{e\mu} \right)^{1/2} (X)^{3/2} \quad (3)$$

where μ is the mobility of the charge carrier and J is the current density. The potential and electric field are assumed to be zero at $X = 0$.

The short arc is characterized by very high current densities, 10^3 to 10^8 amps/cm². Emission of current carriers from the cathode is produced by both the Schottky and thermionic processes.

Experimental evidence indicates that the diameter of the arc at the cathode is quite small. The area of the cathode electrode covered by the arc is called the cathode spot and may be 10^{-2} to 10^{-5} cm in diameter.

In the discussion to follow, we shall assume the electrode spacing s to be constant. This appears to be a reasonable assumption for the short arc of a typical relay (Ref. 2). If the circuit contains any inductance, the voltage across the electrodes will not be constant. Thus, the power calculations which follow must be interpreted to be instantaneous quantities.

III. Instantaneous Power

Balance at the Cathode Spot

Some significant information about the energy dissipated by the arc and the material transferred by the contact electrodes can be obtained from a study of the power balance at the cathode spot, anode spot, and the arc region between the electrodes. This analysis is approached by considering separately the rate of energy input and outflow from the cathode spot. The cathode spot is assumed to have negligible energy

storage because of its small size. We shall define the entire region of molten metal to be the cathode spot.

There are five modes of power input to the cathode spot. First, ions are accelerated toward the cathode by the potential distribution of the cathode fall. They may be assumed to acquire a kinetic energy of V_c electron volts. The assumption here is that ions are produced near the cathode fall anode fall interface and there is no rebound upon striking the cathode. We represent the ion current by I_+ and recall that

$$I_+ = n q v_+ \pi a_c^2 \quad (4)$$

where N is the ion density, q the ion charge and v_+ the ion velocity. Thus, $V_c I_+$ is the rate of energy (Joules per sec) or power flow into the cathode spot by the collision energy of the ions.

The second component of energy is released by the electronic neutralizing the ions on the cathode spot surface. Letting the ionization energy be V_i electron volts, the rate at which energy is added to the cathode spot by ionization radiation is $K_{ci} V_i I_+$. K_{ci} is a proportionality constant relating the total energy radiated by the ionization process to the portion incident at the cathode spot. A reasonable estimate for K_{ci} is 0.5. Several values of V_i for gases and metals of interest are, given in Appendix I, No. III.

The total electron current, I , flowing through the cathode spot region will produce a conventional resistive heat loss. Since the cathode spot is not of simple shape (See Section VI), we must write the loss as

$$\int_{\tau_c} j^2 \rho dV \approx I^2 R_c$$

where τ_c is the volume of the cathode spot, j is the cathode spot

incremental current density, and ρ is the resistivity. This power input is represented by an equivalent $I^2 R_c$ for convenience.

A fourth heat input to the cathode spot is the radiation of energy in the cathode fall region. The gases in this region can reach temperatures as high as 3000°K at pressures 10 to 20 times atmospheric pressure. This power input will be denoted by P_{cr} .

The fifth energy input is due to the latent heat of condensation of unionized molten metal atoms in the gas near the cathode spot. This power will be designated by P_{cc} .

Energy is carried away from the cathode spot by three mechanisms. A large component of power is required to overcome the work function, ϕ , of the cathode spot metal. This power is ϕI , where I is the total arc current. The work function for several common materials is tabulated in Appendix II.

A second power outlet from the cathode spot is by way of conduction to the bulk cathode material. Although the cathode spot is not planar, one may approximate the heat flow by

$$4a_c K (T_c - T_o).$$

Here

K = conductivity of the cathode material,

T_c = temperature of the cathode spot,

T_o = temperature of the cathode bulk material.

The third power sink and one of particular interest here is the latent heat of evaporation of the cathode spot. This occurs in two steps. A fixed quantity of heat is required to melt the cathode spot material. A second component of power is removed from the cathode spot by the energy

required to change the molten cathode material to vapor. This rate of energy removal is denoted by P_{ce} . Heat of vaporization for several materials is listed in Appendix III.

Now, if the cathode spot is small, the energy stored there can be neglected; a power balance must exist between the energy input to the cathode spot and the mechanisms for power dissipation. Thus

$$V_c I_+ + K_{ci} V_i I_+ + I^2 R_c + P_{cr} + P_{cc} = \phi I + 2a_c K (T_c - T_o) + P_{ce}. \quad (5)$$

IV. Instantaneous Power

Balance at the Anode Spot

The power balance at the anode spot is similar to that at the cathode spot. Here the kinetic energy of the electron, V_a electron volts, is dissipated to the anode spot in a collision that does not have any rebound. Thus, the collision power input to the anode spot is $V_a I$. Here we assume the total current flow to be due to ions.

At the anode spot an electron gives up an energy of ϕ electron volts when it falls down the potential barrier (height of the potential barrier is the same as the work function, ϕ) at the surface of the anode spot. This power is denoted by ϕI .

As with the cathode spot, an $I^2 R$ loss given by

$$\int_{\tau_a} j^2 \rho dV \approx I^2 R_z$$

will produce heating in the anode spot.

The power input at the anode spot due to the radiation of the cathode fall gas is denoted by P_{ar} . The latent heat of condensing metal vapor

will be designated by P_{ac} .

Energy is removed from the anode spot in two ways. In the first case heat is conducted to the bulk anode material. As before this is denoted by

$$4a_a K (T_a - T_o).$$

The second case is heat removal by evaporation of the anode material. As with the cathode we denote this power by P_{ae} .

Now the power balance equation for the anode can be written.

$$V_a I + \phi I + I^2 R_a + P_{ar} + P_{ac} = 4a_a K (T_a - T_o) + P_{ae}. \quad (6)$$

V. A Significant Result

If we assume

$$\begin{aligned} P_{ar} &\approx P_{cr}, \\ P_{ac} &\approx P_{cc} \\ 4a_a K (T_a - T_o) &\approx 4a_c K (T_c - T_o), \\ (V_c + K_{ci} V_i) I_+ &\approx V_a I, \\ R_a &\approx R_c, \end{aligned} \quad (7)$$

we can subtract equation 5 from equation 6 and obtain

$$\phi I = -\phi I + P_{ae} - P_{ce}$$

or

$$P_{ae} - P_{ce} = 2\phi I \quad (8)$$

Since $2\phi I$ is greater than zero, the rate at which energy is carried from

the anode by the metal vapor is greater than that of the cathode. Thus, the anode deteriorates faster than the cathode. This fact is verified by experimental evidence (Ref. 1).

VI. Temperature Distribution in the Electrodes

The temperature distribution in the electrode face can be calculated and from this knowledge of the melting point of the electrode material, the size of the spot can be determined. We assume the radius of the arc, a , to be much smaller than the radius of the electrode material. Thus, the electrode can be represented by the semi-infinite region, $z < 0$, shown in Figure 2.

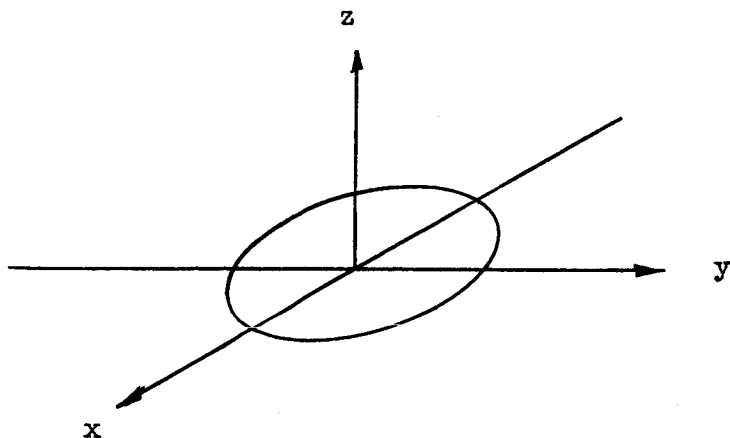


Figure 2

The temperature distribution in the electrode must obey the diffusion equation

$$\frac{\partial \theta}{\partial t} = \lambda \nabla^2 \theta. \quad (9)$$

Here $\lambda = \frac{K}{\rho c}$ is assumed to be constant throughout the electrode. K is

the conductivity of the material, ρ the density, and c the specific heat. The boundary condition applicable to this problem is one in which the heat flux $\frac{\partial \theta}{\partial n}$ is specified across the surface of the electrode. Thus,

$$\frac{\partial \theta}{\partial n} = \phi \quad r \leq a$$

$$\frac{\partial \theta}{\partial n} = 0 \quad r > a.$$

The general condition in which the heat input to the electrode is a control function of time is assumed here. The partial differential equation is not readily solved as it stands. Thus, we assume the solutions $\theta(r, z, t)$ to be a sum of two solutions, a transient solution $v(r, z, t)$ and a steady state solution $U(r, z)$.

$$\theta(r, z, t) = U(r, z) + v(r, z, t) \quad (10)$$

Symmetry eliminates any angular variation in temperature. Substituting (10) into the PDE (9) we obtain two equations to be solved,

$$\nabla^2 U(r, z) = 0 \quad (11)$$

$$\frac{\partial u}{\partial z} = \phi \quad r \leq a$$

$$\frac{\partial u}{\partial z} = 0 \quad r > a$$

and

$$\frac{\partial v}{\partial t} = K \nabla^2 v \quad (12)$$

$$\frac{\partial v}{\partial z} \neq 0 \quad r \geq 0$$

$$v(r, z, 0) = -U(r, z).$$

We solve for the steady state solution first. Multiply both sides of equation (11) by the Hankel kernel $r J_0(r)$ and integrate with respect to r from zero to infinity.

$$\int_0^\infty \frac{\partial^2 U}{\partial r^2} r J_0(r) dr + \int_0^\infty \frac{1}{r} \frac{\partial U}{\partial r} r J_0(r) dr + \frac{\partial^2}{\partial z^2} \int_0^\infty ur J_0(r) dr = 0. \quad (13)$$

We denote the Hankel transform of $u(r, z)$ by

$$U = \int_0^\infty ur J_0(r) dr. \quad (14)$$

Integrating the first integral in (13) by parts we obtain

$$\int_0^\infty \frac{\partial^2 u}{\partial r^2} r J_0(r) dr = r \frac{\partial u}{\partial r} J_0(r) \Big|_0^\infty - \int_0^\infty \frac{\partial u}{\partial r} \frac{d}{dr} [J_0(r)] dr \quad (15)$$

and

$$\begin{aligned} \int_0^\infty \frac{\partial^2 u}{\partial r^2} r J_0(r) dr &= r \frac{\partial u}{\partial r} J_0(r) \Big|_0^\infty - \int_0^\infty \frac{\partial u}{\partial r} J_0(r) dr \\ &+ ur J_1(r) \Big|_0^\infty - r^2 \int_0^\infty ur J_0(r) dr \end{aligned} \quad (16)$$

Now adding the second integral in equation (13) to both sides of equation (16) we obtain

$$\begin{aligned} \int_0^\infty \frac{\partial^2 u}{\partial r^2} r J_0(r) dr + \int_0^\infty \frac{\partial u}{\partial r} J_0(r) dr = \\ r \frac{\partial u}{\partial r} J_0(r) \Big|_0^\infty + ur J_1(r) \Big|_0^\infty - r^2 \int_0^\infty ur J_0(r) dr \end{aligned} \quad (17)$$

Evaluating the limits in (17) and requiring suitable bounds on $\partial U/\partial r$ and U we can write the right hand side as $-\zeta^2 U$. Thus, the transformed partial differential equation becomes the ordinary differential equation,

$$\frac{d^2 U}{dz^2} - \zeta^2 U = 0 \quad (18)$$

with solution

$$U = g(\zeta) e^{\zeta z} + f(\zeta) e^{-\zeta z}.$$

Since $U(\zeta, z)$ must remain finite as z approaches infinity for all ζ , $g(\zeta)$ must be zero. Thus,

$$U = f(\zeta) e^{-\zeta z} \quad (19)$$

Now we calculate the transform of the boundary condition

$$\left. \frac{dU}{dz} \right|_{z=0} = \int_0^\infty \left. \frac{\partial u}{\partial z} \right|_{z=0} r J_0(\zeta r) dr = -\zeta \int_0^a f J_0(\zeta r) dr = -\frac{a\zeta}{\zeta^3} J_0(\zeta a). \quad (20)$$

Also

$$\left. \frac{dU}{dz} \right|_{z=0} = -\zeta f(\zeta) = -\frac{a\zeta}{\zeta^3} J_0(\zeta a),$$

and we have

$$f(\zeta) = \frac{a\zeta}{\zeta^2} J_0(\zeta a). \quad (21)$$

From this we write the transform of the solution

$$U = \frac{a\zeta}{\zeta^2} J_0(\zeta a) e^{-\zeta z} \quad (22)$$

Now we apply the inverse transform and write

$$u(r, z) = a \int_0^{\infty} \frac{e^{-r'z}}{\zeta} J_0(a) J_0(r') dr'. \quad (23)$$

The steps for the transient solution are not carried out here as we are interested primarily in the steady state solution. From equation (23) the temperature at any particular r and z can be calculated. A series approximation to the integral is the most convenient method for determining the required numbers.

Appendix I
Ionization Potentials in Electron Volts
(Ref. 4)

Element	Ionization Level					
	I	II	III	IV	V	VI
Al	5.98	18.74	28.31	119.37	153.4	-
Af	7.6	21.4	35.9	-	-	-
Au	9.2	19.95	-	-	-	-
C	11.3	24.3	47.7	64.2	389.9	487
Cu	7.7	20.2	-	-	-	-
H	13.6	-	-	-	-	-
N	14.5	29.5	47.2	73.5	97.4	586.7
Ni	7.6	18.1	-	-	-	-
O	13.6	34.9	54.9	77.0	109.2	137.5

Appendix II
Work Function in Electron Volts
(Ref. 5)

Aluminum	4.08
Carbon	4.6
Copper	4.38
Gold	4.25
Nickel	5.03
Silver	3.56

Appendix III
Heat of Vaporization
(Ref. 6)

Pressure 760 mm Hg

Element	Temperature	ΔH
	$^{\circ}\text{K}$	Kilocal./mole
Ag	2446	60.72
Al	2600	67.9
Au	2933	74.21
Cu	2855	72.8
Ni	3073	91.0

1. Electric Contacts Handbook; R. Holm; 3rd Edition; Berlin; 1958.
2. Contact Simulation on the Digital Computer; Dec. 1, 1963 - Jan. 31, 1964; NAS 8-2552, Eleventh Interim Report.
3. Physical Electronics; R. L. Ramey; Wadsworth Publishing Co.; Belmont, California; 1961, Pg. 213.
4. Handbook of Chemistry; Lange; Handbook Publishers, Inc.; Sandusky, Ohio; 1956.
5. Handbook of Chemistry and Physics; Hodgman; Chemical Rubber Publishing Co.; Cleveland, Ohio; 1963.
6. American Institute of Physics Handbook; McGraw-Hill; New York, N.Y.; 1957.

TABLE OF CONTENTS

Part D

DESIGN

<u>SUMMARY</u>	<u>Section</u>	<u>Section Report</u>
Force - Physical Shape Relations for the Bipolar Coil Arrangement- - - - -	II	9th
A Study of Pole Face Configurations- - - - -	II	10th
Further Discussion of Pole Face Configurations- - - - -	IV	13th
Relay Drop-Out Time- - - - -	I	12th
Design Modification of the Parallel Coil 300 Ampere Contactor- - - - -	I	13th

Tab Color Code

Orange	9th Interim	1 July - 30 Sept., 1963
Rose	10th Interim	1 Oct. - 30 Nov., 1963
Green	11th Interim	1 Dec., 1963 - 31 Jan., 1964
Blue	12th Interim	1 Feb. - 31 March, 1964
Yellow	13th Interim	1 April - 31 May, 1964

SUMMARY

Part D

Design

This part is mainly concerned with the determination of possible parameters that can be optimized under certain constraint conditions and the application of these results in improving the design of existing units.

Presented in the first section is a study of the pull per watt for circular cores compared to square cores for a given rectangular prism volume occupied by the envelope of each. The results indicate that the circular core is 1.27 times more efficient than the square core.

The second and third sections present a study of the magnetic pull as a function of the apex angle for given core widths or diameters and was made for several configurations, including the circular, wedge and parabolic shapes. The angles for maximum pull are a function of the ratio of the working air gap reluctance to the non-working magnetic circuit reluctance.

The fourth section of this part is the theoretical development of the delay time and armature transit drop-out time as a function of the relay parameters. A rigorous solution of the non linear differential equation which describes the armature transit time in terms of general symbols is not possible as yet. A solution was arrived at by making some practical assumptions which lead to two different conditions of drop out. A weighted combination of these two solutions appears to give a satisfactory relationship for the armature drop-out transit time.

The last section of this part presents a design modification of the economized parallel coil 300 ampere contactor resulting from optimizing the pull per watt. The desire was to be able to eliminate the need for the economized coil arrangement which involves a control switch

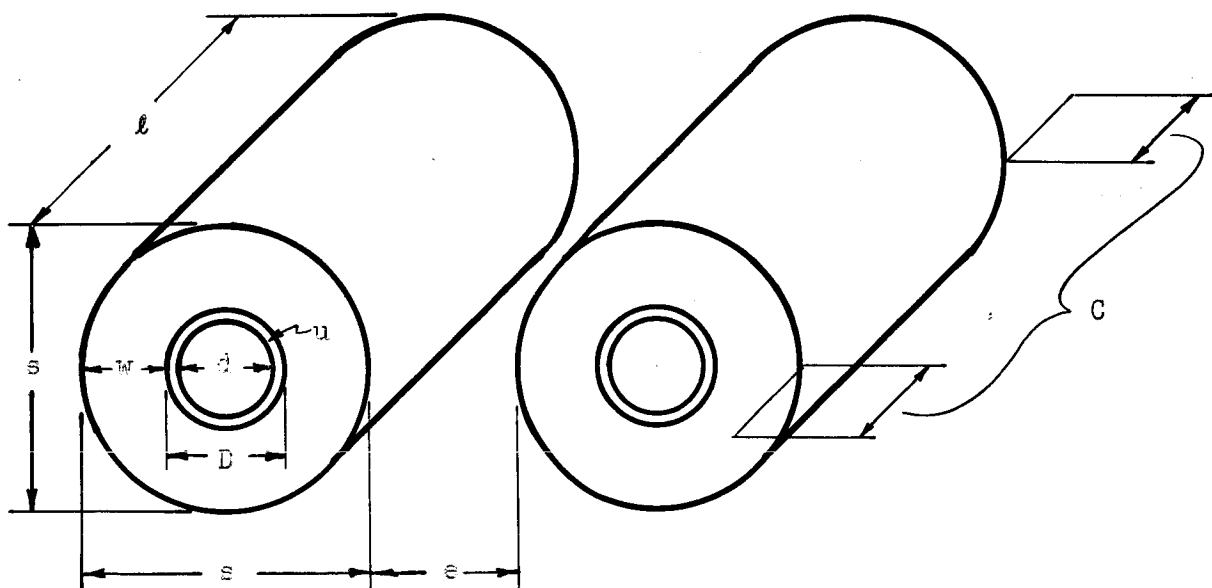
and to develop a one coil unit requiring essentially the same amount of holding coil power as the economized unit. This appears to be possible if the assumption is correct that the single coil mathematical model, with the same number of turns and coil resistance as the two coil unit, represents the two coil unit.

SECTION II

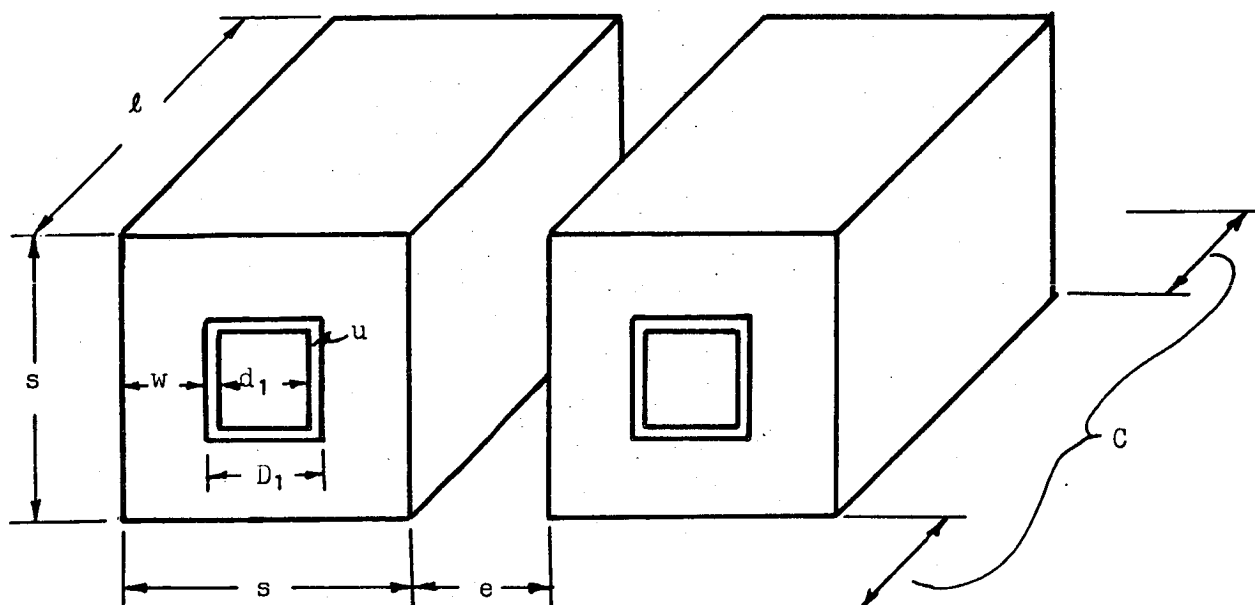
FORCE-PHYSICAL SHAPE RELATIONS FOR THE BIPOLAR TYPE COIL ARRANGEMENT

The following discussion includes some of the basic relations concerning square and circular coils, a development of a relation which obtains the maximum holding force per watt input per unit volume, and a comparison of the holding force per watt input for square and circular coils.

Figures 1 and 2 show the types of coil arrangements considered and Table I is a listing of the parameter symbols and definitions.



Circular Coils
Figure 1



Square Coils
Figure 2

Table I

Parameter Symbols and Definitions

A	= effective area of working air gap = $\pi d^2 a/4$
a	= air gap factor of core diameter
α_0	= air equivalent length of the non-force producing part of the magnetic circuit.
C	= clearance above and below the coils, contains the armature, flux paths, etc.
d	= circular core diameter.
d_1	= square core side.
D	= $d + u$ inside diameter of circular coil.
D_1	= $d_1 + u$ inside length of square coil side.
δ	= diameter of bare wire.
e	= clearance between the two coils.

F = magnetic pull force per pole in grams.
 g_n = winding space factor for the turns.
 g_r = winding space factor affecting the resistance.
 l = coil length.
 L_c = mean length per turn for circular coils.
 L_s = mean length per turn for square coils.
 N_c = number of turns on circular coil.
 N_s = number of turns on square coil.
 P = coil input power in watts.
 R_c = resistance of circular coils.
 R_s = resistance of square coils.
 ρ = resistivity of wire used in coil.
 s = outside diameter of the circular coil or length of the outside width of the square coil.
 u = distance from the core to the coil inside.
 μ_o = permeability of free space = 3.19.
 x_o = length of armature working air gap.

The following discussion does not consider the effects of changes in the reluctance of the flux path through the iron due to changes in the volume occupied by the particular coil configuration. This is believed to be a valid omission, because of the very high relative permeability of the iron as compared to the air gap, except in the limiting cases, such as, the core diameter approaching zero.

From a strictly geometrical approach the number of turns and the mean length per turn can readily be found to be:

$$N_c = \frac{4l g_n (s - D)}{\pi \delta^2} \quad (1)$$

$$N_s = \frac{4\ell g_n (s - D_1)}{\pi\delta^2} \quad (2)$$

$$L_c = \frac{\pi}{2} (s + D) \quad (3)$$

$$L_c = 2 (s + D_1) \quad (4)$$

Using these relations and the basic formula for determining resistance, $R = \frac{\rho N L g_r}{\pi\delta^2/4}$, we have:

$$R_c = \frac{8 \rho \ell_c g_n g_r (s - D)(s + D)}{\pi\delta^4} \quad (5)$$

$$R_s = \frac{32 \rho \ell_s g_n g_r (s - D_1)(s + D_1)}{\pi^2 \delta^4} \quad (6)$$

In a previous Interim Report covering the period 1 October to 30 November 1962, page 7 - II, equation 28, it was shown that

$$F = \frac{4.03 \times 10^{-5} \mu_o N^2 I^2 A}{2 (2 x_o + \alpha)^2} \quad (7)$$

If we consider $F = XI^2$ where X includes all quantities on the right of equation (7) except I^2 , and noting that $P = I^2 R$ we have

$$\frac{F}{P} = \frac{XI^2}{RI^2} = \frac{4.03 \times 10^{-5} \mu_o N^2 A}{2 (2x_o + \alpha)^2 R} \quad (8)$$

With the substitution of equations (1), (3) and (5) into equation

(8) an expression for force per watt for the circular coil construction is obtained.

$$\frac{F}{P} \text{ (circular)} = \frac{4.03 \times 10^{-5} \mu_o \ell g_n (s - D)A}{\pi \rho g_r (2 x_o + \alpha)^2 (s + D)} \quad (9)$$

Using equations (2), (4) and (6) a similar expression for the square coil construction is obtained.

$$\frac{F}{P} \text{ (square)} = \frac{4.03 \times 10^{-5} \mu_o \ell g_n (s - D_1)A}{4 \rho g_r (2 x_o + \alpha)^2 (s + D_1)} \quad (10)$$

As a simplification to a form which shows the effects on F/P due to changes in overall dimensions, i.e. F/P as a function of ℓ and s , and considering D as a fixed quantity, we have

$$\frac{F}{P} = K \frac{\ell (s - D')}{(s + D')} \quad (11)$$

where D' represents either D or D_1 and K incorporates all quantities of equations (9) or (10) not dependent upon ℓ or s .

Investigation is made of force per watt per unit volume to determine an optimum relation between s , ℓ and D , if any. The volume considered here is the volume of the rectangular prism which incloses all dimensions of Figures 1 or 2. The volume for either square or circular coils can therefore be expressed as

$$V = s (\ell + C)(2 s + e) \quad (12)$$

Let the symbol U represent the value of force per watt per unit volume, i. e. $U = F/P/V$. Now from equations (11) and (12) we have

$$U = \frac{K \ell (s - D')}{s (s + D')(\ell + C)(2s + e)} \quad (13)$$

If the partial derivative of U with respect to ℓ is set equal to zero the equation reduces to $C = 0$, which is not the physical situation. This implies that U has no finite extremums as ℓ is varied.

If the partial derivative of U with respect to s is set equal to zero it can be reduced to

$$(s/D')^3 + (e/4D' - 1) (s/D')^2 - (e/2D' + 1) (s/D') - e/4D' = 0 \quad (14)$$

Only one of the three solutions of this equation gives a real positive value for s/D' as e is varied from 0 to D' . This implies that of the three extremums of U as s is varied only one is physically realizable. Since it is intuitively obvious that U is a minimum at $s/D' = 1$ and $s/D' = \infty$ and since only one real extremum occurs between these two minimums it must be a maximum.

A graph of the real positive solutions to equation (14), i.e. s/D' as a function of e/D' , is presented in Figure 3. The coordinates of Figure 3 represent e and s as functions of D' .

A logical continuation as a result of the proceeding development, which relates s , e and D' for maximum force per watt per unit volume, is to investigate the possibility of a relation between ℓ and s or D' for which the maximum force per watt in a fixed volume would exist.

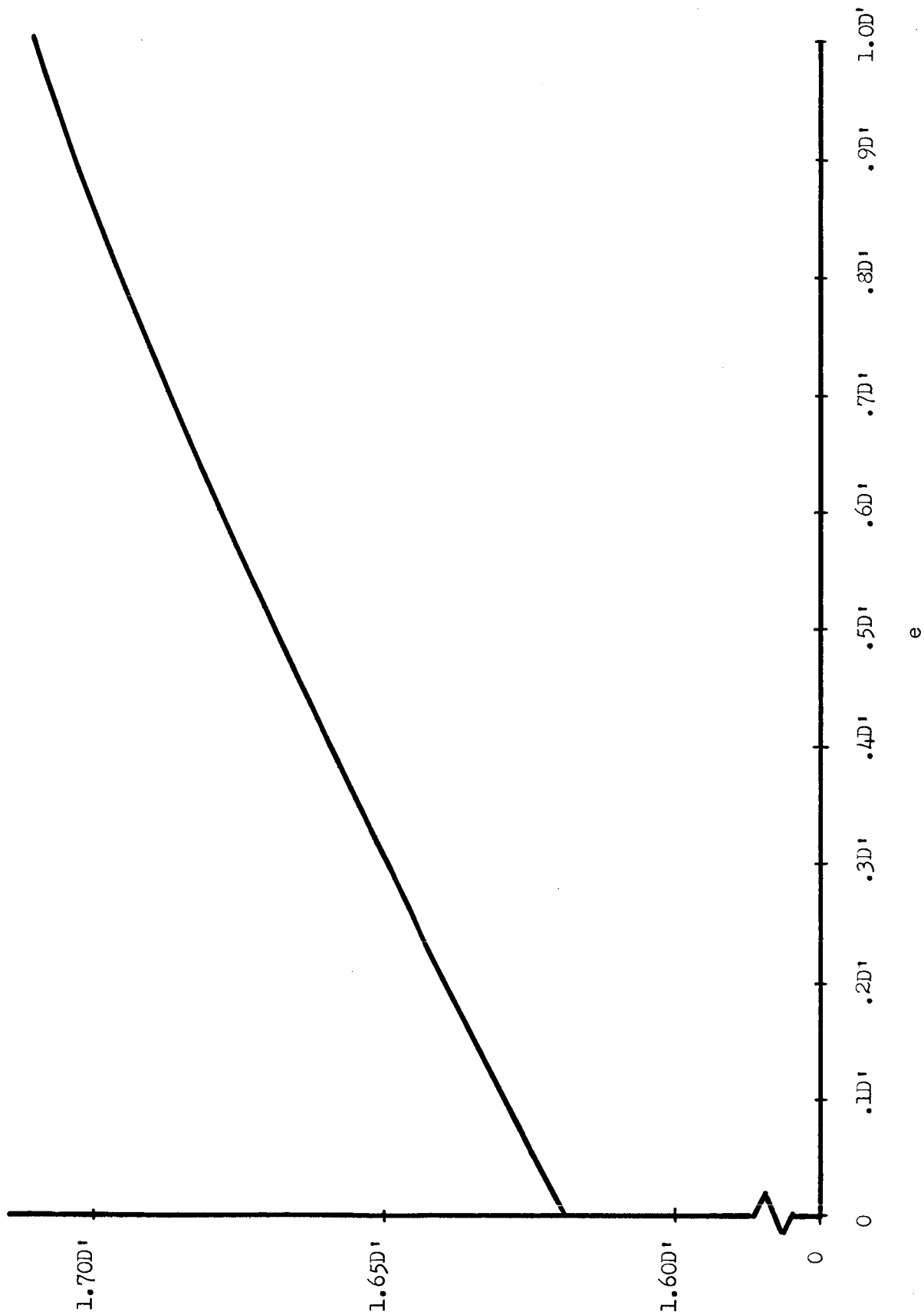


Figure 3 Relation between coil diameter and separation for maximum force per watt per unit volume.

As a first step, equation 10 is rewritten for F/P as a function of the variables ℓ , s and D' such that

$$\frac{F}{P} = \frac{K' \ell (s - D') \pi D'^2}{(s + D') 4} a^2 = \frac{K' (s - D')(D')^2}{s + D'} \ell \quad (15)$$

where D' represents either D or D_1 and $K' = K \pi \gamma^2/4$

If equation (12) is now solved for ℓ , considering V fixed, and substituted into equation (15) we have

$$\frac{F}{P} = \frac{K' (s - D') D'^2}{(s + D')} \left[\frac{V}{s (2s + e)} - C \right] \quad (16)$$

which may be written in the form

$$\frac{F}{P} = \frac{K' (s/D' - 1)}{(s/D' + 1)} \left[\frac{V}{s/D' (2 s/D' + e/D')} - C D'^2 \right] \quad (17)$$

It is noted that if we held e/D' constant as D' is varied then from the previously developed relation for maximum force per watt per unit volume it is seen that s/D' will also be a constant. This results in effectively varying s if F/P for a given volume is to be a maximum.

Figure 4 is a qualitative graph of equation 17. The graph shows that the force per watt for a given volume has no relative extremums as D' (or s) is varied. This graph indicates the most effective design configuration with regard to magnetic force on the armature will be obtained from the smaller diameter coils, which for a fixed volume implies long coils.

The value of F/P goes negative in Figure 4 which is not physically possible because C is held constant as D' is varied. As D' becomes large l must become negative to maintain a constant volume which results in a negative F/P . This relation is also incorrect for very small D' , however, it gives an indication of the behavior of F/P within physical limits.

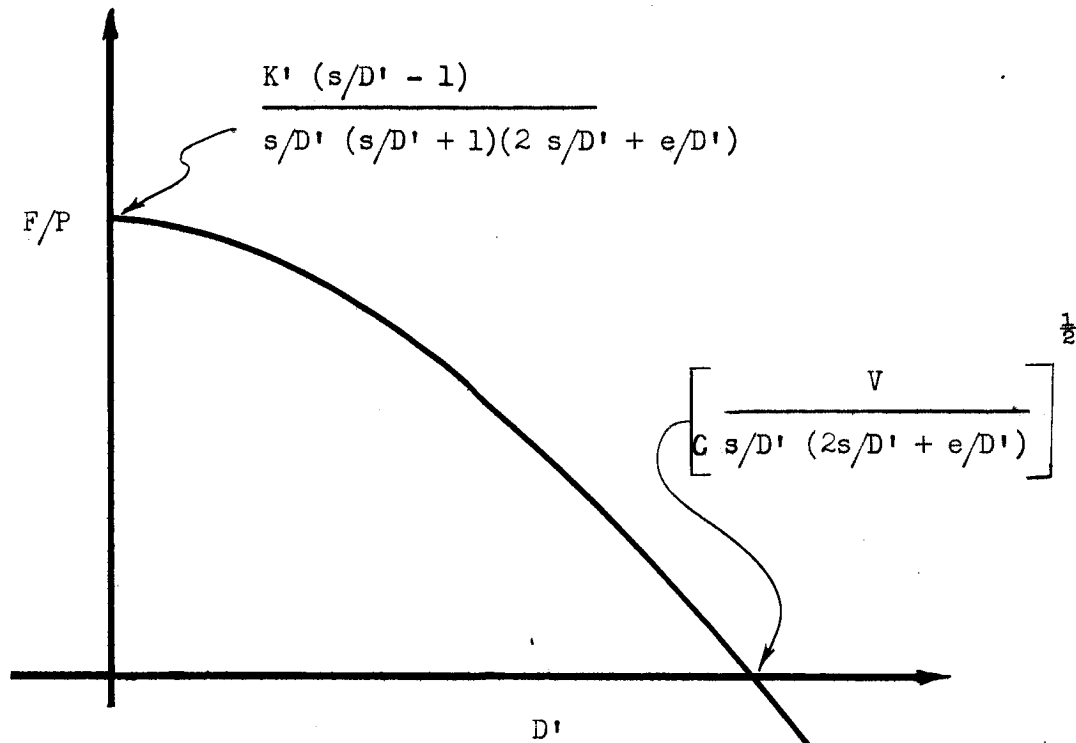


Figure 4

The following is a comparison of the square and circular coils on the basis of the efficiency with which the input power is used to develop magnetic holding force. The comparison is made for both equal volumes and equal weights.

It should be noted that the previous development of the relation between s and D' , which results in the maximum force per watt per unit volume, is independent of whether square or circular coils are considered. Therefore, when square and circular coils are designed for

maximum force per watt per unit volume, such that they occupy the same volume and shape (i.e. such that they have the same s , ℓ and e) then $D = D_1$.

If we now divide equation (9) by equation (10) under the above design we have

$$\frac{F/P \text{ (circular)}}{F/P \text{ (square)}} = \frac{4}{\pi} = 1.273 \quad (18)$$

For comparison on the basis of weight it is assumed that the square and circular coil configuration have the same values of s and D , with ℓ the factor which equalizes the weight. The comparison is equally satisfactory and simplified if we consider only one coil for each case instead of the dual coil arrangement.

ℓ_c = length of circular coil

ℓ_s = length of square coil

d_w = density of winding (wire, insulation, air)

d_c = density of core

W_c = weight of circular coil

W_s = weight of square coil

$$W_c = \ell_c \left[\frac{\pi s^2}{4} - \frac{\pi D^2}{4} \right] d_w + \ell_c \frac{\pi D^2}{4} d_c$$

$$= \ell_c \frac{\pi}{4} (s^2 d_w + (d_c - d_w) D^2) = \ell_c \left[\frac{\pi}{4} \right] K_2$$

$$W_s = \ell_s (s^2 - D^2) d_w + \ell_s D^2 d_c$$

$$= \ell_s (s^2 d_w + (d_c - d_w) D^2) = \ell_s K^2$$

$$\text{For } W_c = W_s$$

$$\frac{W_c}{W_s} = 1 = \frac{l_c \frac{\pi}{4}}{l_s} \quad \text{or} \quad \frac{l_c}{l_s} = \frac{4}{\pi}$$

Now dividing equation (9) by equation (10) again considering ℓ variable

$$\frac{F/P \text{ (circular)}}{F/P \text{ (square)}} = \frac{4l_c}{\pi l_s} = (4/\pi)^2 = 1.621 \quad (19)$$

In conclusion we see that, for coils of which the envelopes occupy the same rectangular prism volume, the circular coils will develop about 1.27 times more magnetic force per watt input than the square coils, as seen from equation (18). If square and circular coils have the same value for s with equal weights the circular coils will develop approximately 1.62 times more force per watt input than the square coils, as seen from equation (19).

SECTION II

A STUDY OF POLE FACE CONFIGURATIONS

This section is concerned with the comparison of the magnetic force developed for four different pole face configurations. The following is not a completely rigorous development because of the restrictions imposed on the models being studied. It is intended, however, to give an indication of the general influence of these configurations on the contactor's performance. Any quantitative application of the results of this development would, of course, depend upon the agreement between the application and its relation to the restrictions imposed on these models.

The models being studied are considered to be in the unoperated condition (i.e. maximum working air gap).

The assumptions, or restriction, made for the magnetic circuitry are:

1. The fringing effect is negligible.
2. The flux is perpendicular to the pole faces and enters or leaves only at the pole faces.
3. The magnetic flux density is constant along the pole face (i.e. no saturation of any part of the pole face).

The comparison of the four configurations is based on the following properties being equal for all configurations:

1. Equal width of the pole face.
2. Equal thickness of the pole face.
3. Equal magnetic reluctance of the magnetic circuit not containing the air gap.
4. Equal ampere turns applied to the total magnetic circuit.
5. Equal travel distance.

Note that the pole face is considered to be of uniform depth and therefore

its plane projection would appear to be representative of some types of rotary armature configurations.

The following is a generalization of the procedure used later for the development of the force equations for the four configurations.

The force in grams from a single pole has been developed in an earlier report as,

$$F = \frac{4.03 \times 10^{-5} B^2 A}{2\mu_0} = \frac{K_1 \Phi_F^2}{A} \quad \text{where } K_1 \text{ is a constant of proportionality}$$

The magnetic relations of interest are

$$\Delta \mathcal{F} = \int H dl = \int B/\mu \, dl \quad \text{where } \mu \text{ is a constant}$$

$$\Delta R = \Delta \mathcal{F}/\Phi = \ell/\mu A \quad \text{for uniform parallel magnetic flux}$$

NOTE: For listing of parameters and symbols used see Table 1.

The five steps in the following mathematical developments are:

1. Let $\mathcal{F} = K_2$ since \mathcal{F} is proportional to the ampere-turns being applied, which is being held constant for this comparison
2. Determine the reluctance of the air gap, R_a , under the stated restrictions.
3. Obtain the total flux, Φ_T .

$$\Phi_T = \frac{\mathcal{F}}{R_T} = \frac{K_2}{R_a + R_c}$$

where R_T is the total reluctance of the magnetic flux path and R_c is the reluctance of the path not including the air gap, a constant for comparison.

4. Determine the force producing flux, Φ_F . Since the flux density along the air gap is considered constant we may write

$$\Phi_F = \frac{\Phi_T}{S} \int \cos Z \, dS$$

where S is the total length of the air gap and Z is the angle between the normal to dS and the direction of force.

5. Determine the force from the previous equation

$$F = \frac{K_1 \Phi_F^2}{A}$$

where A is the area of the air gap. For the comparison purposes here the thickness will be considered one unit, therefore.

$$F = \frac{K_1 \Phi_F^2}{S}$$

Case I

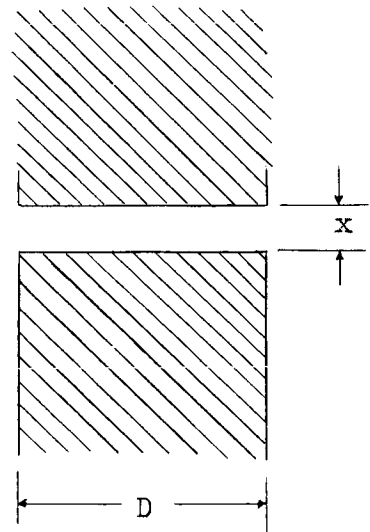
Flat Pole Face

1. $\mathcal{F} = K_2$

2. $\mathcal{R}_a' = \frac{x}{\mu_o D}$

3. $\Phi_T = \frac{K_2}{\mathcal{R}_a' + \mathcal{R}_c} = \frac{K_2}{\frac{x}{\mu_o D} + \mathcal{R}_c}$

4. $\Phi_F = \frac{\Phi_T}{S} \int \cos Z \, dS = \Phi_T$



$$5. F = \frac{K_1 \Phi_T^2}{D} = \frac{K_1 K_2^2}{D \left(\frac{x}{\mu_o D} + R_c \right)^2}$$

Case II

Circular Arc Pole Face

$$1. \mathcal{F} = K_2$$

$$2. \Delta R_a = \frac{\Delta \mathcal{F}}{\Phi(\text{in } \Delta \theta)}$$

$$\Delta \mathcal{F} = \frac{B}{\mu_o} d\ell$$

$$\text{where } B = \frac{\Delta \Phi(\text{in } \Delta \theta)}{\Delta A}$$

$$\Delta A = r \Delta \theta$$

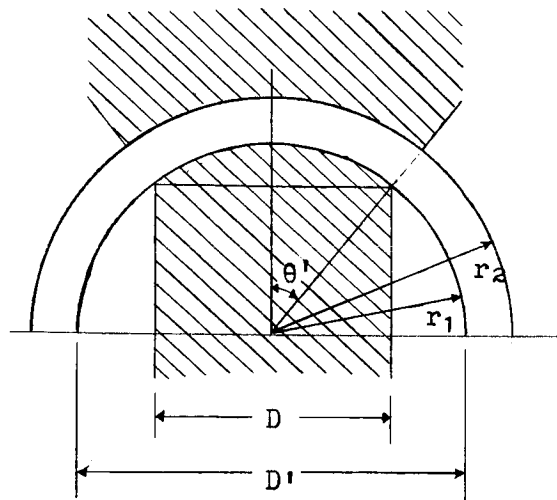
$$\text{and } d\ell = dr$$

therefore

$$\Delta \mathcal{F} = \int_{r_1}^{r_2} \frac{\Delta \Phi(\text{in } \Delta \theta)}{\mu_o \Delta \theta r} dr$$

and

$$\Delta R_a = \int_{r_1}^{r_2} \frac{dr}{\mu_o r \Delta \theta} = \frac{1}{\mu_o \Delta \theta} \ln \frac{r_2}{r_1}$$



In the limit

$$dR_a = \frac{1}{\mu_o d\theta} \ln \frac{r_2}{r_1} \quad \text{or} \quad d\mathcal{P}_a = \frac{1}{dR_a} = \frac{\mu_o d\theta}{\ln \frac{r_2}{r_1}}$$

Then

$$\mathcal{P}_a = \frac{2\mu_o \theta'}{\ln \frac{r_2}{r_1}} \quad \text{or} \quad R_a = \frac{\ln (r_2/r_1)}{2\mu_o \theta'}$$

$$x = r_2 - r_1 \quad \text{or} \quad \frac{r_2}{r_1} = \frac{2x}{D} \sin \theta' + 1$$

$$R_a = \frac{\ln((2x/D) \sin \theta' + 1)}{2\mu_o \theta'}$$

$$3. \quad \Phi_T = \frac{K_2}{R_a + R_c} = \frac{K_2}{\frac{\ln [(2x/D) \sin \theta' + 1]}{2\mu_o \theta'} + R_c}$$

$$4. \quad \Phi_F = \frac{\Phi_T}{S} \int \cos Z \, dS$$

$$\text{where } S = \frac{D\theta'}{\sin \theta'}, \quad dS = \frac{D \, d\theta}{2 \sin \theta'}$$

$$\text{and } Z = \theta$$

$$\Phi_F = \frac{\Phi_T}{S} \, 2 \int_0^{\theta'} \frac{D}{2 \sin \theta'} \cos \theta \, d\theta$$

$$\Phi_F = \frac{K_2 \sin \theta'}{\theta' \left(\frac{\ln [(2x/D) \sin \theta' + 1]}{2\mu_o \theta'} + R_c \right)}$$

$$5. F = \frac{K_1 \Phi_F^2}{S} = \frac{K_1 K_2^2 \sin^3 \theta'}{D \theta'^3 \left(\frac{\ln ((2x/D) \sin \theta' + 1)}{2\mu_o \theta'} + R_c \right)^2}$$

Case III

Wedge Shaped Pole Face

The section of the air gap labeled A is assumed to contribute a negligible amount of force producing flux.

$$1. \mathcal{F} = K_2$$

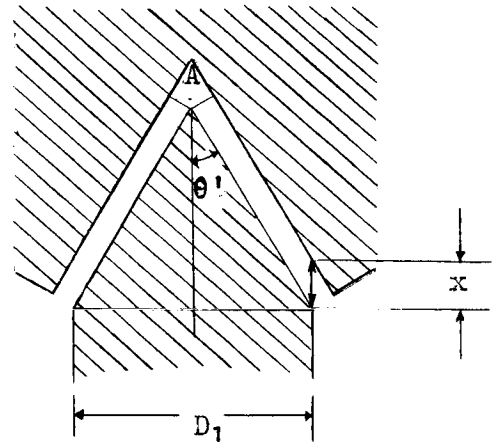
$$2. R_a = \frac{x \sin \theta'}{\mu_o D \sin \theta'}$$

$$= \frac{x \sin^2 \theta'}{\mu_o D}$$

$$3. \Phi_T = \frac{K_2}{R_a + R_c} = \frac{K_2}{\frac{x \sin^2 \theta'}{D\mu_o} + R_c}$$

$$4. \Phi_F = \frac{\Phi_T}{S} \int \cos Z \, dS$$

where $Z = 90^\circ - \theta'$ or $\cos Z = \sin \theta'$

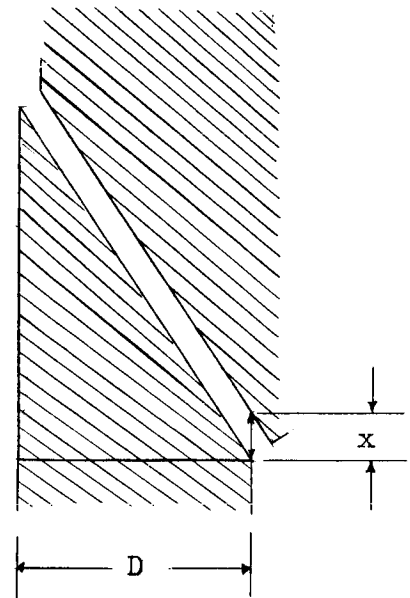


$$S = \frac{D}{\sin \theta'} ; dS = \frac{dD}{\sin \theta'}$$

$$\Phi_F = \frac{K_2 \sin \theta'}{\frac{x \sin^2 \theta'}{D\mu_o} + R_c}$$

$$5. F = \frac{K_1 \Phi_F^2}{S} = \frac{K_1 K_2^2 \sin^3 \theta'}{D \left(\frac{x \sin^2 \theta'}{D\mu_o} + R_c \right)^2}$$

It should be noted that the discussion of the wedge shaped pole face applies equally well to the wedge shaped pole face presented here.



Case IV

Parabolic Shaped Pole Face

The section of the air gap labeled A is assumed to contribute a negligible amount of force producing flux. D is assumed sufficiently greater than x so that the flux lines are essentially parallel.

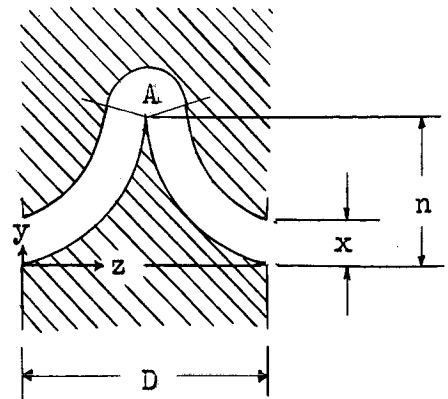
$$1. \quad \mathcal{F} = K_2$$

$$2. \quad y = az^2$$

$$dS = \sqrt{1 + 4a^2 z^2} \, dz$$

$$S/2 = \int_0^{D/2} \sqrt{1 + 4a^2 z^2} \, dz$$

$$S = (D/2) \sqrt{a^2 D^2 + 1} + (1/2a) \ln (aD + \sqrt{a^2 D^2 + 1})$$



$$R_a = \frac{x}{\mu_o S} = \frac{2x}{\mu_o [D \sqrt{a^2 D^2 + 1} + (1/a) \ln (aD + \sqrt{a^2 D^2 + 1})]}$$

$$3. \quad \Phi_T = \frac{K_2}{R_a + R_c}$$

$$4. \quad \Phi_F = \frac{\Phi_T}{S} \int \cos Z \, dS$$

slope of pole face = $2az$

slope of normal to pole face = $-\frac{1}{2az}$

$$\cos Z = \sin \left[\tan^{-1} \left(\frac{-1}{2az} \right) \right] = \frac{1}{\sqrt{4a^2 z^2 + 1}}$$

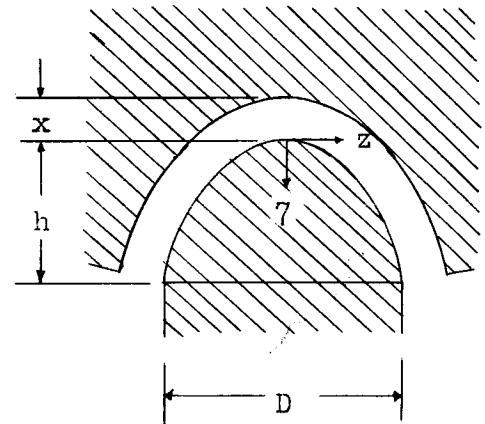
therefore $\Phi_F = \frac{\Phi_T}{S} D$ which reduces to

$$\Phi_F = \frac{DK_2}{\frac{x}{\mu_o} + \frac{1}{2} R_c [D \sqrt{a^2 D^2 + 1} + (1/a) \ln (aD + \sqrt{a^2 D^2 + 1})]}$$

$$5. F = \frac{K_1 \phi^2}{S} = \frac{2K_1 K_2^2}{D Y \left(\frac{x}{D \mu_0} + \frac{1}{2} R_c Y \right)^2}$$

$$\text{where } Y = \sqrt{1 + a^2 D^2} + \frac{1}{aD} \ln (aD + \sqrt{1 + a^2 D^2})$$

It should be noted that the discussion of the parabolic shaped pole face applies equally well to the parabolic shaped pole face presented here, by considering a change of coordinates.



To compare the results of the force produced by the four mathematical models considered here, several graphs are presented.

Figure 1 - To compare the force equations several common quantitative relations had to be chosen. In this figure, relations which are believed to be fairly close to the average for contacts were chosen. These are $x = D/10$ (i.e. the travel distance is one-tenth the pole width) and $R_c = R_a'/10$. The reference for comparison is considered as the flat pole face configuration. The crossing of the 100 percent line is therefore the value at which the force produced by a configuration is equal to that produced by a flat pole face. Note, the second abscissa is for the parabolic shaped pole face and is for the

total heights of the parabola.

Figure 2 - The curves presented are the same as those in Figure 1 except that $R_C = R_a'/50$ and the parabolic shaped pole face is not present because of the unfavorable results of Figure 1.

Figure 3 - The curves presented are the same as those in Figure 2 except that $R_C = \frac{1}{2} R_a'$.

Figure 4 - The results of Figures 1, 2 and 3 show a motion of the maximum value of force for the circular arc and wedge shaped pole face. The curves presented here show the complete motion of these maximums as a function of k where k is defined by

$$R_C = k R_a'$$

In conclusion it is seen that a decided advantage may be obtained from the wedge shaped pole face if R_C is known and small. However, as θ becomes small the mathematical model becomes less correct and the physical problems increase. For the circular arc pole face it is seen that the maximum force always occurs for θ below 27.5 degrees, although, the gain for the maximum is only a few percent improvement over that of a flat pole face. One of the most notable aspects of the curves for the circular arc pole face is the considerable loss in force as θ becomes large, i.e. as the pole face approaches a semicylindrical configuration.

No attempt to experimentally justify the preceding results has been made at this time.

Table 1

A	Area of pole face
a	Specifies the shape of the parabolic pole face $y = az^2$
D	Width of pole face
Δ	Used throughout preceding pages to indicate incremental segments
\mathcal{F}	Magnetomotive force
Φ_F	Component of flux in the direction of force
Φ_T	Total flux
h	Height of parabolic pole face configuration
K_1	Constant of proportionality between force and Φ^2/A where $F = K_1\Phi^2/A$
K_2	Constant magnetic force applied
\mathcal{P}_a	Permeance of air gap, $\mathcal{P}_a = 1/\mathcal{R}_a$
\mathcal{R}_a	Reluctance of air gap
\mathcal{R}_a'	Reluctance of the air gap for the particular case of the flat pole face
\mathcal{R}_C	Reluctance of flux path not including the air gap
S	Total length of air gap. Since the air gap is considered one unit thick $S = A$
x	length of air gap
Y	$\sqrt{1 + a^2D^2} + (1/aD) \ln (aD + \sqrt{1 + a^2D^2})$
θ'	Fixed configuration angle for circular arc and wedge shaped pole faces, (see the appropriate figures on previous pages). Note, that on the graphs the pole face width, D, is considered the constant.

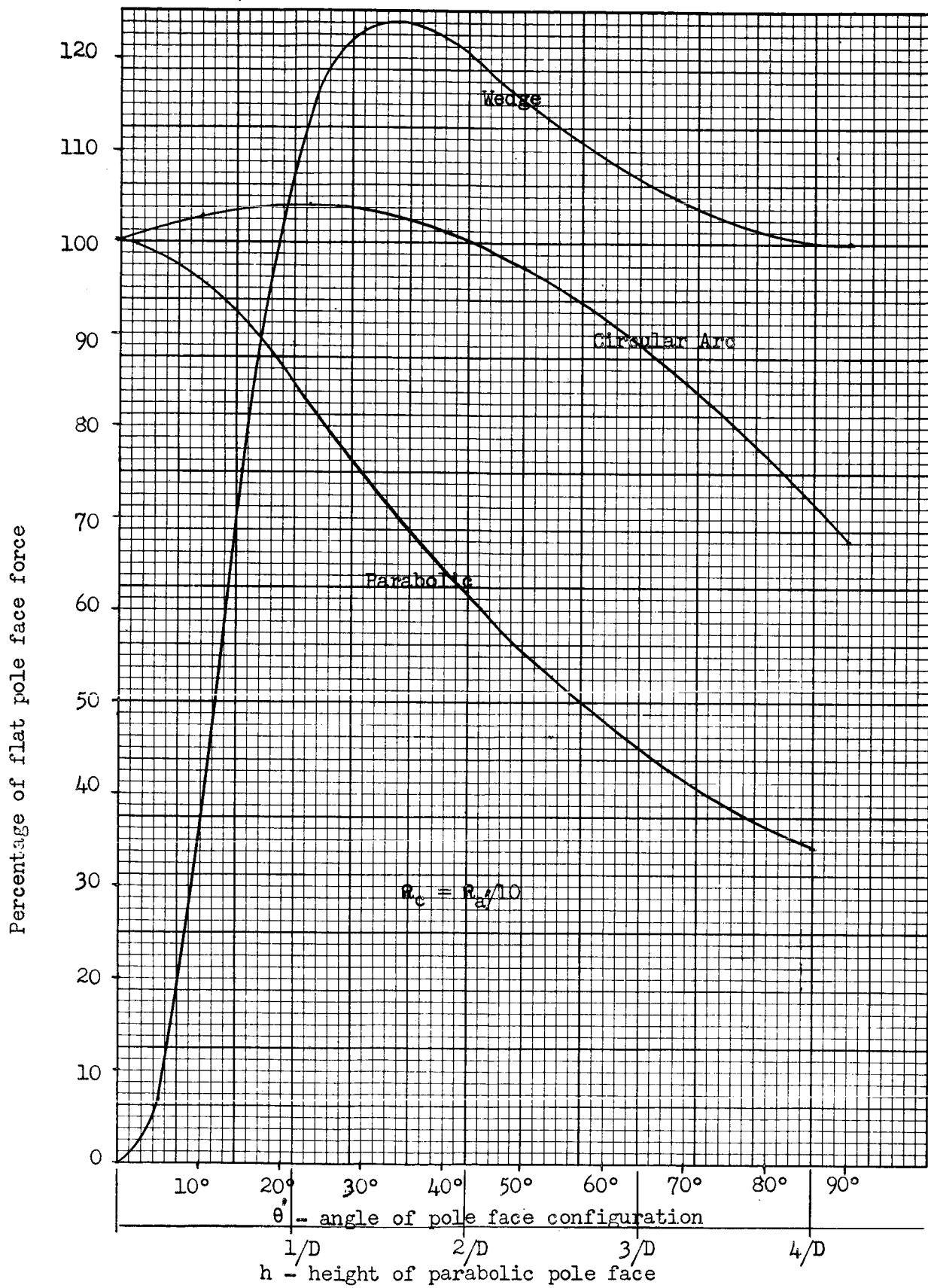


Figure 1
12 - II

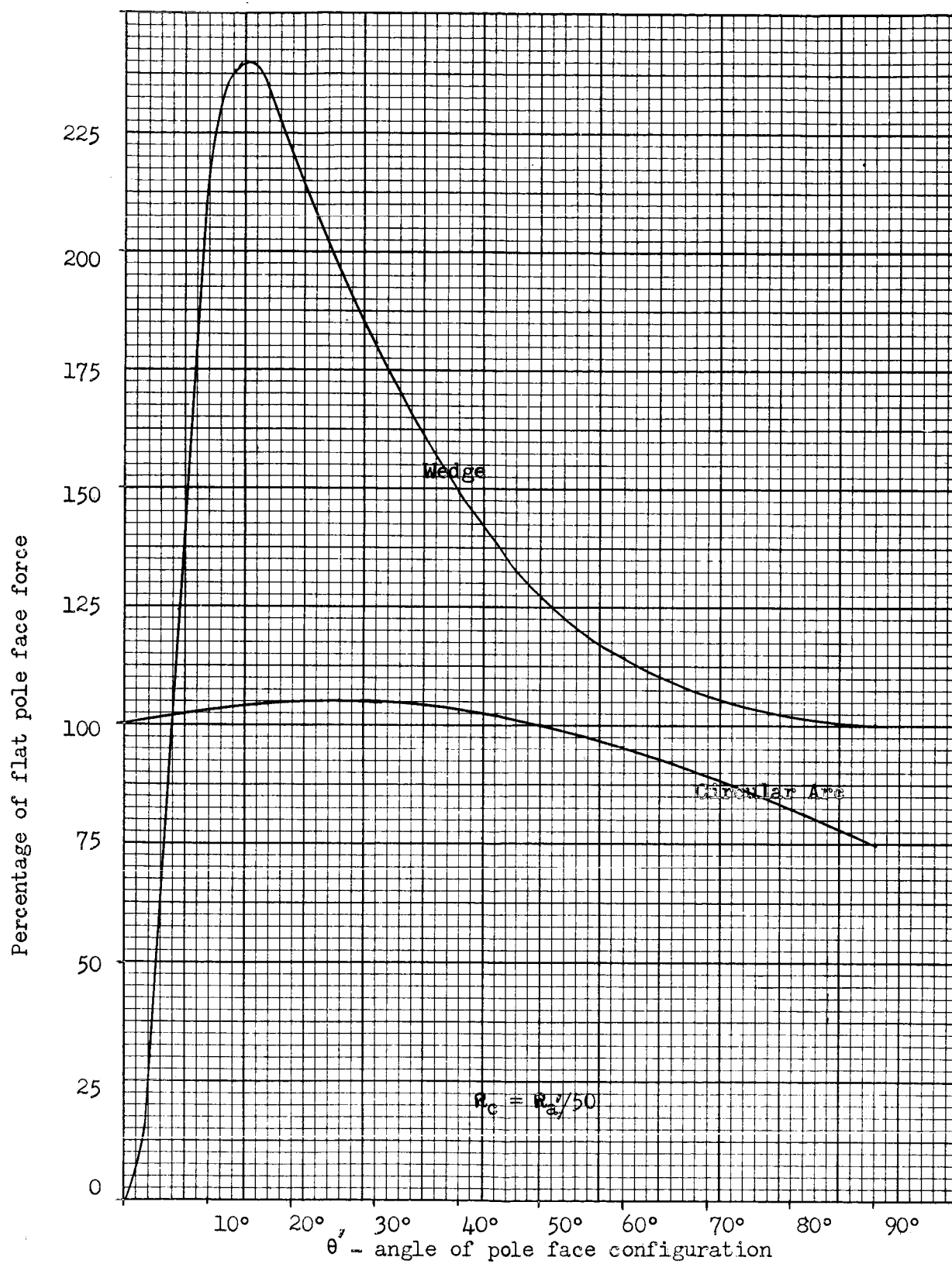


Figure 2

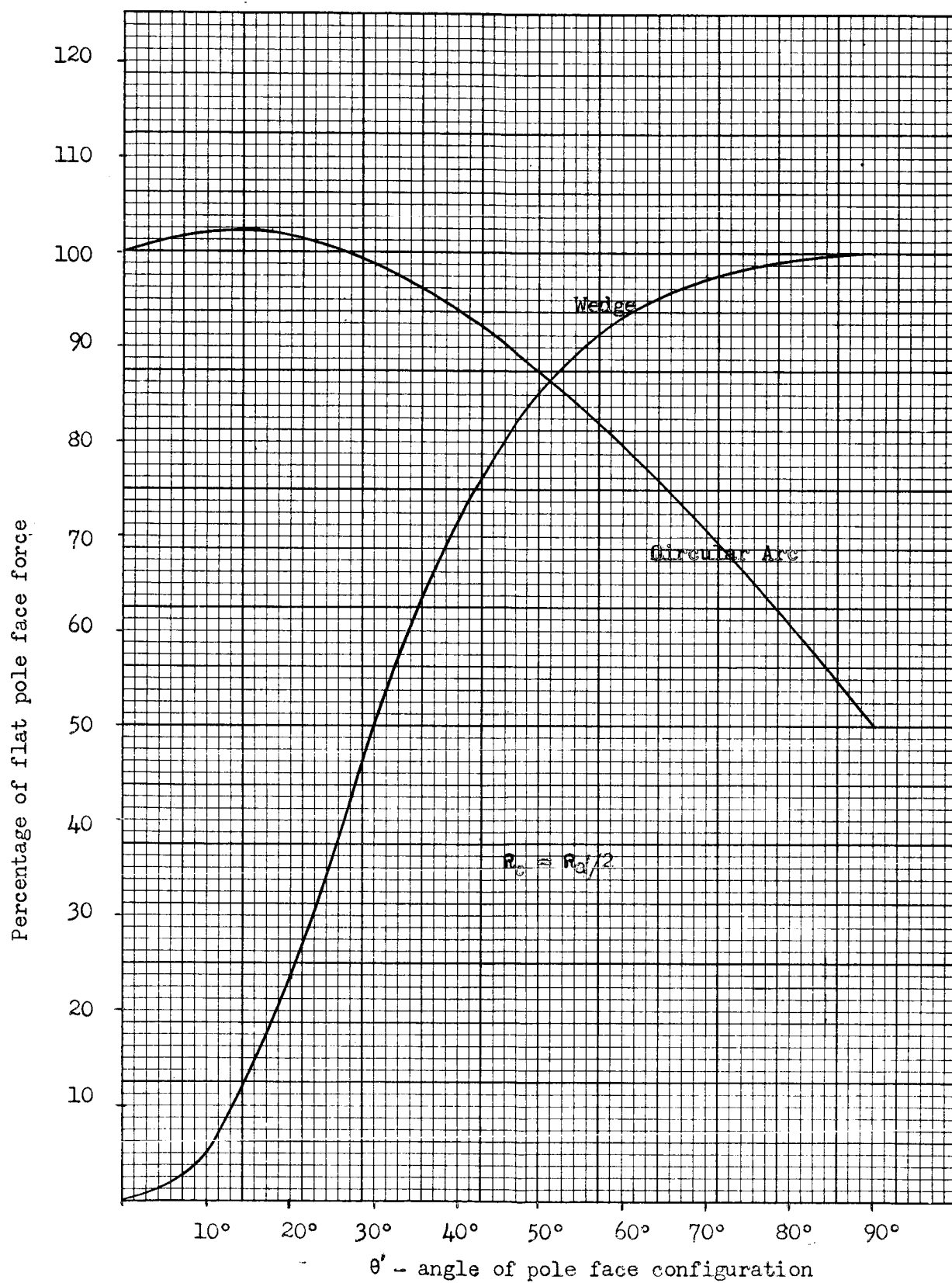


Figure 3

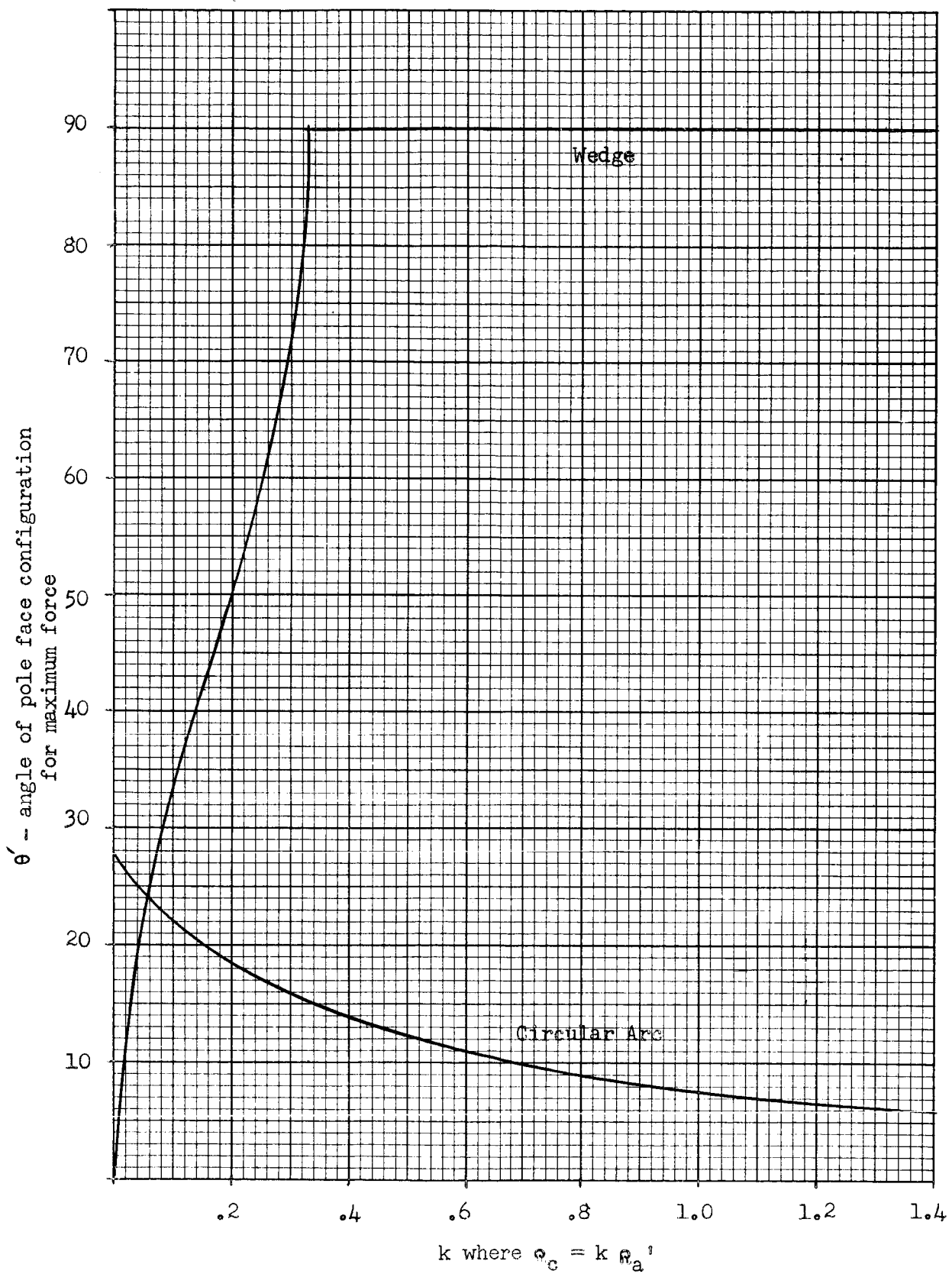


Figure 4

SECTION IV

FURTHER DISCUSSION OF POLE FACE CONFIGURATIONS

From a test report by Sandia Corporation measurements were made on cylindrical solenoids with cone shaped pole faces. These measurements were force displacement curves for several cone angles and for several power inputs.

If an equation is derived with the same assumption and procedure as those in the Tenth Interim Report then the resulting equation for the cone shaped pole face is

$$F = \frac{4K_1 K_2^2 \sin^3 \theta}{\pi D^2 \left[\frac{4x \sin^2 \theta}{\pi \mu_o D^2} + \mathcal{R}_c \right]^2} \quad (1)$$

where: K_1 = constant of proportionality between force and ϕ^2/A as $F = K_1 \phi^2/A$
 K_2 = constant mmf applied
 D = diameter of pole core
 σ = $1/2$ the apex angle of the pole face
 x = length of air gap
 \mathcal{R}_c = reluctance of flux path not including the air gap.
 μ_o = permeability of air

Figures 1 and 2 are copied from the test report of Sandia Corporation for $3/8$ inch diameter cores. It is seen that the values of Figure 1 are very close to one and one half times as large as those in Figure 2 which is the ratio of the different powers applied. This indicates that in this range of measurements the material is not saturating

Equation 1 may be written as

$$F = \frac{C \sin^3 \theta}{[(R_a/R_c) \sin^2 \theta + 1]^2} \quad (2)$$

$$\text{where } C = \frac{4K_1 K_2^2}{\pi D^2 R_c^2} \quad \text{and} \quad R_a = \frac{4x}{\pi \mu_o D^2}$$

The intersection of the 30 degree and 45 degree curves of Figure 1 can be used to solve Equation 2 for C and R_a/R_c . With these quantities a theoretical figure equivalent to Figure 1 can be drawn from Equation 2. This is done in Figure 3.

It is seen from Figures 1 and 3 that the experimental data has approximately the same form as that presented by the equation developed from the simplifying assumptions. It is also seen that the spacings in the range of measurements are not predictable from the equation and therefore neither are the cross over points.

Several empirical modifications to Equation 1 have been tried at this time, all of which were unsuccessful in leading to the experimental results. Close correlation between the theoretical and experimental values is not expected since the assumptions used in developing the equations were based in part upon the fact that the value of x was small compared to the value of D. The experimental data was primarily in the range where x is of the same order of magnitude as D. For values of x comparable to D, the problem involved in the theoretical development is the amount of fringing of the magnetic flux and the manner in which the flux is distributed in the air gap.

The main point obtained from the experimental data is that the maximums predicted do exist and that there seems to be a larger variation than predicted.

The advantage of having an equation, which will give the proper results without neglecting fringing, would result from situations where it is desirable to maximize the force at a given displacement of the armature.

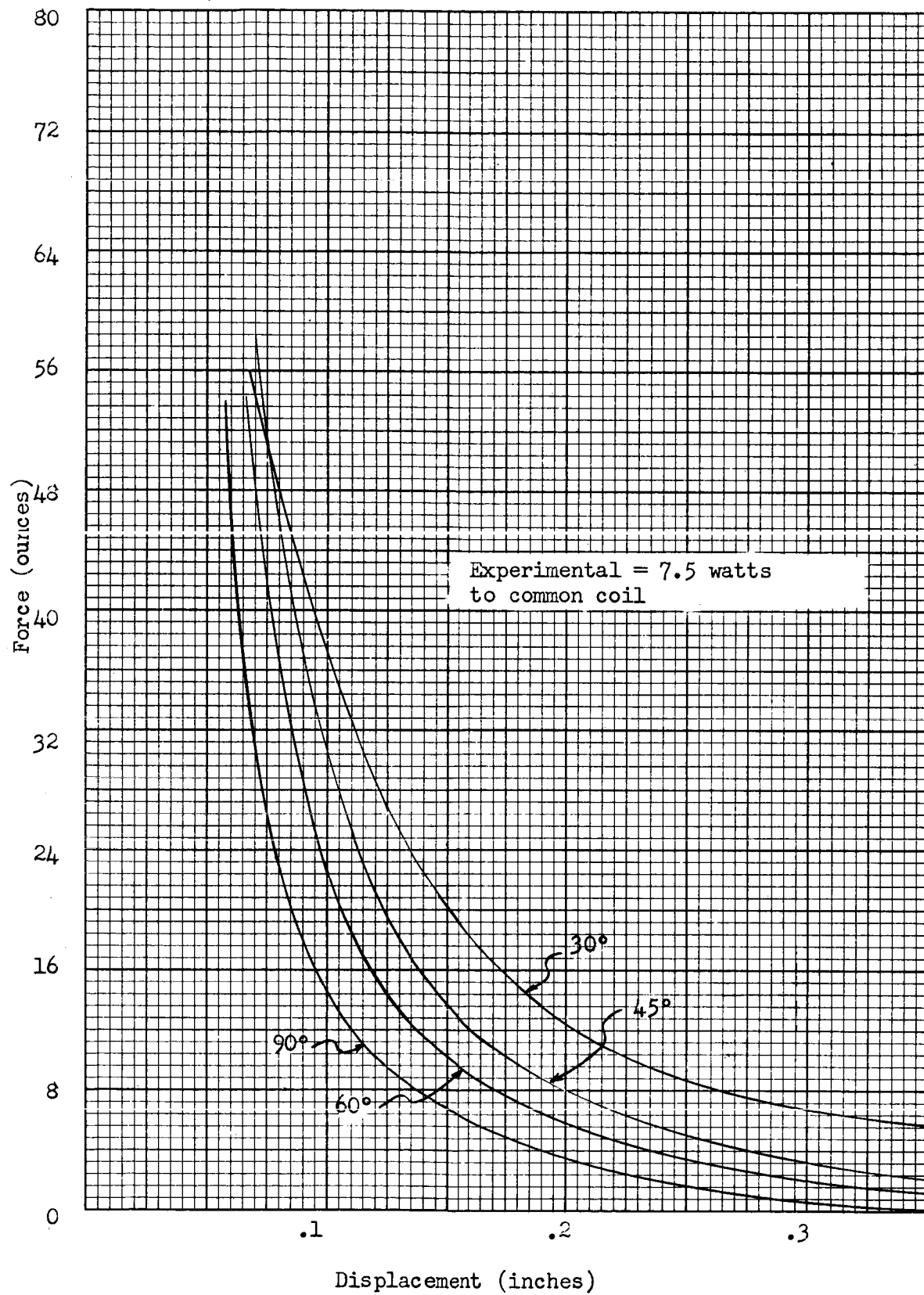


Figure 1

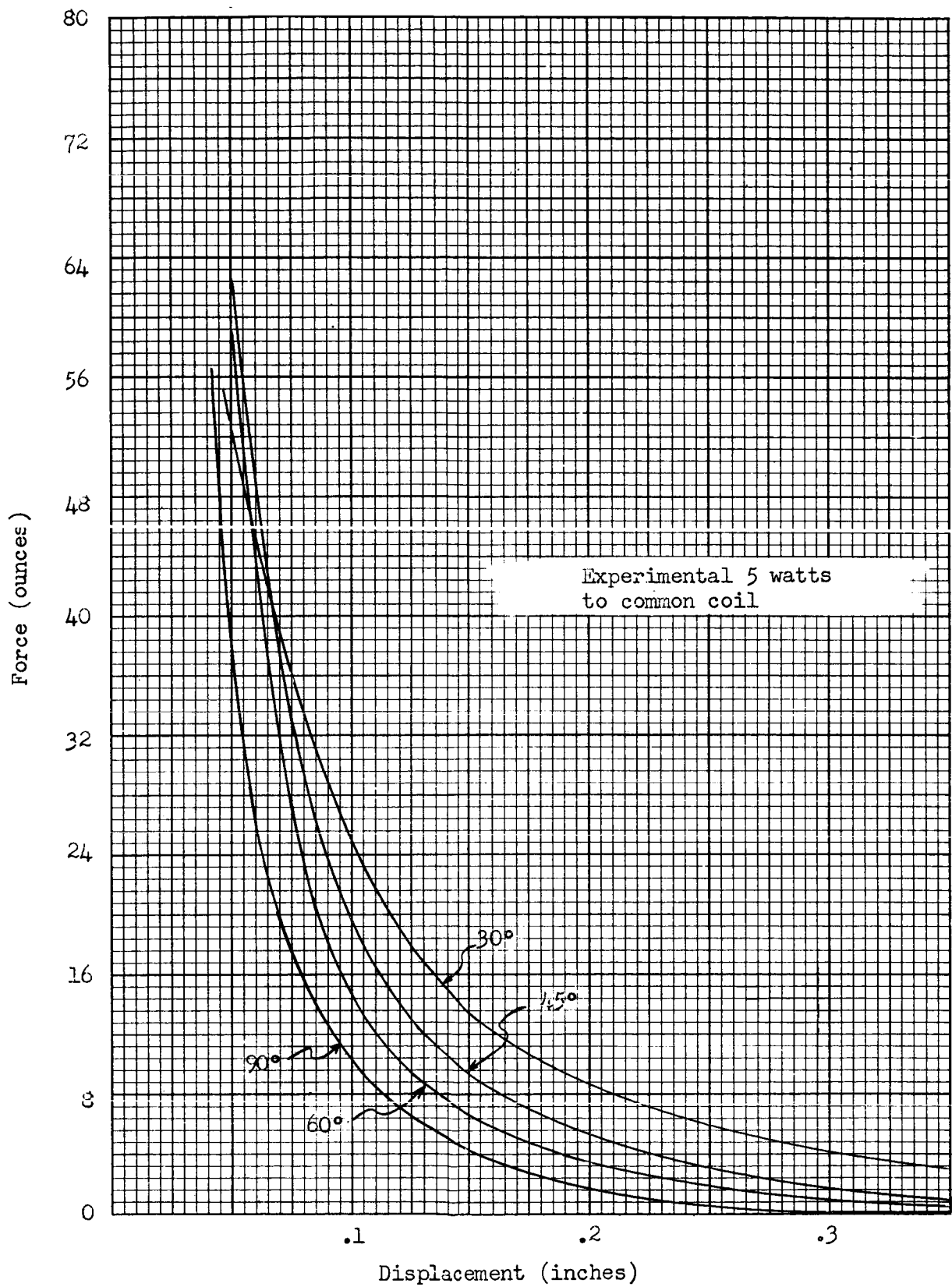


Figure 2

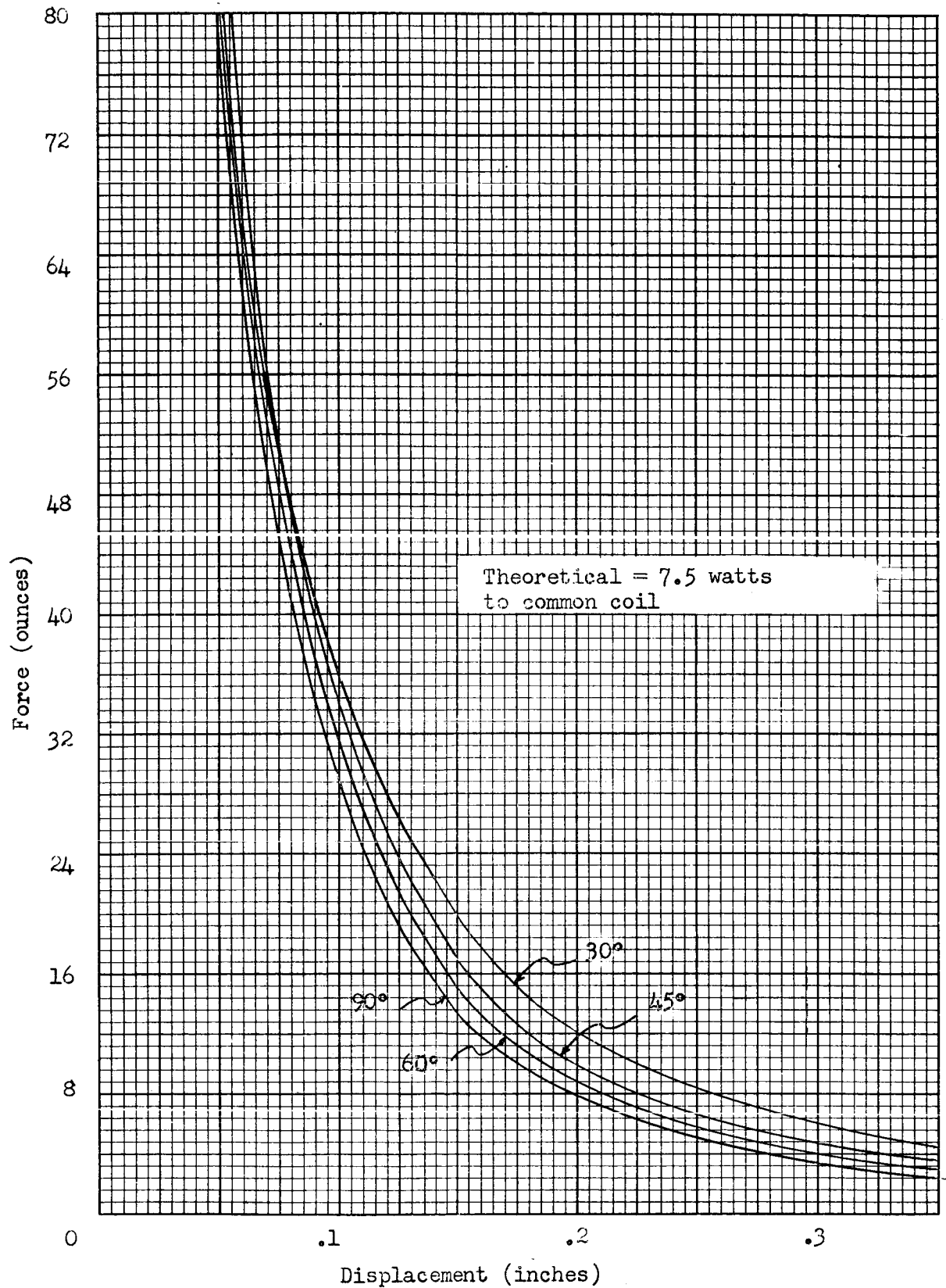


Figure 3

SECTION I

RELAY DROP-OUT TIME

This section is concerned with the determination of an analytical expression for the drop-out time of a relay to be used in the design maps. The drop-out time is considered to be the time interval from the instant the relay is deenergized until the contacts first make contact with their normal deenergized positions (i.e. neglecting opening bounce).

Several important assumptions were made in the following calculations. One of these, that being the magnetic circuit is not saturated, is of primary importance in the determination of the delay time, t_d . Another assumption is that the spring force on the armature has a constant spring constant. This assumption is of primary importance in the determination of the transit drop-out time, t_j . This can be justified by assuming an effective spring constant which includes the armature spring and contact overtravel springs.

Even with these assumptions a straight forward solution of the transit drop-out time involves the solution of two simultaneous non-linear differential equations. No solution in symbolic form is believed to exist for these equations. Therefore, in the solution for the transit drop-out time many hopefully logical approximations and assumptions are made. The ultimate justification of these approximations are results which satisfactorily approximate the actual transit drop-out time. Rough preliminary experiments have given good results. More extensive experimental investigations will be made, however.

The delay time, t_d , is defined as the time interval from the instant the coil is deenergized until the armature moves away from the

core. In the following calculation, t_d , will be approximated by the time interval from the instant the coil is deenergized until the net force on the armature is in the direction to cause release. The force on the armature will be in the direction to cause release at the instant after the spring force is equal to the flux force which can be expressed by the following equation.

$$P_o + kx_o = \frac{4.03 \times 10^{-5} B_d^2 A}{2\mu_o} \quad \text{Eq 1}$$

Where B_d is the flux density at t_d which may be expressed as

$$B_d = \frac{\phi_d}{A} = \frac{Ni_d}{RA} = \frac{Ni_d \mu_o}{\alpha} \quad \text{Eq 2}$$

Where ϕ_d is the total flux and R is the reluctance of the magnetic circuit when the relay is actuated.

Combining Equations 1 and 2 we have

$$i_d = \left[\frac{2(P_o + kx_o)\alpha^2}{4.03 \times 10^{-5} AN^2\mu_o} \right]^{\frac{1}{2}} = 157.5 \frac{\alpha \sqrt{2(P_o + kx_o)}}{N \sqrt{\mu_o A}}$$

from this expression we may obtain

$$\frac{i_d}{i_{ss}} = 157.5 \frac{R_t \alpha \sqrt{2(P_o + kx_o)}}{EN \sqrt{\mu_o A}} = \eta \frac{\alpha \sqrt{P_o + kx_o}}{(\alpha + x_o) \sqrt{P_o}} \quad \text{Eq 3}$$

where η is the stability factor defined in previous reports.

After the coil is deenergized the current will decay exponentially with a time constant of $L_c/(R_c + R_d)$ and at t_d we will have

Note: Table I contains a listing of symbols and definitions.

$$i_d = i_{ss} \exp \left[- \frac{R_c + R_d}{L_c} \right] t_d \quad \text{Eq 4}$$

L_c may be expressed in terms of the relay parameters in the following manner,

$$L_c = N\phi/I \text{ but } \phi = NI/R \text{ or } \phi/I = N/R$$

$$\text{therefore } L_c = N^2/R = \mu_o AN^2/\alpha \quad \text{Eq 5}$$

Substituting Equation 5 into Equation 4 we have

$$\frac{i_d}{i_{ss}} = \exp \left[- \frac{\alpha(R_c + R_d)}{\mu_o AN^2} \right] t_d \quad \text{Eq 6}$$

Equations 3 and 6 may be solved to t_d giving

$$t_d = \frac{\mu_o AN^2}{\alpha(R_c + R_d)} \ln \frac{\alpha(\alpha + x_0) \sqrt{P_o}}{\eta \sqrt{P_o} + kx_0} \quad \text{Eq 7}$$

The transit armature travel drop-out time will be broken down into two separate problems. The first of these will be to determine a drop-out time (j_1) for the case of a greater decrease in flux force than spring force for a constant current of i_d . The second problem will be the determination of a drop-out time (j_2) for the case of comparatively small change in flux force to the change in spring force for a constant current at i_d . These two problems will be shown to lead to the same approximate results with conditional inequalities to be satisfied.

Before proceeding with an approximate solution to the first problem, i.e. determination of j_1 , the dynamic equation of force will be considered in general.

$$F_d \text{ (drop-out force)} = F_s \text{ (spring force)} - F_f \text{ (flux force)} \quad \text{Eq 8}$$

Let x be taken to be zero when the armature is closed and increases positively as the armature opens and let t be zero when $i = i_d$.

Since the flux force $F_f = \frac{B^2 A}{2\mu_0} \propto \frac{i^2}{(\alpha + x)^2}$ because $B = \phi/A = \frac{Ni}{AR} = \frac{\mu_0 Ni}{(\alpha + x)}$ and since $F_f = F_s$ at the instant $t = 0$ we may write

$$F_f = \frac{\alpha^2 F_s(0) i^2}{i_d^2 (\alpha + x)^2} . \text{ The spring force } F_s \text{ is linearly related to the}$$

displacement and using the standard symbols from earlier interim reports may be written as $F_s = P_o + kx_o - kx$. From these considerations we may write Equation 8 as

$$F_d = P_o + kx_o - kx - (P_o + kx_o) \frac{\alpha^2}{(\alpha + x)^2} \frac{i^2}{i_d^2} \quad \text{Eq 9}$$

If we assume that the overall variation in magnitude of $i(t)$ is small (which is generally true for conditions imposed by j_1) we may use $i(t)$ to give the rate of change with respect to time of the force on the armature at $t = 0$ (i.e. $x = 0$ and $d_x/d_t = 0$).

$$\text{Since } i(t) = i_d \exp \left[- \frac{(R_c + R_d)t}{L_c} \right] \text{ and } \frac{di}{dt}(0) = - \frac{i_d(R_c + R_d)}{L_c}$$

$$\left. \frac{d F_d}{dt} \right|_{t=0} = (P_o + kx_o) \frac{2(R_c + R_d)}{L_c} \quad \text{Eq 10}$$

Another condition used in the solution for j_1 is the final force

$$F_d(t) \left| \begin{array}{l} t = j_1 \\ x = x_o \end{array} \right. = P_o - (P_o + kx_o) \frac{\alpha^2}{(\alpha + x_o)^2} \quad \text{Eq 11}$$

Since $F_d = M d^2x/dt^2$ it is seen that Equation 9 is a nonlinear differential equation with respect to time even if i is considered constant for an approximation.

A solution for j_1 will be obtained by assuming a solution for F_d in equation 9 from which j_1 can be obtained from $F_d = M d^2x/dt^2$. The following paragraphs along with Figures 1 through 3 will present the reasoning for selection of the F_d used in the subsequent development.

Figure 1 is an approximate three-dimensional representation of F_d from Equation 2. Plotted in the $F - t$ plane is the variation of force due to the change in current if the armature did not move, however, since this force is small only the initial slope and a short interval of time later is of interest (i.e. to about point a). Shortly after the armature begins to move F_d will become the motivating force and will approach a value of approximately $F_s(x_o) - F_f(x_o)$.

Figure 2 (a) is a curve similiar to Figure 1 except that it is for the condition of the flux force, F_f , being negligible as compared to the force of the spring, F_s , at $x = x_o$. Figure 2 (b) is actually a guess of the force on the armature, F_d , as a function of time resulting from the reasoning presented in the previous paragraph. A function of time which has this shape and can satisfy the initial slope initial value and final value could be

$$F_d(t) = A (1 - Bt)^{\frac{1}{2}} - A \quad \text{Eq 12}$$

where A and B are constants to satisfy the known condition.

Figure 3(a) is another curve similiar to Figure 1 except that it is for the condition of F_f not being negligible as compared to F_s at $x = x_o$. Figure 3 (b) is another guess of the shape of F_d proceeding as above. A simple modification to Equation 12 which would give a curve of this type would be.

$$F_d(t) = A (1 + Bt)^{\frac{1}{2}} - A - F_f(j_1)t/j_1 \quad \text{Eq 13}$$

The constants A and B can be solved for by applying Equations 10 and 11

$$\left. \frac{dF_d(t)}{dt} \right|_{t=0} = \frac{1}{2} AB - F_f(j_1)/j_1 = (P_o + kx_o) \frac{2(R_c + R_d)}{L_c} \quad \text{Eq 14}$$

$$\left. F_d(t) \right|_{t=j_1} = A(1 + Bj_1)^{\frac{1}{2}} - A - F_f(j_1) = P_o - (P_o + kx_o) \frac{\alpha^2}{(\alpha + x_o)^2}$$

$$\text{however, since } F_f(j_1) = (P_o + kx_o) \frac{\alpha^2}{(\alpha + x_o)^2}$$

$$A(1 + Bj_1)^{\frac{1}{2}} - A = P_o \quad \text{Eq 15}$$

The acceleration of the armature is given by $\text{acc.} = F_d(t)/M$
and using the results of Equation 13 we have

$$\text{acc.} = \frac{A}{M} \left[(1 + Bt)^{\frac{1}{2}} - 1 \right] - \frac{F_f(j_1)t}{j_1 M}$$

Integrating and satisfying the initial condition that velocity
at $t = 0$ is zero gives

$$\text{Velocity} = \frac{A}{M} \left[\frac{2(1 + Bt)^{3/2}}{3B} - t - \frac{2}{3B} \right] - \frac{F_f(j_1) t^2}{2j_1 M}$$

Integrating again and satisfying the initial condition that
displacement at $t = 0$ is zero gives

$$x = \frac{A}{M} \left[\frac{4(1 + Bt)^{5/2}}{15B^2} - \frac{t^2}{2} - \frac{2t}{3B} - \frac{4}{15B^2} \right] - \frac{F_f(j_1) t^3}{6j_1 M} \quad \text{Eq 16}$$

For $|Bt| \leq 32$ the quantity $(1 + Bt)^{5/2}$ may be approximated by
the polynomial

$$(1 + Bt)^{5/2} \approx 1 + \frac{5}{2} Bt + \frac{15}{8} B^2 t^2 + \frac{15}{48} B^3 t^3 \quad \text{Eq 17}$$

This is best shown in Figure 5 when both sides of Equation 17 are plotted and the error caused by use of Equation 17 is seen to be small for $Bt < 32$.

If Equation 17 is now substituted into Equation 16 and evaluated for $t = j_1$ we have

$$x_o = \left[\frac{A B}{12M} - \frac{F_f(j_1)}{6j_1 M} \right] j_1^3 \quad \text{Eq 18}$$

From Equation 14 we may substitute for AB in Equation 18 obtaining

$$x_o = \frac{2(P_o + kx_o)(R_c + R_d)}{6ML_c} j_1^3$$

or

$$j_1 = \left[\frac{3ML_c x_o}{(P_o + kx_o)(R_c + R_d)} \right]^{\frac{1}{3}} \quad \text{Eq 19}$$

However, a condition has been imposed on Equation 19 when the approximation in Equation 17 was used. Equations 14 and 15 may be solved for A when $t = j_1$ which results in

$$A = \frac{P_o \delta}{2[2(R_c + R_d)j_1/L_c + j_1 \nabla^2 - \delta]} \quad \text{where } \delta = \frac{P_o}{P_o + kx_o}$$

however, since in general $\nabla^2 \ll 2(R_c + R_d)/L_c$ we have

$$A \approx \frac{P_o \delta}{2[2(R_c + R_d)j_1/L_c - \delta]}$$

Substituting this back into Equation 15 and considering the same inequality to hold as above

$$Bj_1 \approx \frac{8(R_c + R_d)j_1[2(R_c + R_d)j_1/L_c - \delta]}{\delta^2 L_c}$$

Therefore, the condition imposed on Equation 19 is good when the results satisfy Equation 20

$$\left| \frac{(R_c + R_d) j_1 [2(R_c + R_d) j_1 / L_c - \delta]}{\delta^2 L_c} \right| \leq 4 \quad \text{Eq 20}$$

If we now let τ equal the time constant of the discharge circuit $L_c / (R_c + R_d)$ we have

$$\begin{aligned} -4\delta^2 &\leq \frac{j_1}{\tau} \left[2 \frac{j_1}{\tau} - \delta \right] \leq 4\delta^2 \\ 2 \left(\frac{j_1}{\tau} \right)^2 - \delta \frac{j_1}{\tau} - 4\delta^2 &\leq 0 \\ \frac{j_1}{\tau} &\leq 1.68\delta \end{aligned} \quad \text{Eq 21}$$

Where Equation 21 is not the only inequality but the only one of physical interest.

The determination of the transit drop-out time, j_2 , will now be considered. This will be the case when there is a comparatively small change in flux force to the change in spring force for a constant current during the drop-out period. This condition is illustrated in Figure 4. For a force in the direction to release the armature to exist, the current must fall continuously to produce a force less than that of the spring. This condition will be approximated by assuming the force as a function of time is due entirely to the exponential decrease in current. A first order approximation of this force would be,

$$F_d(t) \doteq (P_o + kx_o) \left(1 - \exp \left[- \frac{2(R_c + R_d)}{L_c} t \right] \right) \quad \text{Eq 22}$$

With this approximation the initial slope will be the same as that assumed in Part 2. However, the final value would be larger than actually expected for the assumptions made because the spring force will decrease.

The acceleration of the armature is given by $\text{acc.} = F_d(t)/M$ and using the results of Equation 22 we have

$$\text{acc.} = \frac{(P_o + kx_o)}{M} \left[1 - \exp(-t/\tau) \right]$$

$$\text{where } \tau = \frac{L_c}{2(R_c + R_d)}$$

Integrating and satisfying the initial condition that velocity, v , at $t = 0$ is zero.

$$v = \frac{(P_o + kx_o)}{M} \left[t + \tau \exp(-t/\tau) - \tau \right]$$

Integrating again and satisfying the initial condition that displacement at $t = 0$ is zero

$$x = \frac{(P_o + kx_o)}{M} \left[\frac{t^2}{2} - \tau^2 \exp(-t/\tau) - \tau t + \tau^2 \right] \quad \text{Eq 23}$$

For $t/\tau \leq 1.2$ the quantity $\exp(-t/\tau)$ may be approximated by the polynomial

$$\exp(-t/\tau) \approx \left[1 - t/\tau + \frac{1}{2}(t/\tau)^2 - \frac{2}{15}(t/\tau)^3 \right] \quad \text{Eq 24}$$

This is best shown in Figure 6 where both sides of Equation 24 are plotted and the error caused by use of Equation 24 is seen to be small for $t/\tau < 1.2$.

Substituting Equation 24 into 23 the results reduce to

$$x = \frac{4(P_o + kx_o)(R_c + R_d)}{15 M L_c} t^3 \quad \text{Eq 25}$$

Solving Equation 25 for $t = j_2$ (i.e. $x = x_o$) we have

$$j_2 = \left[\frac{3.75 M x_o L_c}{(P_o + kx_o)(R_c + R_d)} \right]^{\frac{1}{3}} \quad \text{Eq 26}$$

Because the resulting expressions for j_1 and j_2 are almost identical in value and the inequalities to be solved are closely related, these two equations are approximated by one equation.

$$j_3 = \left[\frac{3.5 M L_c x_o}{(P_o + kx_o)(R_c + R_d)} \right]^{\frac{1}{3}} \quad \text{Eq 27}$$

The form of j_3 is not complete for the transit drop-out time because of the inequalities required to be fulfilled and the equations indicate that as the discharge resistance increases toward an open circuit the transit drop-out time approaches zero. It must however, approach some finite time determined by the spring force. This limiting value in drop-out time, j_4 , may be approximated by assuming the spring force to be constant.

$$\text{acceleration} = 1/M (P_o + kx_o)$$

Integrating twice and satisfying the initial conditions of $v = 0$ and $x = 0$ at $t = 0$

$$x_o = \frac{1}{2M} (P_o + kx_o) j_4^2$$

or

$$j_4 = \left[\frac{2M x_o}{P_o + kx_o} \right]^{\frac{1}{2}} \quad \text{Eq 28}$$

Combining Equation 27 and 28 into a complete transit drop-out time equation is the next step. Investigation of the inequalities shows that when they are satisfied j_3 is somewhat larger than j_4 . Experimental evidence seems to indicate, in this region of transition between equations, j_3 and j_4 can be combined as the cube root of the sum of the cubes. This result also satisfied the boundary conditions.

$$j = \left(\left[\frac{3.5 M L_c x_o}{(P_o + kx_o)(R_c + R_d)} \right] + \left[\frac{2 Mx_o}{P_o + kx_o} \right]^{3/2} \right)^{1/3} \quad \text{Eq 29}$$

Further experiments justifying the above results will be made and submitted in the next report along with any required changes.

Throughout the above development of j the M K S system of units has been assumed for convenience in equation manipulations. Now converting Equation 29 to the conventional units used in these reports, where mass and force are in grams and distance is in inches, we have

$$j = \left(\left[\frac{.00906 M x_o L_c}{(P_o + kx_o)(R_c + R_d)} \right] + \left[\frac{.00518 Mx_o}{P_o + kx_o} \right]^{3/2} \right)^{1/3} \quad \text{Eq 30}$$

Table I

A	=	effective area of working air gap
α	=	nonforce producing air equivalent of the magnetic circuit
B_d	=	flux density in air gap at drop-out current i_d
δ	=	$P_o/(P_o + kx_o)$
∇	=	$\alpha/(\alpha + x_o)$
E	=	open circuit supply voltage
ϕ_d	=	total flux in air gap at drop-out current i_d
i_d	=	the current for which the force due to the flux is equal that of the spring with armature in energized position.
i_{ss}	=	steady state coil current when energized
j	=	armature transit time for drop-out cycle
k	=	effective spring constant of spring system
L_c	=	inductance of coil when armature is in the energized position
M	=	effective mass of armature system
μ_o	=	permeability of free space
N	=	coil turns
η	=	design stability factor
P_o	=	effective restoring force on the armature at pick-up
R_c	=	coil resistance
R_d	=	discharge resistance external to coil
R_t	=	total resistance presented to open circuit power supply voltage
\mathcal{R}	=	reluctance of magnetic circuit
t_d	=	time interval from instant supply is removed until force on the armature changes direction
x_o	=	length of armature working air gap

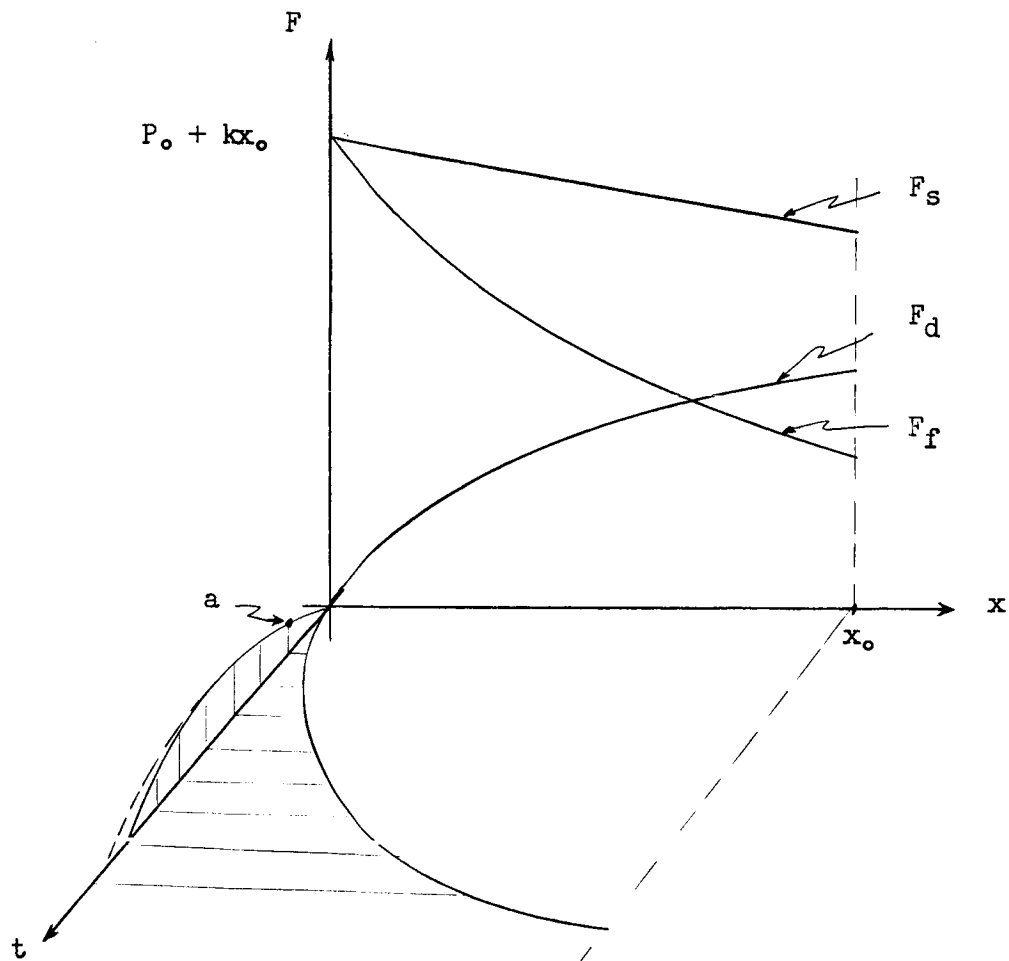


Figure I

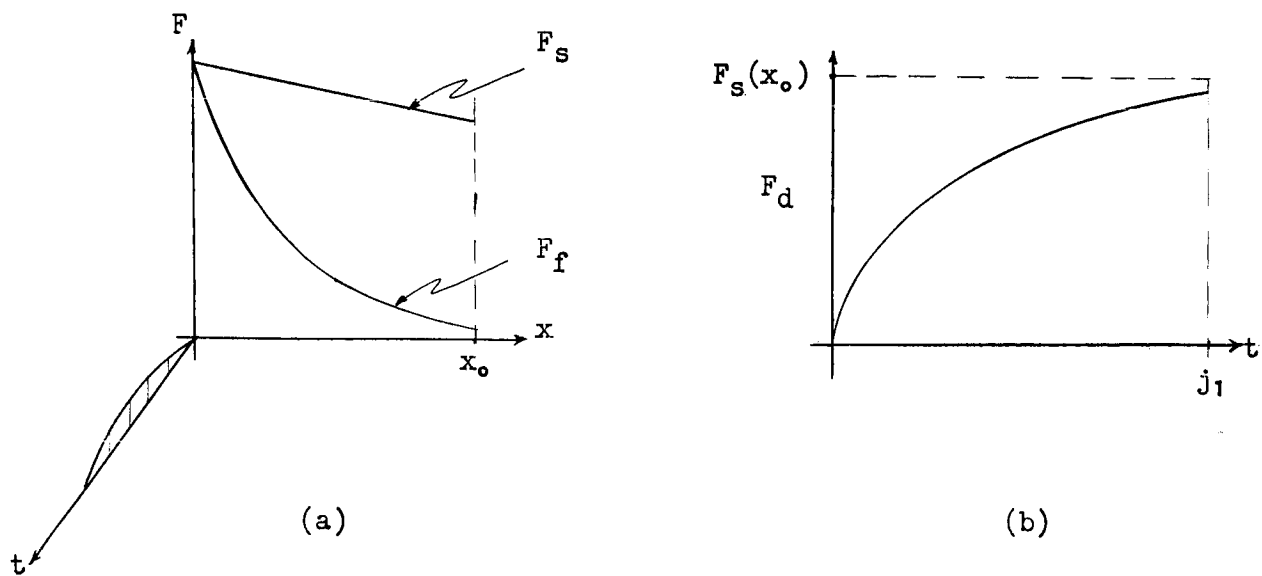


Figure 2

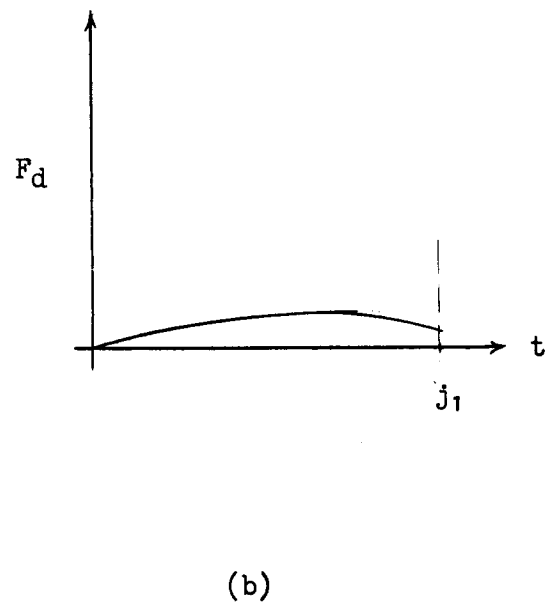
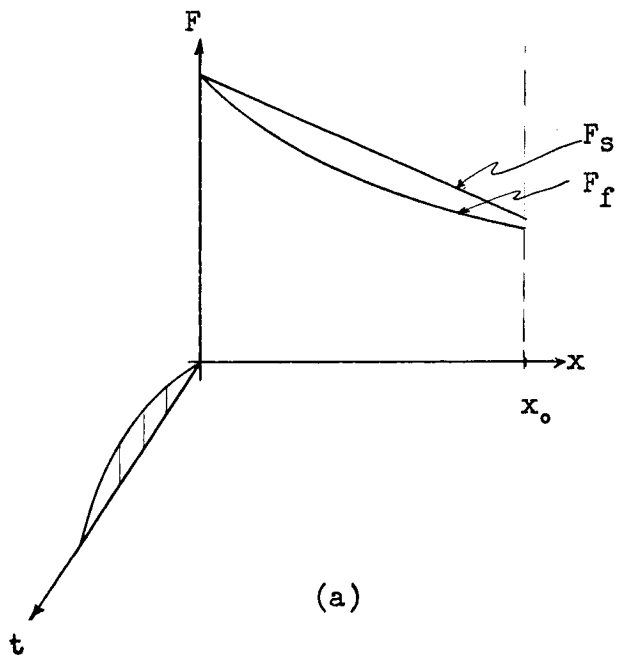


Figure 3

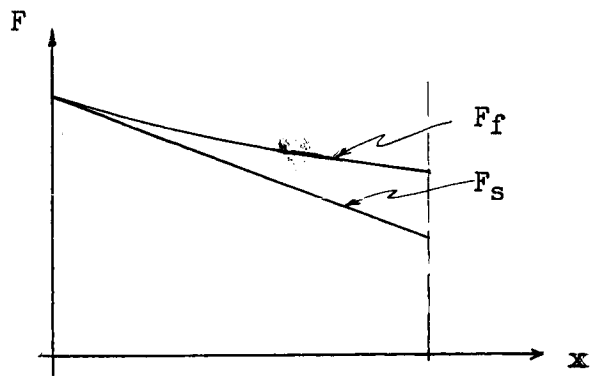
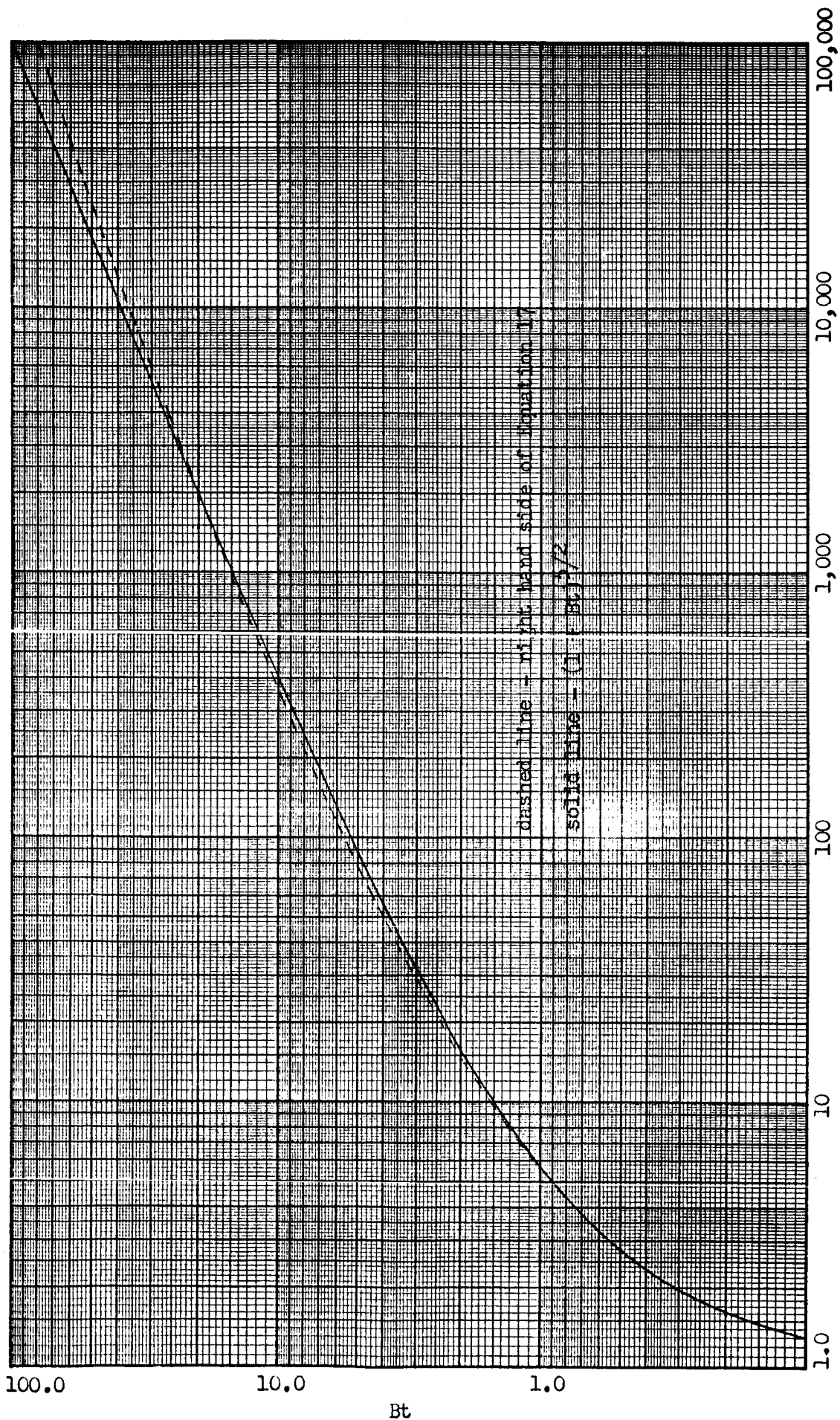


Figure 4



f (Bt) from Equation 17

Figure 5

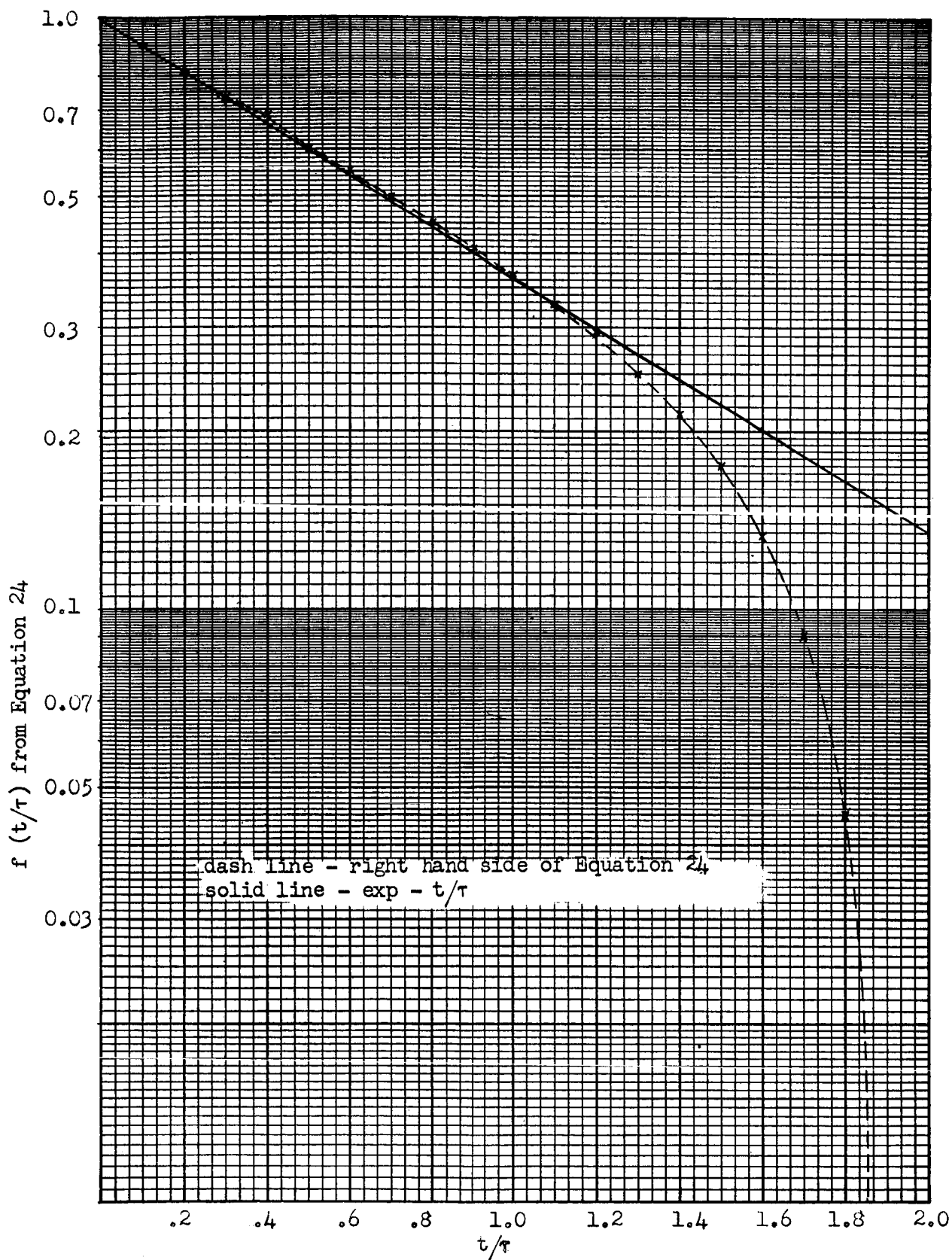


Figure 6

SECTION I

DESIGN MODIFICATION OF THE PARALLEL COIL 300 AMPERE CONTACTOR

The 300 ampere contactor under consideration utilizes a parallel two coil arrangement that uses both coils for operate and one coil for hold. One possible weakness of this arrangement is the possible malfunctioning of the control switch used to switch from the operate to the hold coil arrangement. Failure to open during the operate cycle would result in using about twice the anticipated coil power. Failure to reclose during release would be more drastic since the contactor would not operate on one coil at rated voltage.

The design modification presented here is to consider the result of changing the core diameter to maximize the pull per watt of the core with the hope that a one coil no control switch unit can be made. It is desired to maintain the outside coil dimensions the same and the core dimensions, other than its diameter, also the same. From the mathematical model being used only 9 parameters out of 19 parameters can be fixed or held constant. The other remaining 10 parameters will be subject to change.

The parameters held fixed were:

- coil voltage E
- coil length l
- outside coil diameter s
- working air gap and magnetic circuit $x_0 + \alpha$
- stability factor η
- coil bobbin insulation thickness u
- effective back tension P_0
- mass of moving system M

The only parameter that was desired to be changed was the ratio of the core diameter to the outside core diameter. This ratio is symbolized by β .

The parameters which are subject to change because of changing β are:

- diameter of bare wire δ
- plunger transit time k
- coil turns N
- coil power P

coil resistance R_c
 plunger pick-up time t_p
 total seating time t_s
 cross sectional area of working air gap A
 core diameter d
 ratio of coil bobbin insulation thickness
 to outside coil diameter σ

The relationships used in this mathematical model are as follows:

$$f_1 \quad \eta = 157.5 \frac{R_c(x_o + \alpha)\sqrt{2P_o}}{EN \sqrt{\mu_o A}}$$

$$f_2 \quad t_p = 10^{-8} \frac{N^2 \mu_o A}{(x_o + \alpha)R_c} \ln\left(\frac{1}{1 - \eta}\right)$$

$$f_3 \quad k = (8.66 \times 10^{-3}) \left[\frac{36M x_o^2 R_c}{E^2 \eta (1 - \eta)} \right]^{\frac{1}{3}}$$

$$f_4 \quad P = E^2/R_c$$

$$f_5 \quad R_c = \frac{(0.865 \times 10^{-6}) s^2 \ell (1 - \beta - \sigma)(1 + \beta + \sigma) g_r}{\delta^4}$$

$$f_6 \quad N = \frac{0.637 s \ell (1 - \beta - \sigma) g_n}{\delta^2}$$

$$f_7 \quad \mu_o A = \mu_o (d^2 - d_1^2) \pi/4 \quad (\mu_o = 3.19)$$

d_1 = diameter of hole in core

$$f_8 \quad t_s = t_p + k$$

$$f_9 \quad \beta = d/s$$

$$f_{10} \quad \sigma = u/s$$

In order to check to see if the selected (fixed and those being changed) parameters are non-conflicting the map shown in Figure 1 is used. This map is a listing of the different parameters as rows and the relationships as columns. The selected parameters are marked with a circle in the first column and the determined parameters by a \square or \square . The \triangle is used for those parameters involved in the solution of a set of simultaneous equations. The set of selected parameters are compatible in this case since they resulted in all the remaining parameters being determined through the use of the relationships. The order of solution of the relationships is shown by the alphabetical listing at the bottom of the map. Relationships f_1 , f_5 and f_6 must be solved simultaneously for parameters δ , N and R_c . The solution is outlined as follows:

Relation f_1 can be written as:

$$N = X R_c \quad (1)$$

relation f_6 as

$$N = Y/\delta^2 \quad (2)$$

and relation f_5 as

$$R_c = Z/\delta^4 \quad (3)$$

Solving equations 2 and 3 for δ^4 and setting them equal gives

$$\frac{Y^2}{N^2} = \frac{W}{R_c}$$

or

$$R_c = \frac{WN^2}{Y^2} \quad (4)$$

from equation 1

$$R_c = \frac{N}{X} \quad (4a)$$

therefore

$$\frac{WN^2}{Y^2} = \frac{N}{X} \quad (5)$$

Since W , Y and X are known, then the solution of equation 5 for N gives: $N = Y^2/XW$ where:

$$X = \frac{157.5(x_o + \alpha)\sqrt{2P_o}}{B\eta\sqrt{\mu_o A}} \quad (6)$$

$$Y = 0.637 \text{ sl } (1 - \beta - \sigma)g_n \quad (7)$$

$$W = 0.865 \times 10^{-8} \text{ s}^2 \ell (1 - \beta - \sigma)(1 + \beta + \sigma)g_r \quad (8)$$

g_n and g_r are winding space factors.

Going back to the solution order on the map shows that relationship f_{10} is solved for σ , f_9 for d , f_7 for $\mu_o A$, f_1 , f_5 and f_6 simultaneously for R_o , N and δ . f_2 for t_p , f_3 for k , f_4 for P and f_8 for t_s .

Numerical values for the fixed parameters were obtained from known operating conditions and the drawings which were available. However, two parameters $(x_o + \alpha)$ and P_o were not known. Therefore, a transient test was performed on the engineering sample of the hermetically sealed contactor to obtain data to calculate $(x_o + \alpha)$ and P_o . Since the mathematical model is for a single coil device, an approximation had to be made to make this two parallel coil unit fit the model. The assumption made was that this two coil device was equivalent to a one coil unit having the number of turns equal to the average of the two coils and the total coil resistance measured at the time of the test. Since only the pick-up time was involved then the coil resistance is that of the two coils in parallel.

Relationship f_2 was used to compute $x_o + \alpha$ since the parameters t_p , N , $\mu_o A$, R_o and η were either measured directly or calculated from drawings. A combination of f_1 and f_2 with $(x_o + \alpha)$ eliminated from them was used to compute P_o . This combined equation was

$$t_p = \frac{157.5 \times 10^{-8} N \sqrt{\mu_o A} \sqrt{2P_o}}{\eta} \ln \frac{1}{1 - \eta} \quad (9)$$

The test data (obtained from Figure 7, Section IV, 12th Interim Report) and calculations used for determining P_o and $(x_o + \alpha)$ were:

$$t_p = 13.5 \text{ ms}$$

$$\eta = 0.75$$

$$R_c = 34 \text{ ohms}$$

$$N = 1388$$

$$\mu_o A = 0.922$$

The calculated value of $x_o + \alpha$ is 53.6×10^{-3} inches and P_o is 4750 grams.

With these values then the numerical values of the selected parameters are as follows:

$$E = 28 \text{ volts}$$

$$l = 0.725 \text{ inches}$$

$$s = 1.93 \text{ inches}$$

$$x_o + \alpha = 54 \times 10^{-3} \text{ inches}$$

$$\eta = 0.57$$

$$u = 0.126 \text{ inches}$$

$$P_o = 4750 \text{ grams}$$

$$M = \text{assumed constant}$$

$$R = 0.59 \text{ value to maximize pull per watt}$$

The numerical value of the 10 remaining parameters can now be calculated starting with relationship f_{10} . From relationship f_{10} the value of σ is 0.065. Next the core diameter d is calculated from f_9 as $d = 1.14$ inches. The value of $\mu_o A$ calculated from f_7 is 3.01 lines per amp-turn inch. From equation 5 combined with 6, 7 and 8 the value of N is 1355 turns. By using equation 4a the value of R_c is 45.2 ohms. From equation 3 the value of δ is 1.183×10^{-2} inches which is approximately #29 wire. Now using relationship f_2 the value of t_p

is 19 milliseconds. Relationship f_3 results in k equal to approximately 8 milliseconds. The value of coil power P from f_4 is 17.4 watts. The total seating time t_s from f_8 is 27 milliseconds. These values are tabulated below for convenience.

$\sigma = 0.065$
 $d = 1.14$ inches
 $\mu_o A = 3.01$ lines per amp-turn inch
 $N = 1355$ turns
 $R_c = 45.2$ ohms
 $\delta = 1.183 \times 10^{-2}$ inches
(approx. #29 wire)
 $t_p = 19$ ms
 $k = 8$ ms
 $P = 17.4$ watts
 $t_s = 27$ ms

The steady state power required of the modified unit is essentially the same value as the hold power on the original unit but the modified unit has only one coil and consequently no coil switching contact arrangement. The pick-up time of the modified unit is longer than the original by about 50% but this is caused by the fact that the operate current is less in the modified unit. The outside dimensions and configuration of the modified unit are the same as in the original. The primary change is that the movable core diameter is increased from 0.684" to 1.140" with the associated change in the inside coil diameter and stationary core diameter.

TABLE OF CONTENTS

Part E

VIBRATION

<u>SUMMARY</u>	<u>Section</u>	<u>Section Report</u>
Applications of Vibration Theory in Relay Design- - - - -	IV	9th
Vibration Testing of a 75 Ampere Rotary Type Contactor (part 1)- - - - -	II	12th
Vibration Testing of a 75 Ampere Rotary Type Contactor (part 2)- - - - -	II	13th

Tab Color Code

Orange	9th Interim	1 July - 30 Sept., 1963
Rose	10th Interim	1 Oct. - 30 Nov., 1963
Green	11th Interim	1 Dec., 1963 - 31 Jan., 1964
Blue	12th Interim	1 Feb. - 31 March, 1964
Yellow	13th Interim	1 April - 31 May, 1964

SUMMARY

Part E

Vibration

The objective pursued in this part is to study mathematical models of certain types of spring mass systems, first assuming linear springs and then eventually non-linear springs, in order to better understand the dynamics of the contact system. In order to obtain general solutions of useable form, limitations are put on the number of degrees of freedom in the mathematical model. The dynamics of the actual device may be active in all 6 degrees of freedom with certain ones being the most critical. The problem then is to decide which mathematical model can be used with a particular device in order to obtain the most accurate information.

The first section of this part presents the development of a mathematical model for a two mass two spring linear system and experimental results of a particular power relay which could be represented by this model.

The last two sections of this part present a thorough analysis of the resonant conditions existing in the contactor and container of the 75 ampere rotary type relay. The cantilever way the unit is mounted in the container and the manner in which the contact system is mounted on the coils results in a multimass-spring system with several degrees of freedom. Several different mounting arrangements of the unit inside the container have been evaluated. Improvements have been made with these different arrangements but the shift in the resonant condition is not sufficient yet to decrease the G level experienced by the contacts by the required amount. However, the contact pressure and mass is such that the contacts will withstand 30 or more G's. If the relay and container resonant frequency can be shifted far enough beyond 2000cps then a satisfactory unit can be developed.

SECTION IV

APPLICATIONS OF VIBRATIONS THEORY IN RELAY DESIGN

Introduction

This study was conducted to primarily investigate and attempt to determine the dynamic characteristics of the contact system of a particular type of electromagnetic relay. The development of sophisticated guided missile systems has created applications for this particular make of relay in which its structure would be, in certain cases, subjected to external vibration in various forms.

As the mounting case of the relay is subjected to different types of vibration, the moving components of its contact system may randomly separate from the closed position for small periods of time or they may chatter or bounce indefinitely after initial separation. The cause of initial separation of the closed contacts is the fundamental consideration of this study. Any subsequent motion is beyond the scope of this development.

Use is made of the fundamental theory of contact separation developed by the author and Dr. R. L. Lowery, and Mr. B. C. Riddle during the early months of this year,¹ to explain, theoretically, the motion of the contact system components due to a certain type of external vibration input. Mathematical models tailored to the contact system of the particular relay being considered, are discussed in order to clarify the application of the contact separation theory.

¹Lowery, Dr. R. L., Riddle, B. C. and Stone, G. C., Vibration Control in Relay Design, Part I, Interim Report No. 7 and Part II, Interim Report No. 8, NASA, Contract: NAS 8-2552.

Certain tests in which the components of the relay's contact system were subjected to various types of simulated excitation, were conducted and the results are discussed and compared to the theoretical explanation.

It is well known that the relay designer is being incumbered with a multitude of unsolved problems in the area of contact system component separation due to external vibration. At present, his demand for new knowledge concerning these problems cannot be satisfied. It is the ultimate purpose of this study to gain further information about electromagnetic relay contact system dynamics which may be of value to the relay designer.

Application of Theory

The particular relay considered is shown in Figure 11, page 19. It features three separate contact systems actuated by a single solenoid. These contact systems will be referred to as upper, middle and lower according to the mounting position of each in Figure 11. The middle and lower contact systems are virtually the same. The upper system differs from the other two in that the structure of the permanent contact does not contain the vertical stiffener found on the other two but merely has a small, square shaped piece acting as a stiffener.

External excitation may come from many directions owing to the particular mounting position of the relay and the direction of external vibration. Only external excitation applied in the vertical direction parallel to the longitudinal axis of the solenoid plunger rod will be considered. (See Figure 11).

Mathematical models with controlled parameters are now discussed. For each model, mathematical expressions predicting contact separation criteria are developed.

One other point must be made clear. Only a sinusoidal type input is considered throughout this study.

Stationary Contact Rigid, Translating Contact Flexible

Each contact system of Figure 11 may be considered separately. Let it be represented by Figure 1, page 3.

To begin the mathematical development, a simple case is investigated. The stationary contact is assumed perfectly rigid ($k = \infty$). Overtravel must be provided entirely by the flexibility of the translating contact. Let the translating contact be represented by a mass, m , connected to a weightless linear coil spring with constant, k , as shown in Figure 1.

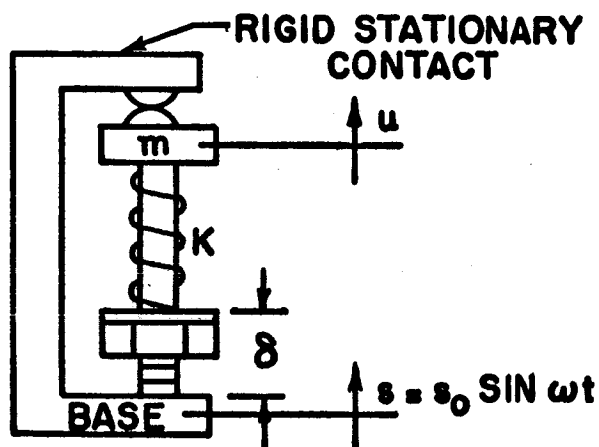


Figure 1

Schematic diagram showing stationary contact rigid, translating contact flexible.

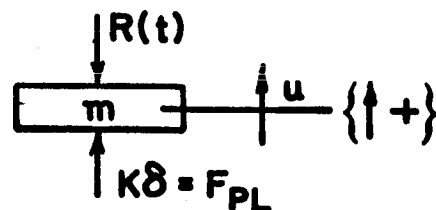


Figure 2

Free body diagram of the system shown in Figure 1.

The linear (force deflection curve is represented by a straight line) spring provides the means for plunger overtravel through the deflection δ , as shown in Figure 1.

Allowing only linear motion along a single axis (single degree of freedom), neglecting damping in the system, and assuming sinusoidal motion of the base

Let: s = absolute displacement of the base
 u = absolute displacement of the movable contact
 k = spring constant of the spring representing the flexibility of the translating contact
 m = mass of the translating contact
 δ = deflection of the translating contact spring from its unloaded length
 $F_{pl} = k\delta$ = translating contact spring preload
 $R(t)$ = time dependent reaction force between the mass and the base

From Figure 2, the differential equation of motion is

$$m\ddot{u} - F_{pl} + R(t) = 0 \quad (1)$$

For $R(t) > 0$ the contacts have not separated and $\ddot{u} = \ddot{s}$

$$\text{Then } R(t) = F_{pl} - m\ddot{s} \quad (2)$$

For contact separation $R(t) = 0$ and

$$F_{pl} = m\ddot{s} \quad (3)$$

or

$$G_L = \frac{F_{pl}}{w} \quad (4)$$

Where $G_L = \frac{\ddot{s}}{g}$ = number of g's acceleration, and $w = mg$

Where $g = 386 \text{ in/sec}^2$

equation (4) indicates that contact breakage will occur only when the base is accelerating upward. Equation (4) is an expression of Newton's second law. Notice that equation (4) is independent of excitation frequency.

As an example using equation (4), let $w = 0.148$ lb. and $F_{pl} = 0.92$ lb., equation (4) yields: $G_L = 6.21$ g's.

Both Contacts Flexible

Both the stationary and translating contacts are considered flexible. The translating contact and its flexibility are represented as shown in Figure 1. The stationary contact and its flexibility can now be replaced by a prismatical cantilever beam. A close inspection must be made of the dynamic characteristics of this beam. A prismatical cantilever beam represents a continuous elastic body and hence possesses infinite number of degrees of freedom (see Figure 3). However, by assuming the form of the deflection curve to be known, Lord Rayleigh (2)¹ has shown that the system can be treated as one with a single degree of freedom as long as only properties involved in the fundamental mode of vibration of the beam are sought.

According to ratio of length to thickness, it will be assumed that the cantilever beam representing the stationary contact must be quite stiff with respect to its mass and length. This assumed characteristic allows the beam to be replaced by a single degree of freedom system.

¹Numbers in parentheses refer to sources listed in the selected bibliography.

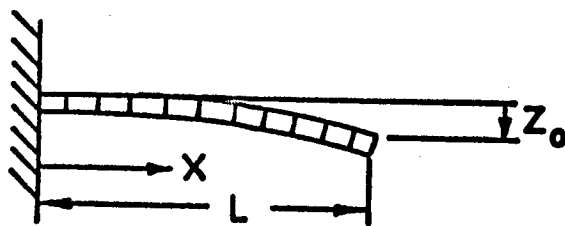


Figure 3

Uniform Cantilever Beam

According to Rayleigh's method, it is assumed that the amplitude of the beam at any point x is given with sufficient accuracy by the statical deflection curve of a weightless cantilever beam with a concentrated load, p , at the end. Writing this equation in the form

$$Z = \frac{1}{2} Z_0 \left[2 \left(\frac{x}{L} \right)^2 - \left(\frac{x}{L} \right)^3 \right] \quad (5)$$

Where $Z_0 = \frac{pL^3}{3EI}$ is the amplitude of the free end, the stiffness at the free end becomes

$$k_{eq} = \frac{3EI}{L^3} \quad (6)$$

The kinetic energy can next be determined by integrating the product of mass and the square of the velocity over the length of the beam

$$\begin{aligned} T_{max} &= \frac{w}{2g} \int_0^L (wZ)^2 dz = \frac{w}{2g} \left(\frac{wZ_0}{2} \right)^2 \int_0^L \left[2 \left(\frac{x}{L} \right)^2 - \left(\frac{x}{L} \right)^3 \right]^2 dx \\ &= \frac{1}{2} \left(\frac{33 wL}{140 g} \right) w^2 Z_0^2 \end{aligned} \quad (7)$$

Where w = weight of the continuous beam per unit length, lb/ft.
 Equation (7) indicates that for the assumed deflection curve, the continuous beam is equivalent in vibration characteristics to that of a weightless beam with a concentrated weight $\left(\frac{33}{140} wL\right)$ at the end.

The cantilever beam can now be replaced by a weightless, linear coil spring with equivalent constant, $k_{eq} = \frac{3EI}{L^3}$, and a lumped mass $m = \frac{33}{140} wL$.

The two contacts and their represented flexibilities are shown in Figure 4.

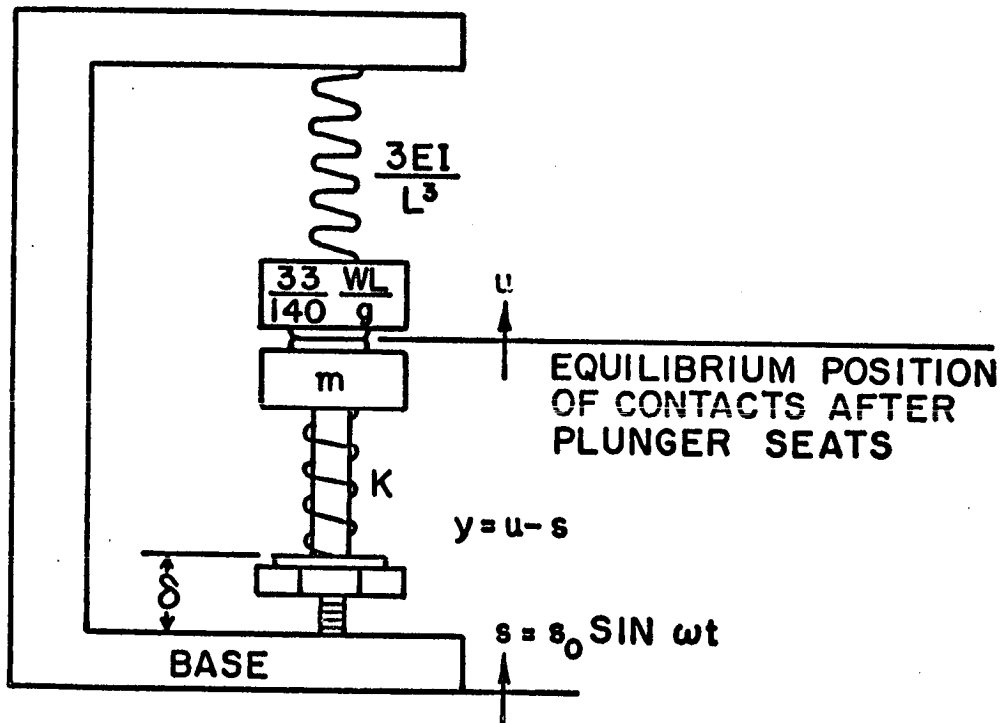


Figure 4

Schematic diagram showing both contacts
 and their represented flexibilities

From Figure 6, it can be seen that plunger overtravel is provided through δ , which is now the sum of the deflections of the translating contact spring and the equivalent stationary contact spring.

Before motion of the system in Figure 4 can be studied, the force-deflection curve of the spring representing the flexibility of each contact must be examined (see Figures 5, 6, 7 and 8).

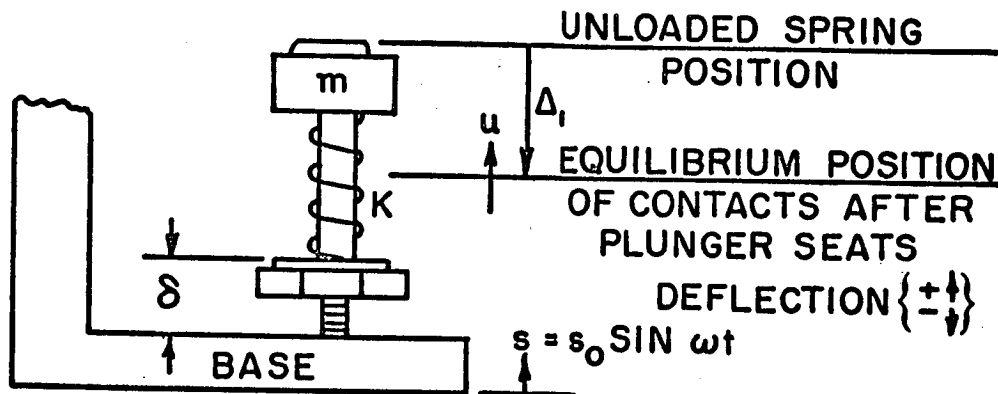


Figure 5

Schematic diagram of translating contact system.

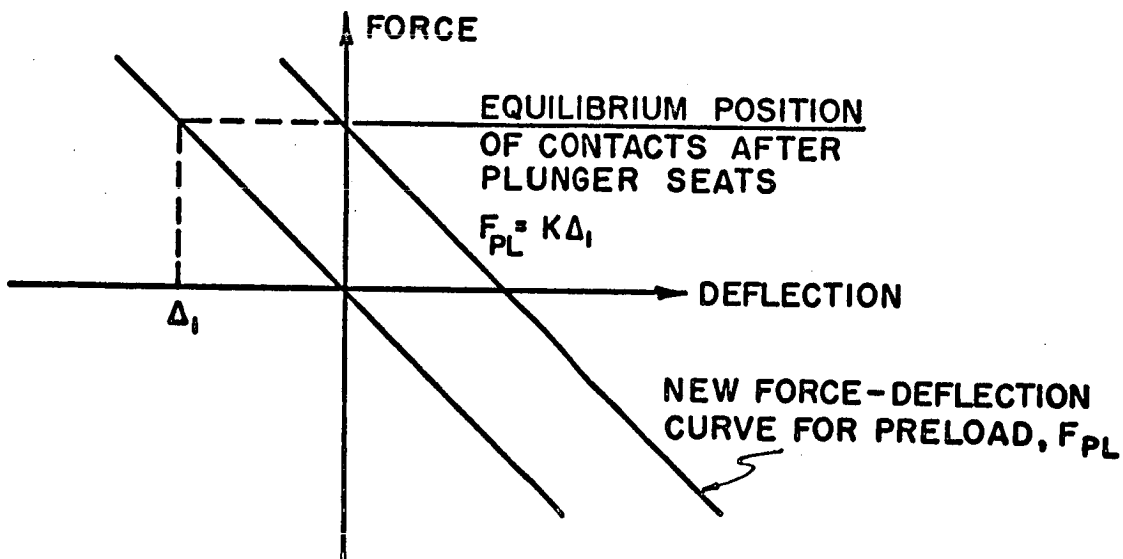


Figure 6

Force-deflection curves for translating contact spring.

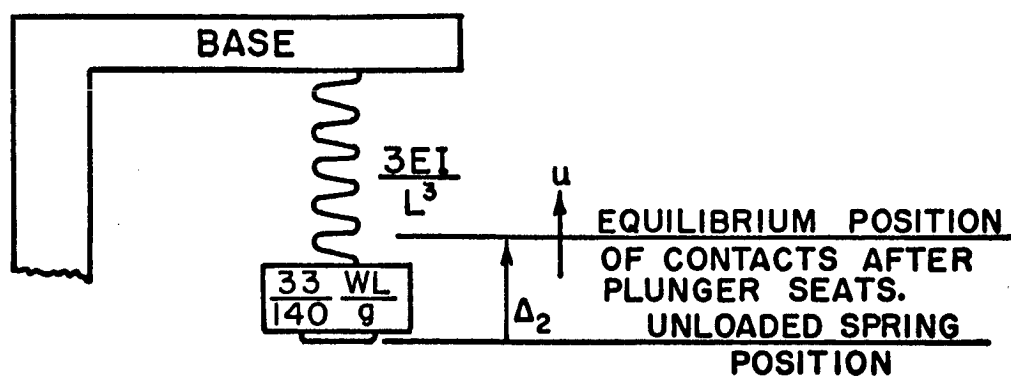


Figure 7

Schematic diagram of stationary contact system.

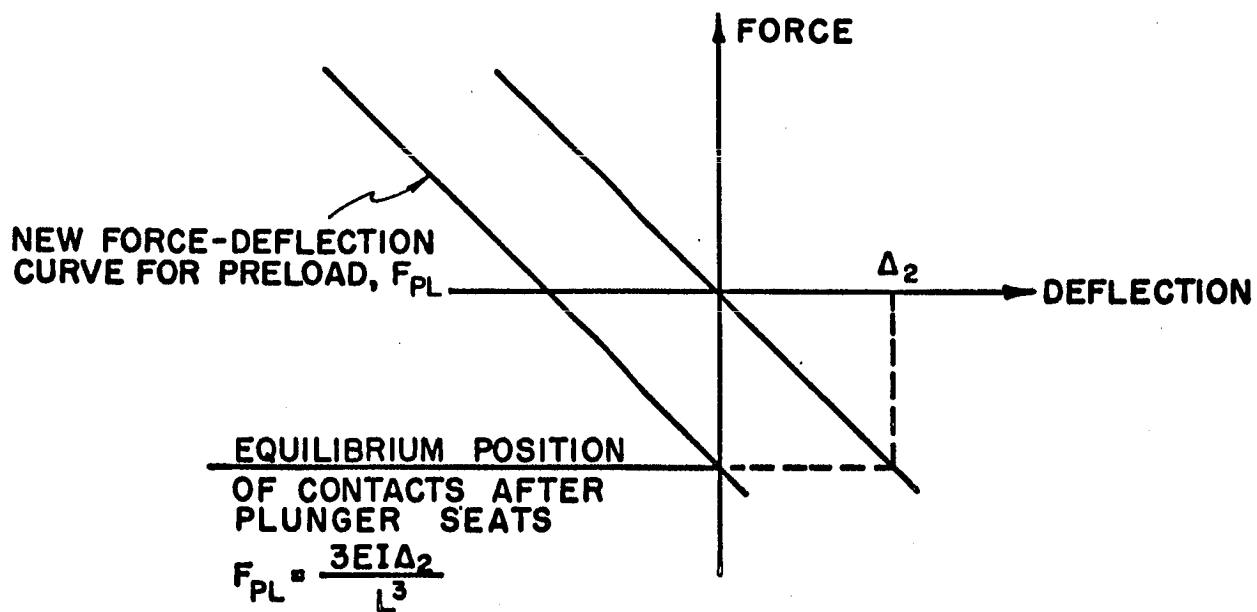


Figure 8

Force-deflection curves for equivalent stationary contact spring.

Each contact spring is deflected an amount, Δ , which has the effect of producing a new force deflection curve for each spring, parallel to the original one, but displaced along the vertical axis of the force-deflection plot (see Figures 6 and 8).

Again, only one degree of freedom is allowed and damping in the system is neglected.

Assuming sinusoidal excitation of the base,

- Let:
- s = absolute displacement of the base
 - u = absolute displacement of the contacts before separation
 - y = $u - s$
 - k = spring constant of the translating contact spring
 - $\frac{3EI}{L^3}$ = spring constant of the equivalent spring representing the stationary contact
 - m = the mass of the translating contact
 - $\left(\frac{33}{140}\right)\left(\frac{WL}{g}\right)$ = the mass of the stationary contact
 - Δ_1 = deflection of the translating contact spring from its unloaded length
 - Δ_2 = deflection of the translating contact spring representing the stationary contact from its unloaded length
 - $F_{p1} = k\Delta_1 = \frac{3EI\Delta_2}{L^3}$ = contact spring preload force
 - $\delta = \Delta_1 + \Delta_2$

Prior to separation, the contacts may be considered coupled and could be replaced by one total mass, $m_t = m + \left(\frac{33}{140}\right)\left(\frac{WL}{g}\right)$. From Figures 9

and 10, the motion equation for the entire system is:

$$m_t \ddot{u} = - \left[\frac{3EI}{L^3} + k \right] y \quad (8)$$

or

$$m_t \ddot{u} + k_t y = 0 \quad (9)$$

substituting $\ddot{y} = \ddot{u} - \ddot{s}$ into equation (8)

$$m_t \ddot{y} + k_t y = - m_t \ddot{s} \quad (10)$$

But:

$$s = s_0 \sin \omega t$$

$$\dot{s} = \omega s_0 \cos \omega t$$

$$\ddot{s} = -\omega^2 s_0 \sin \omega t$$

Therefore:

$$m_t \ddot{y} + k_t y = m_t \omega^2 s_0 \sin \omega t \quad (11)$$

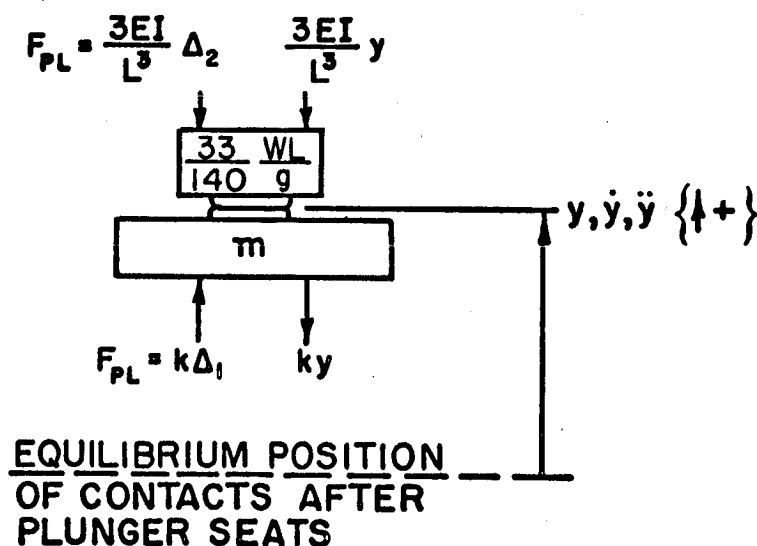


Figure 9

Free body diagram of system immediately before separation
above the contact equilibrium position.

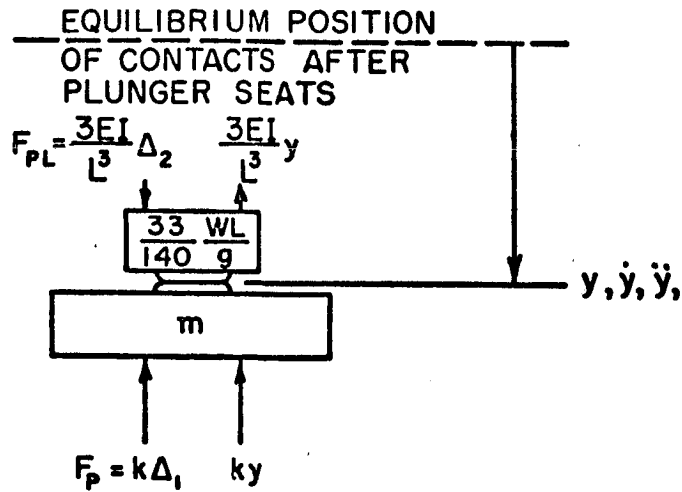


Figure 10

Free body diagram of complete system immediately before separation below the contact equilibrium position.

Since the damping in the system has been assumed negligible, the steady state solution of equation (11) will have the form

$$\begin{aligned} y &= Y \sin \omega t \\ \dot{y} &= Y\omega \cos \omega t \\ \ddot{y} &= -Y\omega^2 \sin \omega t \end{aligned} \tag{12}$$

substituting for y and \ddot{y} in equation (11).

$$-m_t \omega^2 Y + k_t Y = m_t \omega^2 s_o \tag{13}$$

solving for Y :

$$Y = \frac{\omega^2 s_o}{\omega_h^2 - \omega^2} \tag{14}$$

where

$$\omega_n = \sqrt{\frac{k_t}{m_t}} = \sqrt{\frac{k + \frac{3EI}{L^3}}{m + \left(\frac{33}{140}\right)\left(\frac{WL}{g}\right)}} = \text{natural frequency of the system}$$

Separation may occur either above or below the armature seating equilibrium position (see Figures 9 and 10).

Equation (12) shows that for $y > 0$, $\ddot{y} < 0$ and for $y < 0$, $\ddot{y} > 0$. Then if separation is assumed to occur above the equilibrium position, from Figure 9, at the instant that separation occurs, the acceleration of the equivalent mass, $\left(\frac{33}{140}\right)\left(\frac{WL}{g}\right)$, must be greater than the acceleration of mass, m . Dividing the summation of forces on each contact by its mass

$$\frac{-F_{pl} - \frac{3EI}{L^3} y}{\left(\frac{33}{140}\right)\left(\frac{WL}{g}\right)} > \frac{F_{pl} - ky}{m} \quad (15)$$

or

$$F_{pl} < \left[\frac{k - \left(\frac{m}{33 \frac{WL}{140 g}}\right)\left(\frac{3EI}{L^3}\right)}{1 + \frac{m}{\left(\frac{33}{140}\right)\left(\frac{WL}{g}\right)}} \right] (y) \quad (16)$$

If separation is assumed to occur below the equilibrium position, from Figure 10, then, again, the acceleration of the equivalent mass

must be greater than that of mass, m , at the instant that separation occurs.

$$\frac{F_{pl} + ky}{m} < \frac{-F_{pl} + \frac{3EI}{L^3} y}{\left(\frac{33}{140}\right)\left(\frac{wL}{g}\right)} \quad (17)$$

or

$$F_{pl} < \left[\frac{\left(\frac{3EI}{L^3}\right) \left(\frac{m}{\frac{33}{140} \frac{wL}{g}}\right) - k}{1 + \frac{m}{\left(\frac{33}{140}\right)\left(\frac{wL}{g}\right)}} \right] (y) \quad (18)$$

The maximum value of y in equations (16) and (18) will most likely cause separation. Equation (14) expresses the maximum amplitude of y .

Therefore, equations (16) and (18) become

$$F_{pl} < \left[\frac{\omega^2 s_o (k - bk_{eq})}{(1 + b)(\omega_n^2 - \omega^2)} \right] \text{above equilibrium} \quad (19)$$

$$F_{pl} < \left[\frac{-\omega^2 s_o (k - bk_{eq})}{(1 + b)(\omega_n^2 - \omega^2)} \right] \text{below equilibrium} \quad (20)$$

where

$$k_{eq} = \frac{3EI}{L^3}$$

$$b = \frac{m}{\left(\frac{33}{140}\right)\left(\frac{wL}{g}\right)}$$

Let

$$\frac{\ddot{s}}{g} = G_L$$

Then

$$\frac{-\omega^2 s_o}{g} \sin \omega t = G_L$$

If $\sin \omega t = 1$, then $\frac{-\omega^2 s_o}{g} = (G_L)_{\max}$

where G_L = number of g's of acceleration

Then substituting into equations (19) and (20): $(G_L)_{\max} (g) = \omega^2 s_o$,

$$F_{pl} < \left[\frac{-(G_L)_{\max} (g)(k - bk_{eq})}{(1 + b)(\omega_n^2 - \omega^2)} \right] \text{above equilibrium} \quad (21)$$

$$F_{pl} < \left[\frac{(G_L)_{\max} (g)(k - bk_{eq})}{(1 + b)(\omega_n^2 - \omega^2)} \right] \text{below equilibrium} \quad (22)$$

Equations (21) and (22) show that separation can occur at only one position, either above or below plunger seating equilibrium. Due to the arrangement of contact deflection, $F_{pl} \geq 0$, assume that for $k > bk_{eq}$, $\omega < \omega_n$. Then equation (21) cannot be true and (22) holds. For $\omega > \omega_n$ equation (22) cannot be true and (21) holds.

Equation (21) and (22) differ only in sign. If the position where separation occurs is of no consequence,

$$\left| F_{pl} \right| < \left| \frac{(G_{L\max}) (g)(k - bk_{eq})}{(1 + b)(\omega_n^2 - \omega^2)} \right| \quad (23)$$

is valid for any frequency.

Substituting: $g = 386 \text{ in/sec}^2$ and $2\pi f = \omega$

$$|F_{pl}| < \frac{9.78 (G_L)_{\max} \left[k - \left(\frac{m}{33 \text{ WL}} \right) \left(\frac{3EI}{L^3} \right) \right]}{\left(1 + \frac{m}{33 \text{ WL}} \right) (f_n^2 - f^2)} \quad (24)$$

Equation (24) is much more representative of existing plunger type contact systems than equation (4).

It is well to note that equation (24) becomes discontinuous as $f = f_n$. This means that any finite preload force will not be sufficient to insure that the contacts will remain closed if the excitation frequency coincides with the natural frequency of the contact system.

Data and Results

The relay shown in Figure 11, page 19, and also the same relay hermetically sealed within its case, shown in Figure 12, were tested using a sinusoidal input.

A MB Electronics CLOE Exciter Unit was used to generate the simulated external vibration input to the two above mentioned specimens. The CLOE Exciter Table is partially shown in Figure 13, page 21. The Control Cabinet for the CLOE Exciter Table is shown in Figure 14, page 22. This cabinet contains a combination sinusoidal and random type input generator with its amplifier and a multipurpose vibration meter.

Among the many capabilities of this piece of equipment is its specially designed arrangement between the vibration meter and the input generator which enables it to maintain a constant "G" level of

acceleration while automatically sweeping a present frequency range either for a sinusoidal or random type input. This unit can also maintain a constant displacement while automatically sweeping a particular frequency range, "cross-over" at present frequency and maintain a constant "G" level of acceleration for a particular range of frequencies, either for a sinusoidal or random type input.

The CLOE Exciter Unit can produce a rated 1200 lb. force vector. The exciter table weighs 18.1 lbs. which means that the exciter table can reach 1200 lbs. divided by 18.1 lbs. or approximately 66.3 "G's" of acceleration in the "no load" configuration. Neither relay specimen weighed more than 1.5 lbs. which left open the possibility of reaching 1200 lbs. divided by 18.1 lbs. + 1.5 lbs. or approximately 61 "G's" with the specimen attached to the table.

The caseless relay shown in Figure 11 was tested to and including 60 "G's" acceleration using a sinusoidal input. The encased relay shown in Figure 12 was tested to and including 35 "G's" of acceleration using a sinusoidal input to provide a means of comparing data and also for detecting any changes in contact system performance due to the case. The results of these tests are shown in Figures 15 through 20.

Although a test of 10 to 2000 cycles per second frequency range was designated, a larger range was swept in particular instances in which the contacts had separated at a frequency lower than 2000 cps and remained so, as that frequency was reached. For instance, with the encased relay, the frequency range was extended to 2400 cps in order to determine the entire separation range for its upper contact bar.

As a point of clarification, the area inside the curves shown in

Figures 15 through 20 designates the frequencies at which contact separation is continuously maintained for a given "G" level of acceleration.

To further qualify the results in Figure 15 through 20, the CLOE Exciter Unit has two other limitations besides the 66.3 maximum attainable "G" level. At 10 cps, the lowest point of the designated frequency range, due to a displacement limitation of one inch (total), a maximum acceleration of only 5 "G's" can be reached. From 10 to 20 cps the displacement limitation prevails. At 20 cps the maximum attainable acceleration is 20 "G's". From 20 cps to 60 cps a velocity limitation of 70 inches per second prevails. By coincidence the maximum attainable acceleration equals the value of the frequency until, at 60 cps, 60 "G's" can be reached. At 60 cps and higher frequencies the "66.3 G limitation" prevails.

It is felt that the area of contact separation in the range of 400 cps for each contact bar in both specimens was due to the resonance of a system comprised of the mass of the relay attached to a form of cantilever beam, the beam representing the portion of the specimen attachment bracket from its attach points to the exciter table, to the upper attach points of the relay. It is felt that the fundamental natural frequency of this system coincides with 400 cycles approximately. Equation 24 on page 16 produces curves of the same form as that of the theoretical curves shown in Figures 25 through 29, pages 15 - II through 19 - II of "Vibration Control in Relay Design", Part II by Dr. R. L. Lowery, B. C. Riddle and G. C. Stone, Interim Report No. 8, NASA, Contract NAS 8-2552. If the contact separation range in and around 400 cps is ignored, it can be seen that Equation 24, page 16, could be applicable in this particular instance. The "roundness" of the lowest portion of the contact separation curves indicates that some form of damping is present.

The instrumentation for the above tests is shown in Figure 13.

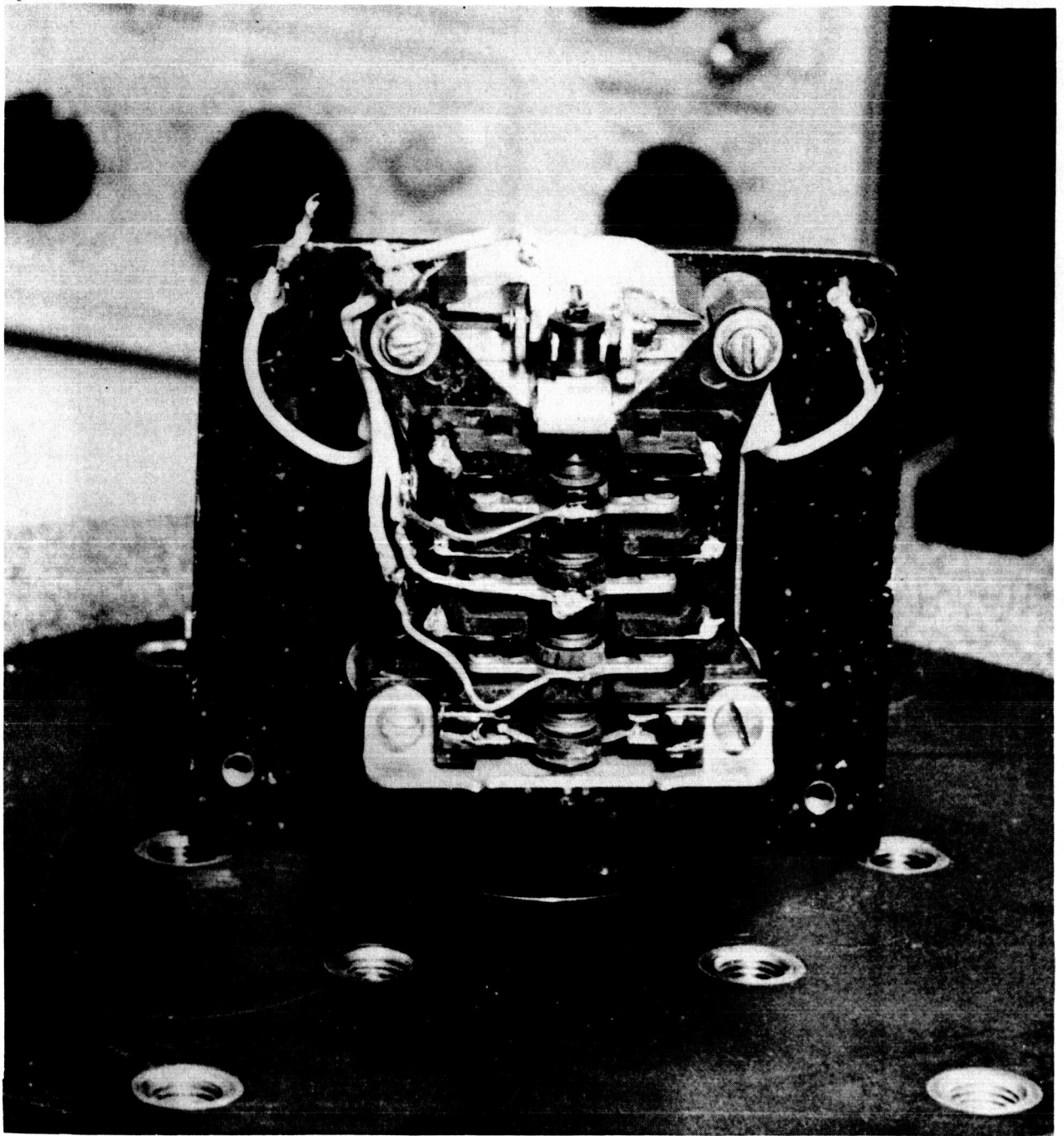


Figure 11

Caseless Relay Mounted on Exciter Table

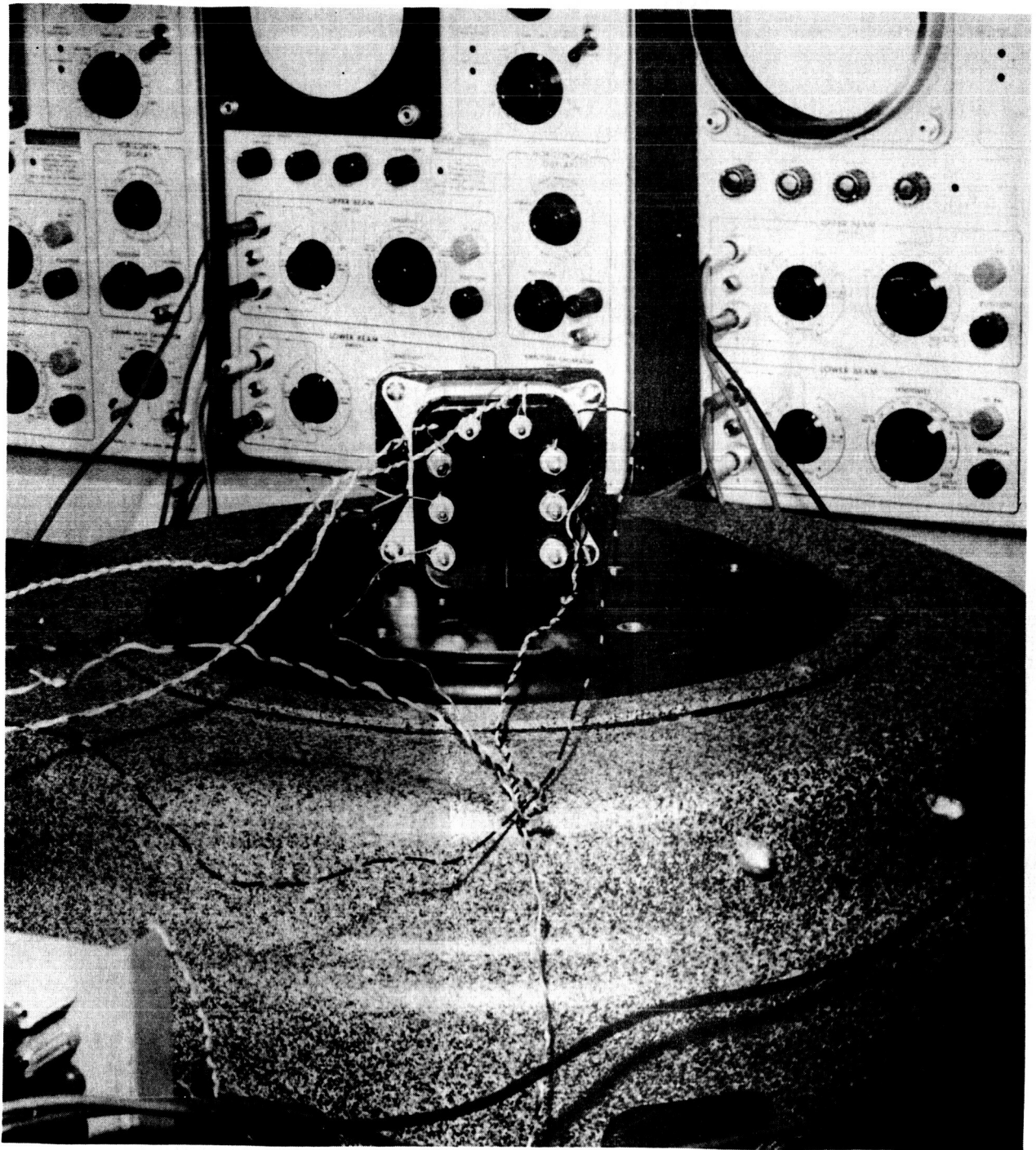


Figure 12
Encased Relay Mounted on Exciter Table

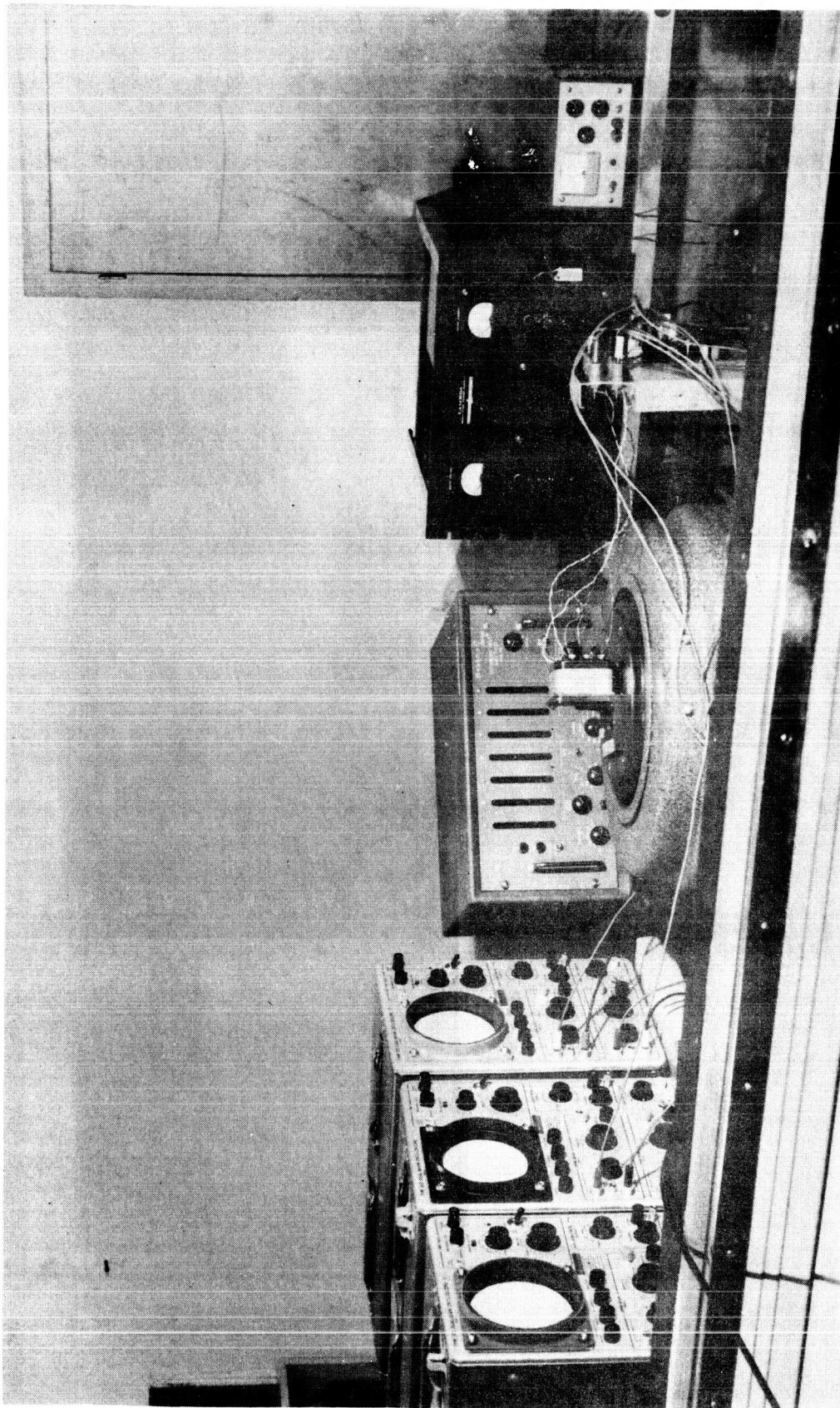


Figure 13
Instrumentation Used in Test Set-up

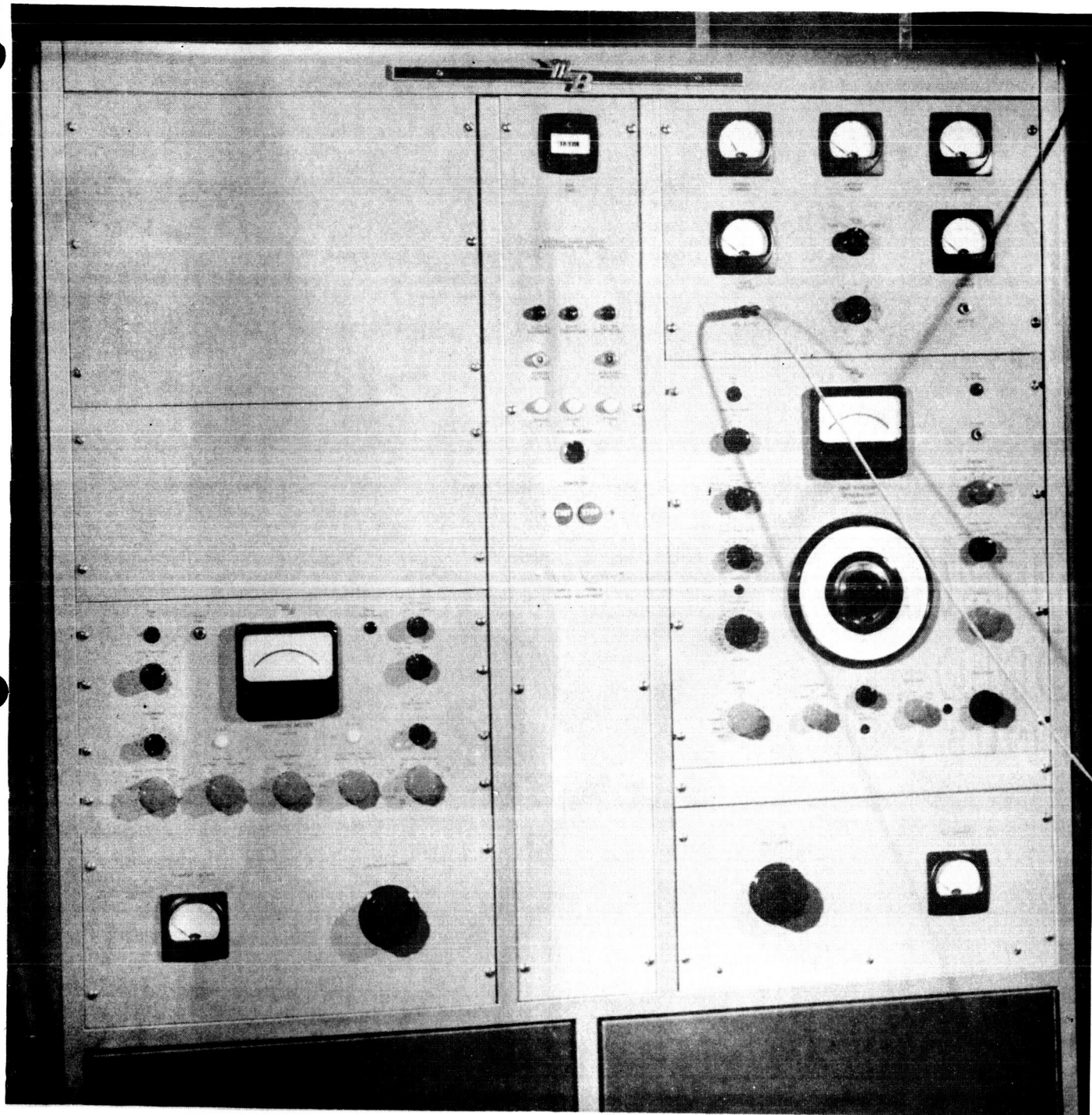


Figure 14
Control Cabinet of CLOE Exciter Unit

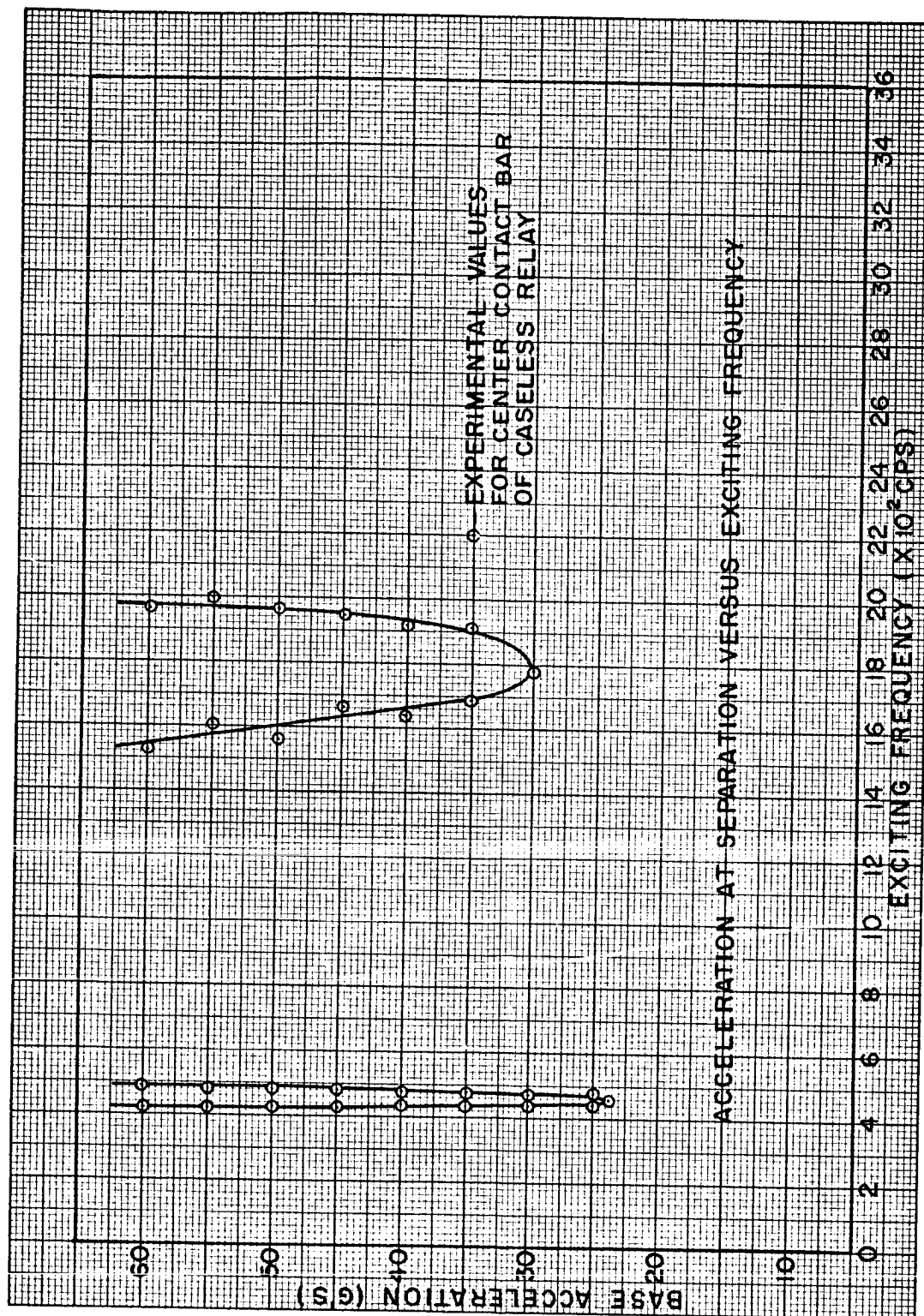


Figure 15

Experimental Data for Upper Contact System of Caseless Relay

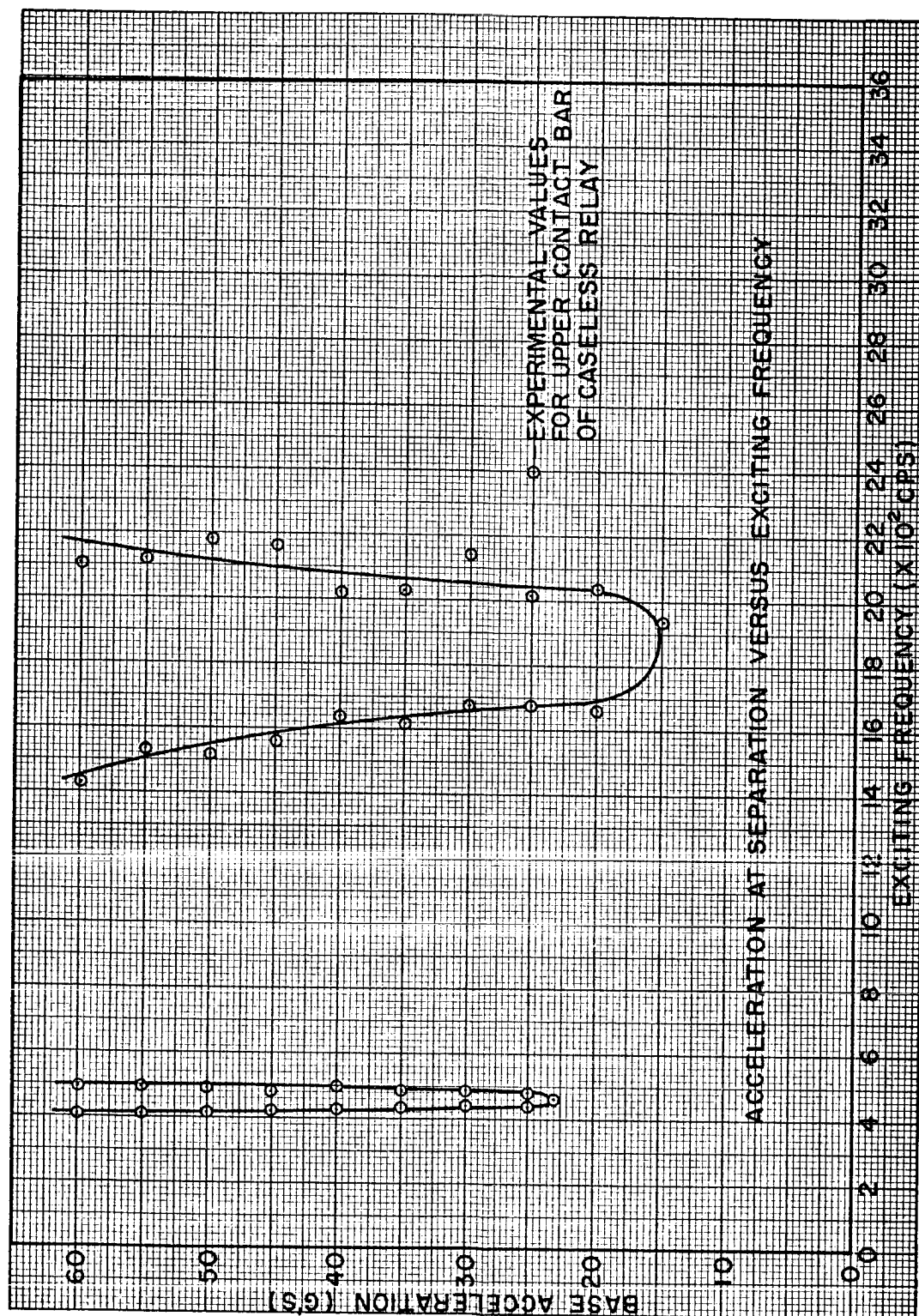


Figure 16

Experimental Data for Center Contact System of Caseless Relay

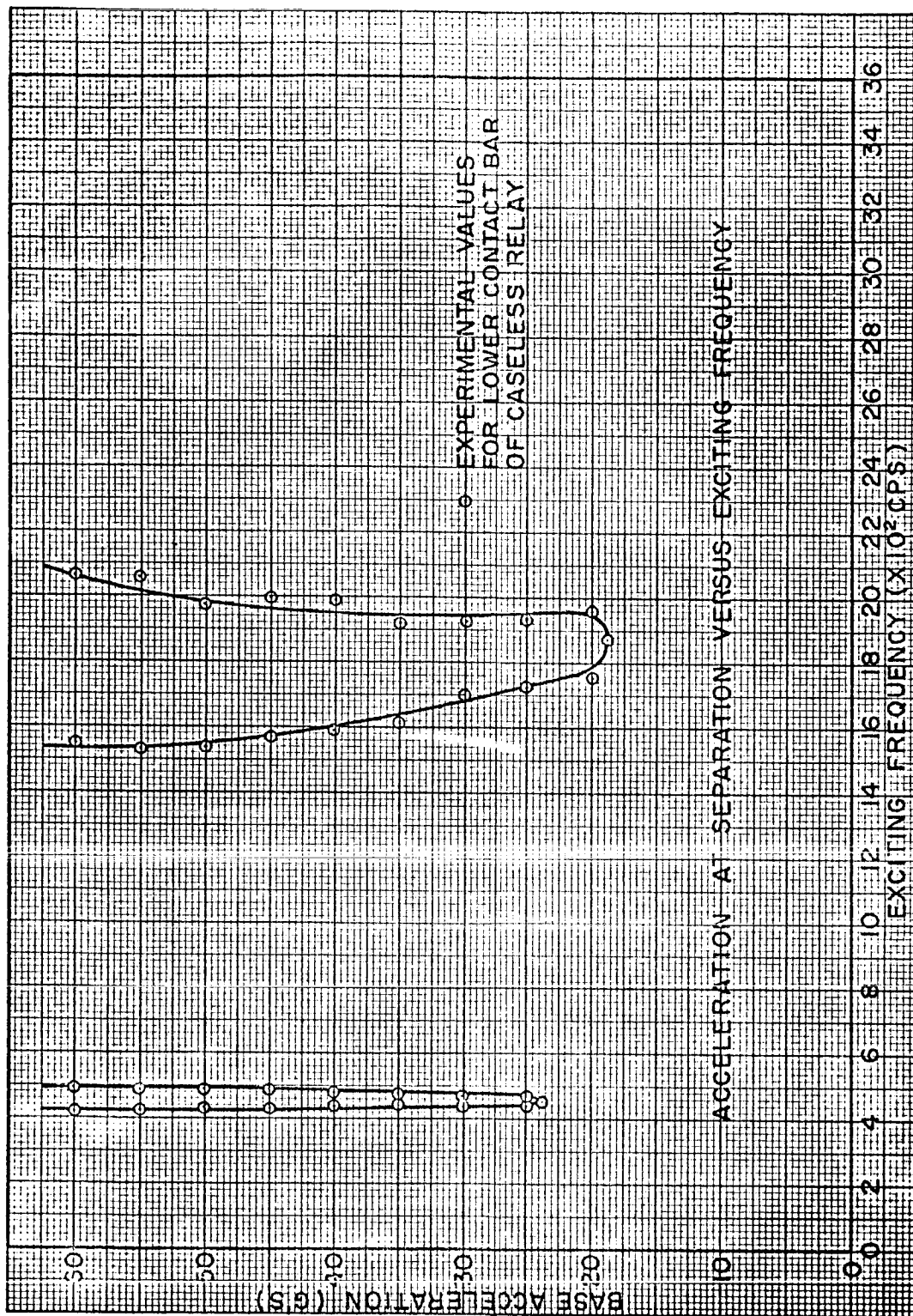


Figure 17

Experimental Data for Lower Contact System of Caseless Relay

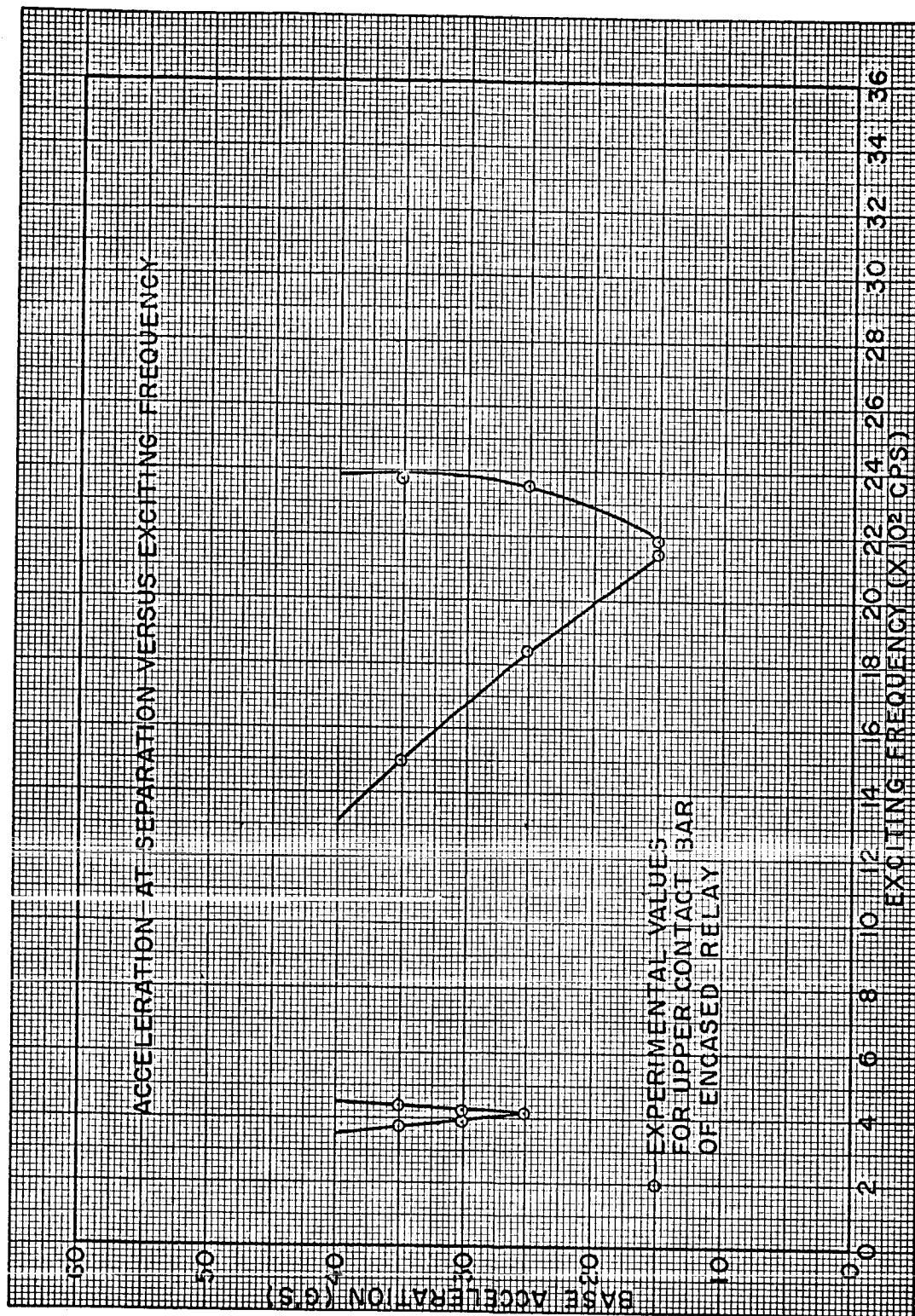


Figure 18

Experimental Data for Upper Contact System of Encased Relay

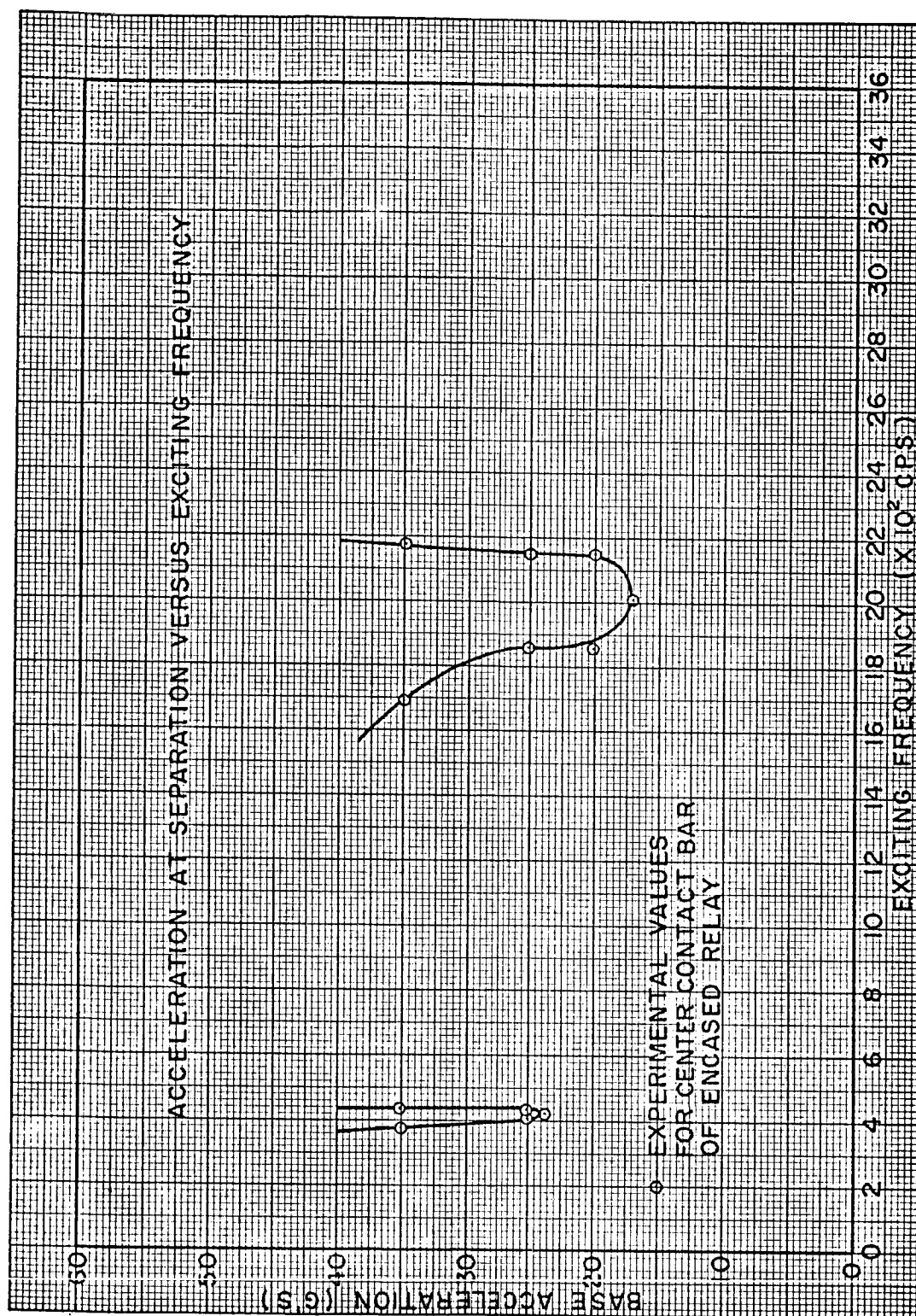


Figure 19

Experimental Data for Center Contact System of Encased Relay

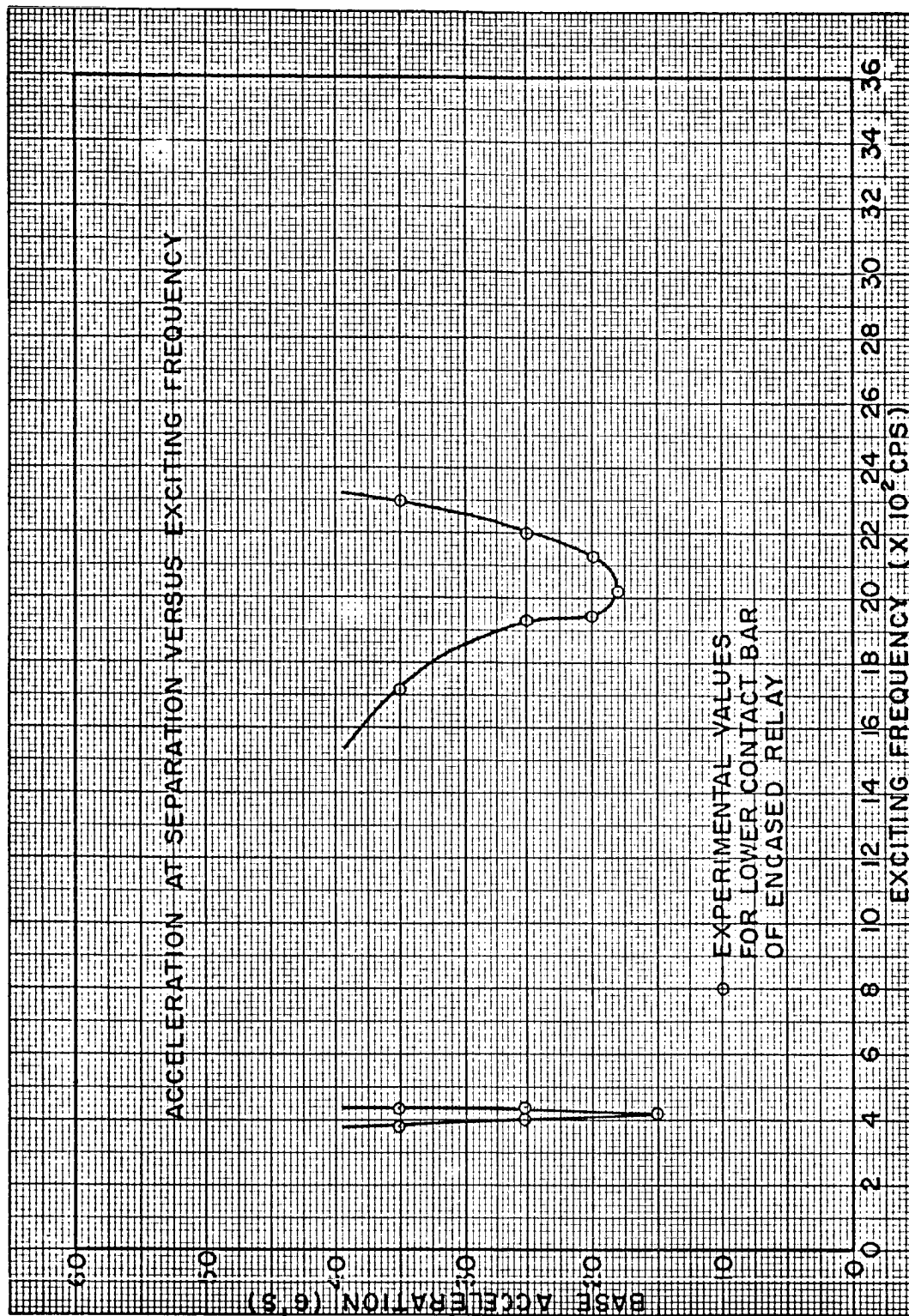


Figure 20

Experimental Data for Lower Contact System of Encased Relay

CONCLUSIONS AND RECOMMENDATIONS

This study has dealt with the basic but general question, "How can the contact system of an electromagnetic plunger type relay be designed so that it is least affected by a given external vibratory excitation"? That question can now be partially answered.

For relays which are analogous to the system in which both contacts are flexible, the contact system should be designed such that the natural frequency of the system is outside the range of required exciting frequencies. It appears that the natural frequency of the system should be below the operating frequency range for best design. However, this may not be possible if the relay is subjected to extremely low frequency external excitation, since reducing the natural frequency of the system requires a softer spring for constant mass. This is not to imply that the mass of the system cannot vary. But, due to electrical current carrying requirements and miniaturization, the mass of the contacts can vary only over a small range. In view of this, it may be easier to change the spring constants in order to alter the system resonant frequency.

Theoretically, according to equation (24), the most desirable condition for this system is that for which $k = bk_{eq}$, since for this case any value of preload would insure that the contacts remain closed at any exciting frequency over any range of acceleration. However, this is most difficult if not impossible to achieve in a given physical system. Manufacturing tolerances would allow some value of difference, no matter how small, between k and bk_{eq} , and the system would once again be governed by a resonance condition, although the

separation g level, at any frequency save resonance, would increase as k approaches bk_{eq} .

Optimum design with respect to the dynamic characteristics of the system could be achieved if the stationary contact is made as rigid as possible in relation to the other system parameters. To further guard against contact separation, the mass of the flexible contact should be made as small as possible.

Recommendations

The dynamic characteristics of the cantilever beam representing the stationary contact should be thoroughly investigated both theoretically and experimentally. Theory should be developed for and tests run on a simulated contact system in which a cantilever beam which is very flexible with respect to its length and mass is resting on a flexible translating contact. Also, the case in which a cantilever beam with a nonuniform cross section is resting on a flexible translating contact should be investigated.

Data from experimentation dealing with the particular relay in this study showed that damping in some form is present in the system. Damping in general should be considered in subsequent studies. Specifically, the separate effects of coulomb and viscous damping should be investigated.

The effect of overtravel spring resonance should be considered in any model having either helical or cantilever type springs in its contact system.

The response from random rather than sinusoidal excitation should be considered in all models. Combined random and sinusoidal inputs might also be considered.

All models should be mounted in various positions and tested to investigate the possibility that multidegrees of freedom cases with coupled modes exist. Certainly, models should be mounted so that external excitation is applied perpendicular to that in Figure 11, since it is felt that excitation from this direction would least affect the contact system.

Stiffer attachment brackets should be used in testing to avoid specimen component resonance similar to that in Figures 15 through 20.

All values of acceleration for the tests of this study were read from the vibration meter of the Exciter Unit. These values come from a signal generator mounted to the exciter table structure. Individual accelerometer transducers should be attached directly to the specimen and their output values should be used in lieu of those from the vibration meter.

A SELECTED BIBLIOGRAPHY

1. MacDuff, John N., and Curreri, John R., Vibration Control, McGraw-Hill Book Co., Inc., New York, 1960.
2. Thomson, William Tyrell, Mechanical Vibrations, Second Edition, Prentice-Hall, Inc., Englewood Cliffs, New Jersey, 1961.

SECTION II

VIBRATION TESTING OF A 75 AMP. ROTARY TYPE RELAY

This discussion deals with the methods used to test the effects of vibration on a rotary relay. Also included are graphs and explanations of the results. The purpose of the tests was to see if the rotary relay functions properly in a vibration environment. It was assumed that the relay failed the test if there was contact breakage or chattering while the relay was energized to its design specifications. The results indicate at what frequency (cycles/sec.) and at what root-mean-square (rms) "g" level the relay contact points broke and when contacts reclosed.

A MB Electronics GIOE Exciter Unit was used to produce the vibration environment. The exciter unit is controlled by a Control Cabinet which contains a combination sinusoidal and random type input generator with its amplifier and a multipurpose vibration meter. The breakage of the contact points was monitored by using a Tektronic Type 551 Dual-Beam Oscilloscope. A breakage duration of 10 micro-seconds was considered a failure. The block diagram in Figure 1 shows the test set-up used while conducting the test to be discussed.

The first test conducted was to determine the lowest and the highest frequency at which the contact points opened (chattered) and reclosed for a specific rms "g" level. The frequency was varied manually and in the areas of interest the frequency was held constant so that maximum energy could be put into the relay. This method of testing was different from the constant sweep method to be discussed. This test was conducted on the "bare" relay. That is, out of its container and without the buss bars from the relay to the Header attached. Two different types of forcing functions were used. These were: Sinusoidal and 100 cycle Narrow-Band Random. The results are

shown in Figure 2. The hashed lines show the frequency range for which the contact points were opened or chattering. The symbol (⊖) is used for a sinusoidal forcing function and the symbol (Δ) is used for a 100 cycle Narrow-Band Random forcing function in this paper. As an example of the results, in Figure 2, at 7 rms g's it can be seen that while exciting the relay with a sinusoidal forcing function the contacts were closed at all frequencies below 710 cycles per sec. At 7 rms "g's" and 710 cps the contacts broke and remained open until a frequency of about 750 cps was reached. Then the contacts closed and remained closed for the duration of this run of the test. A frequency range from 80 cps to 2000 cps was checked at each "g" level. When the relay was being excited by a 100 cycle Narrow-Band Random forcing function of 7 rms "g's" the contact points did not break until a frequency of 575 cps was reached. The contact points remained open between 575 cps and 930 cps then they reclosed. At 1020 cps the contacts again broke or opened and stayed open until a frequency of 1100 cps was reached. Then they again closed. The contacts remained closed for the rest of this test run.

The second test could be considered a continuation of the first, but instead of manually controlling the frequency, the frequency was swept at 30 deg/min constant rate between 80 cps and 2000 cps. The frequency was swept both up and down the frequency scale. Thus, two frequencies for breakage occurred in both the upper and lower failure areas for a specified rms "g" level. These two different break frequencies are caused by the time it takes to build up or dissipate energy in the relay depending on which direction the frequency is being scanned. Therefore, the outer most points on each side of the region the contacts were open is the frequency at which the contacts reclosed. The inner points are when the contacts

opened. These points can be seen in Figure 3 which is the results of this test.

The third test was essentially the same as the second test except the buss bar was attached to the "bare" relay. That is to say, the method of testing was the same only the relay had additional parts attached. The results of this test are shown in Figure 4.

In comparing the results of the three tests, it is obvious that when the relay is excited by either a sinusoidal or random forcing function, the contacts chattered at or below the 3 rms "g" level. Using different test methods and adding the parts to the relay only affected the frequency range at a specific "g" level that the contacts were chattering. These effects were most pronounced when a sinusoidal forcing function was used. An interesting characteristic of all the test was how much larger the frequency range at which the contacts were chattering was when the relay was excited by a random force rather than a sinusoidal force. Adding the buss bars did not affect the rms "g" level at which contact chattering began but did affect the frequency range of chattering.

In addition to the testing being done a separate investigation is being conducted to determine the effects of different parameters on the system.

EFFECTS OF NONLINEAR ELEMENTS IN CONTACTOR ANALYSIS

An investigation is being conducted to determine what effects nonlinear elements have on the sensitivity of contactors to time varying disturbing forces. In particular, it is desired to determine how nonlinearities in overtravel springs affect the separation criteria of contactors when the contactor is subjected to an outside sinusoidal disturbing function.

The investigation has two main purposes: First, to determine whether

certain nonlinearities, particularly from the associated instability standpoint, cause contactor separating to occur with a smaller outside disturbing force than when the overtravel spring is linear, and second, to determine if there is some combination of nonlinearity and physical parameters which will make the contactor system relatively immune to outside disturbing forces as far as contactor separation is concerned.

The investigation is being performed in two concurrent phases, analytical and experimental.

ANALYTICAL PHASE:

The analysis involves a lumped parameter system where the elasticity is presumed to be contained entirely within the restoring springs and the mass entirely within the contactor masses. The second restoring spring is introduced into the system to account for the elasticity of the supposedly rigid contactor and to permit study of the effects of varying the elasticity of the "rigid" element.

Six system parameters are involved in the analysis; two masses, two springs, the overtravel force and the nonlinearity of the overtravel spring.

Whereas the analysis would be simple and straightforward in a linear overtravel spring case, the introduction of a nonlinear overtravel spring complicates the equations of motion to such an extent that closed form solutions are prohibited. The complication results mainly from the overtravel force. Application of a set overtravel force to a nonlinear spring with a symmetric restoring characteristic results in a displacement of the equilibrium position so that the system restoring forces are no longer symmetrical about the static equilibrium position. This factor invalidates the approximate simple harmonic solution for the response curve which is widely used in nonlinear analyses involving symmetric restoring forces.

This complication places the theoretical determination of the response curve beyond the scope of the investigation. However, this does not prevent fulfilling the purposes of the investigation since a unique phase plane delta program has been developed for the IBM 1620 which permits determination of the backbone of the response curve. This can be compared with the measured response curve of the experimental phase in the final data reduction.

Free body analyses of the contactor masses permit determination of the relative displacements of the contactor masses from the equilibrium position at which separation will impend. These are independent of the system disturbing function but, in the nonlinear case, are implicit functions of relative displacement and system parameters. Solutions require fixing certain parameters and resorting to computer root solving techniques. However, the capacity of the IBM 1620 permits determination of meaningful families of curves which clearly indicate the effect of system parameters on the relative displacement of the contactors at impending separation. Although this portion of the investigation is not complete there is ample evidence that system parameters have a marked effect on impending contactor separation.

EXPERIMENTAL PHASE:

A model of the contactor system has been constructed which will be used in attempting experimental verification of the analytical findings. Construction was on an expanded scale in order to permit complete instrumentation of the contactor masses. Instrumentation will include accelerometers, load cell and displacement measuring. Testing will be performed using the MB C-10 Electrical-Mechanical Shaker System to provide the external excitation.

Model design was based on duplication of the analytical lumped parameter system although an appropriate amount of spring mass must be included with contactor mass to duplicate the analytical system. The contactor guides use forced air lubrication in order to eliminate nonlinear friction damping. Very little damping will be present and it will be linear. Provisions were made for varying the nonlinearity of the overtravel spring as well as the stiffness of both. Rigidity of the model is such as to prevent excitation of cross modes and provide reasonable expectation of data repeatability.

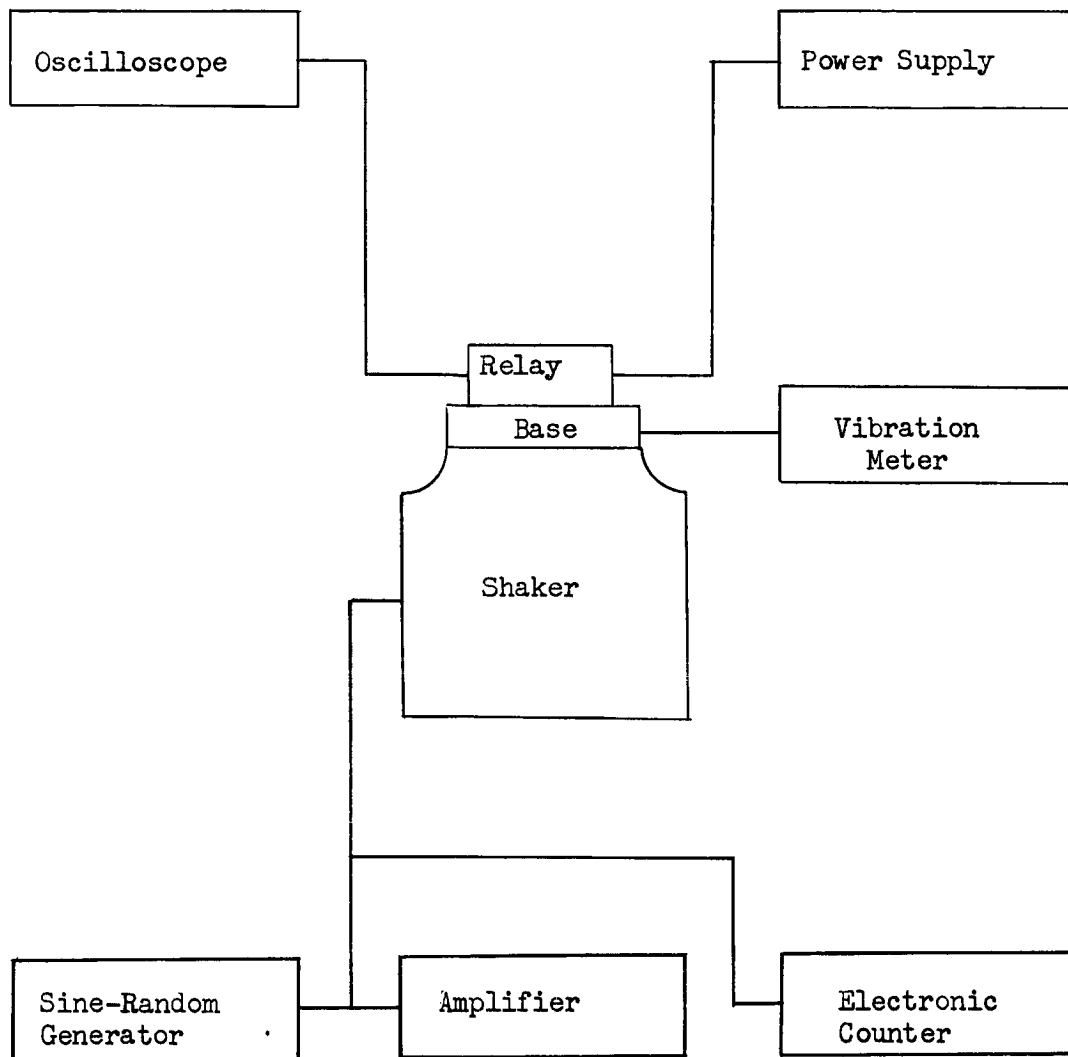
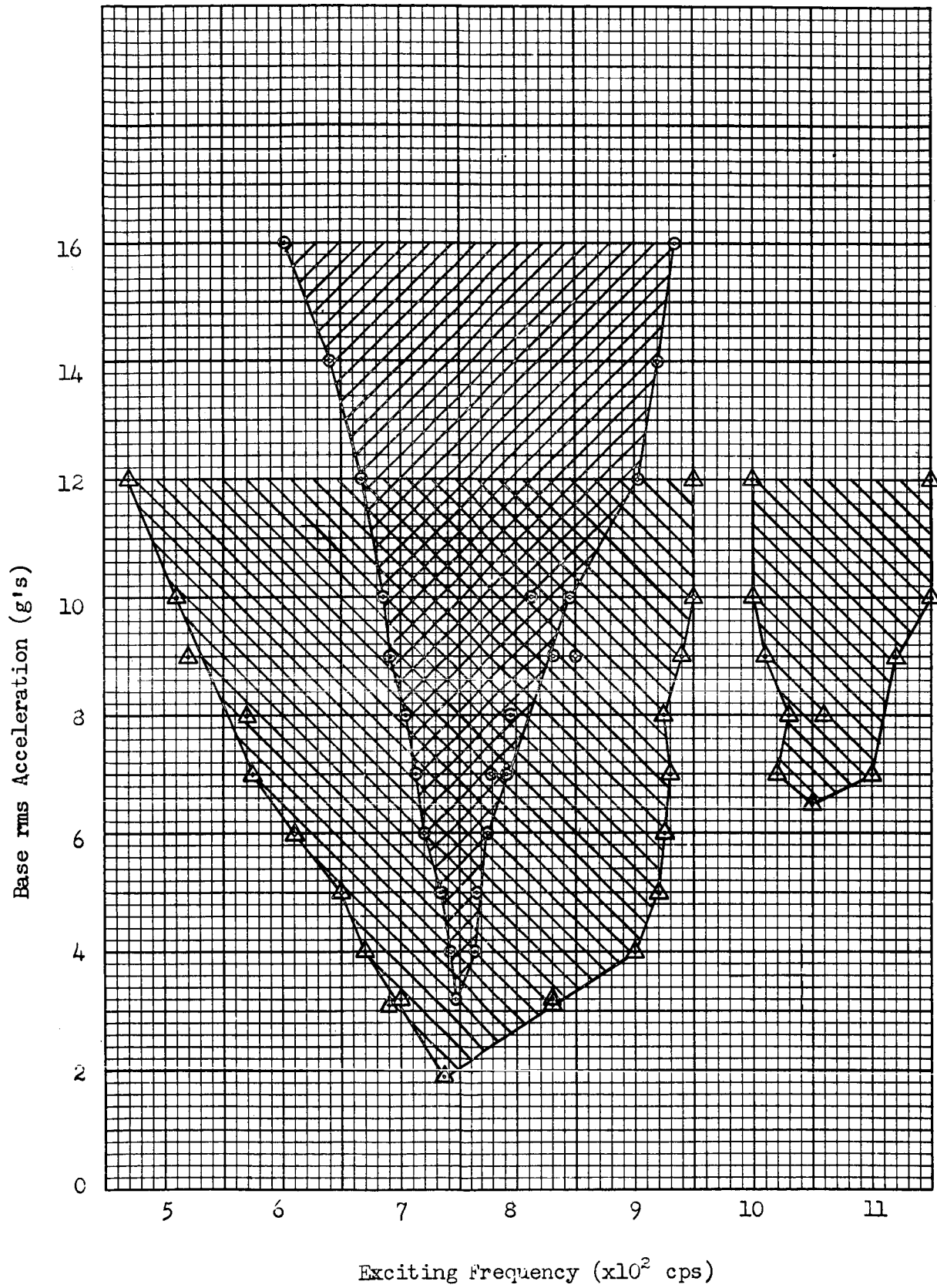


Figure 1
Schematic Diagram of Test Set-up

Acceleration At Separation Versus Exciting Frequency



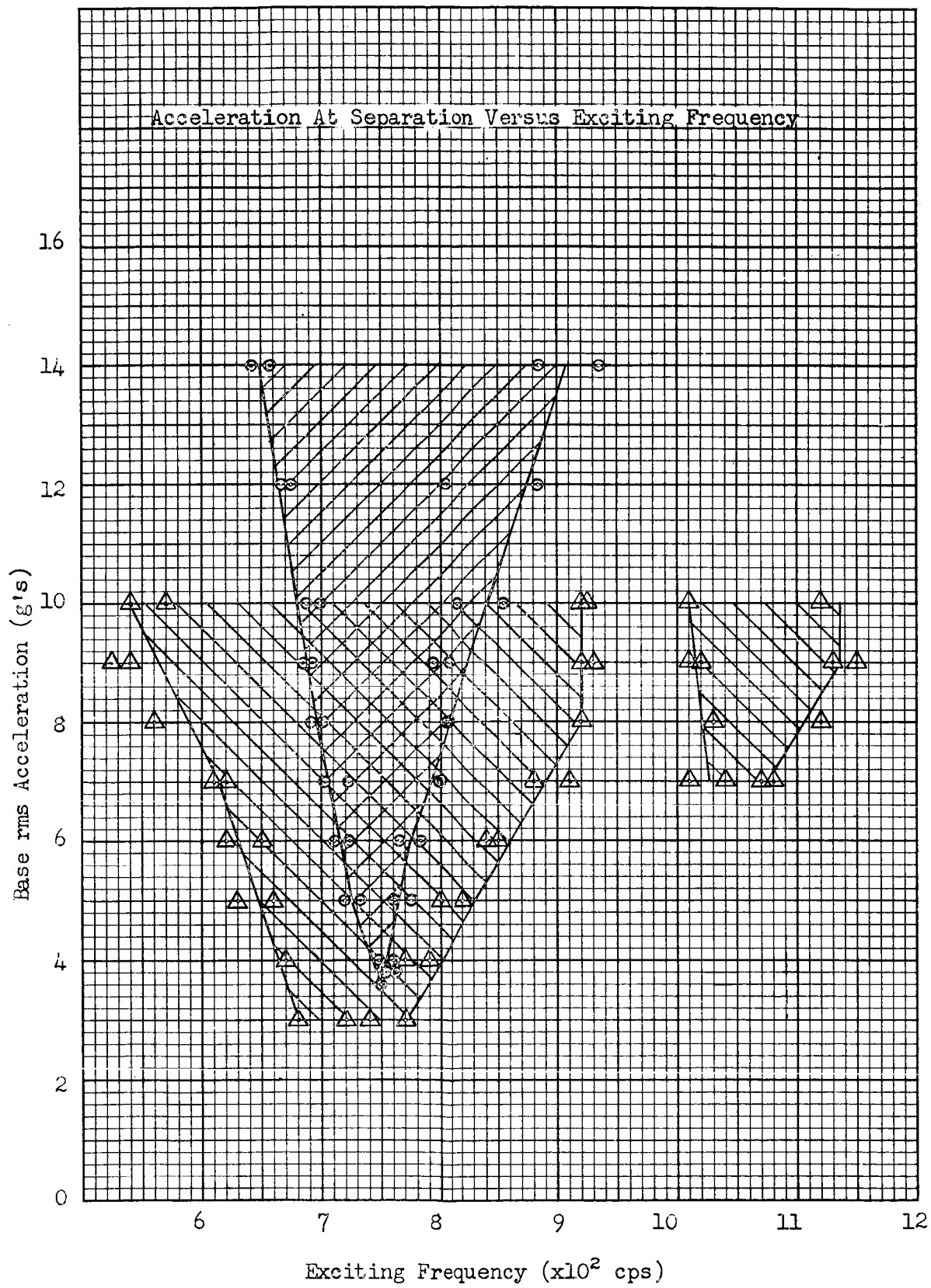
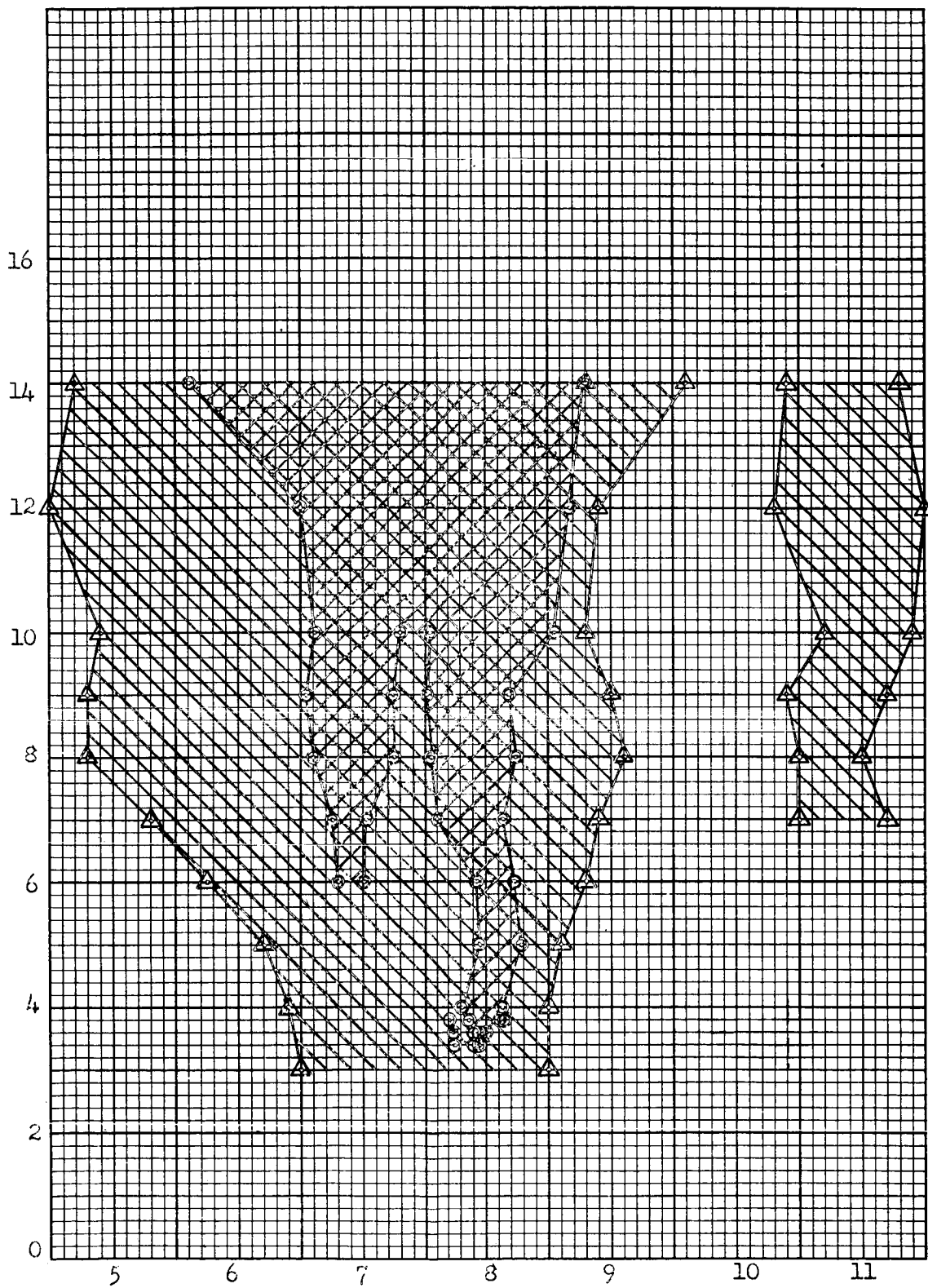


Figure 3

Acceleration At Separation Versus Exciting Frequency



Exciting Frequency ($\times 10^2$ cps)

Figure 4

SECTION II

VIBRATION TESTING OF A 75-AMP ROTARY TYPE RELAY

The first part of this discussion is a continuation of the Twelfth Interim Report. The relay was tested in different stages of assembly from the bare relay to the relay in its container. "Table" accelerations of contact separation versus exciting frequency data were collected. The term "exciting frequency" is the frequency of the driver or table. The latter part of this discussion will be about the frequency response of the relay.

In the Twelfth Interim Report, the relay had been tested from the bare relay to the bare relay with buss bars from the relay to the header attached. The next step was to complete the reassembling of the relay or put it in its container. This will be referred to as relay in the box as compared to the bare relay.

So that more information could be obtained from the test, as accelerometer was attached to the relay. Acceleration from this accelerometer will be called "relay acceleration". Figure 1 shows a schematic diagram of the bare relay, which will be used throughout this discussion with the accelerometer attached. In the Twelfth Interim Report table accelerations at contact separation versus exciting frequency plots were made. In this report a ratio of relay acceleration to sinusoidal table acceleration versus exciting frequency will be plotted. This was done so that the contact separation plot of the relay in the box could be compared to the frequency response of the relay in the box.

A hole was drilled in the relay container so that the accelerometer attached to the relay could be used to obtain data. A test to determine contact separation was conducted on the relay in the box. The test procedure was to set the exciting frequency at a fitted value and vary the

table rms acceleration until separation occurred. Both the table and relay accelerations were recorded. Figure 2 is a table and plot of the results of this test. The plot was made using the ratio of relay acceleration to table accelerations at contact separation versus exciting frequency. The small circles are data points and the lines are interpolated. It should be pointed out that if only table acceleration at contact separation versus exciting frequency would have been plotted, the plot would be the same as those in the Twelfth Interim Report. There could be a small shift along the exciting frequency axis of a few cycles per second. The relay accelerometer indicated the contacts separated at about 40 "g's".

From all tests conducted on this rotary type relay for table acceleration at contact separation versus exciting frequency, it can be seen that at certain exciting frequencies, the contacts separated at table levels below three "g's". The contacts separated in all the stages of assembly but with small shifts along the exciting frequency axis. In an attempt to explain why the relay had this type of response in a sinusoidal vibration environment, frequency response curves were obtained for the relay.

The frequency response curves were found by exciting the table with a constant sinusoidal accelerations and reading the acceleration of the accelerometer attached to the relay. The exciting frequency was swept at a slow rate through a range from 70 cps to 2000 cps. Each test took about an hour and a half. In each case, the relay was energized so that the contacts were closed. Plots were then made of the ratio of the relay acceleration to table acceleration versus exciting frequency. The small circles are data points and the lines are interpolated. Frequency response curves were made for the bare relay, the relay in the box, and the bare relay supported in different manners. Unless otherwise specified, the relay was always supported at the coil end as it would be in its container.

Figure 3 shows the frequency response of the bare relay supported as it would be in the container. The schematic in the upper right hand corner of the figure shows how the relay was supported. Similar schematics will be found on all frequency response curves showing how the relay was supported. From Figure 3 it can be seen that there are three predominant resonant frequencies. The first occurred at about 600 cps, the second at about 1000 cps, and the third at 1500 cps. By looking at the wave shapes of the table and relay accelerometers it was found that as the first resonant frequency was approached the waves were in phase. After passing the first resonance the waves were out of phase. At the second resonant frequency, the waves were about 180° out of phase. And at the third resonant frequency, the waves were varying from 90° to 180° out of phase.

Although the wave shape of the table accelerometer varied very little from a sinusoidal wave, the wave shape of the relay accelerometer was very nonsinusoidal above about 800 cps. At a future date, this wave will be analyzed using a wave analyzer to determine the predominant frequency components. Only the first resonant frequency will be of interest and will be referred to later in this report.

Figure 4 is the frequency response of the relay in the box. The resonant frequencies are at about 650 cps, 1050 cps, 1300 cps, and 1800 cps. Comparing the shape of the first resonant frequency and its location on the exciting frequency axis with the contact separation plot of the relay in the box and its location on the exciting frequency axis it can be seen that they are about the same. This indicates that contact separation occurs as the relay begins to resonate. Contact separation did not occur at the second resonant frequency with table acceleration below 20 "g's". The wave shapes of the table and relay accelerometers at the second resonant frequency were about 180° out of phase.

It can be seen in Figures 3 and 4 that the resonant frequencies are not at any specific harmonic or sub-harmonic of the first resonant frequency. This could mean that each resonant frequency is for different parts of the relay and not a single part or that coupling and nonlinearities are occurring. It is believed that the first resonant frequency is that of the relay. The body of the relay is made up of the coil and shell. The shell is that part of the relay which contains the contacts. (See Figure 1). This same first resonance can be seen in Figure 3 and is seen to be located near the same exciting frequency as in Figure 4. To substantiate the resonance of the body, the bare relay was supported in different manners to see if the first resonant frequency could be changed.

The bare relay was supported at both ends by adding a quarter-inch L-shaped piece of aluminum to the original support. Thus, the body of the relay was fixed to the exciter table at each end. Figure 5 shows the frequency response curve obtained from the bare relay supported at both ends. Now the first predominant resonant frequency occurred at about 1500 cps and the second at about 1850 cps.

Comparing the frequency responses of the bare relay supported at one end, Figure 3, and the bare relay supported at both ends, Figure 5, the first resonant frequency has been shifted along the exciting frequency axis from about 600 cps to about 1500 cps.

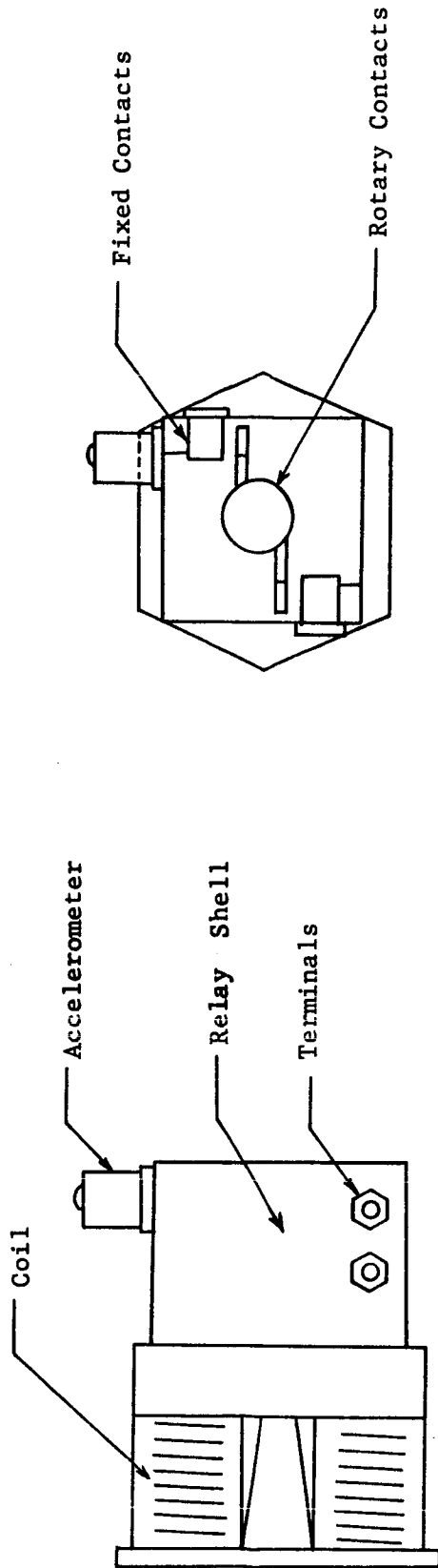
Figures 6 and 7 show the frequency response of the bare relay supported in the middle and at the shell end, respectively. When the relay was supported in the middle, the first resonant frequency was at about 1100 cps. This is a 500 cps increase in the first resonant from the relay support at one end. Supporting the relay in the middle and at the shell end, the first resonant frequency occurred at 550 cps and the second at about 1300 cps. The most predominant resonant frequency was at about 1500 cps.

In the future, different types of damping will be used to try to lower peak values at all resonant frequencies. Also, further investigation will be made on ways to support the relay inside its container and on ways to support the container so that resonant frequencies can be shifted beyond 2000 cps.

TEST CONSIDERATIONS

Excluding the data presented in Figure 7 which was the results of only one test, all other data were collected at least three times on separate days. Resonant peaks shifted along the exciting frequency axis not more than 50 cps if they shifted at all. The peak values at the resonant frequencies varied not more than one unit along the ordinate from one test to the next. All other data points shifted less than 50 cps along the exciting frequency axis and less than one-half a unit along the ordinate. In every test, data were recorded every 10 cps as the exciting frequency was swept from 70 cps to 2000 cps. The data were plotted using 50 cps increments unless additional points were needed for clarification.

Attempts were made to minimize the "cross-talk" of the support used to hold the relay. As long as the relay was not near a resonant condition the cross-talk was less than 15% of the driving "g" force. But in each case as resonance occurred the cross-talk increased. The amount of increase depended on whether the table and relay motions were in or out of phase. When the table and relay motions were in phase the cross-talk increased from about 15% to about 90% of the driving force at resonance. If the table and relay motions were out of phase cross-talk increased to about 200% of the driving force at resonance. The accelerometer used on the relay has a cross sensitivity of 2%



Front View

Side View

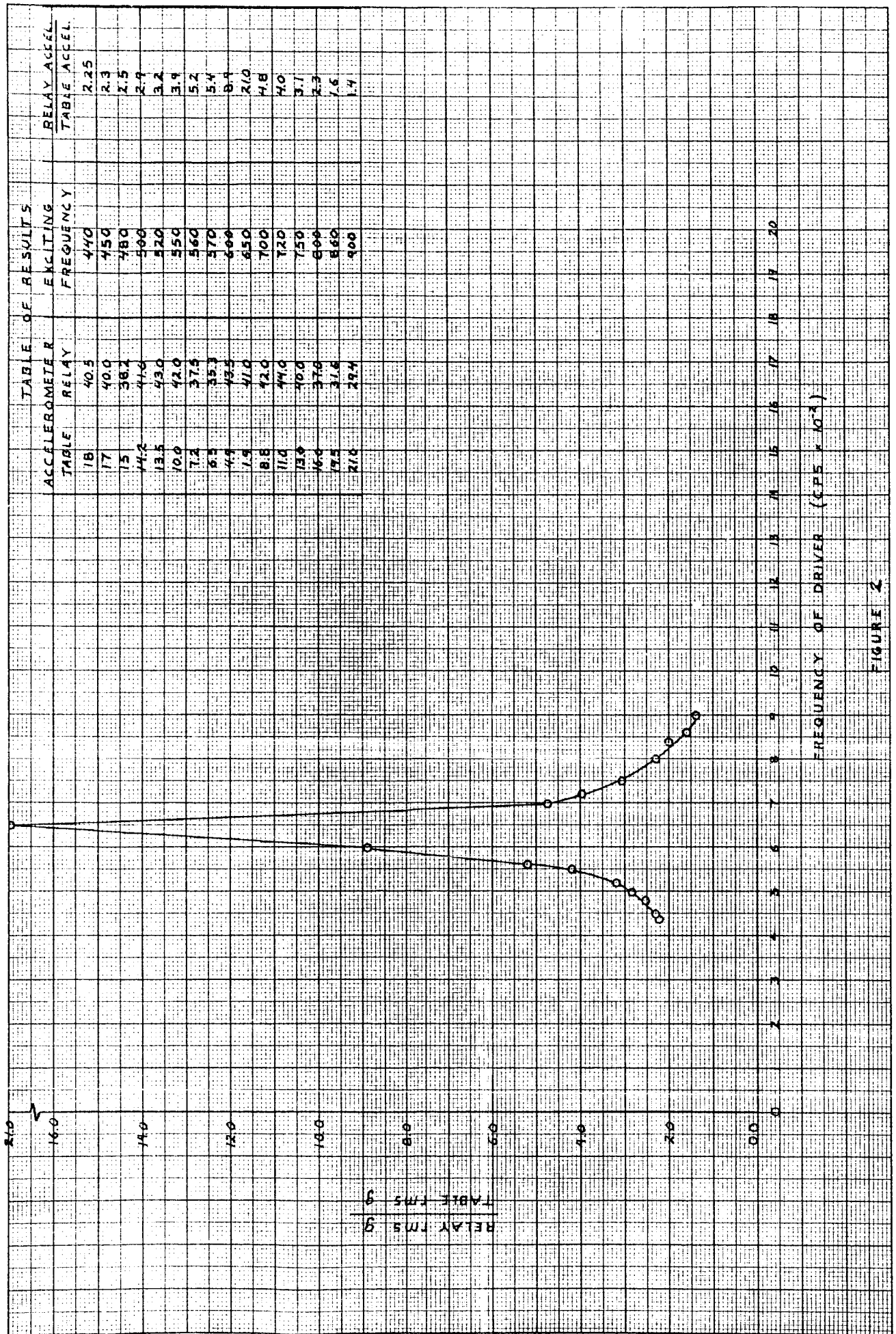
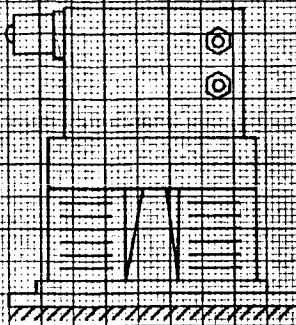
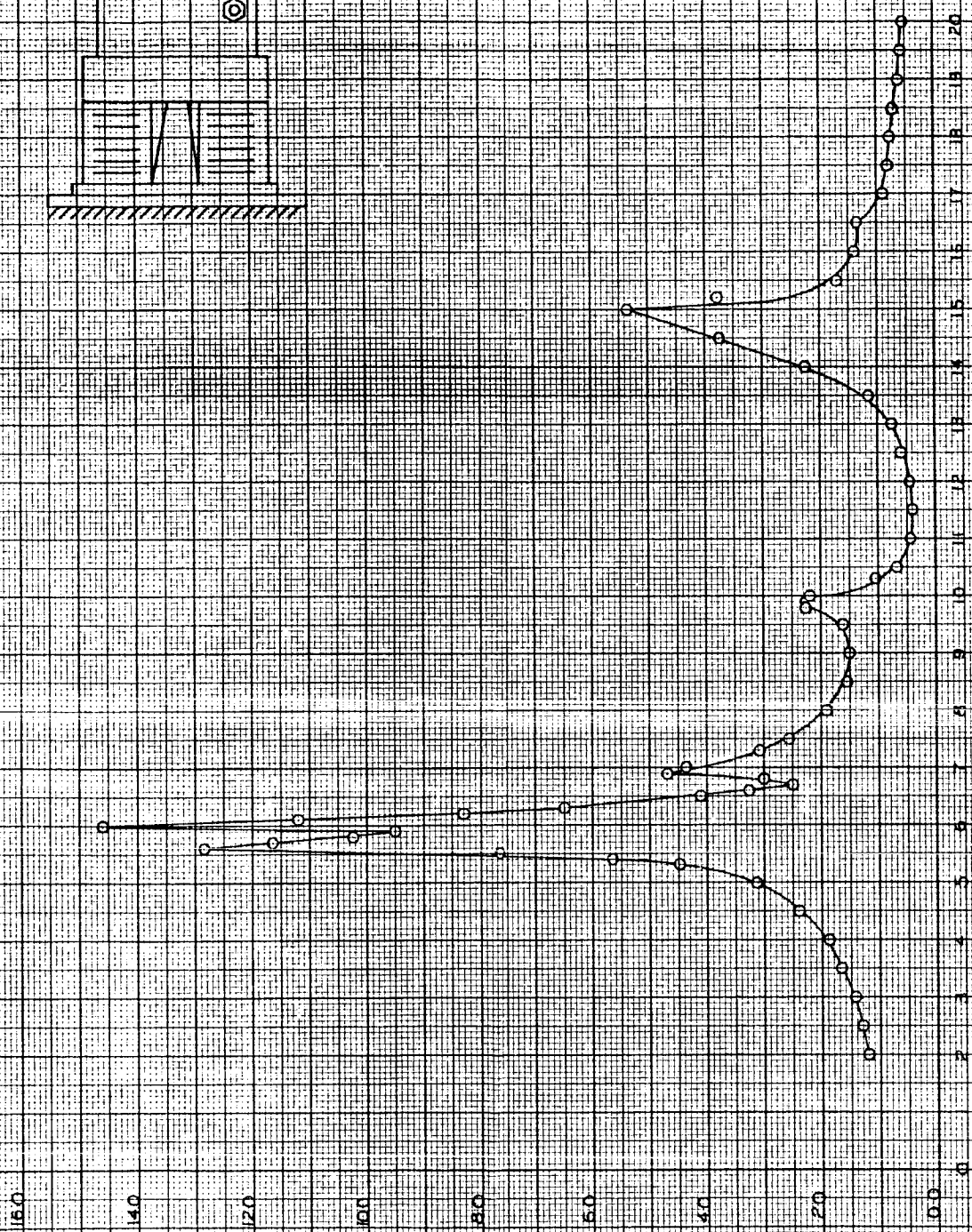


FIGURE 2



RELAY RMS g
TABLE FTS 9



FREQUENCY OF DRIVER (CPS x 10⁻⁴)

FIGURE 3

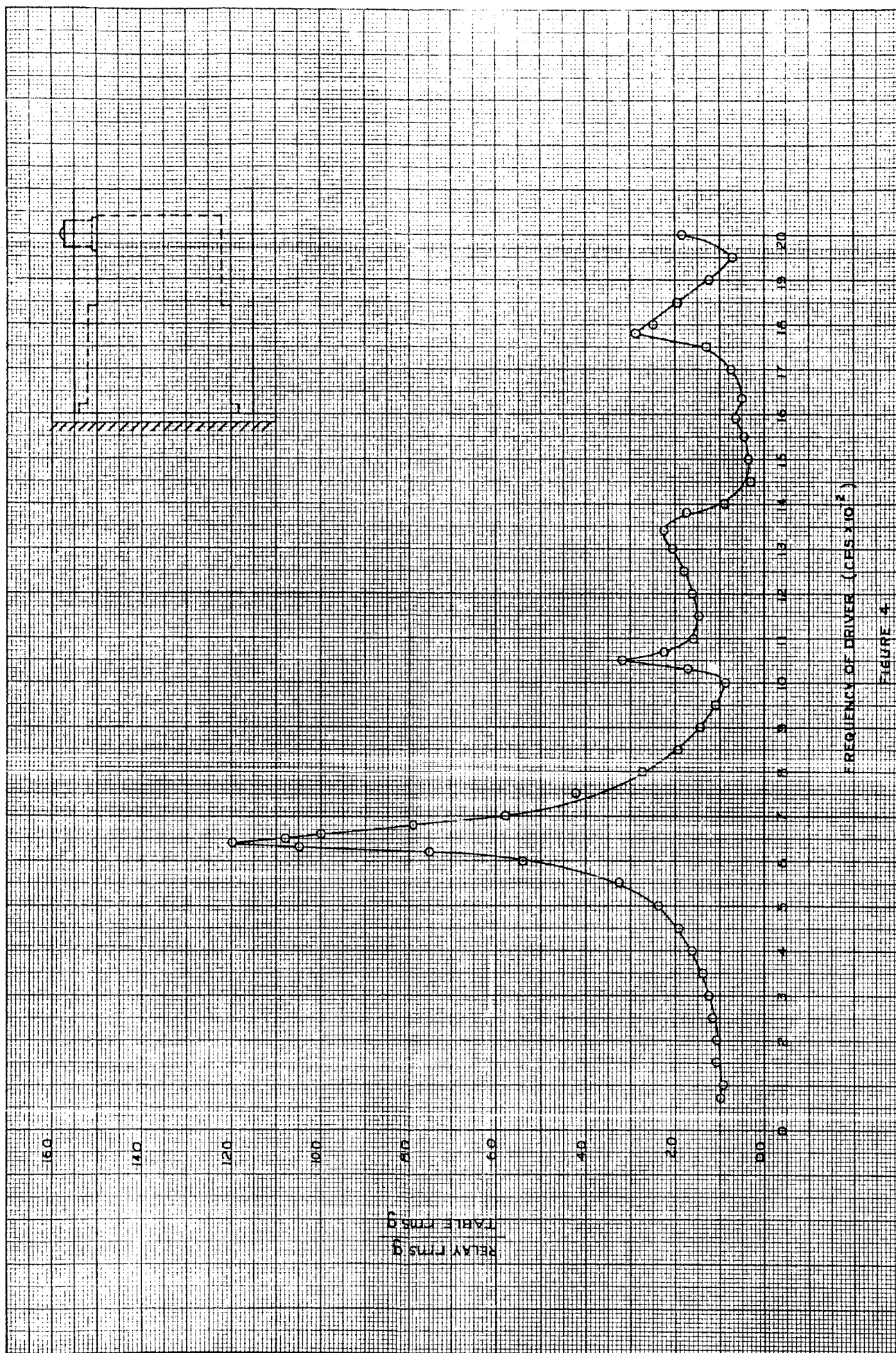
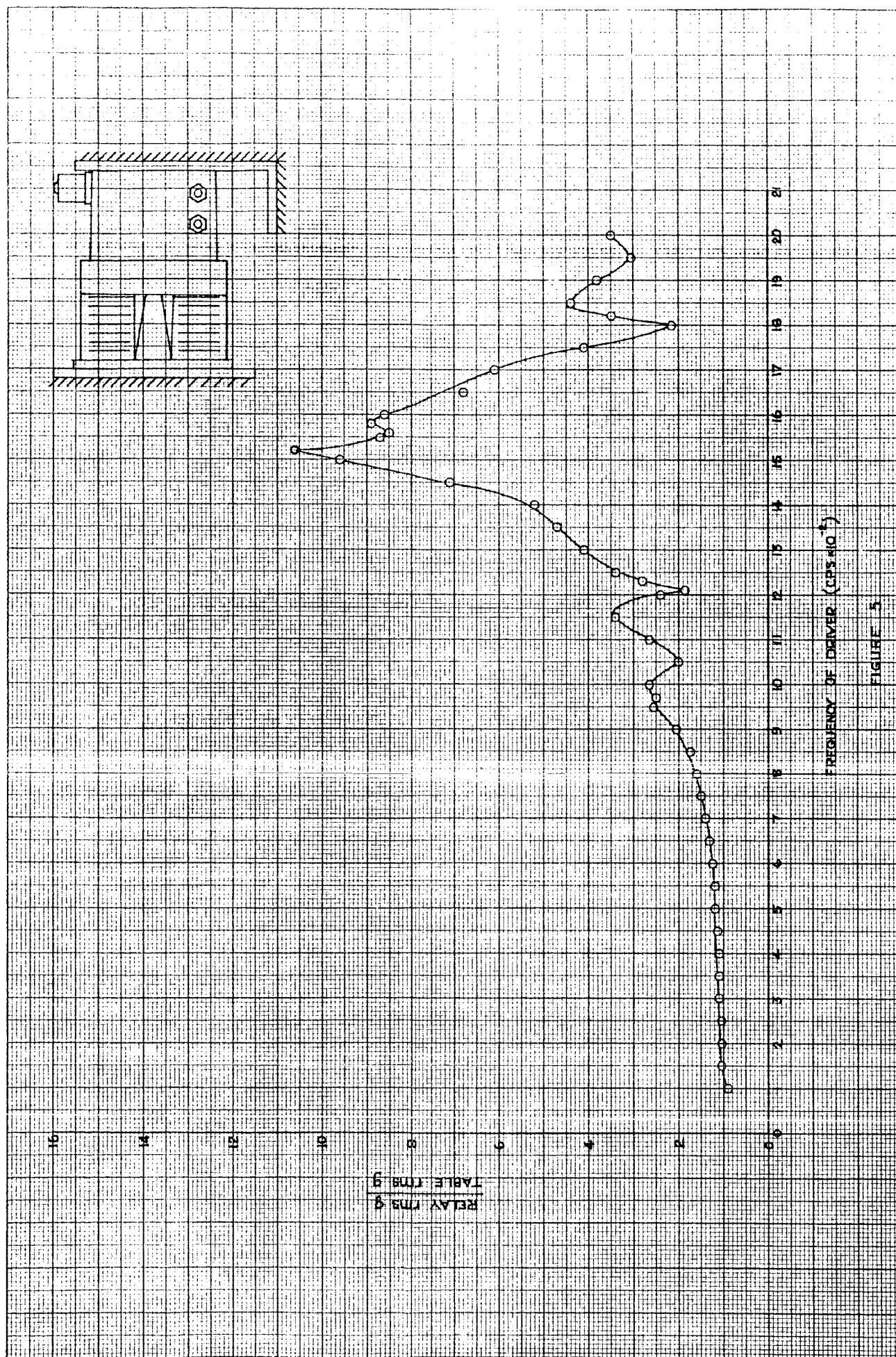
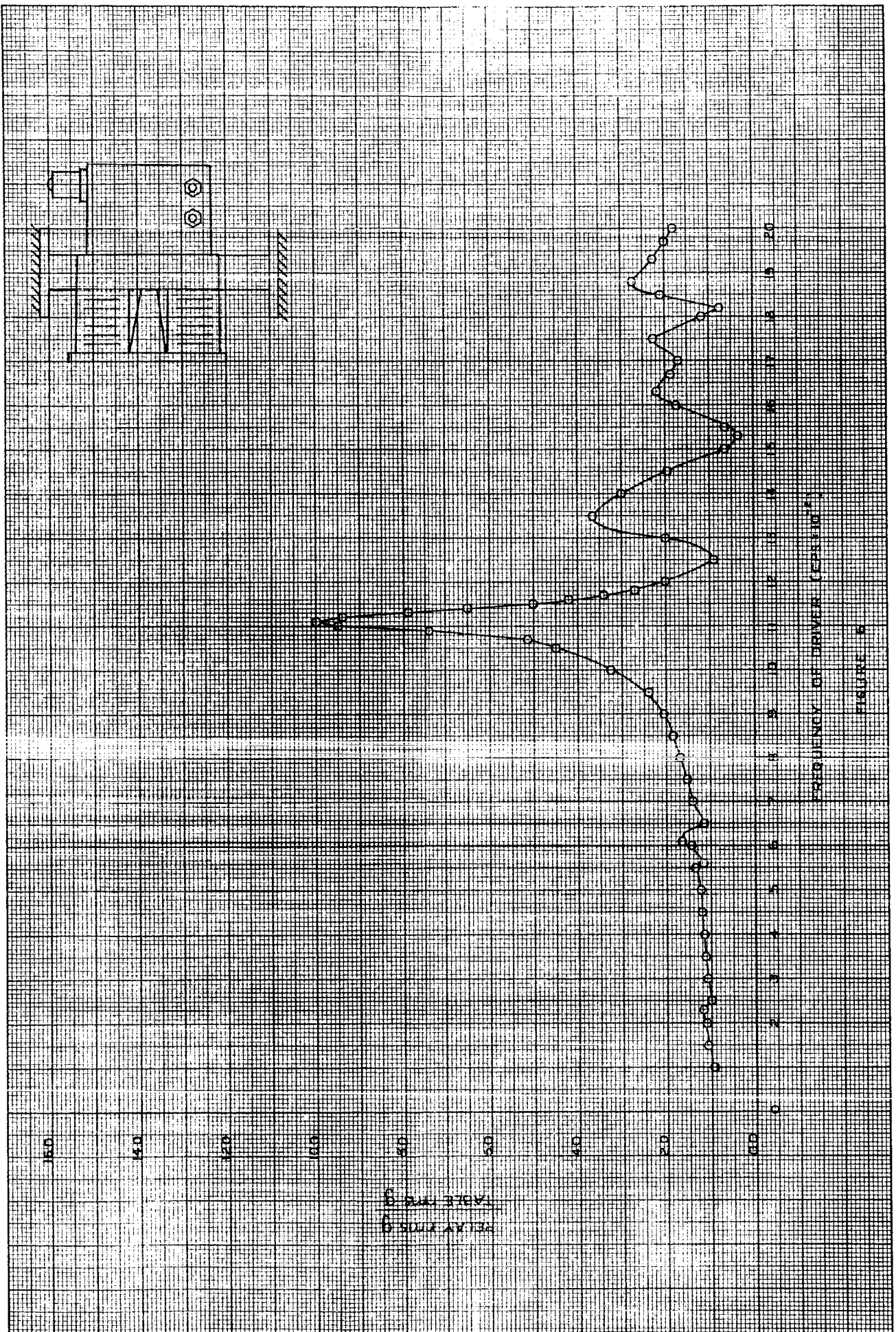


FIGURE 4





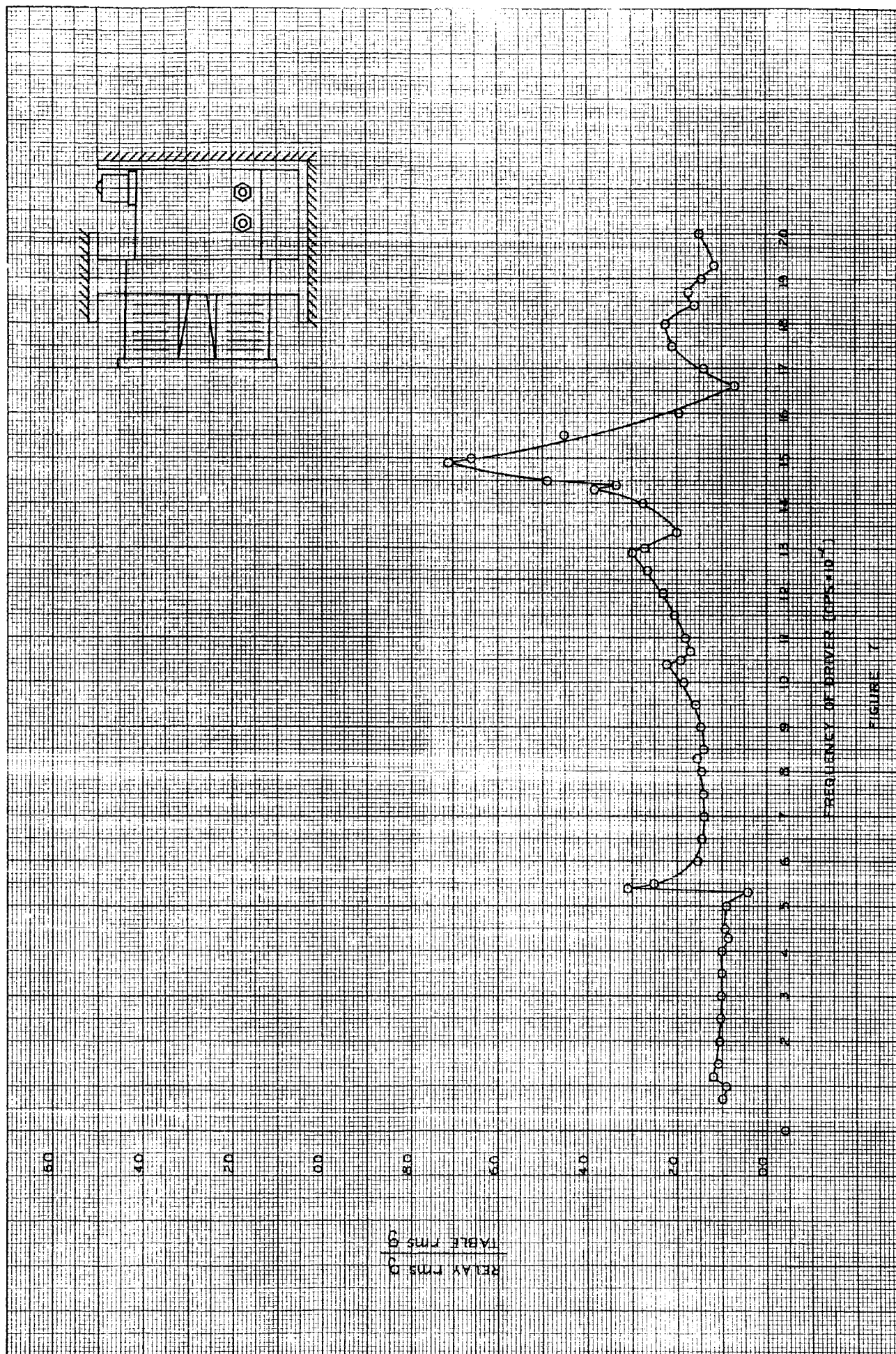


TABLE OF CONTENTS

Part F

DESIGN THEORY

<u>SUMMARY</u>	<u>Section</u>	<u>Interim Report</u>
Use of Abstract Models in Relay Design- - - - -	I	9th
An Investigation of an Alternate Design Map- - - - -	III	9th
Methods for Obtaining Allowed Specification Sets- - - - -	IV	10th

Tab Color Code

Orange	9th Interim	1 July - 30 Sept., 1963
Rose	10th Interim	1 Oct. - 30 Nov., 1963
Green	11th Interim	1 Dec., 1963 - 31 Jan., 1964
Blue	12th Interim	1 Feb. - 31 March, 1964
Yellow	13th Interim	1 April - 31 May, 1964

SUMMARY

Part F

Design Theory

Design theory deals with the problem of knowing when a group of mathematical relationships form an independent set, and also when a set of selected parameters are consistent. Consistent in this sense means that the use of the relationships with a selected set of parameters will not determine any parameter in the selected set by using the other parameters of the same set.

A mapping and decomposition technique was developed which provides a convenient means by which a set of relationships can be checked for independence and a set of selected (specified) parameters can be checked for consistency.

The problem of having to solve a group of simultaneous equations to determine whether or not a given set of parameters is consistent was examined. It was shown that this is a property of the particular form in which the mathematical model is presented. This investigation also indicated that the model could be presented in the form of a linear graph with a one to one correspondance between branches and parameters. The linear graph representation has some disadvantages in that any minimum set of parameters which form a complete loop may or may not be a consistent set. However, any minimum set of parameters which do not form a complete loop is a consistent set.

"USE OF ABSTRACT MODELS IN RELAY DESIGN"

by

Dr. D. D. Lingelbach
Assoc. Professor of Electrical Engineering
Oklahoma State University
Stillwater, Oklahoma

For presentation at

The International Conference on Electromagnetic Relays
Department of Electrical Communications Engineering
Tohoku University
Sendai
JAPAN

October 8 - 11, 1963

Use of Abstract Models in Relay Design

Dr. D. D. Lingelbach
Associate Professor of Electrical Engineering
Oklahoma State University
Stillwater, Oklahoma

The design of a relay, as with other devices, involves some kind of model from which various decisions can be made. Before the device can become a physical reality, the model must present a set of numerical values which are used to produce the device. The determination of the numerical values is essentially the last step in the use of the abstract model, and the model must be of a certain form in order to obtain numerical values from it. There are a number of questions that must be answered which are independent of numerical values. One of these is whether or not the collection of relationships used for the model is independent. Another question is whether or not a set of requirements, given in terms of a restricted set of parameters, is independent. These two questions need to be answered before the numerical values are considered. The second question presented maybe answered at different levels of the system representation. If the requirements do not involve a particular geometrical configuration, then a more basic level of the system model maybe used. The level of the model is determined by the parameters restricted by the requirements. If the requirements involve a geometrical consideration, then a model must be used which contains the parameters representing the geometrical part.

A procedure is presented and illustrated in this paper which allows one to determine whether or not the relationships representing the model are independent. In addition, a scheme is discussed which allows one to take a higher level model and reduce it to a more basic level. Also, an example is given which demonstrates how to determine if a set of restricted parameters is independent or dependent. The problem of starting with a basic level of the model and expanding it to a higher level is presented but as yet no clear cut procedure has been developed to accomplish this expanding directly.

The most effective way to present the concepts involved in using different levels of abstracts or mathematical models is to take a particular model and demonstrate the various operations. The manipulations of abstract models, presented in this paper, allows one to use their own collection of design equations. In addition, this discussion should simplify and present some additional insight into the problem of design.

It seems reasonable to assume that anyone designing relays must use some kind of mathematical model to design from. This model would probably take the form of a collection of algebraic-trigonometric relationships. The algebraic-trigonometric form must be available before numerical values can be obtained for the parameters. However, if one uses this form of the model to make all decisions then a lot of extra work is being

done. A number of decisions can be made by using a model in which only the functional form is presented, not the algebraic-trigonometric form. Whether or not a given set of specified parameters is independent is one problem which can be solved by using the functional form of the model.

In this part of the paper it will be assumed that the individual already has a collection of equations which he uses in relay design. Since each one would probably have a different set of equations for their model of the relay, the model used here is not to be taken as complete but is only used to convey some of the concepts involved in this kind of development.

The model used here for this discussion has 38 parameters and 21 relations. These 21 relationships are shown in the Appendix. The form of the model being discussed is obtained by listing all the different parameters in a row arrangement and relationships in a column arrangement such that only the parameters that occur in a given relationship appear in that column. The 21 relationships and 38 parameters shown in equation form in the Appendix are presented in matrix form in Figure 1.

One important phase of the use of any model is whether or not the physical law relationships making up the model are independent. A decomposition method has been developed which is very useful when the model is of the form shown in Figure 1.¹ This decomposition method is defined as follows:

Let $[(P_i)]$ be the set of parameter sets of the physical law relationships $[f_i]$. Let $[f_k]$ be the subset of relationships such that each parameter set (P_k) has a parameter, say P'_k , such that P'_k does not belong to any other parameter set of $[(P_i)]$. Remove the set of relationships $[f_k]$ from the original set $[f_i]$. Repeat the decomposition process on the parameter sets of the remaining relationships $[f_i] - [f_k]$. If this process terminates with no remaining relationships, the set of relationships $[f_i]$ is said to be decomposable. The physical law relationships are independent, if and only if, they are decomposable.²

This decomposition procedure is illustrated by using the model represented by the matrix shown in Figure 1. The procedure is to mark every parameter that occurs only once on the matrix. This is easily done by examining every row and marking any row which contains only one parameter. The following parameters occur only once in the matrix shown in Figure 1: R_p , c , d' , i , K , m , M , P , r and t_s . According to the decomposition method, each relationship which contains one or more of these "single" parameters is removed from the model.³ The first application of this decomposition method removes relationships h_3 , h_4 , h_7 , h_9 , h_{13} , h_{15} , h_{17} and parameters R_p , c , d' , i , K , m , M , P , r and t_s . This is shown in Figure 2. Removing these relationships and the "single" parameters from

^{1,2} A Theory For Design, C. C. Freeny, Ph.D. Thesis, Oklahoma State Univ., 1963

³ "Single" means the parameter appears in only one relationship of the given or remaining matrix.

the matrix gives a new matrix. This same process is performed on the new matrix resulting in a second new matrix. This procedure is continued until either no "single" parameters occur in the remaining matrix or no relationships remain. For the model in Figure 1, this procedure was applied four times which resulted in no remaining relationships so the physical law relationships of the model are independent.

Once the relationships are shown to be independent then it is possible to use the matrix to determine how many parameters maybe arbitrarily specified and whether or not the set of specified parameters is independent. The number of parameters which can be specified arbitrarily is equal to the number parameters minus the number of relationships in the matrix. In this case 17 parameters can be specified arbitrarily using the matrix in Figure 1 since there are 38 parameters and 21 relationships.

In order to check to see if the 17 specified parameters are independent, or not independent, the following procedure is used with the matrix in Figure 1. Assume the parameters selected to be checked for independence are the following: β , Δ , η , a , c , E , e , m , M , p , P , P_0 , q , r , t_s , u and x_0 .

1. Circle the occurrence of each of the parameters (row) in all relationships (column) and record this by placing a circle in the first column of the matrix.
2. Check each relationship (column) to see if all the parameters in that relationship are circled. If any such condition exists, then that subset of parameters (contained in that relationship) is not independent and any one parameter of that subset must be made unselectable. A new parameter is then selected and steps 1 and 2 repeated. If the condition in step 2 does not exist then go to the next step.
3. Check each relationship (column) to see if all but one parameter in that relationship is circled (selected). If so, that one parameter not circled is enclosed in a square and a square placed in the first column. This parameter, now enclosed by a square, is fixed and is treated as a selected parameter, i.e. all other occurrences of this parameter are circled. This process is continued, rechecking each relationship to see if all but one of the parameters are now circled. Continuing this process will result in all of the parameters being marked either with a circle or square, or the condition in step 2 is obtained, or neither of these conditions occur. If neither of these conditions occur then the situation of m parameters and m relationships with at least one uncircled parameter, will occur. Then the m relationships will have to be solved simultaneously in algebraic form for the m parameters. Whether a unique result is obtained depends on the algebraic form of the m relationships.

The first step of this procedure is shown in Figure 3. Examination of Figure 3 shown that the condition explained in step 2 does not exist. Therefore, the condition explained in step 3 is applied. This shows that relationships h_4 and $h_{1,4}$ satisfy the condition of step 3. Following through with the rest of the procedure gives the result shown in Figure 4. Two sets of relationships had to be solved simultaneously, these were

h_{11} , h_{15} , h_{19} and h_5 , h_6 . The parameters involved in the simultaneous solution are enclosed by a triangle. Since there were five equations solved simultaneously, there were five parameters involved. The result shown by the matrix indicates that the parameters selected are independent, since all the parameters are either marked with a circle, square or triangle. The alphabetical list at the bottom gives the order of solving the equations once numerical values are assigned to the selected parameter. This notation is helpful when it is necessary to determine numerical values for the parameters.

The mathematical model shown by the matrix in Figure 1 contains parameters representing dimensions since the magnetic circuit is included. The parameters b , c , d , e , f , g , h , i , l , m , p , q , r , s , u , x_0 and Δ are dimensional parameters. Sometimes it is desired to know whether or not a set of specified parameters is independent regardless of the particular geometrical form of the device. Certain parameters like coil voltage E , coilpower P , coil resistance R_c , pick-up time t_p , armature transit time k are specified but the particular form of the device is not involved. Therefore, a different level of decision is involved at this point. The problem is whether or not the independency of a set of parameters of this kind can be checked on the matrix in Figure 1? This answer is yes but certain dimensional parameters must be assumed if the matrix shown in Figure 1 is used. This is not usually convenient to do. The most convenient way to change the level of the system is by eliminating the parameters not desired, or more correctly, keeping the ones desired. The desired parameters will be called necessary parameters and the level of the system is changed by the following process.

1. Mark on the matrix in Figure 1 all the necessary (desired) parameters that must remain in the system model.
2. Mark all the parameters that occur only in one relationship that are not necessary parameters.
3. If all "single" parameters are necessary parameters then the system level can not be reduced.¹ If there are "single" parameters which are not necessary then proceed to step 4.
4. Examine each relationship which contains one or more "single" non-necessary parameters. If the relationships contain only "single" non-necessary parameters or "multiple" parameters (necessary or non-necessary) then that relationship is removed from the matrix along with all the "single" non-necessary parameters.² If that relationship contains any "single" necessary parameter then nothing can be removed.

¹ Ibid.

² "Multiple" means the parameters appear in more than one relationship of the remaining matrix.

5. Repeat step 4 until no "single" non-necessary parameters exists unless it is in a relationship containing a "single" necessary parameter.

This procedure is best explained by considering the following example of reducing the system level or order. Assume that the following are the necessary parameters: η , E , k , M , P , P_o , R_c , t_p , t_s and x_o . (Note these parameters do not have to be independent, in fact in general they probably will not be independent). Figure 5 shows the results of performing steps 1 and 2. The necessary parameters are shown by a \checkmark and the "single" non-necessary are shown by a 1.

The parameter R_p is "single" and non-necessary and is only in relationship h_7 . Examination of h_7 shows that it contains, in addition to R_p , only "multiple" parameters so h_7 is removed from the matrix along with R_p . The next "single" parameter is c and it is in relationship h_{17} . Relationship h_{17} contains only "single" non-necessary or "multiple" parameters so it is removed along with the two "single" non-necessary parameters c and i . The parameter d' is next and it is removed along with h_{13} . The next non-necessary "single" parameter is K which is in h_3 . Examination of h_3 shows that it contains a "single" necessary parameter so neither K nor h_3 can be removed. The first three reductions are shown in Figure 5. The final reduced matrix is shown in Figure 6. This matrix contains the necessary parameters plus the additional parameters that are needed to relate the necessary parameters and represents a different level of abstract model since most of the parameters are independent of the geometrical shape of the device. The number of parameters which can be specified arbitrarily using the matrix in Figure 6 is 12. The matrix in Figure 6 can be shown to contain only independent relationships by using the decomposition method described previously in this paper.¹

The matrix in Figure 6 is used to determine whether or not the twelve parameters that are under consideration are independent. Of the seventeen parameters that were used previously in the discussion, only eight are in the matrix in Figure 6 and these are β , η , E , M , P , P_o , t_s and x_o . An additional four parameters can be selected to be specified and these will be $(\alpha, \sigma, l$ and $s)$. Using the matrix in Figure 6 to check these specified parameters for independence gives the result shown in Figure 7. The twelve parameters selected are independent.

The matrix shown in Figure 6 is said to represent a more basic level of the abstract model since most of the parameters are more inclusive in that they are independent of the geometrical form of the device. In addition the size of the matrix is smaller and consequently takes less time to obtain results from it.

Up to this point in the discussion, it has been assumed that the collection of equations were available and the need was to determine whether or not the collection of relations was independent and whether or not a given set of requirements in terms of specified parameters was

¹ A Theory for Design, C. C. Freeny, Ph.D. Thesis, Oklahoma State Univ., 1963

independent. The inverse problem of finding a collection of relationships to form the abstract model is not so well defined, as yet.

One approach is to consider dividing the system or device under consideration into characteristic subsystems. These characteristic subsystems could be those that are associated with a particular form of energy conversion such as the electrical to magnetic conversion subsystem, the magnetic to mechanical conversion subsystem, and the mechanical to electrical conversion (contacts) subsystem. Each general specification such as temperature, shock, vibration is then associated with each subsystem to determine the parameters of the subsystem which are influenced by the specification. The parameters listed are those that are usually restricted by the general requirement and these are called the necessary parameters. The desire then is to develop a model which has the property of consisting of independent relationships, which will relate these, and any other additional parameters, together. The procedure then is to separate the parameters into relationships based on whether or not there are known physical principles which relate any of these parameters to each other or additional parameters. For the class of parameters for which there are known physical principles, choose the physical law relationships which relate only the parameters from the necessary ones. If it is not possible to find physical law relationships which involve only parameters from the necessary class, then form relationships which use the smallest number of additional parameters. This procedure is continued until a model is developed that has the properties discussed earlier in this paper.

The discussion in this paper has tried to show that the functional form of the abstract or mathematical model can be used to make decisions which do not require numerical values. In addition, a scheme has been presented which allows one to determine if a given collection of equations, representing physical principles, are independent or not independent. These equations, which are used to obtain the functional form of the relationships, must show all the parameters involved and the only numerical values allowed are those concerned with units.

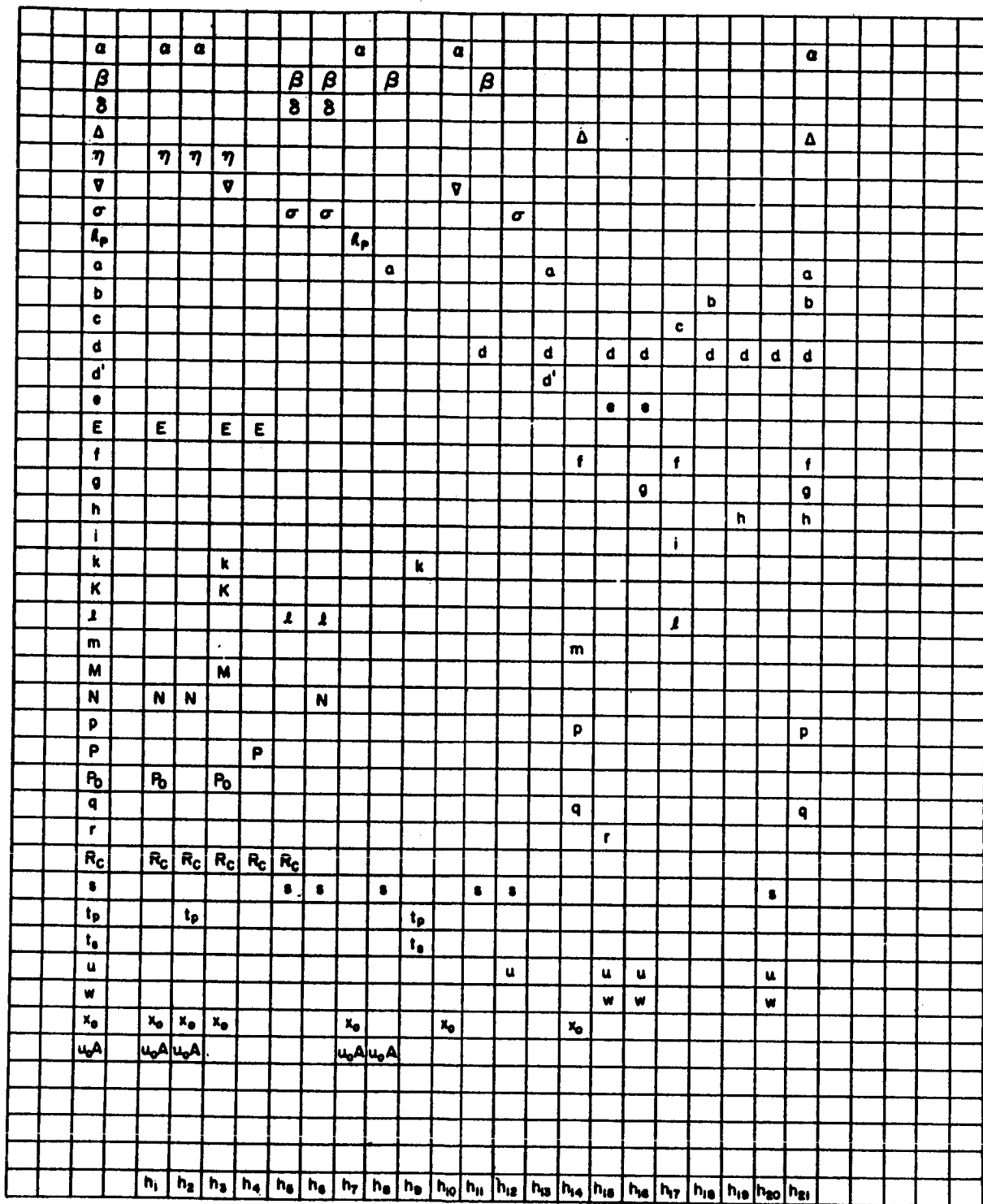


Figure 1

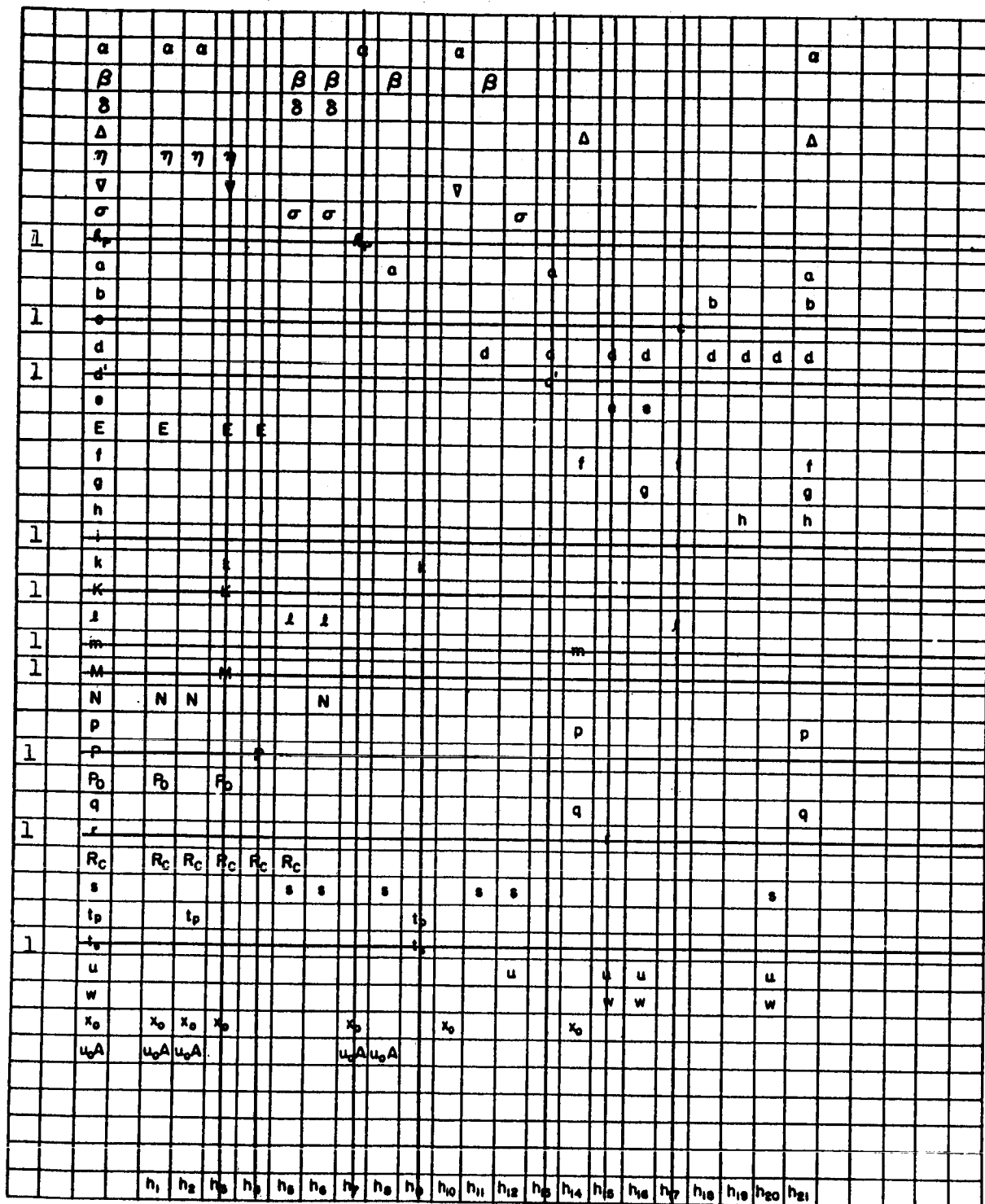


Figure 2

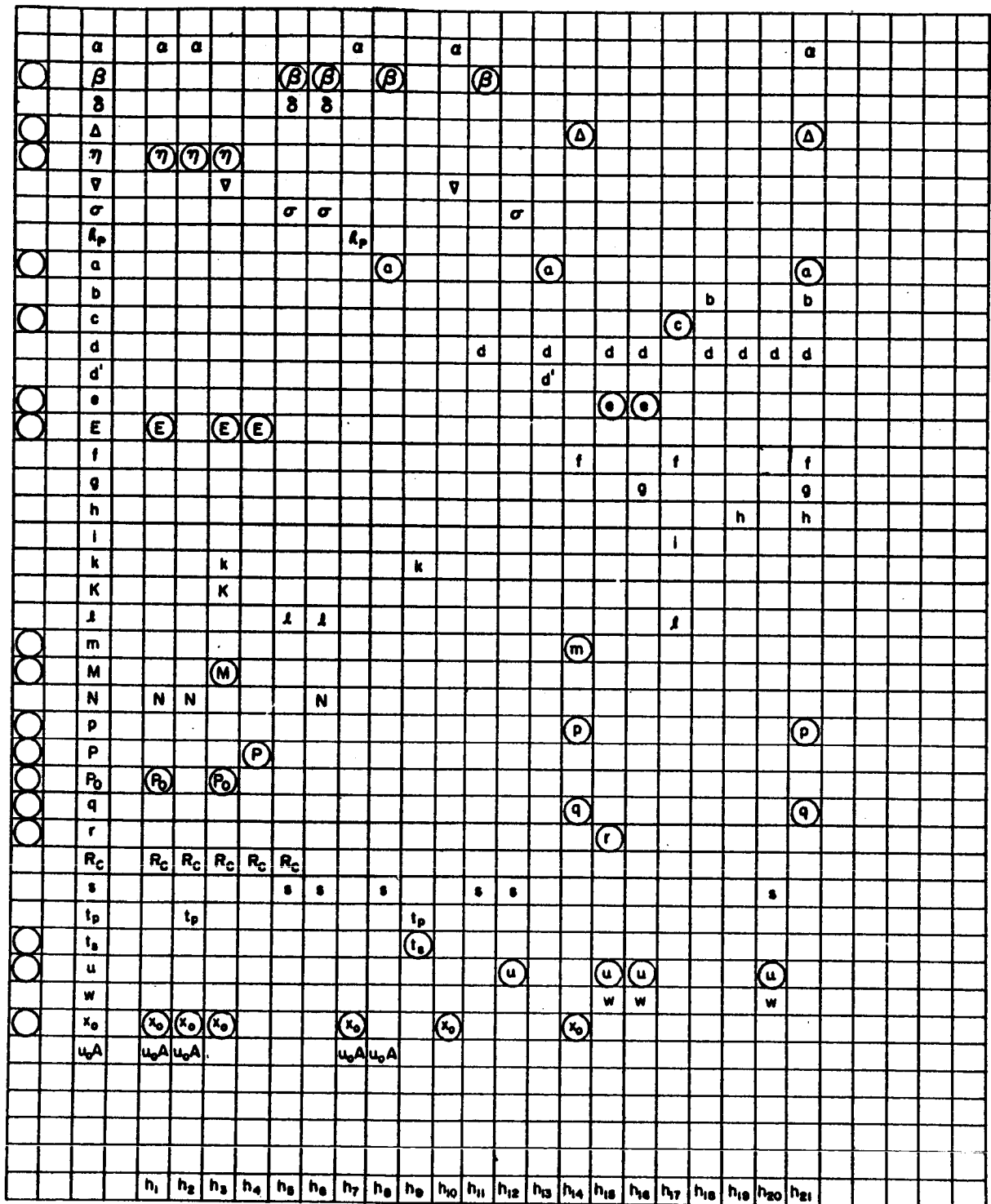


Figure 3

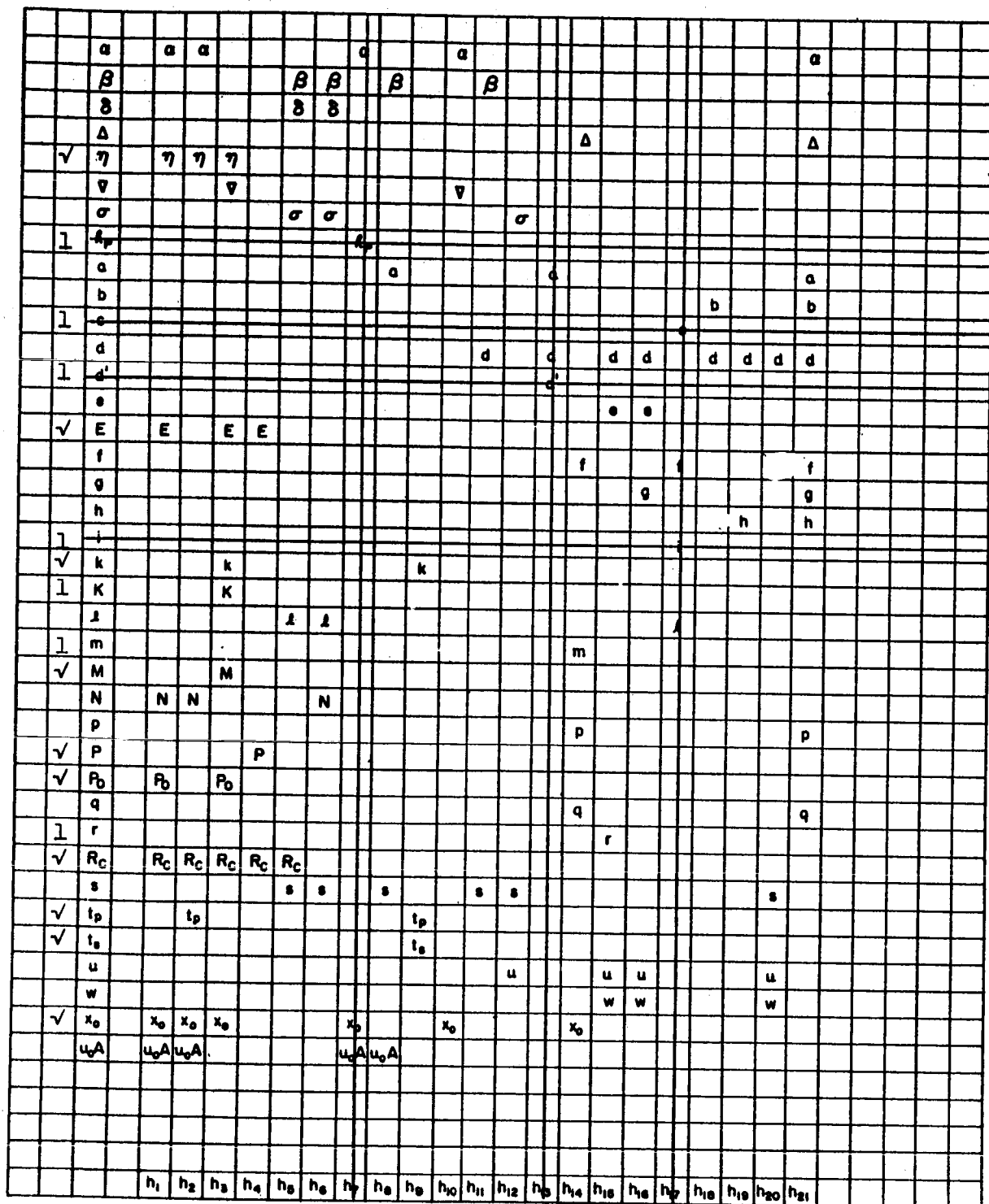


Figure 5

[illegible]

Figure 7

Appendix

$$\begin{aligned}
 h_1 \quad \eta &= 157.5 \frac{R_c(x_o + \alpha)\sqrt{2P_o}}{EN\sqrt{\mu_o A}} \\
 h_2 \quad t_p &= 10^{-8} \frac{N^2\mu_o A}{(x_o + \alpha)R_c} \ln \left[\frac{1}{1 - \eta} \right] \\
 h_3 \quad k &= (8.66 \times 10^{-3}) \left[\frac{18 M x_o^2 R_c}{E^2 \eta(1 - \eta)[1 - \nabla^2(1 + Kx_o/P_o)]} \right]^{\frac{1}{3}} \\
 h_4 \quad P &= E^2/R_c \\
 h_5 \quad R_c &= (.58 \times 10^{-6}) \frac{s^2 (1 - \alpha - \sigma)(1 + \beta + \sigma)l}{\delta^4} \\
 h_6 \quad N &= (.395) \frac{\ell s(1 - \beta - \sigma)}{\delta^2} \\
 h_7 \quad R_p &= (x_o + \alpha)/\mu_o A \\
 h_8 \quad \mu_o A &= \mu_o \pi a^2 s^2 \beta^2/4 \\
 h_9 \quad t_s &= k + t_p \\
 h_{10} \quad \nabla &= \alpha/(x_o + \alpha) \\
 h_{11} \quad \beta &= d/s \\
 h_{12} \quad \sigma &= u/s \\
 h_{13} \quad a &= d'/d \\
 h_{14} \quad m &= \Delta + q + f + p + x_o/2 \\
 h_{15} \quad r &= 4w + 2u + d + e
 \end{aligned}$$

$$h_{16} \quad g = 2w + e + u + d$$

$$h_{17} \quad f = c + l + i$$

$$h_{18} \quad b = 1.4d$$

$$h_{19} \quad h = 1.2d$$

$$h_{20} \quad s = 2w + u + d$$

$$h_{21} \quad \alpha = \left[\frac{\pi d^2 a^2 g}{4hp} + \frac{\pi d^2 a^2 g}{4qb} + 2fa^2 \right] \times 10^{-3} + 2\Delta a^2$$

SECTION III

AN INVESTIGATION OF AN ALTERNATE DESIGN MAP

The relay design map has been used as a method for obtaining allowable design specifications. The procedure used is to select the designated set of parameters and see if they "map through". The results of such an operation will fall into one of three possibilities: (1) If the set maps through, this indicates that the set is an allowable specification set. (2) If the set does not map through because of a contradiction, the set of specifications cannot, in general, be satisfied. (3) If the set fails to map through and there is no apparent contradiction, no information is obtainable from the map and two or more equations must be solved to determine the allowability of the set of parameters in question. In cases (1) and (2) the functional form of the relations is not needed, however, in case (3) no information can be obtained unless the functional form of the relations in question is known. Therefore, it should be kept in mind that the information that can be obtained from the design map is limited to cases in which the functional form of the relations is of no consequence.

An independent set of relations can be altered such that the parameter-relation structure is different but the information and therefore the system which is represented by the relations is unchanged. In view of this possibility, a logical question might be; what effect does this change have on the parameter sets which will or will not map through? An example has been prepared as an answer to this question. The discussion of the example will explain what occurs and why.

An alternate representation of the design map is obtained by allowing line segments to represent parameters and closed loops to

represent relations. This method has been suggested before, but has not been used because of the problem of arranging the line segments to form closed loops corresponding to the relations, without having a particular line (parameter) appear more than once. This problem, it is believed, can be overcome by proper selection of the relations which are to define the system. Proof of this has not yet been obtained, but present results are very promising.

The following examples apply to both questions presented above and will be discussed with both problems in mind.

Consider a relay system defined by the following relations.

$$(1) \quad \eta = (157.5) \left[\frac{R_c (x_o + \alpha) \sqrt{2P_o}}{E N s} \right]$$

$$(2) \quad t_s = (10^{-8}) \frac{N^2 s^2}{(x_o + \alpha)(R_c)} \ln \left[\frac{1}{1 - \eta} \right] +$$

$$(8.66 \times 10^{-3}) \left[\frac{18 M x_o^2 R_c}{E^2 \eta (1 - \eta) [1 - v^2 (1 + K x_o / P_o)]} \right]^{\frac{1}{3}}$$

$$(3) \quad P = E^2 / R_c$$

$$(4) \quad R_c = (.865 \times 10^{-6}) \frac{s^2 (1 - \beta - \sigma)(1 + \beta + \sigma) l g_r}{\delta^4}$$

$$(5) \quad N = \frac{(.637) l s (1 - \beta - \sigma) g_n}{\delta^2}$$

The parameters α , β , σ , g_n , g_r and $[1 - v^2(1 - K x_o / P_o)]$ will be considered constants in the example.

A design map of this system is shown in Figure 1. A specification set, $R_c, N, s, E, x_o, \eta, M$, has been selected for test. The result, shown in Figure 1, leaves the two parameters δ and ℓ undetermined and therefore an appeal to the relations themselves is necessary to determine if the set is an allowable specification set. To do this consider a system defined by the relations (4) and (5). Then the question becomes, is R_c, s and N a specification set for the two relation systems?

$$\text{Let } A = R_c$$

$$B = s$$

$$C = N$$

$$K_1 = \text{constant}$$

$$K_2 = \text{constant}$$

$$\text{Then (4) becomes } A = K_1 \frac{B^2 \ell}{\delta^4}$$

$$\text{and (5) becomes } C = \frac{K_2 \ell B}{\delta^2}$$

Solving for ℓ

$$\ell = \frac{K_3 C^2}{A}$$

Solving for δ

$$\delta = K_4 \sqrt{BC/A}$$

Therefore both ℓ and δ have been determined and the original set of parameters is an allowable specification set.

Now if equations (4) and (5) are combined the result is equation (6)

$$(6) \quad R_c = (2.14 \times 10^{-6}) \left[\frac{N^2 g_r}{\ell^2 g_n^2} \frac{(1 + \theta + \sigma)}{(1 - \theta - \sigma)} \right]$$

If relation (5) in the previous system is replaced by relation (6), a new set of relations is obtained which defines exactly the same system. The map for this system is shown in Figure 2. The same set of parameters that was tested on the map of Figure 1 is shown to map through in Figure 2. Therefore, the set is known to be an allowable specification set. The point of the example is quite clear. A given set of parameters may "map through" on one map and not on another apparently equivalent map. The reason for this result is traced to the maps themselves. Although they are both maps of a set of relations defining a given system, they do not contain the same information. For example, the first map shows it might be possible to solve equation (4) and (5) and obtain a relation involving only R_c and N . Whether or not this can be done cannot be determined from the map itself, and therefore no set of parameters containing both R_c and N would map through the design map in Figure 1.

The map in Figure 2 does not contain this possibility and the set containing R_c and N mapped through. The difference in information contained in the two maps is a result of the particular functional form of the relations themselves.

If the alternate representation were used the design map of Figure 1 would appear as in Figure 3. Note that the parameter N appears twice in the map and there is no possible arrangement that will eliminate this problem since the indicated relation $\{R_c N\}$ is properly contained in a second relation $\{x_o, \eta, P_o, s, R_c, E N\}$.

The map of Figure 2, in alternate representation would appear as in Figure 4. Note that there is no parameter that appears twice and yet all relations appearing in the system are represented. Use of this

design map is quite simple. Any set of parameters which does not form a complete loop is an allowable specification set. These which do form a complete loop may or may not be allowable. This is exactly the same information which can be obtained from the standard design map . The alternate design map is of importance because it allows the listing of all possible sets of parameters which will "map through". The method for doing this will be the topic of a future report.















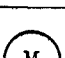
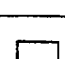
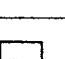
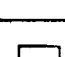
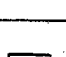
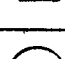
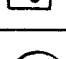




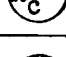
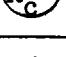
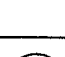

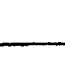


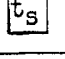

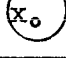
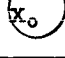

	δ							
	η							7
	E							4
	ℓ							
	M							9
	P							5
	P_o							8
	R_c							1
	s							3
	t_s							10
	x_o							6
	N							2
	0	f_1	f_2	f_3	f_4	f_5		

Figure 1

\square	δ				δ		5
\bigcirc	η	η	η				9
\bigcirc	E	E	E	E			6
\square	ℓ				ℓ	ℓ	3
\bigcirc	M		M				11
\square	P			P			7
\square	P_o	P_o					10
\bigcirc	R_c	R_c	R_c	R_c	R_c	R_c	1
\bigcirc	s	s			s		4
\square	t_s		t_s				12
\bigcirc	x_o	x_o	x_o				8
\bigcirc	N	N	N			N	2
	0	f_1	f_2	f_3	f_4	f_6	

Figure 2

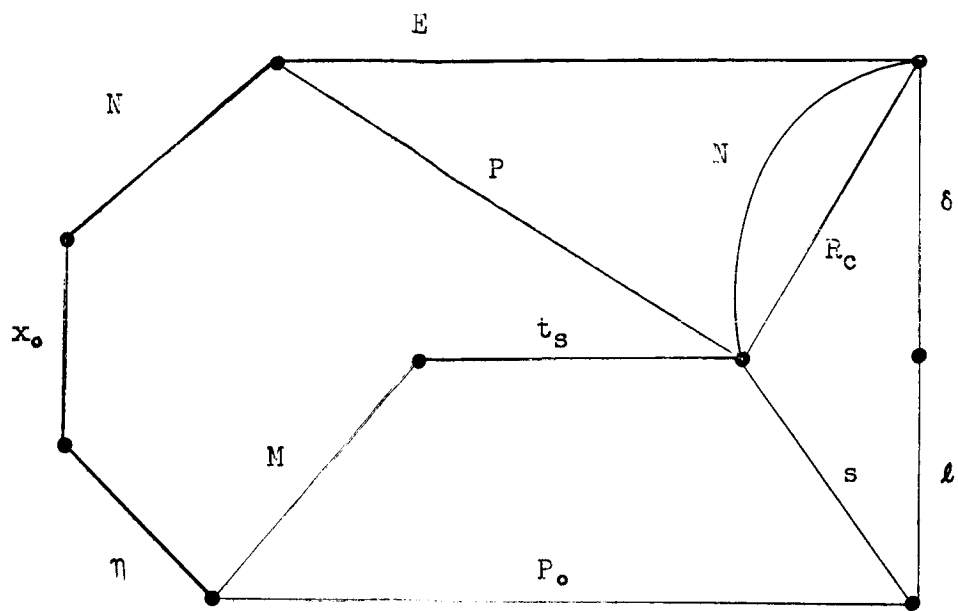


Figure 3

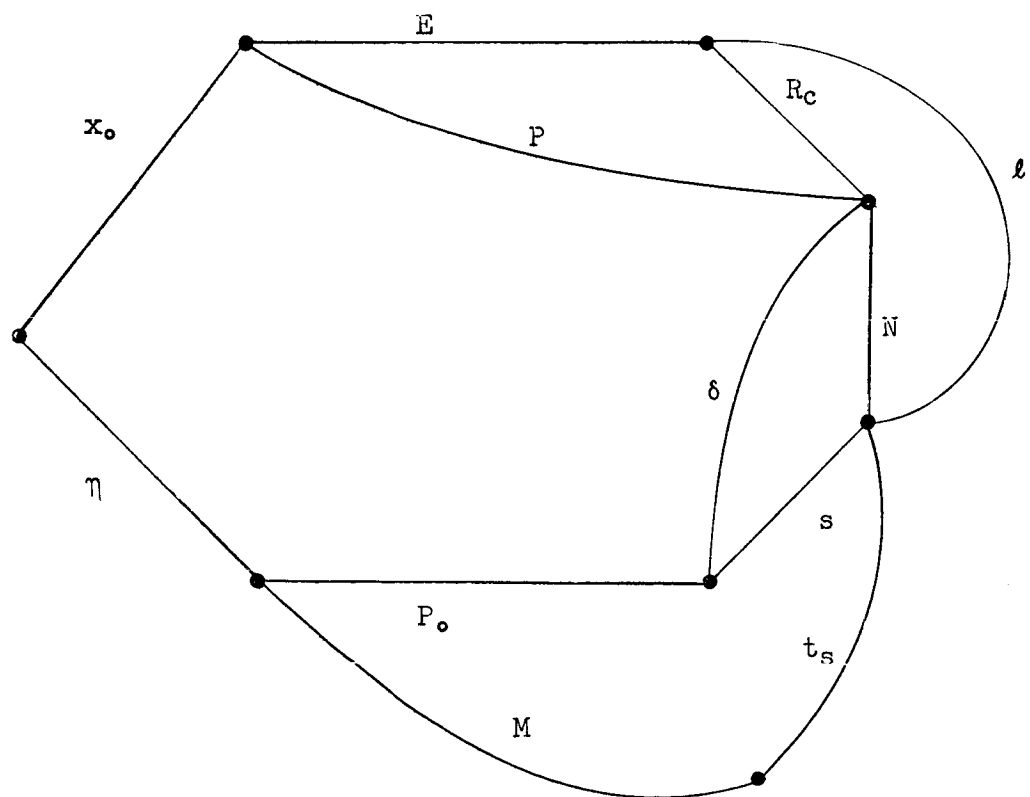


Figure 4

SECTION IV

METHODS FOR OBTAINING ALLOWED SPECIFICATION SETS

An allowed specification set for a system is any set of parameters of that system for which arbitrary scalar values can be selected without any contradictions arising. At present, the design map is used to check a given set of parameters to determine if they are an allowable set. The results are not exact since if the set fails to "map through" some additional test are sometimes required.

When a set of parameters does not give positive results on the design map, it becomes necessary to determine which subset of parameters is causing the contradiction. Once the cause of the difficulty is determined, removal of one or more parameters from the set will give an allowable set.

Determination of the particular subset of the test set which disallows positive results can become quite difficult when the test set has many elements. This section of the report is concerned with the selection of allowed specification sets and presents a method by which these sets can be obtained.

A useful technique employed in the selection of allowable sets is the following decomposition process:

Given a set $[R_i]$ of relations on the parameters $[P_n]$,
discard all relations involving a parameter which appears
in only one relation. Consider those relations remaining as
 $[R_i]$ and again discard those involving unique parameters.
The set $[R_i]$ is said to be decomposable if this process
yields the empty set in a finite number of applications.

It can be shown that decomposibility is a necessary and sufficient condition for independence of the relations under certain conditions. Therefore, the

terms independence and dependence will be used rather than decomposable and non-decomposable.

The key to checking specification sets lies in the fact that every independent set of relations will have at least one allowable specification set. Also, it is known that there does not exist any set of parameters which will map through a dependent set of relations. The obvious result of this is that any subset of parameters, which when deleted from the system leaves the relations independent, is an allowable specification set. Therefore, any subset of the test set may be checked for allowability without the necessity of trying to map it through with the rest of the set. By the same reasoning any set of parameters which when deleted from the system leaves a dependent system, will not map through. If this is the case there is no point in trying to include it in any test set.

The above discussion suggests a method for generating an allowed specification set. That is, select the parameters one by one, testing each time to determine if an independent system remains. If the desired parameters are selected in order of their importance in the design then the best possible specification set is obtained.

An example of this process is given in the sample selection problem which follows.

Consider a relay system defined by the following relations.

- (1) $(\eta, E, P_o, R_c, S, x_o, N)$
- (2) $(\eta, E, M, R_c, t_s, x_o, N)$
- (3) (E, P, R_c)
- (4) (δ, ℓ, R_c, S)
- (5) (δ, ℓ, S, N)

If the set $[N, R_c, \delta, x_o, S, P_o, \eta]$ is selected for test, the results are negative as shown in Figure 1. The original system is independent as shown by the decomposition sets

- a. $[1, 2, 3]$ (first decomposition set)
- b. $[4, 5]$ (second decomposition set)

The system with the test set removed is

- (1) (E)
- (2) (E, M, t_s)
- (3) (E, P)
- (4) (ℓ)
- (5) (ℓ)

which is dependent since the decomposition process yields

- a. $[2, 3]$ (first decomposition set)
- b. $[1]$ (second decomposition set)
- c. $[4, 5]$ (this set is non-decomposable)

This result indicates that the set will not map through and this fact is also exemplified in the results of the mapping in Figure 1. If it is assumed that the desirability of the parameters as members of the specification set is indicated by their order as given above, each subset may be checked for allowability. This process is indicated below.

Step 1: The system with N removed is

- (1) ($\eta, E, P_o, R_c, S, x_o$)
- (2) ($\eta, E, M, R_c, t_x, x_o$)
- (3) (E, P, R_c)
- (4) (δ, ℓ, R_c, S)
- (5) (δ, ℓ, S)

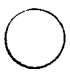





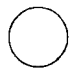









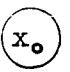
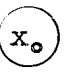



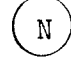
	δ						3
	η	η	η				
	E	E	E	E			
	ℓ						6
	M		M				
	P			P			
	P_o	P_o					
	R_c						2
	S						5
	t_s		t_s				
	x_o						4
	N						1
	0	f_1	f_2	f_3	f_4	f_5	

Figure 1

which has the decomposition classes

- a. [1, 2, 3]
- b. [4]
- c. [5]

Step 2: The system with $[N, R_c]$ removed is

- (1) (η, E, P_o, S, x_o)
- (2) (η, E, M, t_s, x_o)
- (3) (E, P)
- (4) (δ, ℓ, S)
- (5) (δ, ℓ, S)

which, when an attempt at decomposition is made, yields

- a. [1, 2, 3] (first decomposition class)
- b. [4, 5] (non-decomposable)

The implication of step 2 is that no set containing both N and R_c will map through. Since N is considered more desirable than R_c , R_c will be removed from the set of specifications.

Step 3: The system with $[N, \delta]$ removed is

- (1) $(\eta, E, P_o, R_c, S, x_o)$
- (2) $(\eta, E, M, R_c, t_s, x_o)$
- (3) (E, P, R_c)
- (4) (ℓ, R_c, S)
- (5) (ℓ, S)

which has decomposition classes

- a. [1, 2, 3]
- b. [4]
- c. [5]

Step 4: The system with $[N, \delta, x_o]$ removed is

- (1) (η, E, P_o, R_c, S)
- (2) (η, E, M, R_c, t_s)
- (3) (E, P, R_c)
- (4) (ℓ, R_c, S)
- (5) (ℓ, S)

which has decomposition classes

- a. $[1, 2, 3]$
- b. $[4]$
- c. $[5]$

Step 5: The system with $[N, \delta, x_o, S]$ removed is

- (1) (η, E, P_o, R_c)
- (2) (η, E, M, R_c, t_s)
- (3) (E, P, R_c)
- (4) (ℓ, R_c)
- (5) (ℓ)

which has decomposition classes

- a. $[1, 2, 3]$
- b. $[4]$
- c. $[5]$

Step 6: The system with $[N, \delta, x_o, S, P_o]$ removed is

- (1) (η, E, R_c)
- (2) (η, E, M, R_c, t_s)
- (3) (E, P, R_c)
- (4) (ℓ, R_c)
- (5) (ℓ)

which has decomposition classes

- a. [2, 3]
- b. [1]
- c. [4]
- d. [5]

Step 7: The system with $[N, \delta, x_o, S, P_o, \eta]$ removed is

- (1) (E, R_c)
- (2) (E, M, R_c, t_s)
- (3) (E, P, R_c)
- (4) (ℓ, R_c)
- (5) (ℓ)

which has decomposition classes

- a. [2, 3]
- b. [1]
- c. [4]
- d. [5]

Step 7 indicates that an allowable specification set has been obtained, retaining as many as possible of the original test set. An additional parameter may be selected to replace R_c . In practice this procedure is accomplished very easily and quickly and will allow the designer to pinpoint contradictions in the specifications without having to map the entire set through.

It is possible for a single parameter, when removed from the system, to leave a dependent system. It follows then that any set containing this parameter will not map through. The procedure in the example allows a quick check for this possibility.

It might sometimes be desirable to obtain a listing of all sets of parameters which will give positive results on the design map. If the system is represented by a linear graph as was used for an alternate representation in the last report,

it can be shown that the "trees" of the graph are those sets of parameters which give positive results on the design map. A method for obtaining a listing of the trees is given below.

Given a linear graph with V vertices and E edges, form a listing of any $V - 1$ vertex cut sets. (A vertex cut set corresponding to a particular vertex is just a listing of the edges incident to the vertex.) Obtain the Cauchy product of the cut sets and the result is a list of all trees of the graph. (The Cauchy product will be explained in the example).

EXAMPLE:

Consider the system shown in Figure 2

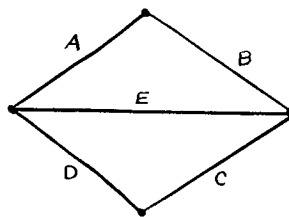


Figure 2

The vertex cut sets are $[A, E, D]$, $[A, B]$, $[B, C, E]$ and $[C, D]$. Select $V - 1$ of these cut sets, $[A, B]$, $[B, C, E]$, $[C, D]$ and arrange them in the following manner:

$$(A + B) (B + C + E) (C + D)$$

Perform ordinary multiplication on the line shown obtaining

$$(AB + AC + AE + BB + BC + BE) (C + D)$$

and

$$ABC + ACC + AEC + BBC + BCC + BEC$$

$$+ ABD + ACD + AED + BBD + BCD + BED$$

Remove all products which contain the same edge twice and all products which appear twice. The result is

$$ABC + AEC + BEC + ABD + ACD + AED + BCD + BED$$

Each of the products in the listing above is a tree of the graph and thus is a listing of the parameter sets which will map through the design map.